Rayonnement des trous noirs en interaction avec des champs bosoniques massifs

Mohamed Ould El Hadj

Université de Corse-Pascal Paoli
École Doctorale Environnement et Société
UMR CNRS 6134 (SPE)

Thèse présentée pour l'obtention du grade de

DOCTEUR EN PHYSIQUE
Spécialité : **Physique Théorique**

Soutenue publiquement par

Mohamed OULD EL HADJ

le : 20/07/2016

Rayonnement des trous noirs en interaction avec des champs bosoniques massifs

---

Directeurs :
M Antoine FOLACCI, Professeur, Université de Corse
M Yves DECANINI, Professeur, Université de Corse

Rapporteurs :
Mme Nathalie DERUELLE, Directrice de recherche au CNRS, Université Paris 7
M Mikhaïl VOLKOV, Professeur, Université de Tours

Jury :
M Luc BLANCHET, Directeur de recherche au CNRS, Université de Paris 6
M Yves DECANINI, Professeur, Université de Corse
Mme Nathalie DERUELLE, Directrice de recherche au CNRS, Université Paris 7
M Antoine FOLACCI, Professeur, Université de Corse
M Mikhaïl VOLKOV, Professeur, Université de Tours

« *Ce n'est pas le doute, c'est la certitude qui rend fou.* »

Friedrich Nietzsche

Remerciements

J'exprime mes profonds remerciements à mes directeurs de thèse, Antoine Folacci et Yves Decanini, pour leur encadrement si efficace, ainsi que leurs conseils si avisés. Je leur dis merci pour leur disponibilité durant toute cette période de thèse, pour tous ces échanges riches d'enseignement qui m'ont permis d'avancer à chaque fois et à mener à bien la tâche qui m'a été confiée. Je leur exprime ma profonde gratitude pour tout ce qu'ils m'ont apporté sur le plan scientifique et humain.

Mes remerciements distingués vont à Mme Nathalie Deruelle, et M. Mikhaïl Volkov d'avoir eu l'amabilité d'accepter d'être les rapporteurs de mon humble travail de thèse, ainsi que M. Luc Blanchet pour son aimable collaboration. Ils m'ont fait l'honneur d'avoir accepté de faire partie de mon jury de thèse, sur ce je leur exprime toute ma reconnaissance.

Je remercie chaleureusement Andreï, avec qui j'ai partagé mon bureau, pour toutes ces discussions scientifiques et amicales, pour son aide, avec Gauthier, dans la préparation de mon pot de thèse. Merci à tous les docteurs et futurs docteurs, Andreï, Damien, David, Éric, Gauthier, Jean-Baptiste, Romain, Sandrine, Tom et Wani et ainsi que Aurélia et Damien, pour leur sympathie et tous ces moments conviviaux qu'on a partagés ensemble et que j'apprécie tellement. Mes remerciements vont également aux chercheurs du laboratoire SPE (UMR CNRS 6134) pour leur accueil et sympathie, merci donc à Pierre Simonnet, Stéphane Ancey, Rachel Baïle, Catherine Ducourtioux, Nicolas Heraud, Jean-François Muzy, Marie-Laure Nivet, Sonia Ternengo, aux techniciens Antoine Pieri et Yves Thibaudat. Mes remerciements à mes amis Juba, Abdellah, Farid, Madjid, Lamara, Mebrouk (Blo), Mustapha, Farouk et Ahmed qui m'ont toujours encouragé et entouré de leur soutien. Je prie toutes celles et tous ceux que je n'ai pas nommés ici de m'excuser.

Je ne crois pas pouvoir trouver des mots justes pour dire à ma famille, mes parents, mes sœurs, Nora et Malika, mes frères, Boukhalfa et Rabah, mes chaleureux remerciements et ma profonde gratitude, pour leurs encouragements et leur soutien indéfectible dans tout ce que j'entreprends et depuis toujours. Merci du fond du cœur.

Je tiens, pour terminer, à dire mes remerciements à la Collectivité Territoriale de Corse pour son soutien financier sans lequel ce travail de thèse n'aurait pas pu voir le jour.

Ait Mislaiene, le 8 septembre 2016

Abstract

Radiation from black holes interacting with massive bosonic fields

This thesis focuses on the radiation from black holes interacting with massive bosonic fields (the scalar, Proca and Fierz-Pauli fields). We studied more particularly the influence of the resonance spectrum (quasinormal modes or quasibound states) on the response of the black hole to an external perturbation. This work is the first step to highlight new effects in the radiation from supermassive black holes which could allow us to test the various massive gravity theories or to further support Einstein's general relativity.

More precisely :

– In order to circumvent the numerous difficulties associated with massive gravity theories and black hole perturbation in this context, we worked at first on a toy model where the graviton field is replaced by a massive scalar field linearly coupled to a particle plunging into the Schwarzschild black hole. We studied the role of the field mass on the structure of the black hole responses and compared our results with those obtained for the massless field. We highlighted unexpected effects due to the mass parameter and in particular the excitation of the quasibound states of the black hole in addition to that of its quasinormal modes as well as the possible vanishing of the waveform when the particle moves on a quasi-circular trajectory.

– We also considered the excitation of quasinormal modes of the Schwarzschild black hole because, from an observational point of view, they are supposed to provide a direct proof of the existence of the black holes. We have shown numerically and analytically the presence of a resonant behaviour of the quasinormal excitation factors which, theoretically, could lead to giant and slowly decaying ringings. This behaviour has been highlighted on the Fierz-Pauli field and we have generalized it to the other bosonic fields (the scalar and Proca fields). However, by working on a Cauchy problem, we also showed that, contrary to what occurs for massless fields, the quasinormal ringing cannot be clearly individualized on a waveform and its giant character is in fact neutralized due to the coexistence of two phenomena (i) the excitation of quasibound states which blur the quasinormal contribution and (ii) the evanescent nature of the particular partial modes which could excite the quasinormal modes whose excitation factor has a resonant behaviour.

Keywords : Radiation of black holes, massive bosonic fields, quasinormal modes, quasibound states, waveforms.

Table des matières

Introduction

« Why do you spend so much time and energy testing General Relativity ? We know that the theory is right. »

Une remarque faite en privé par
S. Chandrasekhar à C. Will

Albert Einstein a publié, le 25 novembre 1915, après huit années de travail acharné, la version définitive de sa théorie de la relativité générale [1]. La théorie de la relativité (restreinte et générale) est l'une des théories les plus révolutionnaires de l'histoire des sciences, au même titre que la théorie quantique et, dans le domaine des sciences naturelles, la théorie de l'évolution. Elle a bouleversé radicalement notre compréhension du réel ; les entités fondamentales de la physique (espace, temps, matière et énergie) que l'on croyait immuables ne le sont plus désormais. Il n'y a pas d'espace fixe, pas non plus de temps absolu ; mais *"l'espace en tant que tel et le temps en tant que tel sont voués à disparaître comme des ombres, et seule une certaine union des deux conservera une certaine réalité."* [1] Et cet espace-temps, maintenant unifié, se distord et se dilate ; il interagit avec la matière, il est dynamique.

La relativité générale ne décrit pas seulement avec élégance mathématique l'interaction gravitationnelle, mais elle fait aussi des prédictions fascinantes. L'une des prédictions majeures, due à Einstein en 1916, est l'existence d'un nouveau type d'ondes [2], les ondes gravitationnelles qui sont des vibrations de l'espace-temps propageant le champ gravitationnel. Le 14 septembre 2015, soit un siècle après, les deux interféromètres de Michelson kilométriques d'Advanced LIGO (*Laser Interferometer Gravitational-Wave Observatory*) ont observé le passage des ondes gravitationnelles et on a baptisé ce signal GW150914 [3]. Ainsi, on dispose pour la première fois d'une détection directe des ondes gravitationnelles. En fait, la première preuve indirecte de l'existence des ondes gravitationnelles remonte aux années soixante-dix. La découverte du pulsar binaire PSR 1913+16 par les deux astrophysiciens Taylor et Hulse en 1974 [4] et les observations ultérieures de sa perte d'énergie par Taylor et Weisberg [5] furent interprétées comme la conséquence de l'émission d'ondes gravitationnelles. Une autre prédiction majeure de la relativité générale qui a été confirmée en même temps que la détection directe des ondes gravitationnelles est l'existence des trous noirs [3]. Ces mystérieux objets sont restés longtemps une solution mathématique, mais non physique des équations d'Einstein et ceci jusqu'aux années soixante où une nouvelle génération de physiciens théoriciens a apporté une explication physique convaincante à ce qui était jusqu'alors une singularité mathématique. De plus, depuis les années soixante-dix, on dispose de fortes présomptions observationnelles en faveur de leur existence, ou plutôt de l'existence d'objets extrêmement massifs

1. Hermann Minkowski lors d'une conférence devant la 80^{e} Assemblée des médecins et scientifiques allemands à Cologne, le 21 septembre 1908, cité par Kip S. Thorne dans son livre *''Trous noirs et distorsions du temps"*

et compacts, tels les quasars et les sources X binaires. Mais, tant qu'on n'aura pas observé l'horizon des événements d'un trou noir, on ne disposera pas de véritables preuves directes de l'existence de tels objets. Une des méthodes utilisée pour mettre en évidence l'existence de trous noirs est l'analyse du rayonnement gravitationnel généré, par exemple, par la coalescence de deux corps compacts du type trous noirs ou étoiles à neutrons. Cette analyse devrait nous permettre l'observation d'une "sonnerie" amortie due aux modes résonnants du trou noir final. Les fréquences et les taux d'amortissement de ces sonneries définissent le spectre complexe des résonances du trou noir, autrement dit, ses modes quasi-normaux (QNMs ou *Quasinormal modes*) . Ces sonneries sont considérées comme l'empreinte digitale de ce trou noir : elles constitueraient une preuve directe de son existence et permettraient de déterminer ses caractéristiques physiques tels que sa masse et son moment angulaire (voir les Réfs. [6–9] pour des articles de revue sur le sujet des QNMs). Et comme nous l'avons déjà mentionné ci-dessus, on dispose maintenant d'une preuve directe de l'existence de trous noirs. En effet, l'analyse du signal gravitationnel GW150914 faite par les chercheurs de LIGO et leurs collaborateurs de l'interféromètre Virgo, selon un modèle basé sur la relativité générale, a montré la présence des QNMs (la sonnerie) du trou noir final d'une masse d'environ 60 fois la masse du Soleil issu de la coalescence de deux trous noirs. Chacun a une masse environ 25 fois plus grande que celle du Soleil (pour plus de détails sur les caractéristiques physiques du trou noir détecté ainsi que du trou noir binaire dont il est issu, le lecteur peut se reporter aux Réfs. [3, 10, 11]).

La relativité générale d'Einstein est une théorie solidement établie qui a connu d'immenses succès. Et, bien qu'un siècle après sa formulation, deux de ses prédictions majeures viennent d'être confirmées, à savoir les ondes gravitationnelles et les trous noirs, des raisons théoriques et expérimentales laissent penser qu'elle n'est pas une théorie définitive de la gravitation. Du point de vue théorique, la relativité générale donne une description purement classique de la gravitation et, de ce fait, elle ne rend pas compte du monde quantique. À de très petites échelles (les échelles de Planck), les effets quantiques du champ gravitationnel deviennent si importants que leur analyse nécessite une véritable théorie de la gravitation quantique. D'autre part, et dans certaines conditions, elle prévoit l'existence de singularités géométriques de l'espace-temps, par exemple, lors de l'effondrement conduisant à la formation des trous noirs, ainsi que pour certains modèles cosmologiques dont celui du *Big-Bang*, et c'est dans ces singularités même que l'on se trouve face aux limites de la théorie là où elle n'est plus applicable [12]. On peut penser qu'au voisinage d'une singularité la courbure de l'espace-temps devient si grande qu'on peut s'attendre à des effets quantiques importants. Ceux-ci pourraient même éviter l'apparition de telles singularités. D'un point de vue expérimental, de nombreuses observations, réalisées depuis 1998 viennent transformer radicalement notre vision de la gravitation. Ces observations nous montrent, tout particulièrement et contrairement à ce que la relativité générale prédit, que l'Univers est en expansion accélérée. Des modifications de la théorie d'Einstein sont alors inévitablement envisagées. En l'absence d'une théorie de la gravité quantique qui serait en mesure de décrire la gravitation à toutes les échelles (microscopique ou macroscopique), une approche phénoménologique du problème a été adoptée. Ainsi, des théories alternatives à la relativité générale ont été proposées afin d'explorer d'autres pistes qui pourront servir de guide à une formulation cohérente et complète de la gravitation. Faire l'hypothèse, par exemple, d'une masse pour le graviton, cette particule qui est le médiateur de l'in-

teraction gravitationnelle, en est une. Le lecteur peut se reporter à la Réf. [13] et à ses références pour une liste quasi-exhaustive des théories de gravité allant au delà de la relativité générale.

On dispose aujourd'hui de quelques contraintes expérimentales sur la limite supérieure de la masse du graviton. Il est très important de noter que les masses limites dépendent fortement du modèle théorique considéré mais aussi des expériences réalisées. De plus, on doit souligner ici que l'hypothétique graviton massif serait certainement une particule ultralégère. Ainsi, l'étude du rayonnement gravitationnel des pulsars binaires, PSR B1913+16 et PSR B1534+12, a permis d'estimer la borne supérieure de la masse du graviton à $\mu_g \leqslant 7{,}6\times10^{-20}\,\mathrm{eV/c^2} \approx 1{,}35\times10^{-54}\,\mathrm{kg}$ [14]. Pour rappel, cette limite a été obtenue dans le cadre de la théorie de Fierz-Pauli ordinaire. D'autres limites supérieures de la masse du graviton basées sur différentes données observationnelles ont été obtenues. On peut, par exemple, faire référence à la limite obtenue dans le cadre du système solaire $\mu_g \leqslant 4{,}4\times10^{-22}\,\mathrm{eV/c^2} \approx 7{,}83\times10^{-58}\,\mathrm{kg}$, dans la limite du potentiel de Yukawa [15]. Récemment, une nouvelle contrainte a été obtenue par l'équipe de LIGO et leurs collaborateurs de Virgo en utilisant le signal gravitationnel GW150914 [3]. Leur estimation qui est basée sur la relation de dispersion modifiée [16] contraint la masse du graviton à une borne supérieure $\mu_g \leqslant 1{,}2\times10^{-22}\,\mathrm{eV/c^2} \approx 2{,}13\times10^{-58}\,\mathrm{kg}$ [17] . En fait, et comme nous l'avons déjà mentionné ci-dessus, les contraintes sur la masse du graviton dépendent étroitement du modèle utilisé. En effet, pour les mêmes données observationnelles, la contrainte sur la masse du graviton peut varier, selon le modèle utilisé, d'un seul ordre de grandeur jusqu'à une dizaine. Pour plus d'informations sur les méthodes évoquées ou sur d'autres méthodes expérimentales utilisées pour contraindre la masse du graviton, le lecteur peut se reporter avec profit à la Réf. [18].

Concrètement, même si le graviton est une particule ultralégère, le paramètre physique pertinent dans l'étude du rayonnement gravitationnel des trous noirs et de leurs perturbations est le paramètre de couplage sans dimension

$$\tilde{\alpha} = \frac{2\mathrm{M}\mu}{m_p^2}. \tag{1}$$

Ici, M, μ et $m_p = \sqrt{\hbar c/\mathrm{G}}$ désignent respectivement la masse du trou noir, la masse du graviton au repos et la masse de Planck. Par conséquent, il existe des configurations pour lesquelles le paramètre de couplage $\tilde{\alpha}$ est non-négligeable et pour lesquelles le signal gravitationnel émis par le trou noir perturbé serait considérablement modifié par rapport au cas non-massif. Pour observer de telles modifications, les trous noirs supermassifs sont de très bons candidats en raison de leur grande masse. Rappelons que les études de la source radio compacte Sagittarius A* nous ont révélé l'existence d'un objet compact de masse $(4{,}31\pm0{,}38)\times10^6\,\mathrm{M}_\odot$ au cœur de notre Galaxie, qui serait un trou noir supermassif (voir la Réf. [19] et ses références). Un autre exemple, encore plus intéressant, est le trou noir supermassif de masse $(1{,}7\pm0{,}3)\times10^{10}\,\mathrm{M}_\odot$ au cœur de la galaxie lenticulaire NGC 1277 [20]. Des trous noirs encore plus massifs pourraient être découverts dans l'avenir étant donné que la plupart des galaxies devraient en abriter en leur cœur [21]. Ainsi, si on considère, par exemple, un objet compact (trou noir stellaire, étoile à neutron, naine blanche…) capturé par un trou noir supermassif ayant une masse comprise entre $10^6\,\mathrm{M}_\odot$ à $2\times10^{10}\,\mathrm{M}_\odot$, tout en supposant que

la masse du graviton soit de l'ordre $\mu_g \approx 1{,}35 \times 10^{-54}\,\mathrm{kg}$ [14], nous aurons le paramètre de couplage $\tilde{\alpha}$ compris entre 5×10^{-3} et 20. Nous choisissons cette valeur pour la masse du graviton parce que c'est celle obtenue dans le cadre du modèle théorique de Fierz-Pauli et que c'est ce modèle qui va nous intéresser par la suite.

Les configurations de type EMRI (*Extreme Mass Ratio Inspiral*), i.e., un système binaire asymétrique où la masse de l'objet compact qui chute dans le trou noir est négligeable devant celle de ce dernier, sont d'un intérêt primordial en physique fondamentale. En effet, avant la phase plongeante, l'objet compact évolue au voisinage du trou noir supermassif en effectuant des milliers de cycles sur des orbites quasi-circulaires, tout en émettant des ondes gravitationnelles que l'on devrait pouvoir détecter à l'aide des futurs détecteurs spatiaux comme eLISA (*evolving Laser Interferometer Space Antenna*) dédiés à l'étude du rayonnement gravitationnel à basse fréquence dont la bande passante est comprise entre $10^{-4}\,\mathrm{Hz}$ et $1\,\mathrm{Hz}$ [22]. Le rayonnement contient des informations sur la géométrie de l'espace-temps, la masse du trou noir supermassif et son moment angulaire. Après avoir extrait les informations codées dans ces ondes gravitationnelles, on devrait pouvoir non seulement déterminer la masse du trou noir supermassif et son moment angulaire, avec une erreur de l'ordre de 0,01 % à 0,1 %, mais aussi construire la carte "exacte" de la structure de l'espace-temps au voisinage de l'horizon du trou noir supermassif et mettre de fortes contraintes sur la masse du graviton. Cette carte de l'espace-temps nous permettrait de tester en champ fort les différentes structures géométriques prédites par les théories alternatives et/ou de vérifier le théorème de non-chevelure de la relativité générale (i.e., le fait que tous les trous noirs non chargés en rotation sont décrits par la géométrie de Kerr [23]). Certes, les ondes gravitationnelles émises durant cette phase encodent des informations qui nous permettraient de reconstruire la structure géométrique de l'espace-temps extérieur de l'objet central, de remonter à sa masse et son moment angulaire, par contre la présence ou non d'un horizon des événements ne serait indiquée qu'au cours du régime plongeant. En effet, lors du régime plongeant, le signal généré pendant cette phase porte l'empreinte digitale du trou noir. Ainsi, les EMRIs peuvent être utilisées pour contraindre les différentes théories alternatives (et pas seulement les théories de la gravité massive) et tester la relativité générale avec des précisions inégalées.

Les systèmes binaires de type EMRI peuvent être décrits dans le cadre de la théorie des perturbations des trous noirs. En effet, dès lors qu'on se place dans l'approximation $m/\mathrm{M} \ll 1$ où m et M qui sont respectivement la masse de l'objet compact (trou noir, étoile à neutron, naine blanche…) et M la masse du trou noir supermassif, l'objet compact peut être considéré comme une "particule" (dans le sens où sa structure interne n'intervient pas dans l'étude du problème) se déplaçant au voisinage (grande vitesse et champ fort) ou loin (faible vitesse et champ faible) du trou noir supermassif. La théorie des perturbations est une approche qui a été développée par Regge et Wheeler dans un article publié en 1957 [24] concernant une étude sur la stabilité du trou noir de Schwarzschild en présence d'une perturbation extérieure. Ces travaux ont été suivis par ceux de Vishveshwara [25] et de Zerilli [26] ainsi que par le travail de Moncrief, en 1974 [27], dans lequel il proposa un nouveau formalisme pour traiter les perturbations du trou noir de Schwarzschild. La théorie des perturbations peut être utilisée pour modéliser les effets de l'action du champ créé par une particule en mouvement sur elle-même (problème dit de la *self-force*). Une vaste littéra-

ture existe traitant de ces problèmes et de leurs variantes (les perturbations du trou noir de Kerr, le rayonnement gravitationnel généré par une particule en chute radiale, le régime plongeant, les perturbations du second ordre...). Le lecteur peut, par exemple, se reporter avec profit aux Réfs. [28–62] et à leurs références.

Comme nous l'avons déjà mentionné ci-dessus, les systèmes EMRIs sont de très bons candidats pour les détecteurs spatiaux, néanmoins, ils ne peuvent pas être observés par les détecteurs terrestres (advanced LIGO, advanced Virgo, GEO600, KAGRA...). En effet, les détecteurs terrestres sont principalement dédiés à la détection d'ondes gravitationnelles dans une gamme de fréquences comprise entre 1 Hz et 10^3 Hz. Parmi les sources astrophysiques les plus prometteuses pour les détecteurs terrestres, on a la coalescence d'un système binaire d'astres compacts ayant une masse allant de quelques masses solaires à une centaine de masses solaires, plus particulièrement les trous noirs binaires (comme GW150914) et les étoiles à neutrons binaires (voir, par exemple, la Réf. [63] et ses références pour plus de détails sur la formation des systèmes binaires et les contraintes observationnelles). L'étude de l'évolution de ces systèmes binaires compacts et leur rayonnement gravitationnel dans le cadre de la théorie de la relativité générale a requis le développement de différentes méthodes d'approximation. Ainsi, dans l'hypothèse du champ faible (grande distance entre les deux objets) et pour des systèmes binaires de faible vitesse orbitale, on peut, par exemple, modéliser la dynamique et les formes d'ondes gravitationnelles générées au cours de la phase "quasi-circulaire", en utilisant l'approximation dite *post-newtonienne* développée à des ordres élevés. Il existe une importante littérature traitant des développements théoriques de l'approximation post-newtonienne et des différentes approches adoptées (voir, par exemple, les Réfs. [64–94] ainsi que les Réfs. [95–99] pour des travaux récents). Aujourd'hui, le développement post-newtonien permet d'avoir une excellente description du mouvement du système binaire et de son rayonnement gravitationnel au cours de la phase quasi-circulaire. Cependant, passée cette phase, le système binaire entame la phase plongeante où le développement post-newtonien doit être remplacé par une résolution numérique directe des équations d'Einstein. Afin de décrire toutes les phases (quasi-circulaire, plongeante, fusion...) du rayonnement gravitationnel d'un système binaire compact, une autre méthode a été proposée en 1999 par Buonnano et Damour [100, 101] dite *Effective One Body approach*. L'idée est de décrire toute la dynamique d'un système binaire de masse m_1 et m_2 en le réduisant à une dynamique effective d'une particule test de masse réduite $\mu = m_1 m_2/\mathrm{M}$, se déplaçant sur un espace-temps effectif décrit par l'extérieur d'un trou noir de Schwarzschild de masse $\mathrm{M} = m_1 + m_2$. Pour plus de détail sur les développements théoriques et le formalisme utilisé dans cette méthode, le lecteur peut, par exemple, consulter les travaux récents de Damour [102, 103]. Le lecteur peut aussi se référer aux Réfs. [104–109] pour ses applications dans le cadre des trous noirs en rotation, et voir également les Réfs. [110–115] pour les problèmes liés à la *self-force* . Toutefois, pour construire la totalité du signal gravitationnel émis par un système binaire et notamment durant la dernière phase de coalescence, les formes d'ondes sont ajustées en se basant sur certains modèles connus en relativité numérique (voir, par exemple, les Réfs. [116–121] sur la construction des formes d'ondes en *Effective One Body approach*). En effet, la relativité numérique permet à présent, grâce aux développements technologiques et au perfectionnement des algorithmes de calcul, de résoudre numériquement les équations d'Einstein et de décrire en détail la dynamique d'un système binaire ainsi que de modéliser sa forme d'onde lors de la phase

de coalescence. Les formes d'ondes obtenues en relativité numérique servent comme modèle de comparaison pour les autres méthodes (voir, par exemple, les Réfs. [122–127] et leurs références pour les récents développements et résultats obtenus en relativité numérique).

Ainsi, l'analyse très précise du signal gravitationnel dans les détecteurs terrestres et/ou spatiaux des systèmes binaires (EMRIs, compacts, ...) repose sur le degré de parachèvement des modèles théoriques (théorie des perturbations, approximation post-newtonienne, *Effective One Body approach*,...) ainsi que la compréhension "complète" de ces processus dans le cadre des théories alternatives. Afin de tirer le meilleur parti de toute l'information contenue dans ce signal et de déceler les possibles déviations à la relativité générale en champ fort prédites dans le cadre des théories alternatives de la gravitation, il est indispensable de disposer d'un catalogue de formes d'ondes le plus complet possible. Aujourd'hui, la comparaison du signal GW150914 avec un modèle basé sur la relativité numérique montre un bon accord avec la théorie de la relativité générale, cependant cette analyse ne permet pas de trancher ou non définitivement en faveur de la théorie d'Einstein (voir, par exemple, la Réf. [128]). Par exemple, si on considère les théories de gravité massive, la très faible valeur du paramètre sans dimension $\tilde{\alpha} \approx 1{,}08 \times 10^{-10}$ calculée pour le trou noir final, tout en tenant compte de la contrainte donnée sur la masse de graviton massif, laisse penser que les effets engendrés par la présence de la masse du graviton (dispersion du signal, présence des modes quasi-liées en plus des QNMs ...) ne peuvent être décelés et sont probablement noyés dans le bruit.

D'énormes efforts ont été consacrés ces dernières années à l'extension de la relativité générale en une théorie de spin-2 massif. Cette activité trouve ses origines dans les travaux de Fierz et Pauli, à la fin des années trente [129, 130]. Les motivations, au départ, étaient purement théoriques car il est tout à fait naturel d'étudier les possibles déformations de la relativité générale en prenant comme paramètre la masse du graviton. Mais aussi, trait à souligner, ces déformations peuvent découler de théories des champs sur un espace-temps ayant des dimensions supplémentaires. C'est le cas, par exemple, dans le modèle de *"brane world"* proposé par Dvali, Gabadaze et Porrati [131], où un modèle de gravité non-massive sur un espace-temps à 5D induit un modèle de gravité massive sur un espace-temps à 4D. En outre, et c'est sans doute la raison principale de leurs succès, ces théories de la gravité massive expliquent, sans recourir à une hypothétique énergie sombre, l'expansion accélérée de l'Univers. La référence [132] peut être utilisée comme guide dans la vaste littérature concernant les aspects théoriques de la gravité massive et permet aussi de suivre l'évolution rapide de ce domaine. Il est important de rappeler ici que des pathologies entachent ces théories, ce qui pourrait mettre en doute leur viabilité ; mais, récemment, divers mécanismes ont été proposés pour y remédier (voir, par exemple, la Réf. [133]).

Cela nous conduit, par conséquent, à reconsidérer dans le cadre de la gravité massive le rayonnement gravitationnel des trous noirs et à étudier particulièrement leurs perturbations dans ce contexte. C'est un problème difficile, mais qui pourrait devenir un thème "à la mode" dans les années à venir. À ce sujet, on peut citer quelques travaux accomplis récemment [134–140]. Ces travaux portent essentiellement sur le problème fondamental de la stabilité des trous noirs ainsi que sur leur existence dans le cadre de la gravité massive. Les résultats, évidemment, dépendent fortement du modèle de gravité massive considéré et des différents paramètres mis en jeu. Mais

une fois admise la stabilité de ces solutions, il devient réellement intéressant de travailler sur la structure du signal émis par un trou noir perturbé par une source extérieure, dans la perspective de tester, dans un avenir proche, les diverses théories du spin-2 massif avec les futures générations de détecteurs d'ondes gravitationnelles.

Depuis les années soixante-dix, de nombreuses études dans le domaine fréquentiel et/ou temporel concernant les champs massifs (ici, notre discussion n'est pas limitée seulement au spin-2 massif) se propageant sur l'extérieur d'un trou noir ont montré que le paramètre de masse induit d'importantes modifications qui influencent d'une manière directe ou non le signal émis par les trous noirs perturbés. Nous soulignons, par exemple, que le spectre de résonance est complètement modifié quand le paramètre de masse n'est pas nul. En effet, en plus des fréquences complexes associées aux QNMs, il est nécessaire de tenir compte de celles correspondant aux modes quasi-liées (QBSs ou *Quasibound states*) (voir, par exemple, les Réfs. [141–144] pour des travaux pionniers sur ce sujet, ainsi que les Réfs. [136, 145] pour des articles récents concernant les champs de spin-1 et de spin-2 massifs). Les champs bosoniques massifs sont un ingrédient incontournable pour des théories fondamentales au-delà du modèle standard des particules élémentaires. Il en est de même pour le modèle standard de la cosmologie basé sur la relativité générale d'Einstein. Ils sont prédits dans le cadre de la théorie des cordes ainsi que par des théories des champs de dimensions supplémentaires. Ils pourraient ainsi contribuer à l'explication de la matière noire dans l'Univers en plus de son expansion accélérée. Cependant, les particules associées sont légères et minimalement couplées avec le secteur visible (matière ordinaire) et elles ont ainsi, jusqu'à présent, échappé à la détection. En revanche, il est très excitant de réaliser que les champs bosoniques ultralégers, interagissant avec des trous noirs, conduisent théoriquement à des effets "macroscopiques" (voir, par exemple, les Réfs. [136–138, 145–160] pour les travaux récents à ce sujet) qui pourraient fournir des preuves directes de l'existence de ces nouvelles particules et contraindre les paramètres des théories associées.

Il faut toutefois noter que les études concernant la thématique du rayonnement classique des trous noirs en présence des champs massifs se sont focalisées sur des aspects très particuliers comme la détermination numérique du spectre des fréquences quasi-normales, l'excitation des QNMs associés, la détermination du spectre des fréquences quasi-liées, leurs rôles dans le contexte des instabilités des trous noirs en rotation, le comportement de la queue du signal dans le cadre des perturbations des trous noirs, etc.... D'autre part, ces aspects sont généralement considérés séparément les uns des autres. Mais, quand on aborde le problème de la construction des formes d'ondes générées par une perturbation arbitraire du trou noir et son interprétation physique, ces différents aspects doivent être examinés en même temps, ce qui complique grandement la tâche. Si nous travaillons dans le régime des faibles masses (ou, plus précisément, des faibles $\tilde{\alpha}$), il semblerait, *mutatis mutandis*, que les enseignements tirés des études des champs non-massifs fournissent un bon guide. Sinon, nous sommes confrontés à de nombreuses difficultés. Il est possible de surmonter les difficultés liées au numérique mais, du point de vue théorique, la situation est beaucoup plus délicate et, en particulier, l'identification sans ambiguïté de différentes contributions ("la pêche initiale", la contribution des QNMs, la contribution des QBSs, la contribution de la queue...) dans les formes d'ondes n'est pas aussi naturelle et aisée que pour les champs non-massifs.

Ainsi, dans la perspective de tester la gravité massive, nous nous proposons d'étudier, dans ce manuscrit de thèse, les perturbations des trous noirs par une source extérieure, de construire les formes d'onde associées et d'analyser leur contenu spectral dans l'espoir d'apporter quelques éclairages. Ce manuscrit de thèse est organisé de la façon suivante. Nous nous intéresserons, d'abord, aux géodésiques de l'espace-temps de Schwarzschild, avec un bref rappel de ses propriétés géométriques, tout en nous focalisant sur les géodésiques suivies par une particule massive, notamment les orbites circulaires et la trajectoire plongeante (Chap. 1). Nous formulerons la théorie générale d'un champ scalaire massif se propageant sur l'espace-temps de Schwarzschild, nous donnerons les équations gouvernant la dynamique du système champ-particule et l'expression de la réponse détectée par un observateur à grande distance du trou noir pour une trajectoire quelconque de la particule. Nous soulignerons, ensuite, le rôle important des modes résonants du trou noir dans l'analyse et l'interprétation des réponses observées (Chap. 2). Nous aborderons les aspects numériques du problème, notamment la manière dont nous construirons les réponses associées aux trous noirs perturbés par une source extérieure et leurs formes d'ondes. Nous décrirons, par la suite, les algorithmes de recherche des fréquences complexes des QNMs et des QBSs (Chap. 3). Dans la possibilité de tester la gravité massive dans le contexte de la physique des trous noirs, nous considérerons une particule plongeant dans le trou noir de Schwarzschild de l'ISCO (*Innermost Stable Circular Orbit*), i.e., la dernière orbite circulaire stable, ou légèrement au-dessous de l'ISCO. Afin de contourner les nombreuses difficultés théoriques liées à la gravité massive, nous utiliserons un "modèle-jouet" dans lequel nous remplacerons le champ de graviton par un champ scalaire massif et nous supposerons un couplage linéaire entre la particule et le champ scalaire. Nous tracerons les formes d'ondes générées par une particule plongeante et étudierons leur contenu spectral. Ceci nous permettra de comprendre et d'interpréter quelques effets qui surviennent dans le régime plongeant et qui ne sont pas présents dans le cas du champ non massif tels que (i) la décroissance et l'annulation de l'amplitude du signal généré quand la particule est en mouvement en orbite quasi-circulaire au voisinage de l'ISCO lorsque le paramètre de masse augmente, et (ii) en plus de l'excitation des QNMs, l'excitation des QBSs du trou noir (Chap. 4). Nous considérerons, au chapitre suivant (Chap. 5), les perturbations du trou noir de Schwarzschild dans le cadre de la gravité massive (spin-2 massif) et nous nous focaliserons uniquement sur les QNMs. Nous montrerons l'existence d'un nouvel effet dans la physique des trous noirs : les coefficients d'excitation présentent un comportement résonant qui devrait induire des sonneries d'amplitude géante et à faible décroissance temporelle. Nous allons, généraliser nos résultats obtenus dans le chapitre précédent pour le champ de spin-2 massif au champ scalaire massif (spin-0) et au champ de Proca (spin-1). Nous montrerons numériquement que les facteurs d'excitation des QNMs ont un comportement résonant et nous confirmerons analytiquement ces résultats en utilisant des considérations semi-classiques basées sur les propriétés des géodésiques circulaires instables suivies par les particules massives en orbite autour du trou noir de Schwarzschild. *Mutatis mutandis*, comme pour le champ de spin-2 massif, ce comportement résonant des coefficients d'excitation devrait induire des sonneries d'amplitude géante et à faible décroissance temporelle (Chap. 6). Enfin, nous reviendrons sur le champ de spin-2 massif, nous considérerons que la perturbation est décrite par un problème de Cauchy avec des données initiales gaussiennes et nous limiterons notre étude au mode impair $\ell = 1$ de la théorie du Fierz-Pauli dans l'espace-temps de Schwarzschild. En considérant la totalité du signal généré par la perturbation, nous montrerons alors que les sonneries géantes sont neutralisées

dans la forme d'onde (Chap. 7). Pour terminer, nous récapitulerons, dans une conclusion générale, les différents résultats obtenus et nous donnerons quelques extensions possibles de notre travail.

Tout au long de ce manuscrit, nous allons utiliser les conventions de Misner, Thorne et Wheeler [161]. Nous considérerons, particulièrement, que la signature de la métrique est du type $(-,+,+,+)$, que le tenseur de Riemann vérifie

$$\nabla_\mu \nabla_\nu \omega_\rho - \nabla_\nu \nabla_\mu \omega_\rho = R^\sigma{}_{\rho\nu\mu}\, \omega_\sigma \tag{2}$$

et que le tenseur de Ricci est donné par

$$R_{\mu\nu} = R^\rho{}_{\mu\rho\nu}. \tag{3}$$

Nous donnerons nos résultats numériques en utilisant la constante de couplage sans dimension $\tilde{\alpha}$ et nous travaillerons dans un système d'unités naturelles tel que $\hbar = G = c = 1$.

CHAPITRE 1

Géodésiques de l'espace-temps de Schwarzschild

« La matière indique à l'espace-temps comment se courber, l'espace-temps indique à la matière comment se déplacer. »

John Archibald Wheeler

La première solution exacte des équations d'Einstein dans le vide fut découverte en 1916 par Karl Schwarzschild [162]. Cette solution de Schwarzschild décrit la géométrie de l'espace-temps à l'extérieur d'une distribution de masse sphérique et statique. Schwarzschild cherchait, effectivement, la métrique $g_{\mu\nu}$ associée à un champ gravitationnel *statique* et à *symétrie sphérique* défini dans le vide. Il est admis qu'un espace-temps est *statique*, si sa métrique est (i) indépendant de la coordonnée temps, et (ii) si l'intervalle d'espace-temps est invariant sous la transformation $t \to -t$. La symétrie sphérique impose, de plus, que la métrique $g_{\mu\nu}$ soit *isotrope* : l'espace-temps est identique dans toutes les directions. Pour plus de rigueur nous renvoyons le lecteur à l'ouvrage de Wald [163]. En fait, la solution de Schwarzschild décrit non seulement d'une manière parfaite la géométrie de l'espace-temps à l'extérieur d'un astre stationnaire à symétrie sphérique, mais elle prédit aussi l'existence de nouveaux objets baptisés trous noirs par John A. Wheeler en 1968.

Dans ce chapitre, après quelques considérations préliminaires sur la géométrie de l'espace-temps de Schwarzschild (Sec. 1.1), nous allons décrire d'une manière générale les géodésiques suivies par les particules massives (Sec. 1.2). Pour ce faire, nous allons résoudre les équations des géodésiques tout en tenant compte de la staticité et de la symétrie sphérique qui caractérisent la métrique de Schwarzschild. Enfin, nous nous intéresserons de plus près à deux types particuliers de trajectoire des particules massives, les orbites circulaires et la trajectoire spirale (Sec. 1.3) et (Sec. 1.4). Pour plus de détails sur ces différents sujets, le lecteur peut se reporter aux Réfs. [161, 164–166].

1.1. Considérations préliminaires

La solution de Schwarzschild permet de décrire l'extérieur d'un trou noir de masse M statique et à symétrie sphérique. C'est la variété

$$\mathcal{M} =]-\infty, +\infty[_t \times]2\mathrm{M}, +\infty[_r \times \mathrm{S}^2, \tag{1.1.1}$$

munie de la métrique

$$ds^2 = g_{\mu\nu}(x)dx^\mu dx^\nu = -\left(1-\frac{2M}{r}\right)dt^2 + \frac{1}{\left(1-\frac{2M}{r}\right)}dr^2 + r^2\, d\sigma_2^2, \tag{1.1.2}$$

où $d\sigma_2^2 = d\theta^2 + \sin^2\theta d\varphi^2$ désigne la métrique de la sphère unité S^2. La surface définie par $r = 2M$ (rayon de Schwarzschild) est l'horizon du trou noir. Le tenseur métrique est donc diagonal et donné par

$$g_{\mu\nu} = \mathrm{diag}\left[-\left(1-\frac{2M}{r}\right), \left(1-\frac{2M}{r}\right)^{-1}, r^2, r^2\sin^2\theta\right]. \tag{1.1.3}$$

Son déterminant g s'écrit

$$\sqrt{-g} = \sqrt{-\det g_{\mu\nu}} = r^2\sin\theta \tag{1.1.4}$$

et son inverse est donné par

$$g^{\mu\nu} = \mathrm{diag}\left[-\left(1-\frac{2M}{r}\right)^{-1}, \left(1-\frac{2M}{r}\right), r^{-2}, r^{-2}\sin^{-2}\theta\right]. \tag{1.1.5}$$

1.2. Géodésiques des particules massives

Les particules massives se mouvant dans un espace-temps courbe suivent des lignes d'Univers qui sont appelées *géodésiques*. Celles-ci correspondent aux lignes de plus "courte distance" entre deux points de l'espace-temps ou, plus exactement, extrémisent l'action

$$S_{\text{particule}} = -m_0\int_\gamma d\tau = -m_0\int_\gamma \sqrt{-g_{\mu\nu}(z(\lambda))\frac{dz^\mu(\lambda)}{d\lambda}\frac{dz^\nu(\lambda)}{d\lambda}}\,d\lambda. \tag{1.2.1}$$

Leurs équations sont obtenues en écrivant les équations d'Euler-Lagrange pour le lagrangien

$$\mathcal{L}\left(z(\lambda), \frac{dz(\lambda)}{d\lambda}\right) = \sqrt{-g_{\mu\nu}(z(\lambda))\frac{dz^\mu(\lambda)}{d\lambda}\frac{dz^\nu(\lambda)}{d\lambda}}, \tag{1.2.2}$$

c'est-à-dire

$$\frac{d}{d\lambda}\left(\frac{\partial\mathcal{L}}{\partial\left(\frac{dz^\alpha}{d\lambda}\right)}\right) = \frac{\partial\mathcal{L}}{\partial z^\alpha}. \tag{1.2.3}$$

Après intégration, on obtient l'équation des géodésiques

$$\frac{d^2z^\delta}{d\lambda^2} + \Gamma^\delta_{\mu\nu}\frac{dz^\mu}{d\lambda}\frac{dz^\nu}{d\lambda} = 0. \tag{1.2.4}$$

où $\Gamma^\delta_{\mu\nu}$ désignent les symboles de Christoffel de deuxième espèce associés au tenseur métrique $g_{\mu\nu}$ et donnés par

$$\Gamma^\delta_{\mu\nu} = -\frac{1}{2}g^{\delta\alpha}\left[\frac{\partial g_{\alpha\mu}}{\partial z^\nu} + \frac{\partial g_{\alpha\nu}}{\partial z^\mu} - \frac{\partial g_{\mu\nu}}{\partial z^\alpha}\right]. \tag{1.2.5}$$

Après ces généralités, nous revenons à l'espace-temps de Schwarzschild. Dans ce *background* les seuls symboles de Christoffel non nuls sont

$$\Gamma^t_{tr} = \Gamma^t_{rt} = \frac{M}{r(r-2M)}, \tag{1.2.6a}$$

$$\Gamma^r_{tt} = \frac{M(r-2M)}{r^3}, \tag{1.2.6b}$$

$$\Gamma^r_{rr} = -\frac{M}{r(r-2M)}, \tag{1.2.6c}$$

$$\Gamma^r_{\theta\theta} = -(r-2M), \tag{1.2.6d}$$

$$\Gamma^r_{\varphi\varphi} = -(r-2M)\sin^2\theta, \tag{1.2.6e}$$

$$\Gamma^\theta_{r\theta} = \Gamma^\theta_{\theta r} = \frac{1}{r}, \tag{1.2.6f}$$

$$\Gamma^\theta_{\varphi\varphi} = -\sin\theta\cos\theta, \tag{1.2.6g}$$

$$\Gamma^\varphi_{r\varphi} = \Gamma^\varphi_{\phi r} = \frac{1}{r}, \tag{1.2.6h}$$

$$\Gamma^\varphi_{\varphi\theta} = \Gamma^\varphi_{\theta\varphi} = \frac{\cos\theta}{\sin\theta}. \tag{1.2.6i}$$

Les équations des géodésiques s'obtiennent alors en substituant les symboles de Christoffel (1.2.6) dans l'équation des géodésiques (1.2.4). Ce calcul conduit à quatre équations

$$\frac{d^2t}{d\lambda^2} + \frac{2M}{r(r-2M)}\frac{dr}{d\lambda}\frac{dt}{d\lambda} = 0, \tag{1.2.7a}$$

$$\frac{d^2r}{d\lambda^2} + \frac{M(r-2M)}{r^3}\left(\frac{dt}{d\lambda}\right)^2 - \frac{M}{r(r-2M)}\left(\frac{dr}{d\lambda}\right)^2 - (r-2M)\left[\left(\frac{d\theta}{d\lambda}\right)^2 + \sin^2\theta\left(\frac{d\varphi}{d\lambda}\right)^2\right] = 0, \tag{1.2.7b}$$

$$\frac{d^2\theta}{d\lambda^2} + \left(\frac{2}{r}\right)\frac{d\theta}{d\lambda}\frac{dr}{d\lambda} - \sin\theta\cos\theta\left(\frac{d\varphi}{d\lambda}\right)^2 = 0, \tag{1.2.7c}$$

$$\frac{d^2\varphi}{d\lambda^2} + \left(\frac{2}{r}\right)\frac{d\varphi}{d\lambda}\frac{dr}{d\lambda} + 2\frac{\cos\theta}{\sin\theta}\frac{d\theta}{d\lambda}\frac{d\varphi}{d\lambda} = 0. \tag{1.2.7d}$$

Il est vrai que la résolution de ce jeu d'équations couplées est une tâche très ardue mais tout sera considérablement simplifié du fait du haut degré de symétrie de la métrique de Schwarzschild. Nous savons qu'il existe quatre *vecteurs de Killing*, trois associés à la symétrie sphérique et un aux translations dans le temps. Chacun d'eux correspond à une constante du mouvement pour une particule libre. En effet, si κ^μ est un vecteur de Killing, nous savons que

$$\kappa_\mu \frac{dz^\mu}{d\lambda} = \text{Constante}. \tag{1.2.8}$$

Au lieu d'écrire maintenant les expressions explicites des quatre quantités conservées associées aux vecteurs de Killing, nous nous penchons, d'abord, sur l'équation (1.2.7c). On remarque immédiatement que $\theta = \pi/2$ est une solution de cette équation. En raison de la symétrie sphérique de la métrique de Schwarzschild, on peut donc se contenter de considérer des particules en mouvement dans le *plan équatorial* paramétré par $\theta = \pi/2$, sans perdre en généralités. Les deux vecteurs de

Killing restants sont alors le vecteur de Killing de genre temps $\xi = \frac{\partial}{\partial t}$ de composantes covariantes

$$\xi_\mu = \left(-\left(1 - \frac{2M}{r}\right), 0, 0, 0\right), \tag{1.2.9}$$

et le vecteur de Killing $\zeta = \frac{\partial}{\partial \varphi}$ de composantes covariantes

$$\zeta_\mu = \left(0, 0, 0, r^2 \sin^2\theta\right). \tag{1.2.10}$$

On déduit de l'équation (1.2.8) (cf. (1.2.9) et (1.2.10)) que les deux quantités conservées sont

$$-\left(1 - \frac{2M}{r}\right)\frac{dt}{d\lambda} = k \tag{1.2.11}$$

et

$$r^2 \frac{d\varphi}{d\lambda} = h. \tag{1.2.12}$$

Ici, Les constantes k et h peuvent être interprétées, en utilisant une parametrisation en temps propre τ, comme l'énergie totale et le moment cinétique par unité de masse d'une particule massive de masse m_0.

On peut maintenant remplacer les équations (1.2.7a) et (1.2.7d) respectivement par (1.2.11) et (1.2.12). Quant à l'équation du second ordre (1.2.7b) elle reste à part. Toutefois, nous pouvons l'intégrer en prenant aussi, au lieu d'un paramètre affine λ quelconque, le temps propre τ de la particule. Nous avons donc

$$g_{\mu\nu}\frac{dz^\mu}{d\tau}\frac{dz^\nu}{d\tau} = -1, \tag{1.2.13}$$

En résumé, les géodésiques du genre temps (celles suivies par une particule massive) paramétrées en temps propre sont décrites dans le plan équatorial par les équations

$$\left(1 - \frac{2M}{r}\right)\frac{dt}{d\tau} = \frac{E}{m_0}, \tag{1.2.14a}$$

$$\left(1 - \frac{2M}{r}\right)\left(\frac{dt}{d\tau}\right)^2 - \left(1 - \frac{2M}{r}\right)^{-1}\left(\frac{dr}{d\tau}\right)^2 - r^2\left(\frac{d\varphi}{d\tau}\right)^2 = 1, \tag{1.2.14b}$$

$$r^2\frac{d\varphi}{d\tau} = \frac{L}{m_0}. \tag{1.2.14c}$$

Ici m_0 est la masse de la particule, E est son énergie totale et L son moment cinétique. En injectant les équations (1.2.14a) et (1.2.14c) dans l'équation (1.2.14b), on obtient l'équation

$$\left(\frac{dr}{d\tau}\right)^2 + \frac{L^2}{m_0^2 r^2}\left(1 - \frac{2M}{r}\right) - \frac{2M}{r} = \left[\left(\frac{E}{m_0}\right)^2 - 1\right]. \tag{1.2.15}$$

qui relie l'énergie totale de la particule à sa coordonnée r. Cette équation interviendra lorsqu'on discutera les orbites circulaires et la trajectoire spirale d'une particule massive. A noter que le membre de droite est une *constante* du mouvement.

1.3. Orbites circulaires

Dans cette section, nous supposons que la particule se meut sur une orbite circulaire avec un rayon r_0, i.e. $r(\tau) = r_0 = \text{Const}$ dans les équations géodésiques (1.2.14) et (1.2.15). Le moment angulaire de la particule, après avoir intégré les équations (1.2.14) et (1.2.15), est

$$\frac{L}{m_0} = \left(\frac{M r_0}{\left(1 - \frac{3M}{r_0}\right)} \right)^{1/2}, \tag{1.3.1}$$

et son énergie

$$\frac{E}{m_0} = \frac{\left(1 - \frac{2M}{r_0}\right)}{\left(1 - \frac{3M}{r_0}\right)^{1/2}}. \tag{1.3.2}$$

De plus, la coordonnée angulaire φ est donnée par

$$\varphi(\tau) = \left(\frac{M}{r_0^3 \left(1 - \frac{3M}{r_0}\right)} \right)^{1/2} \tau \tag{1.3.3}$$

si nous utilisons le temps propre pour décrire le mouvement de la particule et par

$$\varphi(t) = \Omega t \tag{1.3.4}$$

si nous utilisons le temps de Schwarzschild. Dans l'équation (1.3.4)

$$\Omega = \left(\frac{M}{r_0^3} \right)^{1/2}. \tag{1.3.5}$$

Ici, Ω désigne la vitesse angulaire de la particule (i.e. sa fréquence orbitale). On peut noter que, pour une particule se mouvant sur la dernière orbite stable, i.e. ISCO, le rayon r_0 est égal à 6M et la vitesse angulaire est donnée par

$$\Omega_{\text{ISCO}} = \frac{1}{6\sqrt{6}M}. \tag{1.3.6}$$

1.4. Trajectoire spirale d'une particule massive

Nous considérons, maintenant, une particule plongeant dans le trou noir de Schwarzschild à partir de l'ISCO à $r_{\text{ISCO}} = 6M$ où, légèrement au-dessous de l'ISCO. Pour décrire cette trajectoire nous avons besoin du moment angulaire de la particule et de son énergie sur ISCO. Ces deux quantités physiques sont déterminées en utilisant les équations (1.3.1) et (1.3.2), que nous avons déjà établies pour une particule massive en orbite circulaire arbitraire. Nous avons

$$\frac{L_{\text{ISCO}}}{m_0} = 2\sqrt{3}M \tag{1.4.1}$$

et

$$\frac{E_{ISCO}}{m_0} = \frac{2\sqrt{2}}{3}. \tag{1.4.2}$$

En remplaçant L_{ISCO} et E_{ISCO} par leurs expressions (1.4.1) et (1.4.2) dans l'équation (1.2.15), on obtient

$$\left(\frac{dr}{d\tau}\right)^2 = \frac{1}{9}\left(\frac{6M}{r} - 1\right)^3. \tag{1.4.3}$$

Les équations qui vont nous servir à discuter en détail la trajectoire d'une particule plongeant depuis l'ISCO sont donc (cf. (1.2.14a), (1.2.14c) et (1.4.3))

$$\left(1 - \frac{2M}{r}\right)\frac{dt}{d\tau} = \frac{E_{ISCO}}{m_0}, \tag{1.4.4a}$$

$$r^2\frac{d\varphi}{d\tau} = \frac{L_{ISCO}}{m_0}, \tag{1.4.4b}$$

$$\left(\frac{dr}{d\tau}\right)^2 = \frac{1}{9}\left(\frac{6M}{r} - 1\right)^3. \tag{1.4.4c}$$

En tenant compte de (1.4.4a) et (1.4.2), on a

$$\frac{dr}{dt} = -\frac{1}{2\sqrt{2}}\left(1 - \frac{2M}{r}\right)\left(\frac{6M}{r} - 1\right)^{3/2}. \tag{1.4.5}$$

Après intégration de l'équation (1.4.5), on obtient

$$\frac{t(r)}{2M} = \frac{2\sqrt{2}(r - 24M)}{2M\left(\frac{6M}{r} - 1\right)^{1/2}} - 22\sqrt{2}\tan^{-1}\left[\left(\frac{6M}{r} - 1\right)^{1/2}\right] + 2\tanh^{-1}\left[\left(\frac{3M}{r} - \frac{1}{2}\right)^{1/2}\right] + \frac{t_0}{2M} \tag{1.4.6}$$

avec t_0, une constante d'intégration. De la même façon, en utilisant les équations (1.4.4b) et (1.4.4c) tout en tenant compte de (1.4.1), on a

$$\varphi(r) = -\frac{2\sqrt{3r}}{(6M - r)^{1/2}} + \varphi_0 \tag{1.4.7}$$

avec φ_0, une constante d'intégration. Nous pouvons réécrire l'équation spatiale (1.4.7) de la trajectoire d'une particule plongeant sous la forme

$$r(\varphi) = \frac{6M}{[1 + 12/(\varphi - \varphi_0)^2]}. \tag{1.4.8}$$

Les équations (1.4.6) et (1.4.7) (cf. (1.4.8)) décrivent la trajectoire, dans le plan équatorial, d'une particule massive qui plonge depuis l'ISCO dans le trou noir de Schwarzschild.

CHAPITRE 2

Champ scalaire massif se propageant sur l'espace-temps de Schwarzschild

« *The black holes of nature are the most perfect macroscopic objects there are in the Universe : the only elements in their construction are our concepts of the space and time. And since the general theory of relativity provides only a single unique family of solutions for their descriptions, they are the simplest objects as well.* »

Subrahmanyan Chandrasekhar (1984)

Dans ce chapitre, nous allons commencer par dériver l'équation d'onde du champ scalaire Φ (Sec. 2.1). La recherche des modes-solutions de cette équation d'onde (équation de Klein-Gordon) se fera par séparation des variables tout en tenant compte de la symétrie sphérique et de la staticité qui caractérisent l'espace-temps de Schwarzschild. Les ondes partielles obtenues, nous le verrons, satisfont l'équation dite de Regge-Wheeler (Sec. 2.2). Ensuite, nous allons résoudre l'équation de Regge-Wheeler avec source par la méthode des fonctions de Green (Sec. 2.3), et exprimer le champ scalaire pour un observateur à grande distance du trou noir (Sec. 2.4). Enfin, nous terminons ce chapitre par un bref historique de la physique associée aux QNMs et aux QBSs (Sec. 2.5 et Sec. 2.6).

2.1. Equation d'onde

Nous considérons que le *background* gravitationnel $(\mathcal{M}, g_{\mu\nu})$ est l'extérieur du trou noir de Schwarzschild et que le système champ-particule est défini par l'action (voir la Réf. [57])

$$S = S_{\text{champ}} + S_{\text{particule}} + S_{\text{interaction}} \tag{2.1.1}$$

avec

$$S_{\text{champ}} = -\frac{1}{2}\int_{\mathcal{M}} d^4x\sqrt{-g(x)} \times \left[g^{\alpha\beta}(x)\nabla_\alpha\Phi(x)\nabla_\beta\Phi(x) + \mu^2\Phi^2(x)\right], \tag{2.1.2}$$

$$S_{\text{particule}} = -m_0\int_\gamma d\tau = -m_0\int_\gamma \sqrt{-g_{\alpha\beta}(z(\lambda))\frac{dz^\alpha(\lambda)}{d\lambda}\frac{dz^\beta(\lambda)}{d\lambda}}d\lambda \tag{2.1.3}$$

et

$$S_{\text{interaction}} = \int_{\mathcal{M}} d^4x \sqrt{-g(x)}\, \rho(x)\Phi(x). \tag{2.1.4}$$

Ici $S_{\text{champ}} = S_{\text{champ}}[\Phi, g_{\alpha\beta}]$ est une fonctionnelle du champ scalaire réel et massif Φ et de la métrique $g_{\alpha\beta}$ de l'espace-temps. Dans l'expression $S_{\text{particule}}$, m_0 désigne la masse de la particule et $d\tau$ est la différentielle du temps propre le long de sa ligne d'Univers γ d'équation $z^\alpha = z^\alpha(\lambda)$, λ étant un paramètre affine. $S_{\text{particule}} = S_{\text{particule}}[z(\lambda), g_{\alpha\beta}]$ est donc une fonctionnelle de la trajectoire $z^\alpha = z^\alpha(\lambda)$ et de la métrique $g_{\alpha\beta}$ de l'espace-temps. Enfin, $S_{\text{interaction}} = S_{\text{interaction}}[z(\lambda), \Phi, g_{\alpha\beta}]$ est une fonctionnelle de la trajectoire $z^\alpha = z^\alpha(\lambda)$, du champ scalaire Φ et de la métrique $g_{\alpha\beta}$. Il faut préciser que le champ et la particule sont couplés par l'intermédiaire de la densité de charge

$$\rho(x) = q\int_\gamma d\tau \delta^4(x, z(\tau)) = q\int_\gamma d\tau \frac{\delta^4(x - z(\tau))}{\sqrt{-g(x)}} \tag{2.1.5}$$

associée à la charge scalaire q de la particule.

Les équations du mouvement s'obtiennent par extrémisation de l'action (2.1.1)

$$\frac{\delta S}{\delta \Phi} = 0. \tag{2.1.6}$$

Rappelons que la dérivée fonctionnelle $\frac{\delta S}{\delta \Phi}$ est définie à partir de la variation de δS obtenue en considérant la variation infinitésimale $\Phi \to \Phi + \delta\Phi$ par la relation

$$\delta S = \int_{\mathcal{M}} d^4x \frac{\delta S}{\delta \Phi}\delta\Phi. \tag{2.1.7}$$

Après intégration, et en laissant tomber les termes de bord, le champ scalaire vérifie l'équation dite de Klein-Gordon

$$\left(\Box - \mu^2\right)\Phi = -\rho, \tag{2.1.8}$$

avec $\Box = g^{\alpha\beta}\nabla_\alpha\nabla_\beta$ qui est l'opérateur d'alambertien en espace-temps courbe et ρ est donnée par (2.1.5).

2.2. Equation de Regge-Wheeler avec source

La staticité de l'espace-temps de Schwarzschild ainsi que sa symétrie sphérique permettent de rechercher les solutions de (2.1.8) par séparation de variables t, r, θ et φ, en introduisant les décompositions

$$\Phi(t, r, \theta, \varphi) = \frac{1}{\sqrt{2\pi}}\int_{-\infty}^{+\infty} d\omega\, e^{-i\omega t} \times \sum_{\ell=0}^{+\infty}\sum_{m=-\ell}^{+\ell} \frac{\phi_{\omega\ell m}(r)}{r} Y_{\ell m}(\theta, \varphi) \tag{2.2.1}$$

et

$$\rho(t, r, \theta, \varphi) = \frac{1}{\sqrt{2\pi}}\int_{-\infty}^{+\infty} d\omega\, e^{-i\omega t} \times \sum_{\ell=0}^{+\infty}\sum_{m=-\ell}^{+\ell} \frac{\rho_{\omega\ell m}(r)}{r} Y_{\ell m}(\theta, \varphi), \tag{2.2.2}$$

où les $Y_{\ell m}(\theta,\varphi)$ sont les harmoniques sphériques habituelles avec $\ell \in \mathbb{N}$ et $m = -\ell, -\ell+1, \ldots, +\ell$.

Nous remplaçons Φ dans le membre de gauche de l'équation (2.1.8) par son expression (2.2.1), on obtient

$$\left(\Box - \mu^2\right)\Phi = \frac{1}{\sqrt{2\pi}} \int_{-\infty}^{+\infty} d\omega\, e^{-i\omega t} \sum_{\ell=0}^{+\infty} \sum_{m=-\ell}^{+\ell} \left\{ \left[\left(1 - \frac{2M}{r}\right) \frac{1}{r} \frac{d^2}{dr^2} + \frac{2M}{r^3} \frac{d}{dr} \right.\right.$$
$$\left.\left. + \left(1 - \frac{2M}{r}\right)^{-1} \frac{\omega^2}{r} - \frac{2M}{r^4} - \frac{\ell(\ell+1)}{r^3} - \mu^2 \right] \phi_{\omega \ell m}(r) \right\} Y_{\ell m}(\theta,\varphi). \quad (2.2.3)$$

Les équations (2.1.8) et (2.2.3) (cf. (2.2.2)) montrent que les ondes partielles $\phi_{\omega\ell m}$ vérifient

$$\left(1 - \frac{2M}{r}\right) \frac{d}{dr} \left[\left(1 - \frac{2M}{r}\right) \frac{d}{dr} \right] \phi_{\omega \ell m}(r)$$
$$+ \left[\omega^2 - \left(1 - \frac{2M}{r}\right) \left(\frac{\ell(\ell+1)}{r^2} + \frac{2M}{r^3} + \mu^2 \right) \right] \phi_{\omega \ell m}(r) = -\left(1 - \frac{2M}{r}\right) \rho_{\omega \ell m}. \quad (2.2.4)$$

C'est l'équation de Regge-Wheeler avec source.

Lorsqu'on travaille à l'extérieur du trou noir de Schwarzschild, il est plus naturel d'utiliser la coordonnée r_* dite coordonnée de Regge-Wheeler ou encore coordonnée de la tortue, définie par

$$\left(1 - \frac{2M}{r}\right) \frac{d}{dr} = \frac{d}{dr_*}. \quad (2.2.5)$$

Cette équation différentielle ne donne r_* en fonction de r qu'à une constante [1] près. On a

$$r_* = r + 2M \ln\left(\frac{r}{2M} - 1\right) + \text{Const} \quad (2.2.6)$$

avec $r \in]2M, +\infty[$ et $r_*(r) \in]-\infty, +\infty[$. Nous rappelons que $r_*(r)$ est bijective. Ceci implique l'existence de la fonction réciproque $r(r_*)$ donnée par

$$r(r_*) = 2M \left\{ 1 + W\left[e^{\frac{r_* - 2M + \text{Const}}{2M}} \right] \right\} \quad (2.2.7)$$

où W est la fonction de Lambert.

Dans la variable r_*, l'équation de Reege-Wheeler (2.2.4) peut s'écrire

$$\left[\frac{d^2}{dr_*^2} + \omega^2 - V_\ell(r) \right] \phi_{\omega \ell m} = -\left(1 - \frac{2M}{r}\right) \rho_{\omega \ell m}, \quad (2.2.8)$$

1. Remarque : On fixera Const = 0 sans perdre en généralités dans tous nos calculs, sauf mention contraire. Dans ce cas, sa valeur sera donnée.

où $V_\ell(r)$ désigne le potentiel de Reege-Wheeler donné par

$$V_\ell(r) = \left(1 - \frac{2M}{r}\right)\left(\mu^2 + \frac{\ell(\ell+1)}{r^2} + \frac{2M}{r^3}\right). \tag{2.2.9}$$

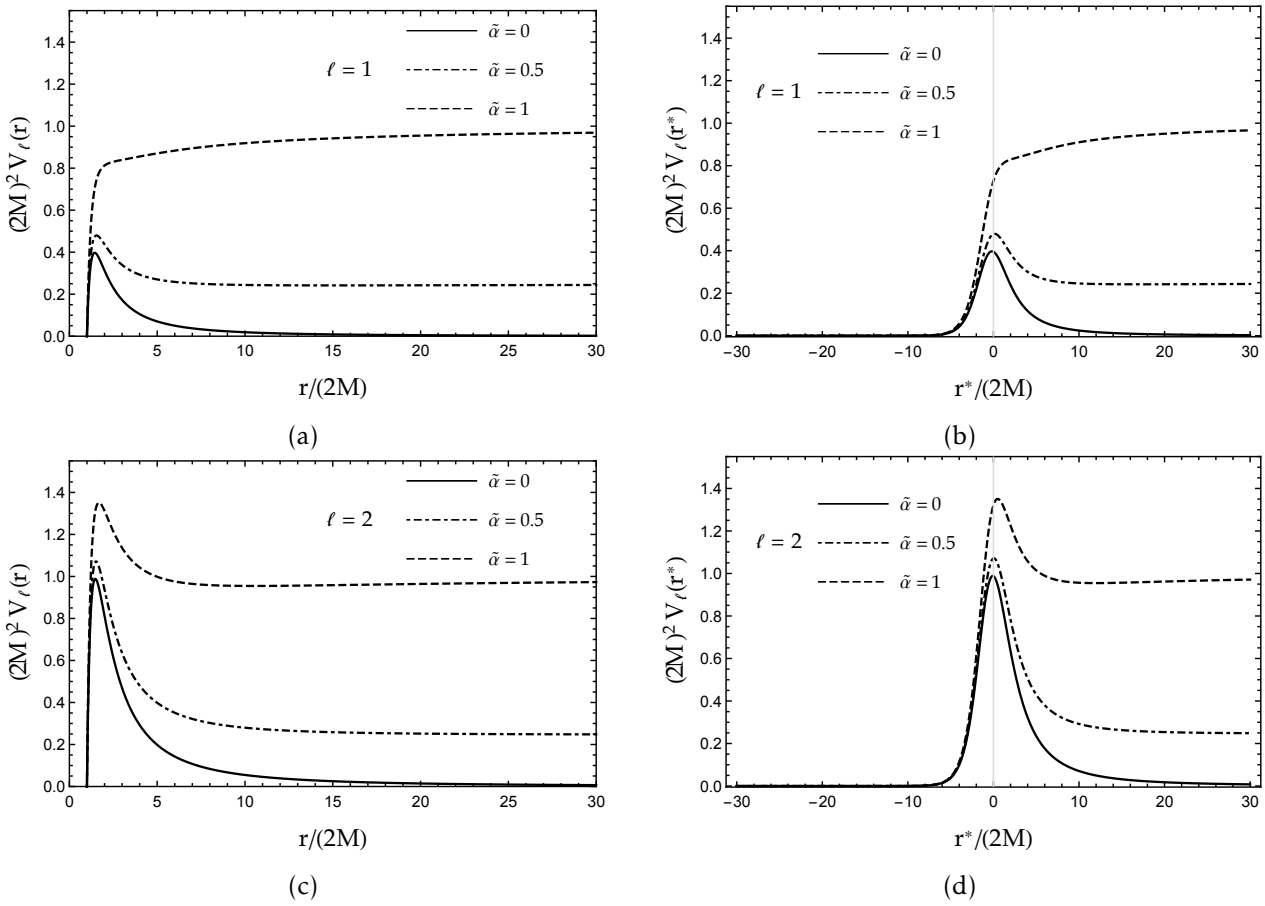

FIG. 2.1. – Le potentiel de Regge-Wheeler V_ℓ pour les modes $\ell = 1, 2$, correspondant, respectivement, aux valeurs $\tilde{\alpha} = 0, 0.5$ et 1 du paramètre de masse réduit, en fonction de la coordonnée r (a) et (c) et, de la coordonnée r_* (b) et (d). La constante dans l'expression (2.2.6) est fixée de sorte que $r_* = 0$ pour $r = 3M$.

La forme de l'équation (2.2.8) est, ce que l'on peut bien remarquer, de type-Schrödinger indépendante du temps. Ce qui fait qu'on peut envisager le problème de perturbation des trous noirs comme un problème de diffusion en mécanique quantique où $V_\ell(r)$ joue le rôle d'un potentiel effectif. On doit cette remarque à Chandrasekhar (voir, aussi, l'ouvrage de V. P. Frolov et I. D. Novikov [167]). L'effet d'un trou noir sur le champ scalaire peut être "visualisé" en examinant la forme du potentiel (2.2.9). En effet, si on considère une onde qui arrive de l'infini spatial (ou monte de l'horizon), elle se réfléchira partiellement sur la barrière de potentiel, et sera transmise, aussi, partiellement par cette même barrière en une composante qui rentre dans l'horizon (ou transmise à l'infini spatial) (voir Fig. 2.1). Il est à noter que le potentiel de Regge-Wheeler possède un maximum proche de $r = 3M$. Cette surface dite "sphère des photons" du trou noir de Schwarzschild est associée à l'interprétation des QNMs dans le cas du champ non-massif. Dans le cas du champ massif, en plus d'un maximum, le potentiel possède un minimum qu'on associe aux QBSs.

2.3. Solution générale de l'équation d'onde avec source

Dans cette section, pour résoudre l'équation de Regge-Wheeler avec source (2.2.8), nous employons la machinerie des fonctions de Green (pour plus de précisions sur ce type de techniques nous renvoyons le lecteur à l'ouvrage de Morse et Feshbach [168] et e.g. la Réf. [169] pour son utilisation dans le cadre de la physique des trous noirs). La première étape consiste à construire une fonction de Green adaptée (Sous-Sect. 2.3.1), puis dans un second temps, nous obtiendrons les réponses partielles $\phi_{\omega\ell m}(r)$ par convolution de la source avec cette fonction de Green (Sous-Sec. 2.3.2).

2.3.1. Construction de la fonction de Green

On considère une fonction de Green $G_{\omega\ell}(r_*, r'_*)$ qui vérifie

$$\left[\frac{d^2}{dr_*^2} + \omega^2 - V_\ell(r)\right] G_{\omega\ell}(r_*, r'_*) = -\delta(r_* - r'_*). \tag{2.3.1}$$

Le comportement du potentiel $V_\ell(r)$ influe sur les solutions de (2.3.1). On peut noter que pour $r_* \to -\infty$ ($r \to 2M$), $V_\ell(r) \to 0$ et $\delta(r_* - r'_*) = 0$. On a

$$G_{\omega\ell}(r_*, r'_*) \underset{r_*\to-\infty}{\sim} e^{\pm i\omega r_*}. \tag{2.3.2}$$

De même, pour $r_* \to +\infty$ ($r \to +\infty$), $V_\ell(r) \to \mu^2$ et $\delta(r_* - r'_*) = 0$. On a

$$G_{\omega\ell}(r_*, r'_*) \underset{r_*\to+\infty}{\sim} \left[\frac{\omega}{p(\omega)}\right]^{1/2} e^{\pm i\left[p(\omega)r_* + \frac{M\mu^2}{p(\omega)}\ln\left(\frac{r}{M}\right)\right]}. \tag{2.3.3}$$

Puisque cette fonction de Green n'est pas définie de manière unique, nous choisissons, parmi toutes les possibilités, de travailler avec celle qui vérifie les conditions aux limites suivantes

$$G_{\omega\ell}(r_*, r'_*) \underset{r_*\to-\infty}{\sim} e^{-i\omega r_*} \tag{2.3.4a}$$

et

$$G_{\omega\ell}(r_*, r'_*) \underset{r_*\to+\infty}{\sim} \left[\frac{\omega}{p(\omega)}\right]^{1/2} e^{+i\left[p(\omega)r_* + \frac{M\mu^2}{p(\omega)}\ln\left(\frac{r}{M}\right)\right]}. \tag{2.3.4b}$$

Ce choix nous permettra de construire une solution physique de l'équation de Regge-Wheeler avec source (2.2.8).

La solution du problème (2.3.1)-(2.3.4) est de la forme

$$G_{\omega\ell}(r_*, r'_*) = \begin{cases} K_{\omega\ell}(r'_*)\,\phi^{\text{in}}_{\omega\ell}(r_*) & r_* < r'_*, \\ \widetilde{K}_{\omega\ell}(r'_*)\,\phi^{\text{up}}_{\omega\ell}(r_*) & r_* > r_*, \end{cases} \tag{2.3.5}$$

où les quantités $K_{\omega\ell}(r_*)$ et $\widetilde{K}_{\omega\ell}(r'_*)$ sont des constantes d'intégration vis-à-vis de la coordonnée r_* et

sont donc *a priori* des fonctions de r'_*. Ici, $\phi^{\rm in}_{\omega\ell}$ et $\phi^{\rm up}_{\omega\ell}$ sont deux solutions linéairement indépendantes de l'équation de Regge-Wheeler homogène (sans source)

$$\left[\frac{d^2}{dr_*^2}+\omega^2-V_\ell(r)\right]\phi_{\omega\ell}=0. \tag{2.3.6}$$

Lorsque $\mathrm{Im}(\omega)>0$, $\phi^{\rm in}_{\omega\ell}$ est définie d'une manière unique par son comportement rentrant à l'horizon des évènements $r=2M$ (i.e., pour $r_*\to-\infty$)

$$\phi^{\rm in}_{\omega\ell}(r)\underset{r_*\to-\infty}{\sim}e^{-i\omega r_*}, \tag{2.3.7a}$$

tandis que, à l'infini spatial $r\to+\infty$ (i.e., pour $r_*\to+\infty$), elle a un comportement asymptotique de la forme

$$\phi^{\rm in}_{\omega\ell}(r)\underset{r_*\to+\infty}{\sim}\left[\frac{\omega}{p(\omega)}\right]^{1/2}\left(A^{(-)}_\ell(\omega)e^{-i\left[p(\omega)r_*+\frac{M\mu^2}{p(\omega)}\ln\left(\frac{r}{M}\right)\right]}+A^{(+)}_\ell(\omega)e^{+i\left[p(\omega)r_*+\frac{M\mu^2}{p(\omega)}\ln\left(\frac{r}{M}\right)\right]}\right). \tag{2.3.7b}$$

De même, $\phi^{\rm up}_{\omega\ell}$ est définie d'une manière unique par son comportement purement sortant à l'infini spatial

$$\phi^{\rm up}_{\omega\ell}(r)\underset{r_*\to+\infty}{\sim}\left[\frac{\omega}{p(\omega)}\right]^{1/2}e^{+i\left[p(\omega)r_*+\frac{M\mu^2}{p(\omega)}\ln\left(\frac{r}{M}\right)\right]} \tag{2.3.8a}$$

et à l'horizon, elle a un comportement asymptotique de la forme

$$\phi^{\rm up}_{\omega\ell}(r)\underset{r_*\to-\infty}{\sim}B^{(-)}_\ell(\omega)e^{-i\omega r_*}+B^{(+)}_\ell(\omega)e^{+i\omega r_*}. \tag{2.3.8b}$$

Dans les expressions précédentes, la fonction $p(\omega)=(\omega^2-\mu^2)^{1/2}$ désigne le "nombre d'onde", tandis que les coefficients $A^{(-)}_\ell(\omega)$, $A^{(+)}_\ell(\omega)$, $B^{(-)}_\ell(\omega)$ et $B^{(+)}_\ell(\omega)$ sont des amplitudes complexes. Ici, il est important de mentionner que ces coefficients ainsi que les modes in et up peuvent être définis par un prolongement analytique dans le plan complexe de $p(\omega)$ composé de deux feuillets de Riemann. Pour finir avec les modes in et up, on considère le Wronskien $W_\ell(\omega)$

$$W\left[\phi^{(1)}_{\omega\ell}(r_*),\phi^{(2)}_{\omega\ell}(r_*)\right]\equiv\phi^{(1)}_{\omega\ell}(r_*)\left(\overrightarrow{\frac{d}{dr_*}}-\overleftarrow{\frac{d}{dr_*}}\right)\phi^{(2)}_{\omega\ell}(r_*), \tag{2.3.9}$$

qui est une constante. Son évaluation sur l'horizon ($r_*\to-\infty$) et sur l'infini spatial ($r_*\to+\infty$) pour la combinaison $\phi^{(1)}_{\omega\ell}=\phi^{\rm in}_{\omega\ell}$ et $\phi^{(2)}_{\omega\ell}=\phi^{\rm up}_{\omega\ell}$ nous donne

$$W_\ell(\omega)=2i\omega A^{(-)}_\ell(\omega)=2i\omega B^{(+)}_\ell(\omega). \tag{2.3.10}$$

Maintenant que nous avons défini les modes in et up, nous allons déterminer les constantes $K_{\omega\ell}(r_*)$ et $\widetilde{K}_{\omega\ell}(r'_*)$. Pour cela, nous exploitons ce que l'on sait sur $G_{\omega\ell}$ et sa dérivée. L'idée consiste en l'utilisation des deux expressions (2.3.5) et, partant de chaque région, de venir vers leurs frontières communes (ici, le point $r_*=r'_*$, la position r'_* étant fixée) pour y écrire les conditions de raccordement sur $G_{\omega\ell}$ et sa dérivée. Nous savons que $G_{\omega\ell}$ est continue en $r_*=r'_*$, ce qui nous donne

$K_{\omega\ell}(r'_*) = k\,\phi^{up}_{\omega\ell}(r'_*)$ et $\widetilde{K}_{\omega\ell}(r'_*) = k\,\phi^{in}_{\omega\ell}(r'_*)$ où k est une constante indépendante de r_* et de r'_*. Par contre, la dérivée $\frac{\partial}{\partial r_*}G_{\omega\ell}(r_*, r'_*)$ a un saut en $r_* = r'_*$ dont on trouve l'amplitude en intégrant (2.3.1) par rapport à r_* de part et d'autre de r'_*. L'intégration de la dérivée seconde donne la variation de la dérivée première de part et d'autre de r'_*. Par ailleurs, comme $G_{\omega\ell}$ est une fonction continue, le terme en $(\omega^2 - V_\ell(r))G_{\omega\ell}$ donne zéro. Quant au terme $\delta(r_* - r'_*)$ du second membre, il nous donne 1 par définition de δ.

Ce qui nous donne, après calculs, l'expression définitive de la fonction de Green

$$G_{\omega\ell}(r_*, r'_*) = -\frac{1}{W_\ell(\omega)}\begin{cases}\phi^{in}_{\omega\ell}(r_*)\,\phi^{up}_{\omega\ell}(r'_*), & r_* < r'_*,\\ \phi^{up}_{\omega\ell}(r_*)\,\phi^{in}_{\omega\ell}(r'_*), & r_* > r'_*.\end{cases} \tag{2.3.11}$$

2.3.2. Solution de l'équation de Regge-Wheeler

Nous allons maintenant utiliser la fonction de Green (2.3.11) pour résoudre l'équation de Regge-Wheeler (2.2.8). Parmi toutes les solutions possibles nous allons rechercher celle qui a un comportement rentrant sur l'horizon et sortant à l'infini spatial, c'est-à-dire qui vérifie les conditions aux limites

$$\phi_{\omega\ell m}(r) = \begin{cases} C_{\ell m}(\omega)\, e^{-i\omega r_*}, & r_* \to -\infty,\\ D_{\ell m}(\omega)\, e^{+i\left[p(\omega)r_* + \frac{M\mu^2}{p(\omega)}\ln\left(\frac{r}{M}\right)\right]}, & r_* \to +\infty.\end{cases} \tag{2.3.12}$$

Ces conditions aux limites sont naturelles. En effet, le champ (classique) créé par la particule plongeant dans le trou noir ne peut qu'être absorbé par l'horizon et, d'autre part, rien ne peut revenir de l'infini spatial (conditions de rayonnement de type Sommerfeld - pour plus de détails, sur ce type de conditions nous renvoyons le lecteur à l'ouvrage de Sommerfeld [170]).

En intégrant l'équation (2.3.1), tout en la multipliant par $(1 - 2M/r'(r'_*))\,\rho_{\omega\ell m}(r'_*)$ et en soustrayant le résultat obtenu de l'équation (2.2.8), on en déduit nécessairement

$$\phi_{\omega\ell m}(r_*) = \int_{-\infty}^{+\infty} dr'_* G_{\omega\ell}(r^*, r'_*)\left(1 - \frac{2M}{r'(r'_*)}\right)\rho_{\omega\ell m}(r'_*) + \alpha_\ell(\omega)\phi^{in}_{\omega\ell}(r_*) + \beta_\ell(\omega)\phi^{up}_{\omega\ell}(r_*) \tag{2.3.13}$$

avec $\phi^{in}_{\omega\ell}$ et $\phi^{up}_{\omega\ell}$ qui sont les modes in et up habituels de l'équation de Regge-Wheeler sans source. Pour déterminer les constantes $\alpha_\ell(\omega)$ et $\beta_\ell(\omega)$, nous allons utiliser les conditions aux limites (2.3.12). On a pour $r_* \to -\infty$, $\phi_{\omega\ell m}(r_*) \sim C_\ell(\omega)e^{-i\omega r_*}$. Dans ce cas, on doit prendre $\beta_\ell(\omega) = 0$. Pour $r_* \to +\infty$, $\phi_{\omega\ell m}(r_*) \sim D_\ell(\omega)e^{+i\left[p(\omega)r_* + [M\mu^2/p(\omega)]\ln(r/M)\right]}$. Ici, on doit prendre $\alpha_\ell(\omega) = 0$. En conséquence, on peut réécrire l'expression (2.3.13) sous la forme

$$\phi_{\omega\ell m}(r) = \int_{-\infty}^{+\infty} dr'_* G_{\omega\ell}(r_*, r'_*)\left(1 - \frac{2M}{r'(r'_*)}\right)\rho_{\omega\ell m}(r'_*) \tag{2.3.14}$$

ou, de manière équivalente (cf. Eq. (2.2.5))

$$\phi_{\omega\ell m}(r) = \int_{2M}^{+\infty} dr'\, G_{\omega\ell}(r, r')\rho_{\omega\ell m}(r'). \tag{2.3.15}$$

Ce qui est une solution générale de l'équation de Regge-Wheeler avec source et $G_{\omega\ell}(r_*, r'_*)$ est la fonction de Green qui lui est associée.

2.4. Champ observé à grande distance du trou noir

Il s'agit, dans cette section, de construire la réponse (2.2.1) détectée par un observateur à (t, r, θ, φ)

$$\Phi(t, r, \theta, \varphi) = \frac{1}{r} \sum_{\ell=0}^{+\infty} \sum_{m=-\ell}^{+\ell} \phi_{\ell m}(t, r) Y_{\ell m}(\theta, \varphi) \tag{2.4.1}$$

avec

$$\phi_{\ell m}(t, r) = \frac{1}{\sqrt{2\pi}} \int_{-\infty+ic}^{+\infty+ic} d\omega \, e^{-i\omega t} \phi_{\omega\ell m}(r) \tag{2.4.2}$$

(ici $c > 0$) qui désigne la réponse partielle dans le mode (ℓ, m).

En faisant $r \to +\infty$ dans la solution (2.3.15) tout en tenant compte des équations (2.3.8a), (2.3.10) et (2.3.11), on peut la réduire à une expression asymptotique

$$\phi_{\omega\ell m}(r) = -\frac{1}{2i\omega A_\ell^{(-)}(\omega)} \left[\frac{\omega}{p(\omega)}\right]^{1/2} \times e^{+i\left[p(\omega) r_* + \frac{M\mu^2}{p(\omega)} \ln\left(\frac{r}{M}\right)\right]} \times \int_{2M}^{+\infty} dr' \, \phi^{\text{in}}_{\omega\ell}(r') \, \rho_{\omega\ell m}(r'). \tag{2.4.3}$$

Cependant, il est très important de mentionner que, dans la pratique, si l'on considère que l'observateur est localisé à une distance finie du trou noir (mais toujours plus éloigné du trou noir que la particule), il n'est pas possible d'utiliser le comportement asymptotique (2.3.8a) dans l'équation (2.3.11). Dans ce cas, il est nécessaire d'obtenir les modes $\phi^{\text{up}}_{\omega\ell}(r)$ numériquement en résolvant attentivement l'équation de Regge-Wheeler (2.3.6). C'est le prix à payer afin de tenir compte de la nature dispersive du champ scalaire massif. On doit donc remplacer (2.4.3) par

$$\phi_{\omega\ell m}(r) = -\frac{1}{2i\omega A_\ell^{(-)}(\omega)} \, \phi^{\text{up}}_{\omega\ell}(r) \times \int_{2M}^{+\infty} dr' \, \phi^{\text{in}}_{\omega\ell}(r') \, \rho_{\omega\ell m}(r'), \tag{2.4.4}$$

et la forme d'onde dans le mode (ℓ, m) est donnée par

$$\phi_{\ell m}(t, r) = -\frac{1}{\sqrt{2\pi}} \int_{-\infty+ic}^{+\infty+ic} d\omega \left(\frac{e^{-i\omega t}}{2i\omega A_\ell^{(-)}(\omega)}\right) \times \phi^{\text{up}}_{\omega\ell}(r) \int_{2M}^{+\infty} dr' \phi^{\text{in}}_{\omega\ell}(r') \rho_{\omega\ell m}(r'). \tag{2.4.5}$$

Pour finir, l'expression de la source (2.1.5) pour une trajectoire quelconque, dans le plan équatorial de l'espace-temps de Schwarzschild, est donnée par

$$\rho(x) = q \, \delta(\theta - \pi/2) \int_\gamma \frac{d\tau}{r_p^2(\tau)} \, \delta(t - t_p(\tau)) \times \delta(r - r_p(\tau)) \, \delta(\varphi - \varphi_p(\tau)). \tag{2.4.6}$$

Le lecteur doit bien garder à l'esprit que $x = (t, r, \theta, \varphi)$ désigne le point où l'on veut calculer la densité de charge ρ tandis que les coordonnées $t_p(\tau), r_p(\tau), \pi/2$ et $\varphi_p(\tau)$ repèrent le mouvement de

la particule massive.

2.5. Les modes quasi-normaux

Les QNMs, comme nous l'avons déjà mentionné dans l'introduction, jouent un rôle de premier plan dans la physique des trous noirs. En effet, la mise en évidence de l'existence de ces derniers repose sur l'identification des QNMs dans le signal émis, par exemple, par le trou noir final issu de la coalescence de deux corps compacts. Ces QNMs constitueraient, par conséquent, leur empreinte digitale. Les premiers travaux traitant des QNMs, remontent à plus de quarante ans avec la parution de l'article de Press [171], où il a identifié les résonances (les sonneries) des trous noirs de Schwarzschild à des "*oscillations libres*". Depuis, il est bien connu que les QNMs des trous noirs associées aux champs non massifs peuvent être interprétés en terme d'ondes piégées au voisinage de la sphère des photons, i.e. l'hypersurface sur laquelle une particule de masse nulle se meut en orbite circulaire instable autour du trou noir. Cette séduisante interprétation a été suggérée peu après l'article de Press par Goebel [172] et on la retrouve ensuite dans divers travaux (voir e.g. les Réfs. [173–175] pour une approche basée sur l'eikonale et les Réfs. [176–179] pour une approche basée sur les techniques de pôles de Regge). On peut aussi retrouver les QNMs en astronomie des ondes gravitationnelles et dans toutes les théories des champs en interaction avec des trous noirs, par exemple, dans le cadre de la théorie de la gravité quantique et la théorie des cordes (voir les Réfs. [6–9]).

On définit les QNMs comme étant les solutions de l'équation de Regge-Wheeler sans source (2.3.6) pour lesquelles le Wronskien (2.3.10) s'annule ($A_\ell^{(-)}(\omega) = B_\ell^{(+)}(\omega) = 0$), i.e. les fonctions $\phi^{\text{in}}_{\ell\omega}$ et $\phi^{\text{up}}_{\ell\omega}$ sont linéairement dépendantes et sont complètement entrantes à l'horizon et sortantes à l'infini spatial. Autrement dit, les QNMs ont un comportement purement entrant à l'horizon et purement sortant à l'infini spatial [180]. Ainsi, les zéros du Wronskien se trouvant dans la partie inférieure du plan complexe du premier feuillet de Riemann de $p(\omega)$ (voir Fig. 3.4a) sont les fréquences complexes quasi-normales associées aux QNMs. A noter que le spectre complexe des fréquences quasi-normales est symétrique par rapport à l'axe imaginaire de ω, i.e. si $\omega_{\ell n}$ est une fréquence quasi-normale dans le quatrième quadrant, $-\omega_{\ell n}{}^*$ est sa fréquence quasi-normale symétrique se trouvant dans le troisième quadrant.

2.6. Les modes quasi-liés

Les travaux pionniers qui ont traité des QBSs dataient des années soixante-dix avec la publication de l'article de Deruelle et Ruffini [141] et, peu après, l'article de Damour, Deruelle et Ruffini [142] où ils ont mis en évidence l'existence d'états quasi-liés dans l'équation de Klein-Gordon en étudiant un champ scalaire massif se propageant sur l'espace-temps de Schwarzschild et sur l'espace-temps de Kerr. On les associe, depuis, au minimum du potentiel de Regge-Wheeler (2.2.9). Nous renvoyons le lecteur aux Réfs. [143, 144, 147, 181–197] pour la littérature sur la physique des trous noirs de Schwarzschild, Kerr et Kerr-Newman liée aux QBSs des champs massifs bosoniques

et fermioniques.

Nous précisons que les QBSs ne doivent pas être pris ni confondus avec les QNMs des trous noirs ayant une longue durée de vie. Les QBSs sont définis précisément par leur comportement purement entrant à l'horizon et exponentiellement décroissant à l'infini spatial. Les fréquences complexes $\omega_{\ell n}$ associées aux QBSs sont les zéros du Wronskien donnés par (2.3.10) se trouvant sur la partie inférieure du plan complexe du second feuillet de Riemann de $p(\omega)$ (voir Fig. 3.4b). Et, comme pour les QNMs, le spectre des fréquences quasi-liées est symétrique par rapport à l'axe imaginaire de ω.

CHAPITRE 3

Méthodes numériques

Nous construisons dans ce chapitre les réponses partielles dans un mode (ℓ, m) donné du champ scalaire massif (2.4.3), particulièrement leurs formes d'onde associées (2.4.5). Pour cela, nous devons déterminer numériquement les fonctions $\phi^{\text{in}}_{\omega\ell}$ et $\phi^{\text{up}}_{\omega\ell}$ ainsi que les coefficients $A^{(-)}_{\ell}$ (Sec. 3.1). Nous allons, ensuite, construire numériquement le spectre des fréquences quasi-normales ainsi que le spectre des fréquences quasi-liées (Sec. 3.2) et (Sec. 3.3).

3.1. Résolution numérique de l'équation de Regge-Wheeler sans source

Nous commençons par construire numériquement les fonctions $\phi^{\text{in}}_{\omega\ell}$ et $\phi^{\text{up}}_{\omega\ell}$ solutions de l'équation de Regge-Wheeler sans source (sans second membre) (2.2.4) ou (2.2.8), ainsi que les coefficients $A^{(-)}_{\ell}$. Pour ce faire, on peut adopter une approche "grossière" du problème numérique (voir la Réf. [198]). Nous devons résoudre (2.2.4) ou (2.2.8) sans second membre en partant de la condition aux limites (2.3.7a). On rentre cette condition pour une valeur $r = r_i$ ou $r_* = r_{*i}$ correspondant à un point très proche de l'horizon. On résout alors l'équation de Regge-Wheeler par une procédure de *Runge-Kutta* en s'arrêtant à une valeur $r = r_f$ ou $r_* = r_{*f}$ correspondant à un point "proche" de l'infini spatial. On peut en déduire les coefficients $A^{(-)}_{\ell}$. En effet, comme $r_f \to +\infty$ on a

$$\begin{cases} \left[\frac{\omega}{p(\omega)}\right]^{1/2}\left(A^{(-)}_{\ell}(\omega)e^{-i\left[p(\omega)r_{*f}+\frac{M\mu^2}{p(\omega)}\ln\left(\frac{r_f}{M}\right)\right]}+A^{(+)}_{\ell}(\omega)e^{+i\left[p(\omega)r_{*f}+\frac{M\mu^2}{p(\omega)}\ln\left(\frac{r_f}{M}\right)\right]}\right)=\phi^{\text{in}}_{\omega\ell}(r_{*f}), \\ \left[\frac{\omega}{p(\omega)}\right]^{1/2}\left(A^{(-)}_{\ell}(\omega)e^{-i\left[p(\omega)r_{*f}+\frac{M\mu^2}{p(\omega)}\ln\left(\frac{r_f}{M}\right)\right]}-A^{(+)}_{\ell}(\omega)e^{+i\left[p(\omega)r_{*f}+\frac{M\mu^2}{p(\omega)}\ln\left(\frac{r_f}{M}\right)\right]}\right)=\left(\frac{1}{-ip(\omega)}\right)\left[\frac{d\phi^{\text{in}}_{\omega\ell}(r_*)}{dr_*}\right]_{r_*=r_{*f}}. \end{cases} \tag{3.1.1}$$

On a en particulier

$$A^{(-)}_{\ell}(\omega)=\left\{\frac{p(\omega)}{2\omega}e^{+i\left[p(\omega)r_*+\frac{M\mu^2}{p(\omega)}\ln\left(\frac{r}{M}\right)\right]}\left(\phi^{\text{in}}_{\omega\ell}(r_*)-\left(\frac{1}{ip(\omega)}\right)\frac{d\phi^{\text{in}}_{\omega\ell}(r_*)}{dr_*}\right)\right\}_{r_*=r_{*f}}. \tag{3.1.2}$$

Cependant, en adoptant cette approche, on rencontre inévitablement des problèmes de stabilité numérique et des difficultés liées au fait que les fonctions $e^{\pm i\left[p(\omega)r_{*f}+(M\mu^2/p(\omega))\ln(r_f/M)\right]}$ oscillent "sauvagement" pour $r_* \to \pm\infty$ ce qui rend difficile le choix de r_i et r_f.

Pour une approche plus élaborée de ce problème numérique, nous allons d'abord décrire la solution de l'équation de Regge-Wheeler sans source (2.2.4) ou (2.2.8) pour $r_* \to -\infty$ ou $r \to 2M$ à l'aide d'un développement en série de Taylor convergeant rapidement lorsqu'on est proche de

l'horizon. On l'écrit

$$\phi_{\omega\ell}^{(2M,\pm)} = e^{\pm i\omega r_*(r)} \sum_{n=0}^{+\infty} a_n^{\pm}(2M\omega,\mu,\ell)\left(1-\frac{2M}{r}\right)^n \tag{3.1.3}$$

avec les $a_n^{\pm}$ qui vérifient la relation de récurrence à 5 termes

$$\begin{aligned}
&n\Big[n \pm 2i\,(2M\omega)\Big]a_n^{\pm}\\
&+\Big[\mp 4i\,(2M\omega)(n-1) - 2(n-1)(2n-1) - \ell(\ell+1) - 1 - (2M\mu)^2\Big]a_{n-1}^{\pm}\\
&+\Big[\pm 2i\,(2M\omega)(n-2) + 6(n-2)(n-1) + 2\ell(\ell+1) + 3\Big]a_{n-2}^{\pm}\\
&+\Big[-2(n-3)(2n-3) - \ell(\ell+1) - 3\Big]a_{n-3}^{\pm}\\
&+\Big[(n-3)^2\Big]a_{n-4}^{\pm} = 0
\end{aligned} \tag{3.1.4}$$

et les conditions initiales

$$a_{-3}^{\pm} = a_{-2}^{\pm} = a_{-1}^{\pm} = 0 \quad \text{et} \quad a_0 = 1. \tag{3.1.5}$$

On décrit aussi la solution de l'équation de Regge-Wheeler (2.2.4) sans source ou (2.2.8) pour $r_* \to +\infty$ ou $r \to +\infty$ à l'aide des développements asymptotiques

$$\phi_{\omega\ell}^{(\infty,\pm)} = e^{\pm i\left[p(\omega)r_*(r) + \frac{M\mu^2}{p(\omega)}\ln\left(\frac{r}{M}\right)\right]} \sum_{n=0}^{+\infty} \tau_n^{\pm}(2M\omega,\mu,\ell)\left(\frac{2M}{r}\right)^n \tag{3.1.6}$$

où les $\tau_n^{\pm}$ vérifient la relation de récurrence à 4 termes

$$\begin{aligned}
&\mp\Big[2i\,(2Mp(\omega))\,n\Big]\tau_n^{\pm}\\
&+\Big[(2M\mu)^2 \pm 2i\,(2Mp(\omega))(n-1) \mp 2i\left(\frac{M\mu^2}{p(\omega)}\right)(n-1)\\
&\mp i\left(\frac{M\mu^2}{p(\omega)}\right) - \left(\frac{M\mu^2}{p(\omega)}\right)^2 + n(n-1) - \ell(\ell+1)\Big]\tau_{n-1}^{\pm}\\
&+\Big[\pm 4i\left(\frac{M\mu^2}{p(\omega)}\right)(n-2) \pm 3i\left(\frac{M\mu^2}{p(\omega)}\right) + 2\left(\frac{M\mu^2}{p(\omega)}\right)^2 - 2n^2 + 5n - 3 + \ell(\ell+1)\Big]\tau_{n-2}^{\pm}\\
&+\Big[\mp 2i\left(\frac{M\mu^2}{p(\omega)}\right)(n-3) \mp 2i\left(\frac{M\mu^2}{p(\omega)}\right) - \left(\frac{M\mu^2}{p(\omega)}\right)^2 + (n-2)^2\Big]\tau_{n-3}^{\pm} = 0
\end{aligned} \tag{3.1.7}$$

et les conditions initiales suivantes

$$\tau_{-2}^{\pm} = \tau_{-1}^{\pm} = 0 \quad \text{et} \quad \tau_0^{\pm} = 1. \tag{3.1.8}$$

On initialise, maintenant, la méthode de *Runge-Kutta* à l'aide du développement de Taylor à

l'horizon $\phi^{(2M,-)}_{\omega\ell}$ et on compare le résultat obtenu au point d'arrêt $r_f \to +\infty$ avec

$$\left[\frac{\omega}{p(\omega)}\right]^{1/2} A^{(-)}_{\ell}(\omega)\,\phi^{(\infty,-)}_{\omega\ell}(r_*) + \left[\frac{\omega}{p(\omega)}\right]^{1/2} A^{(+)}_{\ell}(\omega)\,\phi^{(\infty,+)}_{\omega\ell}(r_*). \tag{3.1.9}$$

On en déduit donc très précisément les coefficients $A^{(-)}_{\ell}$

$$A^{(-)}_{\ell}(\omega) = \frac{1}{2i\omega}\left[\frac{\omega}{p(\omega)}\right]^{1/2}\left[\left(1-\frac{2M}{r}\right)\left\{\phi^{\rm in}_{\omega\ell}(r)\left(\frac{\overrightarrow{d}}{dr}-\frac{\overleftarrow{d}}{dr}\right)\phi^{(\infty,+)}_{\omega\ell}(r)\right\}\right]_{r=r_f}. \tag{3.1.10}$$

Cet algorithme nous permet d'obtenir à la fois les modes partiels $\phi^{\rm in}_{\omega\ell}(r)$ et les coefficients $A^{(-)}_{\ell}(\omega)$. Quant aux modes partiels $\phi^{\rm up}_{\omega\ell}(r)$, pour les construire, on initialise la méthode de *Runge-Kutta* avec le développement asymptotique (3.1.6) et on résout l'équation de Regge-Wheeler sans source. Pour assurer une meilleure convergence et obtenir des résultats très stables, il est nécessaire de décoder l'information cachée dans la partie divergente, en réécrivant le développement asymptotique sous forme de sommation de Padé (voir e.g. le chapitre 8 de la Réf. [199]).

3.2. Construction du spectre des fréquences quasi-normales

Nous soulignons, pour commencer, que les premiers travaux relatifs à la détermination des fréquences quasi-normales datent du début des années soixante-dix (voir, e.g., l'article de Davis, Ruffini, Press et Price [29] sur les oscillations du trou noir de Schwarzschild excité par une particule en chute radiale).

Pour construire le spectre des fréquences quasi-normales, on trouve dans la littérature différentes méthodes numériques. La méthode *d'intégration de l'équation de Regge-Wheeler dans le domaine temporel* développé par Vishveshwara [200] est considérée comme l'une des premières méthodes utilisées pour la construction des fréquences quasi-normales. On peut citer, aussi, la méthode *d'intégration directe dans le domaine fréquentiel* développée par Chandrasekhar et Detweiler [180], et la méthode *WKB* suggérée, pour la première fois, par Schutz et Will [201] etc. (voir la section 6.1 de la Réf. [6], pour une liste exhaustive des différentes méthodes numériques pour la construction du spectre des fréquences quasi-normales). La méthode la plus utilisée est celle des *fractions continues* développée par Leaver dans son article de 1985 [202]. Cette méthode fournit des résultats très précis et on peut l'appliquer non seulement dans le cas du trou noirs de Schwarzschild, mais aussi pour le trou noir de Kerr et, avec quelques modifications, pour le trou noir de Reissner-Nordström [203]. A noter que cette méthode de Leaver s'applique dans le cas de la théorie non-massive et qu'elle a été, aussi, généralisée dans le cas de la théorie massive par Konoplya et Zhidenko [204].

Comme nous l'avons déjà mentionné dans la Sec. 2.5, les QNMs sont définis par leur comportement purement entrant à l'horizon et purement sortant à l'infini spatial. Ainsi, les conditions

aux limites satisfaites par les QNMs à l'horizon et à l'infini spatial sont

$$\phi_{\omega\ell}(r) \underset{r\to 2M}{\sim} C_1 \left(\frac{r}{2M}-1\right)^{-i2M\omega}, \tag{3.2.1a}$$

$$\phi_{\omega\ell}(r) \underset{r_*\to+\infty}{\sim} C_2\, e^{ip(\omega)r}\left(\frac{r}{2M}-1\right)^{i2Mp(\omega)} r^{(iM\mu^2/p(\omega))}. \tag{3.2.1b}$$

Les solutions de l'équation de Regge-Wheeler homogène (2.3.6) peuvent être, donc, recherchées sous la forme [204]

$$\phi_{\omega\ell}(r) = e^{ip(\omega)r}\, r^{(i2Mp(\omega)+iM\mu^2/p(\omega))}\left(1-\frac{2M}{r}\right)^{-i2M\omega}\sum_{n=0}^{\infty} a_n\left(1-\frac{2M}{r}\right)^n. \tag{3.2.2}$$

Ici, les a_n vérifient la relation de récurrence à trois termes

$$\alpha_n a_{n+1} + \beta_n a_n + \gamma_n a_{n-1} = 0, \quad n>0, \tag{3.2.3}$$

avec comme conditions initiales

$$\alpha_0 a_1 + \beta_0 a_0 = 0, \tag{3.2.4}$$

où

$$\alpha_n = (n+1)(n+1-4iM\omega), \tag{3.2.5a}$$

$$\beta_n = \frac{M(\omega+p(\omega))\left[4M(\omega+p(\omega))^2 + i(2n+1)(\omega+3p(\omega))\right]}{p(\omega)} - 2n(n+1) - 1 - \ell(\ell+1), \tag{3.2.5b}$$

$$\gamma_n = \left[n - \frac{Mi(\omega+p(\omega))^2}{p(\omega)}\right]^2. \tag{3.2.5c}$$

Les Coefficients $A_\ell^{(-)}$ s'annulent lorsque $\sum_n a_n$ converge. On peut donc utiliser la méthode des fractions continues pour déterminer numériquement les fréquences quasi-normales qui seront les zéros de ces coefficients .

Une autre manière de mettre en pratique la relation de récurrence (3.2.3) consiste en l'utilisation de la méthode du *déterminant de Hill* suggérée par Majumdar et Panchapakesan dans leur article de 1989 [205] pour le champ scalaire non-massif. Cette méthode est surtout employée pour la détermination des valeurs propres des problèmes en mécanique quantique. Nous l'avons modifiée et adaptée aux champs massifs.

Les fréquences quasi-normales sont donc solutions du déterminant de Hill

$$\mathrm{D} = \begin{vmatrix} \beta_0 & \alpha_0 & 0 & 0 & 0 & \dots & \dots & \dots \\ \gamma_1 & \beta_1 & \alpha_1 & 0 & 0 & \dots & \dots & \dots \\ 0 & \gamma_2 & \beta_2 & \alpha_2 & 0 & \dots & \dots & \dots \\ \vdots & \ddots & \ddots & \ddots & \ddots & \ddots & \dots & \dots \\ \vdots & \vdots & \ddots & \gamma_{n-1} & \beta_{n-1} & \alpha_{n-1} & \ddots & \dots \\ \vdots & \vdots & \vdots & \ddots & \gamma_n & \beta_n & \alpha_n & \ddots \\ \vdots & \vdots & \vdots & \vdots & \ddots & \ddots & \ddots & \ddots \end{vmatrix} = 0 \tag{3.2.6}$$

que l'on peut réécrire sous forme d'une relation de récurrence

$$\mathrm{D}_n = \beta_n \mathrm{D}_{n-1} - \gamma_n \alpha_{n-1} \mathrm{D}_{n-2} \tag{3.2.7}$$

avec les conditions initials

$$\mathrm{D}_0 = \beta_0 \qquad \text{et} \qquad \mathrm{D}_1 = \beta_1 \beta_0 - \gamma_1 \alpha_0 \tag{3.2.8}$$

ou, de manière équivalente

$$\begin{aligned} \mathrm{D}_n &= \prod_{k=1}^{n+1} k^2 \mathrm{P}_{n+1} \\ &= 1 \times 2^2 \dots (n-2)^2 (n-1)^2 n^2 (n+1)^2 \mathrm{P}_{n+1}, \end{aligned} \tag{3.2.9}$$

où

$$\mathrm{P}_n = \left(\frac{\beta_{n-1}}{n^2}\right) \mathrm{P}_{n-1} - \left(\frac{\gamma_{n-1}}{n^2}\right)\left(\frac{\alpha_{n-2}}{(n-1)^2}\right) \mathrm{P}_{n-2}, \tag{3.2.10}$$

avec les conditions initiales

$$\mathrm{P}_1 = \beta_0 \qquad \text{et} \qquad \mathrm{P}_2 = \frac{\beta_0 \beta_1 - \gamma_1 \alpha_0}{4}. \tag{3.2.11}$$

Dans la pratique, la recherche des zéros du déterminant de Hill peut se faire, par exemple, en résolvant la relation de récurrence (3.2.10) considérée comme une équation polynomiale en ω. Pour ce faire, on utilise la méthode de *Newton-Raphson*. Les racines de ce polynôme définissent ainsi le spectre des fréquences quasi-normales. Cette méthode est celle mise en pratique dans la Réf. [205].

On peut aussi, en adoptant une nouvelle approche, déterminer les zéros du déterminant de Hill. Nous utilisons, cette fois, une technique basée sur le théorème de l'argument (ou le principe de l'argument) de l'analyse complexe. Nous considérons que la relation de récurrence (3.2.10) décrit une fonction complexe et que les pôles de cette fonction représentent les fréquences quasi-normales. Comme nous l'avons déjà mentionné, elles se trouvent dans la partie inférieure du plan complexe de $p(\omega)$, i.e. dans le troisième et le quatrième cadran. Le spectre des fréquences quasi-normales est symétrique par rapport à l'axe imaginaire de ω, nous allons donc les rechercher seulement dans le quatrième cadran par la méthode du *balayage du plan complexe*.

Pour commencer, nous délimitons une zone à balayer (voir Fig. 3.1). Nous définissons, ensuite, un cercle que nous prenons comme notre contour d'intégration, et qui sera divisé en petits arcs. Nous utilisons une méthode d'intégration numérique adaptée pour évaluer notre intégrale. Enfin, nous répétons l'opération en déplaçant le cercle tout au long de la zone délimitée. Il n'y a pas besoin, contrairement aux autres méthodes numériques, d'initialiser avec une valeur au voisinage de la fréquence quasi-normale recherchée. Le balayage se fera d'une manière aveugle dans une zone préalablement délimitée et on doit être sûr de ne rien oublier.

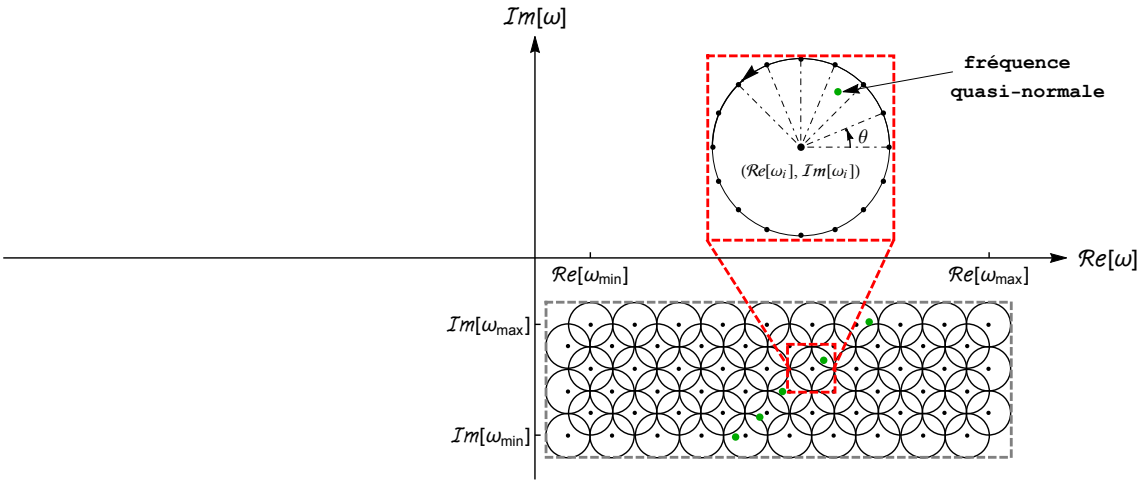

Fig. 3.1. – Plan complexe des fréquences quasi-normales.

Pour terminer cette section, nous donnons un échantillon du spectre des fréquences quasi-normales en fonction du paramètre sans dimension $\tilde{\alpha}$ Fig. 3.2. Nous considérons les modes ($\ell = 1, n = 0, 1$) Fig. 3.2a et les modes ($\ell = 2, n = 0, 1$) Fig. 3.2b et nous montrons l'effet de la masse du champ sur les fréquences quasi-normales complexes $\omega_{\ell n}$. On voit, que lorsque le paramètre de masse augmente, la partie imaginaire des fréquences quasi-normales diminue, par conséquent leurs modes QNMs associés ont une longue durée de vie.

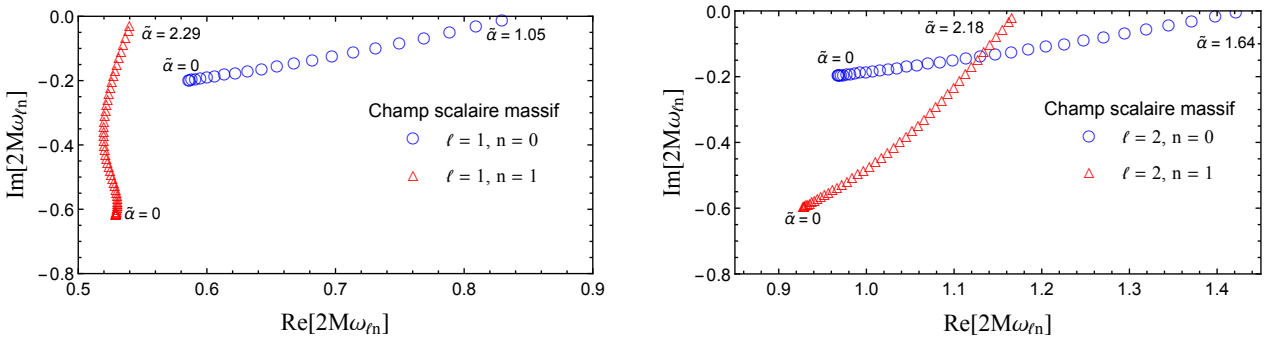

Fig. 3.2. – Les fréquences complexes quasi-normales $2M\omega_{\ell n}$. (a) Pour les modes ($\ell = 1, n = 0, 1$). (b) Pour les modes ($\ell = 2, n = 0, 1$).

3.3. Construction du spectre des fréquences quasi-liées

Les fréquences quasi-liées, comme nous l'avons fait déjà remarquer dans la Sec. 2.6, sont les zéros du Wronskien se trouvant dans la partie inférieure du second feuillet de Riemann de la fonction $p(\omega)$. Certaines des méthodes permettant le calcul des fréquences quasi-normales peuvent être adoptées pour la construction du spectre des fréquences quasi-liées. Le lecteur peut se référer, e.g. à l'article de Dolan [194], où la méthode de Leaver (fractions continues) est utilisée. Pour notre part, nous avons repris la technique qui nous a permis d'obtenir le spectre des fréquences quasi-normales (Sec. 3.2), tout en tenant compte du fait que nous travaillons sur le second feuillet de Riemann associé à $p(\omega)$, d'où la nécessité de prendre $-p(\omega)$ au lieu de $p(\omega)$ (voir Fig. 3.4b).

Nous terminons cette section en donnant un échantillon du spectre des fréquences quasi-liées en fonction du paramètre sans dimension $\tilde{\alpha}$ (Fig. 3.3). Nous présentons les modes $(\ell = 1, n = 0, 1)$ Fig. 3.3a et les modes $(\ell = 2, n = 0, 1)$ Fig. 3.3b et nous montrons l'effet de la masse du champ sur les fréquences quasi-liées complexes $\omega_{\ell n}$.

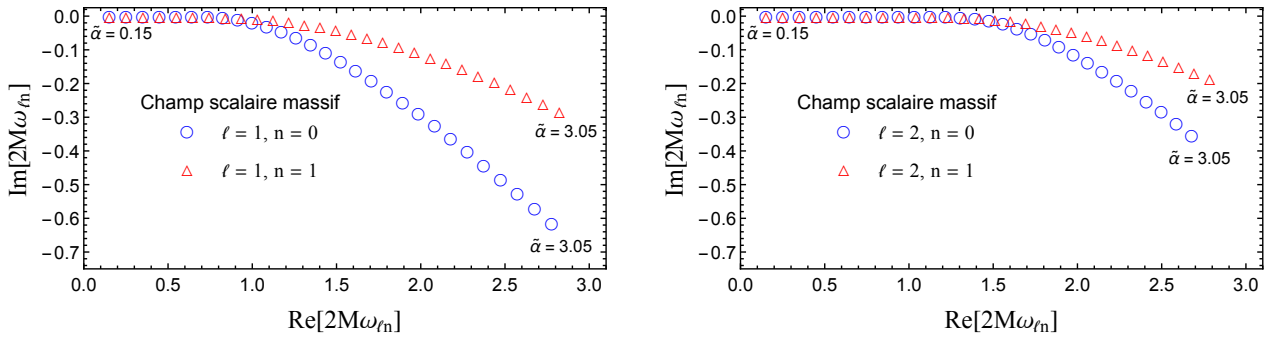

(a) (b)

FIG. 3.3. – Les fréquences complexes quasi-liées $2M\omega_{\ell n}$ pour $\tilde{\alpha} = 0, 0.10, \ldots, 2.95, 3.05$. (a) Pour les modes $(\ell = 1, n = 0, 1)$. (b) Pour les modes $(\ell = 2, n = 0, 1)$

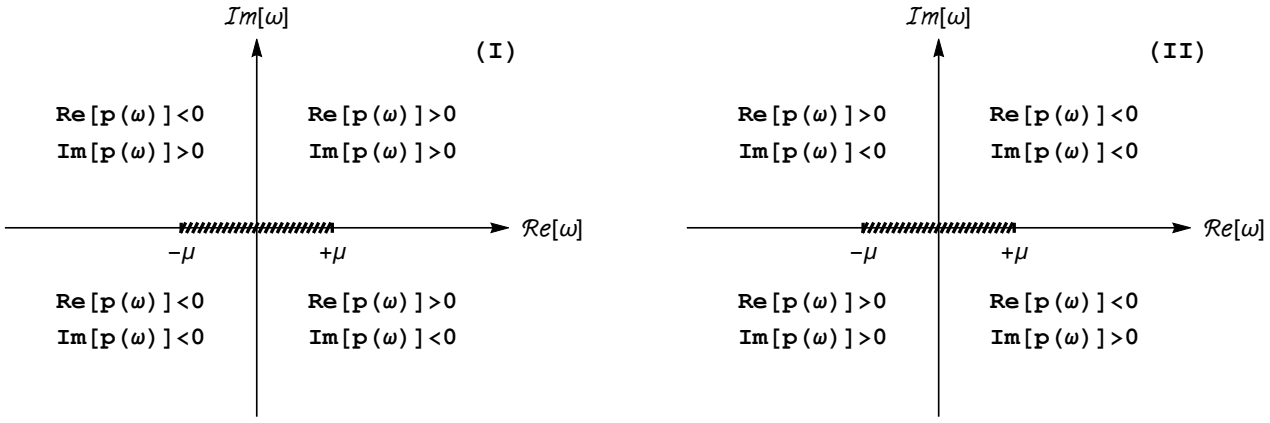

(a) Premier feuillet associé au spectre de fréquences quasi-normales

(b) Second feuillet associé au spectre de fréquences quasi-liées

FIG. 3.4. – Les deux feuillets de la fonction $p(\omega) = \sqrt{\omega^2 - \mu^2} = Re[p(\omega)] + iIm[p(\omega)]$

CHAPITRE 4

Particule plongeant dans le trou noir de Schwarzschild

Dans une perspective de test de la gravité massive dans le cadre de la physique des trous noirs, nous considérerons une particule plongeant à partir de la première orbite stable, i.e., ISCO, dans le trou noir de Schwarzschild. Nous supposons le système trou noir-particule asymétrique, i.e., la masse du trou noir est très grande devant la masse de la particule. Cette hypothèse nous permet de décrire le rayonnement gravitationnel généré par ce système dans le cadre des perturbations du trou noir. Il existe une vaste littérature à ce sujet dans le cadre de la théorie d'Einstein. Le lecteur peut se reporter, par exemple, aux Réfs. [36, 40, 43, 45, 47, 48, 50, 52, 56, 58–60, 100, 101, 206, 207].

Le "régime plongeant" est en vérité, la phase finale de l'évolution d'un objet stellaire aux voisinages d'un trou noir supermassif et le signal émis au cours de cette phase porte l'empreinte digitale du trou noir. Dans le cadre de la gravité massive, en plus des difficultés théoriques mentionnées précédemment, le problème d'excitation du trou noir de Schwarzschild par une particule plongeante est compliqué par des instabilités numériques. Afin de "simplifier" notre tâche, nous examinons dans ce chapitre un modèle-jouet où le champ de gravité massive est remplacé par un champ scalaire massif et nous considérons un couplage linéaire entre le champ scalaire massif et la particule.

PHYSICAL REVIEW D **92,** 024057 (2015)

Waveforms produced by a scalar point particle plunging into a Schwarzschild black hole: Excitation of quasinormal modes and quasibound states

Yves Décanini,[*] Antoine Folacci,[†] and Mohamed Ould El Hadj[‡]

Equipe Physique Théorique–Projet COMPA, SPE, UMR 6134 du CNRS et de l'Université de Corse, Université de Corse, BP 52, F-20250 Corte, France

(Received 30 June 2015; published 31 July 2015)

With the possibility of testing massive gravity in the context of black hole physics in mind, we consider the radiation produced by a particle plunging from slightly below the innermost stable circular orbit into a Schwarzschild black hole. In order to circumvent the difficulties associated with black hole perturbation theory in massive gravity, we use a toy model in which we replace the graviton field with a massive scalar field and consider a linear coupling between the particle and this field. We compute the waveform generated by the plunging particle and study its spectral content. This permits us to highlight and interpret some important effects occurring in the plunge regime which are not present for massless fields, such as (i) the decreasing and vanishing, as the mass parameter increases, of the signal amplitude generated when the particle moves on quasicircular orbits near the innermost stable circular orbit; and (ii) in addition to the excitation of the quasinormal modes, the excitation of the quasibound states of the black hole.

DOI: 10.1103/PhysRevD.92.024057 PACS numbers: 04.30.Db, 04.25.Nx, 04.70.Bw

I. INTRODUCTION

In recent years, theories of massive gravity, i.e., extensions of general relativity mediated by an ultralight massive graviton, are the subject of intense activity, and the internal inconsistencies present in the old Fierz-Pauli theory [1,2] seem to be overcome, such as (i) the discontinuity with general relativity in the limit where the mass of the graviton is taken to zero and (ii) the ghost problem. (See, e.g., Refs. [3] and [4] for reviews on massive gravity, and Ref. [5] for experimental constraints on the mass of the graviton.) Because massive gravity could explain naturally the observed accelerated expansion of the present Universe, i.e., without requiring dark energy or introducing a cosmological constant (see, e.g., Sec. 12 of Ref. [4] and references therein), it has led to numerous works in cosmology. By contrast, it has rarely been the subject of works in black hole (BH) physics. (See, however, Ref. [6] and references therein for recent articles dealing with BH solutions in massive gravity, and Refs. [7–9] for important considerations on the problem of BH stability in massive gravity.) In our opinion, it is in this particular area that, in the near future, theories of massive gravity could be directly tested with the next generations of gravitational wave detectors.

In this article, with the possibility of testing massive gravity in the context of BH physics in mind, we intend to consider the radiation produced by a "particle" plunging from slightly below the innermost stable circular orbit (ISCO) into a Schwarzschild BH. We shall assume an extreme mass ratio for this physical system, i.e., that the BH is much heavier than the particle. Such a hypothesis permits us to describe the emitted radiation in the framework of BH perturbations. Here, two remarks are in order:

(1) In the context of Einstein's general relativity, the problem we consider is of fundamental importance, and there exists a large literature concerning it more or less directly (see, e.g., Refs. [10–25]). Indeed, the "plunge regime" is the last phase of the evolution of a stellar mass object orbiting near a supermassive BH (note that it can also be used to describe the late-time evolution of a binary BH), and the waveform generated during this regime encodes the final BH fingerprint.

(2) The Schwarzschild BH, one of the most important solutions of Einstein's general relativity, is also relevant to massive gravity [6]. Indeed, it is a solution of the pathology-free bimetric theory of gravity discussed by Hassan, Schmidt-May, and von Strauss in Ref. [26] and obtained by extending, in curved spacetime, the fundamental work of de Rham, Gabadadze, and Tolley [27,28].

In the context of the bimetric theory of gravity discussed in Ref. [26], gravitational perturbations of the Schwarzschild BH have been studied by Brito, Cardoso, and Pani [8,9]. This problem is rather difficult and leads to results which generalize the problem of massless spin-2 fluctuations in a nontrivial way. In particular, it is important to recall that (i) the Schwarzschild BH is linearly unstable for small graviton masses, (ii) the $\ell = 1$ modes (the so-called dipole modes) become dynamic, and (iii) except for

[*]decanini@univ-corse.fr
[†]folacci@univ-corse.fr
[‡]ould-el-hadj@univ-corse.fr

the odd-parity dipole modes, all the other dynamical modes are governed by two or three coupled differential equations. All these results make very difficult, in the context of massive gravity, the theoretical analysis of the gravitational radiation produced by a particle falling into a Schwarzschild BH on an arbitrary trajectory. To our knowledge, there does not exist any work dealing fully with this fundamental problem. In a recent paper [29] (see also Ref. [30] for a more complete study including analytical results and extension to other bosonic fields), we have partially considered it by only focusing on some aspects linked with the excitation of quasinormal modes (QNMs). We have shown that, in rather large domains around critical values of the graviton mass, the excitation factors of the long-lived QNMs have a strong resonant behavior which induces, as a consequence, the existence of giant and slowly decaying ringings. This unexpected effect was obtained in a rather restricted context: (i) we only focused on the odd-parity dipole modes; (ii) the source of the distortion of the BH was described by an initial value problem with Gaussian initial data; and (iii) we did not take into account the full response of the BH but only the part associated with QNMs, and therefore we neglected various important effects linked with quasibound states (QBSs) which could blur the QNM contribution.

Preliminary unpublished investigations have permitted us to understand that, in massive gravity, in addition to the theoretical difficulties previously mentioned, the problem of the excitation of a Schwarzschild BH by a plunging particle is plagued by numerical instabilities. So, in order to simplify our task, both numerically and theoretically, we shall consider in this article a toy model in which we replace the massive spin-2 perturbations with a massive scalar field and consider a linear coupling between the particle and this field. We shall compute the waveform generated by the plunging particle and study its spectral content. This shall permit us to describe the excitation of the QNMs as well as that of the QBSs of the BH, but also to show the influence of the mass on the amplitude of the emitted signal and, more particularly, on the part generated when the particle moves on quasicircular orbits near the ISCO. Of course, we hope to return to the same problem in the context of massive gravity, but we think that the phenomena highlighted with the toy model are still present in this more physical and interesting problem. Furthermore, the lessons we have learned by working with the toy model should allow us to avoid some difficulties due to numerical instabilities.

Our paper is organized as follows: In Sec. II, we describe our toy model, introduce our notations, and establish theoretically the expression of the waveform emitted by a scalar point particle moving on an arbitrary geodesic by using the standard Green's function techniques. These results will be useful both in Sec. III and Appendix A. In Sec. III, from the closed-form expression of the plunge trajectory, we first obtain the general expression of the waveform generated by the plunging particle, and then we focus more particularly on the $(\ell = 2, m = 2)$ mode of the scalar field. We study numerically the corresponding waveform (the so-called quadrupolar waveform) and its behavior as the mass parameter increases and as the observer location changes, and we highlight the excitation of the QNMs and QBSs of the BH. In the Conclusion, we summarize the main results obtained in this article, and we briefly deal with arbitrary (ℓ, m) modes of the scalar field and consider possible extensions of our work. In three Appendixes, we gather some important results which permit us to analyze and interpret the numerical results of Sec. III. In Appendix A, we provide a simple closed form for the emitted waveform when the particle lives on the ISCO. In Appendix B, we consider the weakest damped QNM with $\ell = 2$ and construct numerically its response when it is excited by the plunging particle. In Appendix C, we consider the first QBSs with $\ell = 2$ and determine their complex frequencies.

Throughout this article, we adopt units such that $\hbar = c = G = 1$, and we introduce the reduced mass parameter (a dimensionless coupling constant) $\tilde{\alpha} = 2M\mu/{m_P}^2$, where M, μ, and m_P denote, respectively, the mass of the BH, the mass of the scalar field, and the Planck mass.

II. THE GENERAL SOLUTION OF THE SCALAR WAVE EQUATION WITH SOURCE

A. Our model

We shall consider a point particle with mass m_0 and scalar charge q moving along a world line $\gamma(\lambda)$ in the Schwarzschild spacetime $(\mathcal{M}, g_{\alpha\beta})$. λ is an affine parameter and $(\mathcal{M}, g_{\alpha\beta})$ is the exterior of the Schwarzschild BH of mass M defined by the metric

$$ds^2 = -\left(1-\frac{2M}{r}\right)dt^2 + \left(1-\frac{2M}{r}\right)^{-1}dr^2 + r^2 d\sigma_2^2, \quad (1)$$

where $d\sigma_2^2$ denotes the metric on the unit 2-sphere S^2 and with the Schwarzschild coordinates (t, r) which satisfy $t \in]-\infty, +\infty[$ and $r \in]2M, +\infty[$. In the following, we shall also use the so-called tortoise coordinate $r_* \in]-\infty, +\infty[$ defined from the radial Schwarzschild coordinate r by $dr/dr_* = (1 - 2M/r)$ and given by $r_*(r) = r + 2M\ln[r/(2M) - 1]$. We recall that the function $r_* = r_*(r)$ provides a bijection from $]2M, +\infty[to]-\infty, +\infty[$.

The particle is coupled to a scalar field Φ with mass μ, and the dynamics of the system field particle is defined by the action (see also Ref. [31])

$$S = S_{\text{field}} + S_{\text{part}} + S_{\text{int}}, \quad (2)$$

with

$$S_{\rm field} = -\frac{1}{2}\int_{\mathcal{M}} d^4x\sqrt{-g(x)} \times [g^{\alpha\beta}(x)\nabla_\alpha\Phi(x)\nabla_\beta\Phi(x) + \mu^2\Phi^2(x)] \quad (3)$$

and

$$S_{\rm part} = -m_0\int_\gamma d\tau = -m_0\int_\gamma \sqrt{-g_{\alpha\beta}(z(\lambda))\frac{dz^\alpha(\lambda)}{d\lambda}\frac{dz^\beta(\lambda)}{d\lambda}}d\lambda \quad (4)$$

and

$$S_{\rm int} = \int_{\mathcal{M}} d^4x\sqrt{-g(x)}\rho(x)\Phi(x). \quad (5)$$

Here $S_{\rm field} = S_{\rm field}[\Phi, g_{\alpha\beta}]$ denotes the action of the scalar field Φ. $S_{\rm part} = S_{\rm part}[z(\lambda), g_{\alpha\beta}]$ is the action of the particle, τ denotes its proper time, and the equations $z^\alpha = z^\alpha(\lambda)$ describe its world line. $S_{\rm int} = S_{\rm int}[z(\lambda), \Phi, g_{\alpha\beta}]$ is an interaction term describing the coupling of the particle and the field. It should be noted that they are coupled via the charge density

$$\rho(x) = q\int_\gamma d\tau\delta^4(x, z(\tau)) = q\int_\gamma d\tau\frac{\delta^4(x - z(\tau))}{\sqrt{-g(x)}} \quad (6)$$

associated with the charged scalar particle.

B. Wave equation and Regge-Wheeler equation with source

The wave equation governing the scalar field Φ is obtained by extremization of the action (2). We have

$$(\Box - \mu^2)\Phi = -\rho, \quad (7)$$

where the source ρ is given by (6).

Due to both the staticity and the spherical symmetry of the Schwarzschild background, we can solve Eq. (7) by introducing the decompositions

$$\Phi(t, r, \theta, \varphi) = \frac{1}{\sqrt{2\pi}}\int_{-\infty}^{+\infty} d\omega e^{-i\omega t} \times \sum_{\ell=0}^{+\infty}\sum_{m=-\ell}^{+\ell}\frac{\phi_{\omega\ell m}(r)}{r}Y_{\ell m}(\theta, \varphi) \quad (8)$$

and

$$\rho(t, r, \theta, \varphi) = \frac{1}{\sqrt{2\pi}}\int_{-\infty}^{+\infty} d\omega e^{-i\omega t} \times \sum_{\ell=0}^{+\infty}\sum_{m=-\ell}^{+\ell}\frac{\rho_{\omega\ell m}(r)}{r}Y_{\ell m}(\theta, \varphi), \quad (9)$$

where $Y_{\ell m}(\theta, \varphi)$ are the standard spherical harmonics with $\ell \in \mathbb{N}$ and $m = -\ell, -\ell + 1, \ldots, +\ell$. The wave equation (7) reduces then to the Regge-Wheeler equation with source

$$\left[\frac{d^2}{dr_*^2} + \omega^2 - V_\ell(r)\right]\phi_{\omega\ell m} = -\left(1 - \frac{2M}{r}\right)\rho_{\omega\ell m}. \quad (10)$$

In Eq. (10), $V_\ell(r)$ denotes the Regge-Wheeler potential given by

$$V_\ell(r) = \left(1 - \frac{2M}{r}\right)\left[\mu^2 + \frac{\ell(\ell+1)}{r^2} + \frac{2M}{r^3}\right]. \quad (11)$$

C. Construction of the Green's function

In order to solve the Regge-Wheeler equation (10), we shall use the machinery of Green's functions (see Ref. [32] for generalities on this topic and e.g., Ref. [33] for its use in the context of BH physics). We consider the Green's function $G_{\omega\ell}(r_*, r'_*)$ defined by

$$\left[\frac{d^2}{dr_*^2} + \omega^2 - V_\ell(r)\right]G_{\omega\ell}(r_*, r'_*) = -\delta(r_* - r'_*), \quad (12)$$

which can be written as

$$G_{\omega\ell}(r_*, r'_*) = -\frac{1}{W_\ell(\omega)}\begin{cases}\phi^{\rm in}_{\omega\ell}(r_*)\phi^{\rm up}_{\omega\ell}(r'_*), & r_* < r'_*,\\ \phi^{\rm up}_{\omega\ell}(r_*)\phi^{\rm in}_{\omega\ell}(r'_*), & r_* > r'_*.\end{cases} \quad (13)$$

Here $W_\ell(\omega)$ denotes the Wronskian of the functions $\phi^{\rm in}_{\omega\ell}$ and $\phi^{\rm up}_{\omega\ell}$. These two functions are linearly independent solutions of the homogenous Regge-Wheeler equation

$$\left[\frac{d^2}{dr_*^2} + \omega^2 - V_\ell(r)\right]\phi_{\omega\ell} = 0. \quad (14)$$

When $\mathrm{Im}(\omega) > 0$, $\phi^{\rm in}_{\omega\ell}$ is uniquely defined by its purely ingoing behavior at the event horizon $r = 2M$ (i.e., for $r_* \to -\infty$)

$$\phi^{\rm in}_{\omega\ell}(r) \underset{r_*\to-\infty}{\sim} e^{-i\omega r_*}, \quad (15a)$$

while at spatial infinity $r \to +\infty$ (i.e., for $r_* \to +\infty$), it has an asymptotic behavior of the form

$$\phi^{\rm in}_{\omega\ell}(r) \underset{r_*\to+\infty}{\sim} \left[\frac{\omega}{p(\omega)}\right]^{1/2} \times (A^{(-)}_\ell(\omega) e^{-i[p(\omega)r_*+[M\mu^2/p(\omega)]\ln(r/M)]} + A^{(+)}_\ell(\omega) e^{+i[p(\omega)r_*+[M\mu^2/p(\omega)]\ln(r/M)]}). \quad (15b)$$

Similarly, $\phi^{\rm up}_{\omega\ell}$ is uniquely defined by its purely outgoing behavior at spatial infinity

$$\phi^{\rm up}_{\omega\ell}(r) \underset{r_*\to+\infty}{\sim} \left[\frac{\omega}{p(\omega)}\right]^{1/2} e^{+i[p(\omega)r_*+[M\mu^2/p(\omega)]\ln(r/M)]}, \quad (16a)$$

and at the horizon, it has an asymptotic behavior of the form

$$\phi^{\rm up}_{\omega\ell}(r) \underset{r_*\to-\infty}{\sim} B^{(-)}_\ell(\omega) e^{-i\omega r_*} + B^{(+)}_\ell(\omega) e^{+i\omega r_*}. \quad (16b)$$

In the previous expressions, the function $p(\omega) = (\omega^2-\mu^2)^{1/2}$ denotes the "wave number," while the coefficients $A^{(-)}_\ell(\omega)$, $A^{(+)}_\ell(\omega)$, $B^{(-)}_\ell(\omega)$, and $B^{(+)}_\ell(\omega)$ are complex amplitudes. Here, it is important to note that these coefficients as well as the in and up modes can be defined by analytic continuation on the two-sheet Riemann surface associated with $p(\omega)$. By evaluating the Wronskian $W_\ell(\omega)$ at $r_* \to -\infty$ and $r_* \to +\infty$, we obtain

$$W_\ell(\omega) = 2i\omega A^{(-)}_\ell(\omega) = 2i\omega B^{(+)}_\ell(\omega). \quad (17)$$

D. Solution of the wave equation with source

Using the Green's function (13), we can show that the solution of the Regge-Wheeler equation with source (10) is given by

$$\phi_{\omega\ell m}(r) = \int_{-\infty}^{+\infty} dr'_* G_{\omega\ell}(r_*, r'_*)\left(1-\frac{2M}{r'(r'_*)}\right)\rho_{\omega\ell m}(r'_*) \quad (18)$$

or, equivalently, by

$$\phi_{\omega\ell m}(r) = \int_{2M}^{+\infty} dr' G_{\omega\ell}(r,r')\rho_{\omega\ell m}(r'). \quad (19)$$

As a consequence, the response (8) detected by an observer at (t,r,θ,φ) is given by

$$\Phi(t,r,\theta,\varphi) = \frac{1}{r}\sum_{\ell=0}^{+\infty}\sum_{m=-\ell}^{+\ell}\phi_{\ell m}(t,r)Y_{\ell m}(\theta,\varphi), \quad (20)$$

where

$$\phi_{\ell m}(t,r) = \frac{1}{\sqrt{2\pi}}\int_{-\infty+ic}^{+\infty+ic} d\omega e^{-i\omega t}\phi_{\omega\ell m}(r) \quad (21)$$

(here $c>0$) denotes the partial response corresponding to the (ℓ,m) mode.

For $r \to +\infty$, the solution (19) reduces to the asymptotic expression

$$\phi_{\omega\ell m}(r) = -\frac{1}{2i\omega A^{(-)}_\ell(\omega)}\left[\frac{\omega}{p(\omega)}\right]^{1/2} \times e^{+i[p(\omega)r_*+[M\mu^2/p(\omega)]\ln(r/M)]} \times \int_{2M}^{+\infty} dr' \phi^{\rm in}_{\omega\ell}(r')\rho_{\omega\ell m}(r'). \quad (22)$$

This result is a consequence of Eqs. (13), (16a), and (17). However, it is very important to note that, in practice, if we consider that the observer is located at a finite distance from the BH, it is not possible to use the asymptotic behavior (16a) in Eq. (13), but it is necessary to obtain $\phi^{\rm up}_{\omega\ell}(r)$ numerically by solving carefully the Regge-Wheeler equation (14): this is the price to pay in order to take into account the dispersive nature of the massive scalar field. In that case, assuming that the observer is located beyond the source, we must replace (22) with

$$\phi_{\omega\ell m}(r) = -\frac{1}{2i\omega A^{(-)}_\ell(\omega)}\phi^{\rm up}_{\omega\ell}(r) \times \int_{2M}^{+\infty} dr' \phi^{\rm in}_{\omega\ell}(r')\rho_{\omega\ell m}(r'), \quad (23)$$

and then we have for the (ℓ,m) waveform

$$\phi_{\ell m}(t,r) = -\frac{1}{\sqrt{2\pi}}\int_{-\infty+ic}^{+\infty+ic} d\omega\left(\frac{e^{-i\omega t}}{2i\omega A^{(-)}_\ell(\omega)}\right) \times \phi^{\rm up}_{\omega\ell}(r)\int_{2M}^{+\infty} dr' \phi^{\rm in}_{\omega\ell}(r')\rho_{\omega\ell m}(r'). \quad (24)$$

E. General expression of the source

By extremization of the action (4), we can obtain the equations governing the timelike geodesic γ followed by the massive particle. We shall denote by $t_p(\tau)$, $r_p(\tau)$, $\theta_p(\tau)$, and $\varphi_p(\tau)$ its coordinates, and we remark that, without loss of generality, its trajectory can be considered to lie in the BH equatorial plane, so we assume that $\theta_p(\tau) = \pi/2$. We have

$$\left(1-\frac{2M}{r_p}\right)\frac{dt_p}{d\tau} = \frac{E}{m_0}, \quad (25a)$$

$$r_p^2\frac{d\varphi_p}{d\tau} = \frac{L}{m_0}, \quad (25b)$$

and

$$\left(\frac{dr_p}{d\tau}\right)^2+\frac{L^2}{m_0^2r_p^2}\left(1-\frac{2M}{r_p}\right)-\frac{2M}{r_p}=\left[\left(\frac{E}{m_0}\right)^2-1\right], \tag{25c}$$

where E and L are, respectively, the energy and the angular momentum of the particle. Here, it is important to recall that E and L are two conserved quantities.

For the general trajectory previously described, the expression (6) of the source is then given by

$$\rho(x)=q\delta(\theta-\pi/2)\int_\gamma\frac{d\tau}{r_p^2(\tau)}\delta(t-t_p(\tau)) \times\delta(r-r_p(\tau))\delta(\varphi-\varphi_p(\tau)). \tag{26}$$

III. WAVEFORMS EMITTED BY A SCALAR POINT PARTICLE ON A PLUNGE TRAJECTORY

A. Source due to a scalar point particle on a plunge trajectory

In this section, we consider a particle plunging into the BH from the ISCO at $r_{\rm ISCO}=6M$ or, more precisely, from slightly below the ISCO. In order to describe its trajectory, we need its angular momentum and its energy on the ISCO. They are determined by using Eqs. (A1) and (A2), which have been established for an arbitrary circular trajectory. We have

$$\frac{L_{\rm ISCO}}{m_0}=2\sqrt{3}M \tag{27a}$$

and

$$\frac{E_{\rm ISCO}}{m_0}=\frac{2\sqrt{2}}{3}. \tag{27b}$$

Substituting $L_{\rm ISCO}$ and $E_{\rm ISCO}$ into the geodesic equations (25a)–(25c), we obtain after integration

$$\frac{t_p(r)}{2M}=\frac{2\sqrt{2}(r-24M)}{2M(6M/r-1)^{1/2}}-22\sqrt{2}\tanh^{-1}[(6M/r-1)^{1/2}] +2\tanh^{-1}[(3M/r-1/2)^{1/2}]+\frac{t_0}{2M} \tag{28}$$

and

$$\varphi_p(r)=-\frac{2\sqrt{3r}}{(6M-r)^{1/2}}+\varphi_0, \tag{29}$$

where t_0 and φ_0 are two arbitrary integration constants. From (29), we can write the spatial trajectory of the plunging particle in the form

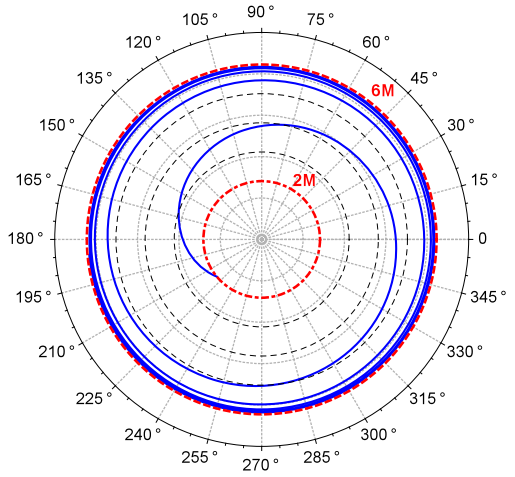

FIG. 1 (color online). The plunge trajectory obtained from Eq. (30). Here, we assume that the particle starts at $r=r_{\rm ISCO}(1-\epsilon)$ with $\epsilon=10^{-2}$, and we take $\varphi_0=0$. The red dashed line at $r=6M$ and the red dot-dashed line at $r=2M$ represent the ISCO and the horizon, respectively.

$$r_p(\varphi)=\frac{6M}{[1+12/(\varphi-\varphi_0)^2]}. \tag{30}$$

This trajectory is displayed in Fig. 1.

After integration and by using, in particular, the change of variable $\tau\to\varphi_p(\tau)$, Eq. (26) leads to

$$\rho(t,r,\theta,\varphi)=\frac{1}{2\pi}\int_{-\infty}^{+\infty}d\omega e^{-i\omega t}\sum_{\ell=0}^{+\infty}\sum_{m=-\ell}^{+\ell}\left\{\frac{3q}{\sqrt{r}} \times\frac{e^{i[\omega t_p(r)-m\varphi_p(r)]}}{(6M-r)^{3/2}}Y^*_{\ell m}\left(\frac{\pi}{2},0\right)\right\}Y_{\ell m}(\theta,\phi), \tag{31}$$

and we can then show that (31) can be written in the form (9) with

$$\rho_{\omega\ell m}(r)=\frac{3q\sqrt{r}}{\sqrt{2\pi}}\frac{e^{i[\omega t_p(r)-m\varphi_p(r)]}}{(6M-r)^{3/2}}Y^*_{\ell m}\left(\frac{\pi}{2},0\right). \tag{32}$$

B. Quadrupolar waveform produced by the plunging particle

From Eq. (24) with the source term given by Eq. (32), we can now obtain numerically the partial waveform $\phi_{\ell m}(t,r)$ emitted by the plunging particle. In this section, we shall only focus on the $(\ell=2,m=2)$ mode of the scalar field, and we shall emphasize the role of the mass parameter μ and the location of the observer.

In Figs. 2, 3, and 4, we display the partial waveforms corresponding, respectively, to the values $\tilde{\alpha}=0$, 0.25, and 0.35 of the reduced mass parameter. For each one, we consider that the observer is located at $r=10M$, $20M$, and

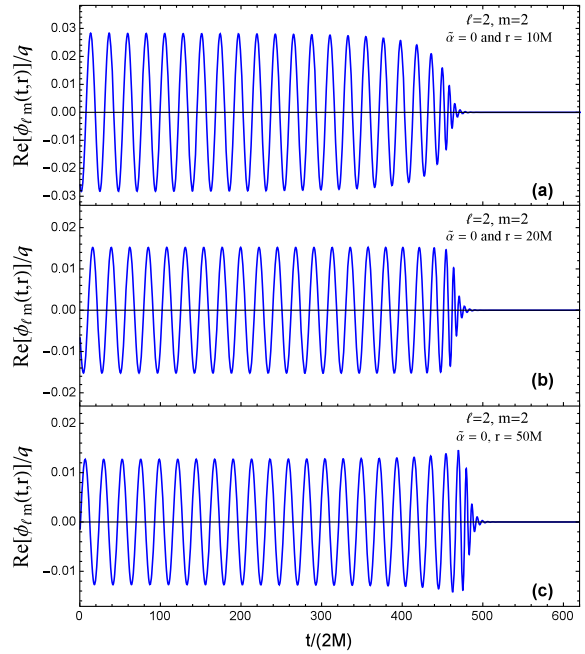

FIG. 2 (color online). Quadrupolar waveforms produced by the plunging particle. The results are obtained for a massless scalar field ($\tilde{\alpha} = 0$), and the observer is located at (a) $r = 10M$, (b) $r = 20M$, and (c) $r = 50M$.

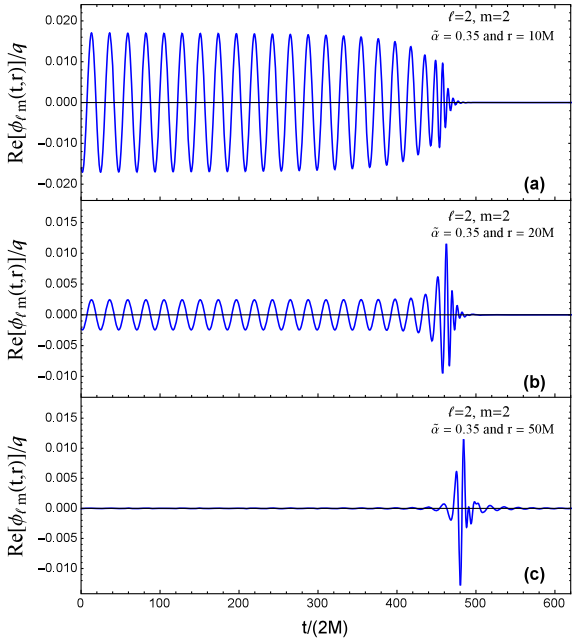

FIG. 4 (color online). Quadrupolar waveforms produced by the plunging particle. The results are obtained for a massive scalar field ($\tilde{\alpha} = 0.35$ is above the threshold $\tilde{\alpha}_c \approx 0.2722$), and the observer is located at (a) $r = 10M$, (b) $r = 20M$, and (c) $r = 50M$.

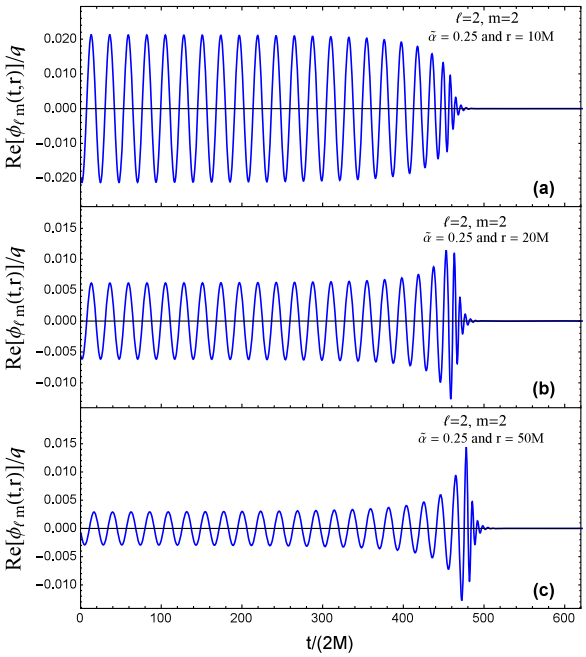

FIG. 3 (color online). Quadrupolar waveforms produced by the plunging particle. The results are obtained for a massive scalar field ($\tilde{\alpha} = 0.25$ is below the threshold $\tilde{\alpha}_c \approx 0.2722$), and the observer is located at (a) $r = 10M$, (b) $r = 20M$, and (c) $r = 50M$.

$50M$. The waveforms have been obtained by assuming that the particle starts at $r = r_{\mathrm{ISCO}}(1-\epsilon)$ with $\epsilon = 10^{-4}$, and furthermore, we have taken $\varphi_0 = 0$ and $t_0/(2M) = 500$ in order to shift the interesting part of the signal in the window $t/(2M) \in [0, 600]$. To construct these waveforms and, in particular, to obtain the functions $\phi^{\mathrm{in}}_{\omega\ell}$ and $\phi^{\mathrm{up}}_{\omega\ell}$ as well as the coefficient $A^{(-)}_{\ell}(\omega)$, we have numerically integrated the Regge-Wheeler equation (14) with the Runge-Kutta method. The initialization of the process has been achieved with Taylor series expansions converging near the horizon, and we have compared the solutions to asymptotic expansions with ingoing and outgoing at spatial infinity that we have decoded by Padé summation. Moreover, in Eq. (24), we have discretized the integral over ω. For $\tilde{\alpha} = 0$, 0.25, and 0.35, in order to obtain numerically stable waveforms, we can limit the range of frequencies to $-6 \leq 2M\omega \leq +6$ and take for the frequency resolution $2M\delta\omega = 1/10000$. It should be noted, however, that in order to extract correctly the spectral content of the signals (see Sec. III E), it is necessary to work with higher-frequency resolutions which strongly depend on the mass parameter $\tilde{\alpha}$. For example, for $\tilde{\alpha} = 0$ it is sufficient to take $2M\delta\omega = 1/10000$, while for $\tilde{\alpha} = 0.35$, we have worked with $2M\delta\omega = 1/100000$.

For the massless scalar field (see Fig. 2), the waveforms can be decomposed in three phases: (i) an "adiabatic phase" corresponding to the quasicircular motion of the particle near the ISCO (see Fig. 1), (ii) a ringdown phase due to the

excitation of QNMs, and (iii) a late-time phase. Such a decomposition remains roughly valid for the massive field (compare Figs. 3 and 4 with Fig. 2), but now, as we shall see in more detail in the following subsections, the behavior of the signal is modified by the excitation of the QBSs, and moreover, at a large distance from the BH, it strongly depends on a threshold value $\tilde{\alpha}_c$ of the dimensionless coupling constant $\tilde{\alpha}$ which separates the regions where the (ℓ, m) mode of the field is propagating (but dispersive) or evanescent. This threshold corresponds to the mass parameter $\mu_c = 2\Omega_{\rm ISCO}$, where $\Omega_{\rm ISCO}$ denotes the angular velocity of the particle moving on the ISCO or, in other words, its orbital frequency. The existence of this threshold and its consequences are discussed in detail in Appendix A.

C. The adiabatic phase and the circular motion of the particle on the ISCO

In Figs. 5 and 6, we compare the quadrupolar waveform produced by the plunging particle we have obtained in Sec. III B with the quadrupolar waveform produced by a particle orbiting the BH on the ISCO we discuss in Appendix A. We consider two particular masses given by $\tilde{\alpha} = 0.25$ and $\tilde{\alpha} = 0.35$, i.e., one below the threshold value $\tilde{\alpha}_c \approx 0.2722$ and the other one above, but the discussion remains valid even for other masses if they are not too large. In the adiabatic phase, the waveform emitted by the plunging particle is described very accurately by the waveform emitted by the particle living on the ISCO. This can be easily understood by noting that the initial position of the plunging particle is very close to the ISCO so that it undergoes an adiabatic inspiral along a sequence of quasicircular orbits near the ISCO. As a consequence, the comments made in Appendix A (see also Fig. 13) permit us to understand the behavior of the waveform in the adiabatic phase and to interpret Figs. 3 and 4. It is, in particular, important to note that in the adiabatic phase,

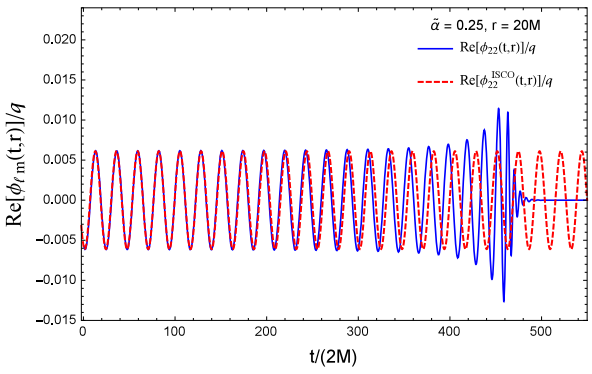

FIG. 5 (color online). Quadrupolar waveforms produced by the plunging particle (blue line) and by a particle orbiting the BH on the ISCO (red dashed line). The reduced mass $(\tilde{\alpha} = 0.25)$ is below the threshold $(\tilde{\alpha}_c \approx 0.2722)$.

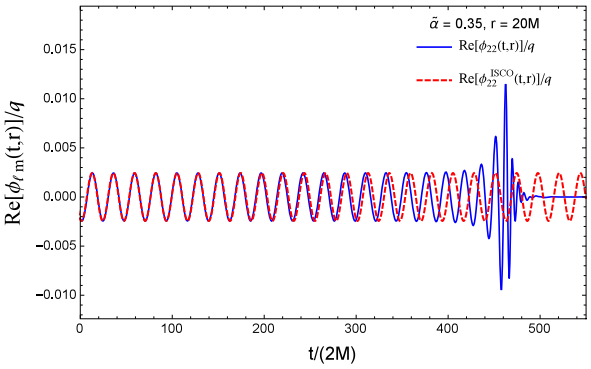

FIG. 6 (color online). Quadrupolar waveforms produced by the plunging particle (blue line) and by a particle orbiting the BH on the ISCO (red dashed line). The reduced mass $(\tilde{\alpha} = 0.35)$ is above the threshold $(\tilde{\alpha}_c \approx 0.2722)$.

(1) For a given "distance" r of the observer, the waveform amplitude decreases as the mass increases and vanishes for large masses.
(2) Above the threshold, for an observer at spatial infinity, the waveform amplitude vanishes. (However, as we shall see in Sec. III E, this result is slightly modified due to the excitation of the long-lived QBSs.)

D. The ringdown phase and the excitation of QNMs

In Figs. 7 and 8, we compare the quadrupolar waveform produced by the plunging particle we have obtained in Sec. III B with the quadrupolar quasinormal waveform $\phi_{220}^{\rm QNM}$ given by Eq. (B3), which corresponds to the fundamental $(\ell = 2, n = 0)$ QNM we discuss in Appendix B. We have considered two locations for the observer ($r = 10M$ and $r = 50M$) and three particular reduced masses given by $\tilde{\alpha} = 0$, 0.25, and 0.35. When the reduced mass $\tilde{\alpha}$ and the distance r are not too large, the quasinormal waveform describes very accurately the ringdown phase. However, we have checked that if the reduced mass $\tilde{\alpha}$ or the distance r increases, the agreement is not so good [cf. e.g., Fig. 8(c), where $\tilde{\alpha}$ and r are both large]. In our opinion, this is due to the excitation of QBSs (see Sec. III E) which blur the QNM contribution.

E. Excitation of QBSs

In this subsection, we focus on the spectral content of the waveform by considering separately the adiabatic and the late-time phases. The associated spectral contents can be obtained by using the Fourier transform machinery and limiting the time integrations to the considered phase.

In Figs. 9 and 10, we display the spectral content of the adiabatic phase of the quadrupolar waveform produced by the plunging particle. For a reduced mass parameter $\tilde{\alpha}$ below the threshold $\tilde{\alpha}_c$ (see Fig. 9), we can observe a peak at $\omega = 2\Omega_{\rm ISCO}$. It is, of course, associated with the

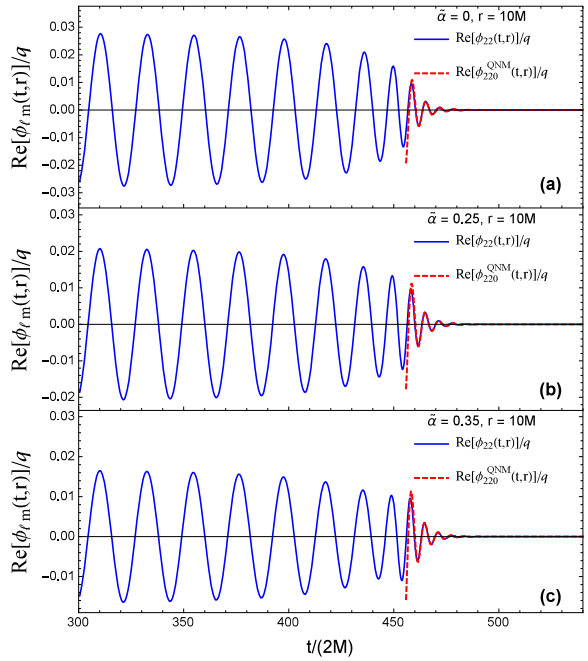

FIG. 7 (color online). Comparison of the quadrupolar waveform produced by the plunging particle (blue line) and the quadrupolar quasinormal waveform (red dashed line). The results are obtained for an observer at $r = 10M$.

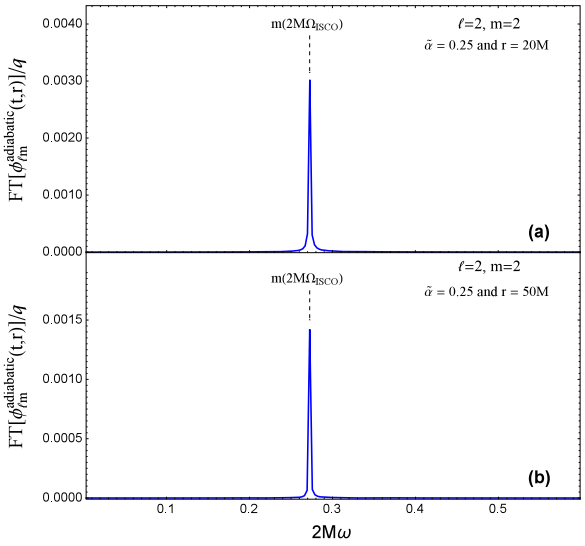

FIG. 9 (color online). Spectral content of the adiabatic phase of the quadrupolar waveform produced by the plunging particle. The results are obtained for a massive scalar field ($\tilde{\alpha} = 0.25$ is below the threshold $\tilde{\alpha}_c \approx 0.2722$), and the observer is located at (a) $r = 20M$ and (b) $r = 50M$. We observe the signature of the quasicircular motion of the plunging particle.

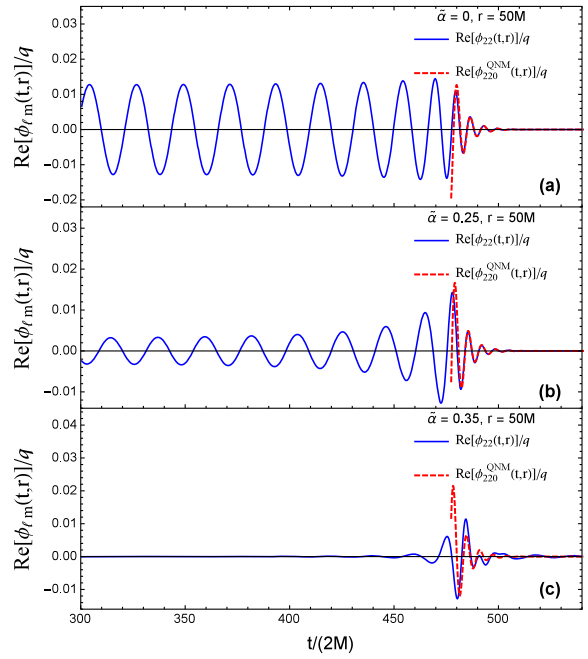

FIG. 8 (color online). Comparison of the quadrupolar waveform produced by the plunging particle (blue line) and the quadrupolar quasinormal waveform (red dashed line). The results are obtained for an observer at $r = 50M$.

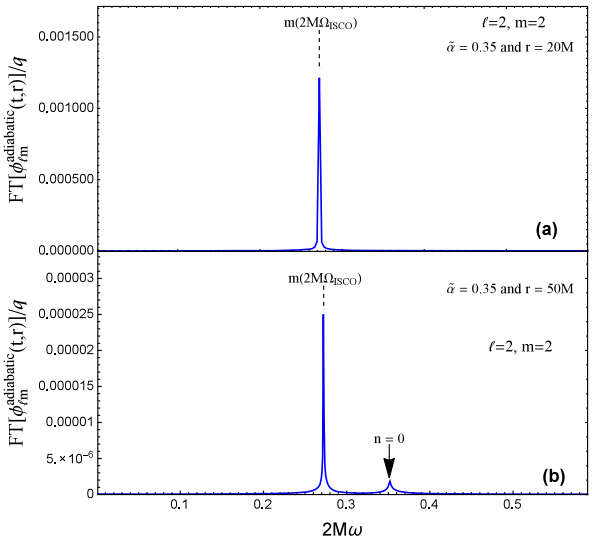

FIG. 10 (color online). Spectral content of the adiabatic phase of the quadrupolar waveform produced by the plunging particle. The results are obtained for a massive scalar field ($\tilde{\alpha} = 0.35$ is above the threshold $\tilde{\alpha}_c \approx 0.2722$), and the observer is located at (a) $r = 20M$ and (b) $r = 50M$. We observe, in addition to the signature of the quasicircular motion of the plunging particle, that of the first long-lived QBS.

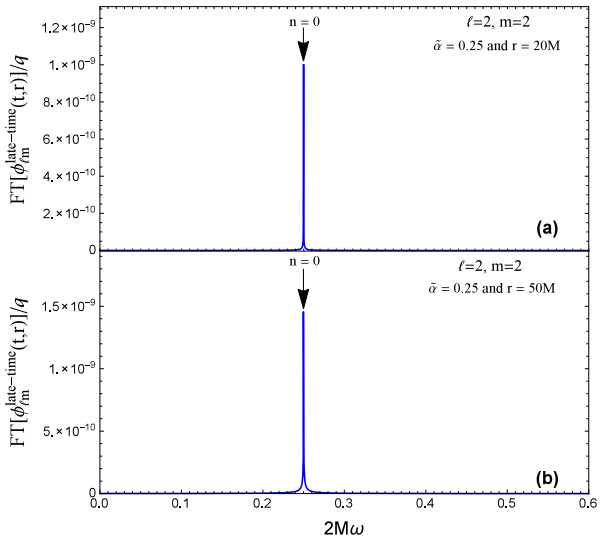

FIG. 11 (color online). Spectral content of the late-time phase of the quadrupolar waveform produced by the plunging particle. The results are obtained for a massive scalar field ($\tilde{\alpha} = 0.25$ is below the threshold $\tilde{\alpha}_c \approx 0.2722$), and the observer is located at (a) $r = 20M$ and (b) $r = 50M$. We observe the signature of the first long-lived QBS.

quasicircular motion of the plunging particle near the ISCO. For a reduced mass parameter $\tilde{\alpha}$ above the threshold $\tilde{\alpha}_c$ (see Fig. 10), the same peak at $\omega = 2\Omega_{\mathrm{ISCO}}$ is present. However, it is important to note that its height decreases very rapidly as the distance r of the observer increases. This is due to the evanescent character of the $(\ell = 2, m = 2)$

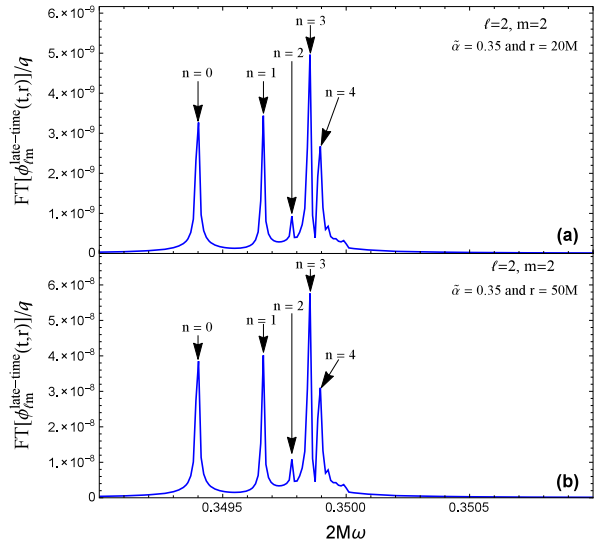

FIG. 12 (color online). Spectral content of the late-time phase of the quadrupolar waveform produced by the plunging particle. The results are obtained for a massive scalar field ($\tilde{\alpha} = 0.35$ is above the threshold $\tilde{\alpha}_c \approx 0.2722$), and the observer is located at (a) $r = 20M$ and (b) $r = 50M$. We observe the signature of the first long-lived QBSs.

mode below $\tilde{\alpha}_c$. It is, moreover, very interesting to remark the presence of another peak at a frequency corresponding to the real part of the complex frequency of the first long-lived QBS (see Table II). In other terms, we can observe the excitation of the first QBS in the adiabatic phase. As we have already noted in Sec. III C, above the threshold, for an observer at a large distance from the BH, the contribution of the quadrupolar waveform associated with the quasicircular motion vanishes, but the QBSs pick up the slack.

In Figs. 11 and 12, we display the spectral content of the late-time phase of the quadrupolar waveform produced by the plunging particle. We can observe the excitation of QBSs (see also Table II). We can also note that, as the reduced mass parameter $\tilde{\alpha}$ increases, the spectrum of the frequencies of the QBSs spreads more and more, and it is then possible to separate the different excitation frequencies.

IV. CONCLUSION AND PERSPECTIVES

If the graviton has a mass, the study of the gravitational radiation generated by a particle plunging into a BH is certainly a problem of fundamental importance whose solution could help us to test the various massive gravity theories. Because this problem seems to us rather difficult, theoretically as well as numerically, we have chosen to work with a toy model where the massive spin-2 perturbations of the BH are replaced by a massive scalar field, and we have considered that this field and the plunging particle are linearly coupled. In our opinion, the study of the scalar radiation generated by the plunging particle has permitted us to exhibit some features that should also be present in the solution of the analogous problem in massive gravity, because they are directly associated with characteristics shared by the massive scalar and spin-2 fields, such as (i) the propagating or evanescent nature of the partial modes and (ii) the existence of QBSs.

In this article, by limiting our study to the case of the Schwarzschild BH and to the $(\ell = 2, m = 2)$ mode of the scalar field, we have more particularly shown that

(1) The waveform produced by a particle plunging into a Schwarzschild BH from slightly below the ISCO can be roughly decomposed in three phases: (i) an adiabatic phase corresponding to the quasicircular motion of the particle near the ISCO, (ii) a ringdown phase due to the excitation of QNMs, and (iii) a late-time phase.

(2) In the adiabatic phase, for an observer at a large distance from the BH, the behavior of the waveform depends on a threshold value $\tilde{\alpha}_c$ of the reduced mass parameter $\tilde{\alpha}$. This threshold corresponds to the mass parameter $\mu_c = 2\Omega_{\mathrm{ISCO}}$, where Ω_{ISCO} denotes the orbital frequency of the particle moving on the ISCO. This threshold value separates the dispersive and the evanescent regimes. Above the threshold, for an observer at spatial infinity, the waveform amplitude vanishes. For a given distance r of the observer,

the waveform amplitude decreases as the mass increases and vanishes for large masses.

(3) The ringdown phase (oscillations and damping) is very well described from the excitation of the first QNM, i.e., the least damped one.

(4) In the late-time phase, whatever the mass parameter, we can observe the excitation of QBSs. In the adiabatic phase, the excitation of QBSs only occurs for masses above the threshold. These QBSs could dominate the signal at a large distance from the BH.

(5) For large masses, the ringdown phase is modified by the excitation of QBSs which blur the QNM contribution.

It should be noted that, *mutatis mutandis*, the behaviors of an arbitrary (ℓ, m) waveform and of the quadrupolar waveform generated by the plunging particle are quite similar. In general, the waveform amplitude in the adiabatic phase decreases as ℓ increases or m decreases (see Figs. 14 and 15). However, it should be noted that this does not remain true around the threshold values for an observer at a large distance from the BH (see Fig. 14).

We hope in the near future to extend this work to the massive spin-2 perturbations of the Schwarzschild BH and to consider higher values of the mass parameter in order to check if the intrinsic giant ringings predicted in our previous works [29,30] are generated in physical processes. With this aim in view, there remain a lot of theoretical and numerical difficulties to overcome.

ACKNOWLEDGMENTS

We gratefully acknowledge Thibault Damour for drawing some years ago the attention of one of us (A. F.) to the plunge regime. We wish also to thank Andrei Belokogne for various discussions and the "Collectivité Territoriale de Corse" for its support through the COMPA project.

APPENDIX A: WAVEFORMS PRODUCED BY A SCALAR POINT PARTICLE LIVING ON THE ISCO

In this Appendix, we provide a simple closed-form expression for the emitted waveform when the particle lives on the ISCO, and we analyze its behavior as the reduced mass parameter $\tilde{\alpha}$ increases and as the distance r of the observer changes. These results are helpful in order to describe the adiabatic phase of the waveform emitted by a point particle on a plunge trajectory (see Sec. III C).

1. Source due to a point particle on a circular orbit and associated waveform

Here, we assume that the particle moves on a circular orbit with radius r_0; i.e., we have $r_p(\tau) = r_0 = \text{Const.}$ in the geodesic equations (25). After integration, they provide for the angular momentum and the energy of the particle,

$$\frac{L}{m_0} = \left(\frac{M r_0}{1 - 3M/r_0}\right)^{1/2} \tag{A1}$$

and

$$\frac{E}{m_0} = \frac{(1 - 2M/r_0)}{(1 - 3M/r_0)^{1/2}}. \tag{A2}$$

Moreover, we find that the angular coordinate φ_p is given by

$$\varphi_p(\tau) = \left(\frac{M}{r_0^3(1 - 3M/r_0)}\right)^{1/2} \tau \tag{A3}$$

if we use the proper time to describe the particle motion and by

$$\varphi_p(t) = \Omega t \tag{A4}$$

if we use the Schwarzschild time. In Eq. (A4),

$$\Omega = \left(\frac{M}{r_0^3}\right)^{1/2} \tag{A5}$$

denotes the angular velocity of the particle (i.e., its orbital frequency).

After integration and by using, in particular, the change of variable $\tau \to \varphi_p(\tau)$, we can show that (26) can be written in the form (9) with

$$\rho_{\omega\ell m}(r) = \frac{\sqrt{2\pi} q}{r_0}\left(1 - \frac{3M}{r_0}\right)^{1/2} \times \delta(r - r_0)\delta(\omega - m\Omega) Y^*_{\ell m}\left(\frac{\pi}{2}, 0\right). \tag{A6}$$

The (ℓ, m) waveform produced by the particle orbiting the BH on a circular orbit with radius r_0 can now be obtained by substituting the source term (A6) in Eq. (24). After integration, we have

$$\phi_{\ell m}(t, r) = -\frac{q}{2ir_0}\left(1 - \frac{3M}{r_0}\right)^{1/2} Y^*_{\ell m}\left(\frac{\pi}{2}, 0\right) \times \left[\frac{\phi^{\text{up}}_{\omega\ell}(r)\phi^{\text{in}}_{\omega\ell}(r_0)}{\omega A^{(-)}_{\ell}(\omega)} e^{-i\omega t}\right]_{\omega = m\Omega}. \tag{A7}$$

It should be noted that (i) $\phi_{\ell -m} = (-1)^m \phi^*_{\ell m}$, so we can limit our study to the modes with $m \geq 0$; and (ii) $\phi_{\ell m} = 0$ for $\ell - m$ odd. This will simplify the discussions in the next subsection.

2. Waveforms for a particle on the ISCO

We now specialize to the point particle living on the ISCO, i.e., we assume that $r_0 = 6M$ in the waveform (A7), and we note also that (A5) reduces to

$$\Omega_{\mathrm{ISCO}} = \frac{1}{6\sqrt{6}M}. \tag{A8}$$

We intend to highlight both the influence of the mass μ of the scalar field and the distance r of the observer, and to show more particularly that the classical and well-known results concerning the massless field cannot be naively extended to massive fields.

In Fig. 13, we focus on the $(\ell = 2, m = 2)$ waveform. For an observer at spatial infinity, the behavior of the waveform amplitude depends in a complex way on the mass of the scalar field. This is due to the term $p(\omega = m\Omega_{\mathrm{ISCO}}) = [(m\Omega_{\mathrm{ISCO}})^2 - \mu^2]^{1/2}$, which is implicitly present in the expression (A7) of the waveform. Indeed, depending on whether $\mu < \mu_c$ or $\mu > \mu_c$ with

$$\mu_c = m\Omega_{\mathrm{ISCO}}, \tag{A9}$$

this term is responsible for the propagating (but dispersive) or evanescent character of the (ℓ, m) mode of the massive field. In Fig. 13, we observe the decreasing of the waveform amplitude when the reduced mass parameter $\tilde{\alpha}$ increases, and we note that, above the threshold value $\tilde{\alpha}_c$ corresponding to μ_c, the amplitude vanishes. As a consequence, above $\tilde{\alpha}_c$, the excitation of the system scalar field–BH by a particle orbiting on the ISCO cannot be observed at spatial infinity. This abrupt behavior remains valid for large distances (for $r \geq 50M$) but is smoothed for short distances with a vanishing of the amplitude for large masses. As a consequence, for "very" massive scalar fields, the excitation of the system scalar field–BH by a particle orbiting ISCO cannot be observed whatever the distance.

In Figs. 14 and 15, we show that the behavior of the $(\ell = 2, m = 2)$ waveform can also be observed for arbitrary (ℓ, m) waveforms. Moreover, in Fig. 14, it is

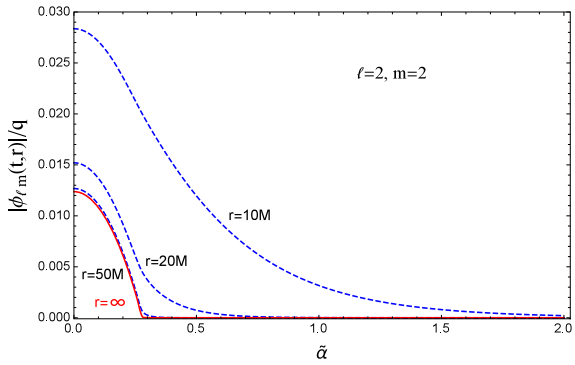

FIG. 13 (color online). Waveform amplitudes for a particle on the ISCO and reduced masses in the range $\tilde{\alpha} \in [0, 2]$. The results are obtained from (A7) for the particular $(\ell = 2, m = 2)$ mode. We study the role of the location of the observer. For an observer at a large distance from the BH, the transition between the propagating (but dispersive) and evanescent behaviors of the response occurs at $\tilde{\alpha}_c \approx 0.2722$.

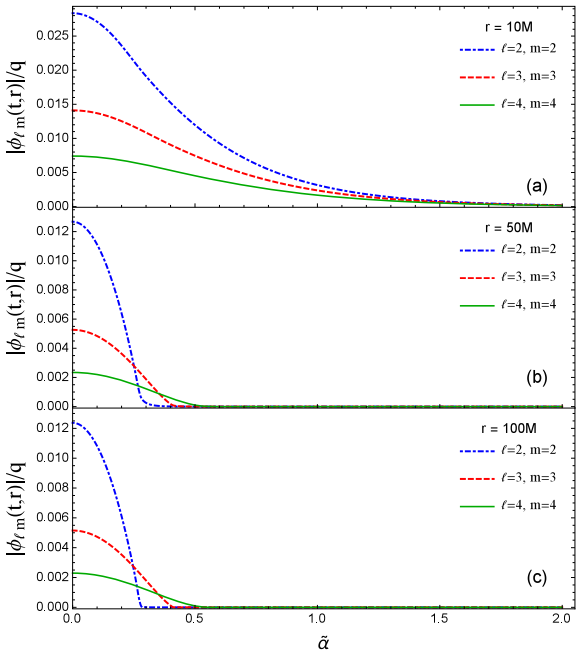

FIG. 14 (color online). Waveform amplitudes for a particle on the ISCO and reduced masses in the range $\tilde{\alpha} \in [0, 2]$. The results are obtained from (A7) for some $(\ell, m = \ell)$ modes and an observer at (a) $r = 10M$, (b) $r = 50M$, and (c) $r = 100M$. The transition between the propagating (but dispersive) and evanescent behaviors of the response occurs at $\tilde{\alpha}_c \approx 0.2722$ for the $(\ell = 2, m = 2)$ mode, at $\tilde{\alpha}_c \approx 0.4082$ for the $(\ell = 3, m = 3)$ mode, and at $\tilde{\alpha}_c \approx 0.5443$ for the $(\ell = 4, m = 4)$ mode.

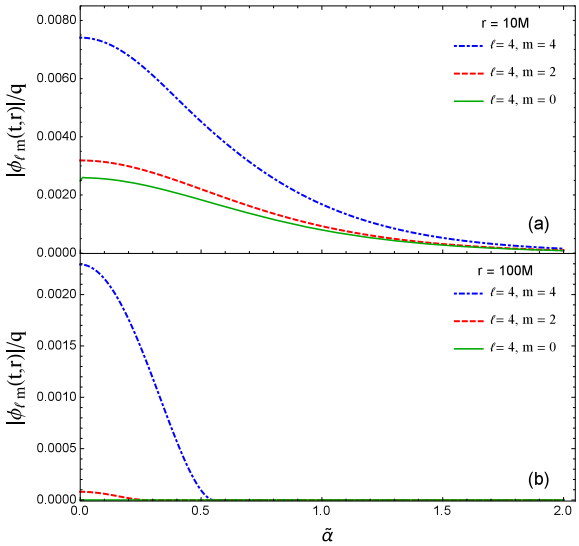

FIG. 15 (color online). Waveform amplitudes for a particle on the ISCO and reduced masses in the range $\tilde{\alpha} \in [0, 2]$. The results are obtained from (A7) for modes with angular momentum $\ell = 4$. We study the influence of the azimuthal number m for an observer at (a) $r = 10M$ and (b) $r = 100M$.

interesting to note that, in a large domain around the particular threshold masses, the mode with the lowest ℓ does not provide the greatest waveform amplitudes. In this, a massive field is completely different from a massless one. Furthermore, in Fig. 15 we can observe that, for a given ℓ, the waveform amplitude decreases with m, and therefore that the $(\ell, m = \pm\ell)$ modes induce the highest amplitudes. Such behavior is well known for massless fields, and we can see that it remains valid for massive fields.

APPENDIX B: QUASINORMAL FREQUENCIES, QNMs AND ASSOCIATED RINGINGS

In this Appendix, we consider the weakest damped QNM with $\ell = 2$, and we obtain numerically its response when it is excited by the plunging particle. This result is helpful in order to describe the ringdown phase of the waveform emitted by a point particle on a plunge trajectory (see Sec. III D).

The response of a QNM to an excitation (the so-called quasinormal waveform or, in other words, the associated ringing) can be constructed from (i) the intrinsic characteristics of the BH (the quasinormal frequency $\omega_{\ell n}$, the QNM itself and the corresponding excitation factor $\mathcal{B}_{\ell n}$—here $n = 0$ corresponds to the fundamental QNM, i.e., the least damped one and $n = 1, 2, \ldots$ to the overtones), and (ii) the source of the excitation. In the following subsections, we describe this construction.

1. Quasinormal frequencies and excitation factors

We recall that the quasinormal frequencies $\omega_{\ell n}$ are the zeros of the Wronskian $W_\ell(\omega)$ given by Eq. (17) lying in the lower part of the first Riemann sheet associated with the function $p(\omega) = (\omega^2 - \mu^2)^{1/2}$ (see Fig. 16), and that the corresponding excitation factors are defined by

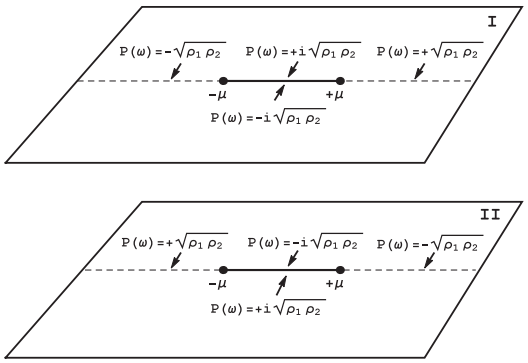

FIG. 16. The two Riemann sheets of the function $p(\omega) = (\omega^2 - \mu^2)^{1/2}$ and the branch cut we have chosen. We have introduced the polar coordinates (ρ_1, θ_1) and (ρ_2, θ_2) such that $\omega - \mu = \rho_1 e^{i\theta_1}$ and $\omega + \mu = \rho_2 e^{i\theta_2}$. Here $0 \leq \theta_1, \theta_2 < 2\pi$.

$$\mathcal{B}_{\ell n} = \left[\frac{1}{2p(\omega)}\frac{A_\ell^{(+)}(\omega)}{\frac{dA_\ell^{(-)}(\omega)}{d\omega}}\right]_{\omega=\omega_{\ell n}}. \tag{B1}$$

It should be noted that when the Wronskian $W_\ell(\omega)$ vanishes (i.e., if $\omega = \omega_{\ell n}$), the functions $\phi^{\rm in}_{\omega\ell}$ and $\phi^{\rm up}_{\omega\ell}$ are linearly dependent and propagate inward at the horizon and outward at spatial infinity, such behavior defining the QNMs.

We also recall that the complex spectrum of the quasinormal frequencies is symmetric with respect to the imaginary ω axis. In other words, if $\omega_{\ell n}$ is a quasinormal frequency lying in the fourth quadrant, $-\omega^*_{\ell n}$ is the symmetric quasinormal frequency lying in the third one. In Table I, we have considered the least damped $\ell = 2$ QNM, and we have given its quasinormal frequency ω_{20} with the positive real part and the associated excitation factor $\mathcal{B}_{20}$ for three particular values of the reduced mass parameter $\tilde{\alpha}$. The results have been obtained by using the numerical methods described in Sec. II of Ref. [30].

2. Quasinormal waveforms

We now deform the contour of integration in Eq. (24) in order to extract a residue series over the quasinormal frequencies. It is given by

$$\phi^{\rm QNM}_{\ell m}(t, r) = \sum_{n=0}^{+\infty} \phi^{\rm QNM}_{\ell mn}(t, r) \tag{B2}$$

with

$$\phi^{\rm QNM}_{\ell mn}(t, r) = \sqrt{2\pi}(\mathcal{C}_{\ell mn}\phi^{\rm up}_{\omega_{\ell n}\ell}(r_*)e^{-i\omega_{\ell n}t} + \mathcal{D}_{\ell mn}[\phi^{\rm up}_{\omega_{\ell n}\ell}(r_*)]^* e^{i\omega^*_{\ell n}t}). \tag{B3}$$

Here $\mathcal{C}_{\ell mn}$ and $\mathcal{D}_{\ell mn}$ denote the extrinsic excitation coefficients defined by

$$\mathcal{C}_{\ell mn} = \mathcal{B}_{\ell n}\left[\int_{2M}^{+\infty} dr' \frac{\phi^{\rm in}_{\omega\ell}(r')\rho_{\omega\ell m}(r')}{[\omega/p(\omega)]A^{(+)}_\ell(\omega)}\right]_{\omega=\omega_{\ell n}} \tag{B4}$$

and

TABLE I. Evolution of the quasinormal frequency and the excitation factor of the fundamental $\ell = 2$ QNM.

(ℓ, n)	$\tilde{\alpha}$	$2M\omega_{\ell n}$	$\mathcal{B}_{\ell n}$
(2,0)	0	$0.96729 - 0.19352i$	$0.11935 + 0.01343i$
(2,0)	0.25	$0.97717 - 0.19012i$	$0.12241 + 0.00737i$
(2,0)	0.35	$0.98669 - 0.18684i$	$0.12548 + 0.00091i$

$$\mathcal{D}_{\ell mn} = [\mathcal{B}_{\ell n}]^* \left[\int_{2M}^{+\infty} dr' \frac{\phi^{\rm in}_{\omega\ell}(r')\rho_{\omega\ell m}(r')}{[\omega/p(\omega)]A^{(+)}_{\ell}(\omega)} \right]_{\omega=-\omega^*_{\ell n}}. \tag{B5}$$

The first term in Eq. (B3) is the contribution of the quasinormal frequency $\omega_{\ell n}$ lying in the fourth quadrant of the first Riemann sheet of $p(\omega)$, while the second one is the contribution of $-\omega^*_{\ell n}$, i.e., its symmetric with respect to the imaginary axis. The expression (B3) has been simplified by using some symmetry properties in the change $\omega_{\ell n} \to -\omega^*_{\ell n}$ and, in particular,

$$p(-\omega^*_{\ell n}) = -[p(\omega_{\ell n})]^*, \tag{B6a}$$

$$\phi^{\rm in}_{-\omega^*_{\ell n}\ell} = [\phi^{\rm in}_{\omega_{\ell n}\ell}]^*, \tag{B6b}$$

$$\phi^{\rm up}_{-\omega^*_{\ell n}\ell} = [\phi^{\rm up}_{\omega_{\ell n}\ell}]^*. \tag{B6c}$$

It should be noted that, in our problem, the spherical symmetry of the Schwarzschild BH is broken due to the asymmetric plunging trajectory. It is this dissymmetry which, in connection with the presence of the azimuthal number m, forbids us to gather the two terms in Eq. (B3).

Let us finally remark that $\phi^{\rm QNM}_{\ell mn}(t,r)$ does not provide physically relevant results at "early times" due to its exponentially divergent behavior as t decreases. It is necessary to determine, from physical considerations when this is possible or by using a numerical approach, the time beyond which this waveform can be used, i.e., the starting time $t_{\rm start}$ of the BH ringing.

TABLE II. Complex frequencies $\omega_{\ell n}$ of the first long-lived QBSs.

(ℓ, n)	$\tilde{\alpha}$	$2M\omega_{\ell n}$
(2,0)	0	…
(2,0)	0.25	$0.24978 - 6.08009 \times 10^{-17} i$
(2,1)		$0.24988 - 3.63454 \times 10^{-17} i$
(2,0)	0.35	$0.34940 - 1.08832 \times 10^{-14} i$
(2,1)		$0.34966 - 1.03797 \times 10^{-14} i$
(2,2)		$0.34978 - 3.90581 \times 10^{-15} i$
(2,3)		$0.34985 - 2.42608 \times 10^{-15} i$
(2,4)		$0.34989 - 1.59115 \times 10^{-15} i$

APPENDIX C: COMPLEX FREQUENCIES OF THE FIRST QBSs

The complex frequencies $\omega_{\ell n}$ of the QBSs are the zeros of the Wronskian $W_\ell(\omega)$ given by Eq. (17) lying in the lower part of the second Riemann sheet associated with the function $p(\omega) = (\omega^2 - \mu^2)^{1/2}$ (see Fig. 16). Their spectrum is symmetric with respect to the imaginary ω axis. They can be numerically obtained by using the method which has permitted us to determine in Sec. 1 of Appendix B the quasinormal frequencies, but now, because we are working on the second Riemann sheet associated with $p(\omega)$, it is necessary to use $-p(\omega)$ instead of $p(\omega)$ (see also Fig. 16). In Table II, we have given a sample of the complex frequencies of the long-lived QBSs relevant to the spectral content of the waveform emitted by the plunging particle (see Sec. III E).

[1] M. Fierz, Helv. Phys. Acta **12**, 3 (1939).
[2] M. Fierz and W. Pauli, Proc. R. Soc. A **173**, 211 (1939).
[3] K. Hinterbichler, Rev. Mod. Phys. **84**, 671 (2012).
[4] C. de Rham, Living Rev. Relativity **17**, 7 (2014).
[5] A. S. Goldhaber and M. M. Nieto, Rev. Mod. Phys. **82**, 939 (2010).
[6] M. S. Volkov, Classical Quantum Gravity **30**, 184009 (2013).
[7] E. Babichev and A. Fabbri, Classical Quantum Gravity **30**, 152001 (2013).
[8] R. Brito, V. Cardoso, and P. Pani, Phys. Rev. D **88**, 023514 (2013).
[9] R. Brito, V. Cardoso, and P. Pani, Phys. Rev. D **87**, 124024 (2013).
[10] S. L. Detweiler and E. Szedenits, Astrophys. J. **231**, 211 (1979).
[11] K. Oohara and T. Nakamura, Prog. Theor. Phys. **70**, 757 (1983).
[12] A. Buonanno and T. Damour, Phys. Rev. D **59**, 084006 (1999).
[13] A. Buonanno and T. Damour, Phys. Rev. D **62**, 064015 (2000).
[14] A. Ori and K. S. Thorne, Phys. Rev. D **62**, 124022 (2000).
[15] J. G. Baker, B. Bruegmann, M. Campanelli, C. Lousto, and R. Takahashi, Phys. Rev. Lett. **87**, 121103 (2001).
[16] L. Blanchet, M. S. Qusailah, and C. M. Will, Astrophys. J. **635**, 508 (2005).
[17] M. Campanelli, C. Lousto, and Y. Zlochower, Phys. Rev. D **73**, 061501 (2006).
[18] T. Damour and A. Nagar, Phys. Rev. D **76**, 064028 (2007).
[19] U. Sperhake, E. Berti, V. Cardoso, J. A. Gonzalez, B. Bruegmann, and M. Ansorg, Phys. Rev. D **78**, 064069 (2008).
[20] Y. Mino and J. Brink, Phys. Rev. D **78**, 124015 (2008).
[21] S. Hadar and B. Kol, Phys. Rev. D **84**, 044019 (2011).
[22] S. Hadar, B. Kol, E. Berti, and V. Cardoso, Phys. Rev. D **84**, 047501 (2011).
[23] R. H. Price, G. Khanna, and S. A. Hughes, Phys. Rev. D **88**, 104004 (2013).

[24] S. Hadar, A. P. Porfyriadis, and A. Strominger, Phys. Rev. D **90**, 064045 (2014).
[25] S. Hadar, A. P. Porfyriadis, and A. Strominger, arXiv: 1504.07650.
[26] S. Hassan, A. Schmidt-May, and M. von Strauss, J. High Energy Phys. 05 (2013) 086.
[27] C. de Rham and G. Gabadadze, Phys. Rev. D **82**, 044020 (2010).
[28] C. de Rham, G. Gabadadze, and A. J. Tolley, Phys. Rev. Lett. **106**, 231101 (2011).
[29] Y. Decanini, A. Folacci, and M. Ould El Hadj, arXiv: 1401.0321.
[30] Y. Decanini, A. Folacci, and M. Ould El Hadj, Phys. Rev. D **89**, 084066 (2014).
[31] E. Poisson, A. Pound, and I. Vega, Living Rev. Relativity **14**, 7 (2011).
[32] P. M. Morse and H. Feshbach, *Methods of Theoretical Physics* (McGraw-Hill, New York, 1953).
[33] R. Breuer, P. Chrzanowksi, H. Hughes, and C. W. Misner, Phys. Rev. D **8**, 4309 (1973).

CHAPITRE 5

Sonneries géantes induites par la gravité massive

Dans ce chapitre, nous considérons exclusivement le champ de spin-2 massif du fait de son importance théorique et aussi en raison de la fascinante conséquence observationnelle que nos résultats prédisent pour un tel champ. Notre étude sera limitée à la théorie de Fierz-Pauli dans l'espace-temps de Schwarzschild [136] que l'on peut obtenir, par exemple, en linéarisant la théorie de "*ghost-free bimetric*" de Hassan, Schmidt-May et von Strauss (inspirés dans leurs recherches par les travaux fondamentaux de de Rham, Gabadadze et Tolley [208, 209]) discutée dans la Réf. [210]. En outre, nous nous focalisons principalement sur le mode impair $\ell = 1$ de ce champ (des résultats similaires peuvent être obtenus pour d'autres mode - voir Chap. 6) et sur les QNMs associés.

Nous allons d'abord mettre en évidence numériquement le comportement résonant des facteurs d'excitation du QNM ($\ell = 1, n = 0$) et discuter brièvement ses harmoniques. Ce comportement se produit dans un large domaine autour de la valeur critique du paramètre de masse μ du champ où, en plus, les QNMs sont faiblement amortis. En conséquence, il devrait induire des sonneries d'amplitude géante et à faible décroissance temporelle. Nous les construisons directement à partir des fonctions de Green retardées (un point de vue dit intrinsèque) et nous les comparons avec les sonneries générées par le QNM impair ($\ell = 2, n = 0$) de la théorie d'Einstein.

Dans une perspective de considérations observationnelles, il est nécessaire de vérifier qu'une perturbation réelle du trou noir ne neutralise pas l'effet résonant précédemment discuté. Pour cela, on étudie, ensuite, les sonneries construites à partir des coefficients d'excitation quasi-normaux (un point de vue dit extrinsèque) car ils permettent d'inclure la contribution de la perturbation dans la réponse du trou noir (voir la Réf. [211] pour une claire distinction entre les facteurs d'excitation quasi-normaux et les coefficients d'excitation quasi-normaux).

Giant black hole ringings induced by massive gravity

Yves Décanini,[1,*] Antoine Folacci,[1,†] and Mohamed Ould El Hadj[1,‡]

[1] *Equipe Physique Théorique - Projet COMPA, SPE, UMR 6134 du CNRS et de l'Université de Corse, Université de Corse, BP 52, F-20250 Corte, France*

(Dated: January 3, 2014)

A distorted black hole radiates gravitational waves in order to settle down in one of the geometries permitted by the no-hair theorem. During that relaxation phase, a characteristic damped ringing is generated. It can be theoretically constructed from the black hole quasinormal frequencies (which govern its oscillating behavior and its decay) and from the associated excitation factors (which determine intrinsically its amplitude) by carefully taking into account the source of the distortion. Here, by considering the Schwarzschild black hole in the framework of massive gravity, we show that the excitation factors have an unexpected strong resonant behavior leading to giant ringings which are, moreover, slowly decaying. Such extraordinary black hole ringings could be observed by the next generations of gravitational wave detectors and allow us to test the various massive gravity theories or their absence could be used to impose strong constraints on the graviton mass.

PACS numbers: 04.70.Bw, 04.30.-w, 04.25.Nx, 04.50.Kd

Introduction.— Gravitational waves, a major prediction of Einstein's general relativity, should be observed directly in a near future by the next generations of gravitational wave detectors. Another fascinating prediction of Einstein's theory, the existence of black holes (BHs), should be simultaneously confirmed. Indeed, if in its final stage the astrophysical process generating the observed gravitational radiation involves a distorted BH, the signal is then dominated, at intermediate time scales, by a characteristic damped ringing. It is due to the BH which radiates away all its distortions in the form of gravitational waves and relaxes toward a state permitted by the no-hair theorem. The frequencies and decay rates describing that ringing define the complex resonance spectrum of the BH. They are linked to its quasinormal modes (QNMs) [1–4], i.e., to those mode solutions of the wave equation which propagate inward at the horizon and outward at spatial infinity, and they can be considered as the BH fingerprint : they indicate beyond all doubt the existence of a horizon and they could be used to determine unambiguously the mass as well as the angular momentum of the BH.

These last years, generalizations of general relativity mediated by a massive spin-2 particle are the subject of intense activity (see Ref. [5] for a recent review). They have their source in the 70-year old Fierz-Pauli theory [6]. They are motivated by purely theoretical considerations (the study of the deformations of general relativity with the graviton mass as deformation parameter) but they also arise from field theories in spacetimes with extra dimensions. Furthermore, and this is surely the main raison of their success, they could explain, without dark energy, the accelerated expansion of the present Universe. Of course, a hypothetical massive graviton is surely an ultralight particle (see Ref. [7] for a description of the experimental constraints on the graviton mass but note that the mass limit strongly depends on the theory considered).

It is therefore natural to study BH perturbations and to reconsider gravitational radiation from BHs in massive gravity. It is only very recently that some works on this subject by Babichev and Fabbri [8] and by Brito, Cardoso and Pani [9, 10] have been achieved. They mainly discuss the fundamental problem of BH stability and therefore the existence of BHs in massive gravity. Of course, this depends on the model of gravity considered but, once we assume stability, it becomes really interesting to work on the structure of the signal emitted by a distorted BH with in mind the possibility to test, in a near future, the various massive spin-2 field theories with gravitational wave detectors.

Since the seventies, an increasing number of frequency- and time-domain studies dealing with massive fields propagating in BH spacetimes have highlighted the important modifications induced by the mass parameter which concern more or less directly the signal emitted by a distorted BH : (i) the resonance spectrum is enriched by the complex frequencies corresponding to quasibound states (see Refs. [11–14] for important pioneering works and Ref. [9] for a recent study in massive gravity); (ii) as the mass parameter increases, the quasinormal frequencies migrate in the complex plane, a behavior observed numerically by various authors (see, e.g., Refs. [15, 16] for pioneering works and Ref. [9] for a recent study in massive gravity) and analytically described recently [17, 18]; (iii) at very late time (i.e., after the quasinormal ringing), the signal emitted by the relaxing BH is not described by the usual power-law tail behavior [19] but, roughly speaking, by oscillations with a slowly-decaying amplitude (see, e.g., Ref. [20] as well as Ref. [21] for a recent study in massive gravity).

In a future article [22], we intend to discuss as fully

as possible a new effect with amazing consequences : for massive bosonic fields in the Schwarzschild spacetime, the excitation factors of the QNMs have a strong resonant behavior which induces giant ringings. It is a totally unexpected effect. Indeed, until now it was assumed that, for massive fields, quasinormal ringings are less easily excited (see the introduction of Ref. [23] and references therein). We shall describe this effect numerically and confirm it analytically from semiclassical considerations based on the properties of the unstable circular geodesics on which a massive particle can orbit the BH.

In this letter, we only consider the massive spin-2 field because of its theoretical importance and due to the fascinating observational consequences that our results predict for such a field. We limit our study to the Fierz-Pauli theory in the Schwarzschild spacetime [9] which can be obtained, e.g., by linearization of the ghost-free bimetric theory of Hassan, Schmidt-May and von Strauss discussed in Ref. [24] and which is inspired by the fundamental work of de Rham, Gabadadze and Tolley [25, 26]. Furthermore, we mainly focus on the odd-parity $\ell = 1$ mode of this field (similar results can be obtained for the other modes - see also Ref. [22]) and on the associated QNMs. Our letter is organized as follows. We first establish numerically the resonant behavior of the excitation factor of the $(\ell = 1, n = 0)$ QNM (and briefly discuss its overtones). It occurs in a large domain around a critical value of the mass parameter where the QNM is, in addition, weakly damped. As a consequence, it induces giant and slowly decaying ringings. These are constructed directly from the retarded Green function (an intrinsic point of view) and we compare them with the ringing generated by the odd-parity $(\ell = 2, n = 0)$ QNM of the massless theory which, in the context of Einstein gravity, provides one of the most important contribution to the BH ringing. With in mind observational considerations, it is necessary to check that a realistic perturbation describing the BH distortion does not neutralize the resonant effect previously discussed and to study ringings constructed from the quasinormal excitation coefficients (an extrinsic point of view) because they permit us to include the contribution of the perturbation into the BH response [27]. We then describe the perturbation by an initial value problem, an approach which has regularly provided interesting results [27–29]. We show that the excitation coefficient of the $(\ell = 1, n = 0)$ QNM also has a resonant behavior which still leads to giant and slowly decaying ringings. In a conclusion, we discuss some possible extensions of our work and its interest for gravitational wave astrophysics and theoretical physics.

Throughout this letter, we display our numerical results by using the dimensionless coupling constant $\tilde{\alpha} = 2M\mu/{m_{\rm P}}^2$ (here M, μ and $m_{\rm P} = \sqrt{\hbar c/G}$ denote respectively the mass of the BH, the rest mass of the graviton and the Planck mass). We adopt units such that $\hbar = c = G = 1$ and assume a harmonic time dependence $\exp(-i\omega t)$ for the spin-2 field. We describe the exterior of the Schwarzschild BH by using both the radial coordinate $r \in]2M, +\infty[$ and the so-called tortoise coordinate $r_* \in]-\infty, +\infty[$ given by $r_*(r) = r + 2M \ln[r/(2M) - 1]$.

Resonant behavior of the quasinormal excitation factors and associated "intrinsic" giant ringings.— In Schwarzschild spacetime, the partial amplitude $\phi(t, r)$ describing the odd-parity $\ell = 1$ mode of the massive spin-2 field satisfies [9] (the angular momentum index $\ell = 1$ will be, from now on, suppressed in all the formulas)

$$\left[-\frac{\partial^2}{\partial t^2} + \frac{\partial^2}{\partial r_*^2} - V(r)\right]\phi(t, r) = 0 \tag{1}$$

with the effective potential $V(r)$ given by

$$V(r) = \left(1 - \frac{2M}{r}\right)\left(\mu^2 + \frac{6}{r^2} - \frac{16M}{r^3}\right). \tag{2}$$

The associated retarded Green function can be written as

$$G_{\rm ret}(t; r, r') = -\int_{-\infty+ic}^{+\infty+ic} \frac{d\omega}{2\pi} \frac{\phi_\omega^{\rm in}(r_<)\phi_\omega^{\rm up}(r_>)}{W(\omega)} e^{-i\omega t} \tag{3}$$

where $c > 0$, $r_< = \min(r, r')$, $r_> = \max(r, r')$ and with $W(\omega)$ denoting the Wronskian of the functions $\phi_\omega^{\rm in}$ and $\phi_\omega^{\rm up}$. These two functions are linearly independent solutions of the Regge-Wheeler equation

$$\frac{d^2\phi_\omega}{dr_*^2} + \left[\omega^2 - V(r)\right]\phi_\omega = 0. \tag{4}$$

When $\mathrm{Im}(\omega) > 0$, $\phi_\omega^{\rm in}$ is uniquely defined by its ingoing behavior at the event horizon, i.e., for $r_* \to -\infty$ $\phi_\omega^{\rm in}(r) \sim \exp[-i\omega r_*]$ and, at spatial infinity, i.e., for $r_* \to +\infty$, it has an asymptotic behavior of the form

$$\phi_\omega^{\rm in}(r) \sim \sqrt{\frac{\omega}{p(\omega)}}\left[A^{(-)}(\omega)e^{-i[p(\omega)r_* + [M\mu^2/p(\omega)]\ln(r/M)]} + A^{(+)}(\omega)e^{+i[p(\omega)r_* + [M\mu^2/p(\omega)]\ln(r/M)]}\right]. \tag{5}$$

Similarly, $\phi_\omega^{\rm up}$ is uniquely defined by its outgoing behavior at spatial infinity, i.e., for $r_* \to +\infty$, $\phi_\omega^{\rm up}(r) \sim \sqrt{\omega/p(\omega)}\exp\{+i[p(\omega)r_* + [M\mu^2/p(\omega)]\ln(r/M)]\}$ and, at the horizon, i.e., for $r_* \to -\infty$ it has an asymptotic behavior of the form

$$\phi_\omega^{\rm up}(r) \sim B^{(-)}(\omega)e^{-i\omega r_*} + B^{(+)}(\omega)e^{+i\omega r_*}. \tag{6}$$

Here $p(\omega) = \sqrt{\omega^2 - \mu^2}$ denotes the "wave number" while $A^{(-)}(\omega)$, $A^{(+)}(\omega)$, $B^{(-)}(\omega)$ and $B^{(+)}(\omega)$ are complex amplitudes which, like the in- and up- modes, can be defined by analytic continuation in the full complex ω-plane (or, more precisely, in a well-chosen multi-sheeted Riemann surface). By evaluating the Wronskian $W(\omega)$ at $r_* \to -\infty$ and $r_* \to +\infty$, we obtain $W(\omega) = 2i\omega A^{(-)}(\omega) = 2i\omega B^{(+)}(\omega)$.

If the Wronskian $W(\omega)$ vanishes, the functions $\phi^{\rm in}_\omega$ and $\phi^{\rm up}_\omega$ are linearly dependent and propagate inward at the horizon and outward at spatial infinity, a behavior which defines the QNMs. The zeros of the Wronskian lying in the lower part of the complex ω-plane are the frequencies of the $\ell = 1$ QNMs. They are symmetrically distributed with respect to the imaginary ω-axis. The contour of integration in Eq. (3) may be deformed in order to capture them [28]. By Cauchy's Theorem, we can extract from the retarded Green function (3) a residue series over the quasinormal frequencies ω_n lying in the fourth quadrant of the complex ω-plane. We then obtain the contribution describing the BH ringing. It is given by

$$G^{\rm QNM}_{\rm ret}(t;r,r') = 2\,{\rm Re}\left[\sum_n \mathcal{B}_n \tilde{\phi}_{\omega_n}(r)\tilde{\phi}_{\omega_n}(r') \times e^{-i\omega_n t + ip(\omega_n)r_* + ip(\omega_n)r'_* + i[M\mu^2/p(\omega_n)]\ln(rr'/M^2)}\right] \quad (7)$$

where

$$\mathcal{B}_n = \left(\frac{1}{2p(\omega)}\frac{A^{(+)}(\omega)}{\frac{dA^{(-)}(\omega)}{d\omega}}\right)_{\omega=\omega_n} \quad (8)$$

denotes the excitation factor corresponding to the complex frequency ω_n. In Eq. (7), the modes $\tilde{\phi}_{\omega_n}(r)$ are defined by normalizing the modes $\phi^{\rm in}_{\omega_n}(r)$ so that $\tilde{\phi}_{\omega_n}(r) \sim 1$ as $r \to +\infty$. In the sum, $n = 0$ corresponds to the fundamental QNM (i.e., the least damped one) and $n = 1, 2, \ldots$ to the overtones.

Quasinormal retarded Green functions such as (7) do not provide physically relevant results at "early times" due to their exponentially divergent behavior as t decreases. It is necessary to determine, from physical considerations, the time beyond which they can be used and such a time is the starting time $t_{\rm start}$ of the BH ringing. $t_{\rm start}$ can be "easily" obtained for massless fields (see, e.g., Ref. [27]). Indeed, we first note that the QNMs are semiclassically associated with the peak of the effective potential located close to $r_* \approx 0$. Then, by assuming that the source at r'_* and the observer at r_* are far from the BH (i.e., that $r_*, r'_* \gg 2M$) we have $t_{\rm start} \approx r_* + r'_*$ (it is approximatively the time taken for the signal to travel from the source to the peak of the potential and then to reach the observer). For massive fields, the previous considerations must be slightly modified. We take into account the dispersive behavior of the QNMs and define $t_{\rm start}$ from group velocities. From the dispersion relation $p(\omega) = \sqrt{\omega^2 - \mu^2}$, we can show that the group velocity corresponding to the quasinormal frequency ω_n is given by $v_{\rm g} = {\rm Re}[p(\omega_n)]/{\rm Re}[\omega_n]$. Because the peak of the effective potential still remains located close to $r_* \approx 0$, we then obtain $t_{\rm start} \approx (r_* + r'_*){\rm Re}[\omega_n]/{\rm Re}[p(\omega_n)]$ (here, we neglect the contribution of $[M\mu^2/p(\omega_n)]\ln(rr'/M^2)$).

In Fig. 1, we display the effect of the graviton mass on ω_0 (see also Fig. 2 in Ref. [9]) and in Fig. 2, we exhibit

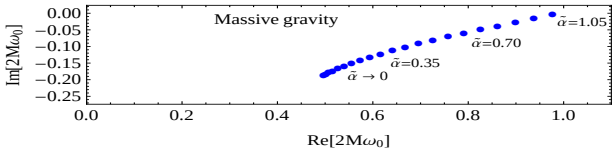

FIG. 1. Complex frequency ω_0 of the odd-parity ($\ell = 1, n = 0$) QNM.

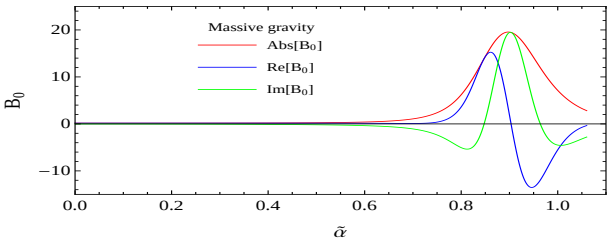

FIG. 2. Resonant behavior of the excitation factor $\mathcal{B}_0$ of the odd-parity ($\ell = 1, n = 0$) QNM. The maximum of $|\mathcal{B}_0|$ occurs for the critical value $\tilde{\alpha} \approx 0.89757$; we then have $2M\omega_0 \approx 0.85969073 - 0.03878222i$ and $\mathcal{B}_0 \approx 3.25237 + 19.28190i$.

the strong resonant behavior of $\mathcal{B}_0$ occurring around the critical value $\tilde{\alpha} \approx 0.90$. The same kind of resonant behavior exists for the excitation factors $\mathcal{B}_n$ with $n \neq 0$ but the resonance amplitude decreases rapidly as the overtone index n increases.

The resonant behavior of the excitation factor $\mathcal{B}_0$ occurring for masses in a range where the QNM is a long-lived mode (see Figs. 1 and 2) induces giant ringings which are, moreover, slowly or even very slowly decaying. In Fig. 3, we plot, for two values of the graviton mass, the BH "intrinsic" ringings constructed from the quasinormal retarded Green function (7) and we compare them to the ringing generated by the odd-parity ($\ell = 2, n = 0$) QNM of the massless spin-2 field with quasinormal frequency $2M\omega_{20} \approx 0.74734337 - 0.17792463i$ and with excitation factor $\mathcal{B}_{20} \approx 0.12690 + 0.02032i$. Similar results can be obtained for various locations of the source and the observer. Giant BH ringings also exist for $n \neq 0$ but with less impressive characteristics.

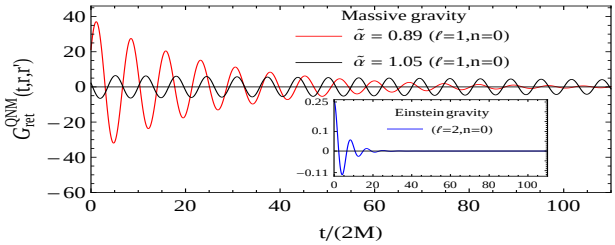

FIG. 3. Extraordinary "intrinsic" ringings induced by massive gravity and comparison with the ringing generated in Einstein gravity. The results are obtained from (7) with $r = 50M$ and $r' = 10M$.

Resonant behavior of the quasinormal excitation coefficients and associated "extrinsic" giant ringings.— In the previous section, we focussed on "intrinsic" ringings, i.e., on ringings directly constructed from the quasinormal retarded Green function and therefore depending only on the BH properties. Of course, with in mind astrophysical applications, it is now necessary to check that giant ringings also exist in the presence of a realistic perturbation or, in other words, that the convolution of the source of the perturbation with the retarded Green function does not modify, in a fundamental way, our results. This is a complex problem and, in this letter, we just discuss some of its elementary aspects.

Some years ago, dealing with the observability of quasinormal ringings, Andersson and Glampedakis associated to each QNM an effective amplitude $h_{\rm eff}$ achievable after matched filtering [30, 31]. For the massive QNMs considered here, it reads

$$h_{\rm eff} \sim {\rm Re}\left[2\sqrt{-{\rm Re}(\omega_n)/{\rm Im}(\omega_n)}\, p(\omega_n)\mathcal{B}_n\right]. \qquad (9)$$

We can use it in order to determine the effective amplitude of the ringings generated by the odd-parity ($\ell = 1, n = 0$) QNM of massive gravity; we obtain $|h_{\rm eff}| \approx 54.74$ for $\tilde{\alpha} = 0.89$ and $|h_{\rm eff}| \approx 13.02$ for $\tilde{\alpha} = 1.05$. For the ringing generated by the odd-parity ($\ell = 2, n = 0$) QNM of Einstein gravity we have $|h_{\rm eff}| \approx 0.40$. This is in perfect agreement with our previous results and suggests that giant BH ringings are astrophysically relevant and observable. However, it should be noted that Andersson-Glampedakis formula must be taken with a pinch of salt. As noted in Ref. [27], it seems helpful only if the quasinormal ringing is excited by localized initial data. So, it is necessary to consider a more general approach.

We now describe the BH perturbation by an initial value problem with Gaussian initial data. More precisely, we consider that, at $t = 0$, the partial amplitude $\phi(t, r)$ governed by (1) satisfies

$$\phi(t = 0, r) = \phi_0(r) \equiv \phi_0 \exp\left[-\frac{a^2}{(2M)^2}(r_* - \beta)^2\right] \qquad (10)$$

and $\partial_t\phi(t = 0, r) = 0$. By Green's Theorem, we can show that the time evolution of $\phi(t, r)$ is described, for $t > 0$, by $\phi(t, r) = \int \partial_t G_{\rm ret}(t; r, r')\phi_0(r')dr'_*$. We can insert (3) into this expression and deform again the contour of integration on ω in order to capture the contributions of the QNMs. We then isolate the BH ringing generated by the initial data:

$$\phi^{\rm QNM}(t, r) = 2\,{\rm Re}\left[\sum_n i\omega_n\mathcal{C}_n \times e^{-i\omega_n t + ip(\omega_n)r_* + i[M\mu^2/p(\omega_n)]\ln(r/M)}\right]. \qquad (11)$$

Here $\mathcal{C}_n$ denotes the excitation coefficient of the QNM with overtone index n. It takes explicitly into account the role of the BH perturbation and is given by

$$\mathcal{C}_n = \mathcal{B}_n \int \frac{\phi_0(r')\phi^{\rm in}_{\omega_n}(r')}{\sqrt{\omega_n/p(\omega_n)}A^{(+)}(\omega_n)}dr'_*. \qquad (12)$$

The excitation coefficients $\mathcal{C}_n$, like the excitation factors $\mathcal{B}_n$, have a resonant behavior but it is now more attenuated. Moreover, the maximum amplitude of the resonance is slightly shifted but still occurs for masses in a range where the QNM is a long-lived mode. In Fig. 4, we exhibit the strong resonant behavior of $\mathcal{C}_0$ for particular values of the parameters defining the initial data (10). It occurs around the critical value $\tilde{\alpha} \approx 0.89$ and is rather similar to the behavior of the corresponding excitation factor $\mathcal{B}_0$. It should be noted that we have checked that it depends very little on the parameters defining the initial data (10) (see Ref. [22] for a detailed study). Of course, for overtones, the resonance is more and more attenuated as the overtone index n increases so, the ringings generated by the fundamental QNM are certainly the most interesting.

In Fig. 5, we plot, for the two values of the graviton mass considered in Fig. 3, the BH "extrinsic" ringings defined by (11) and we compare them to the ringing generated by the odd-parity ($\ell = 2, n = 0$) QNM of the massless spin-2 field. This last one is constructed by noting that, for the same initial data, the excitation coefficient

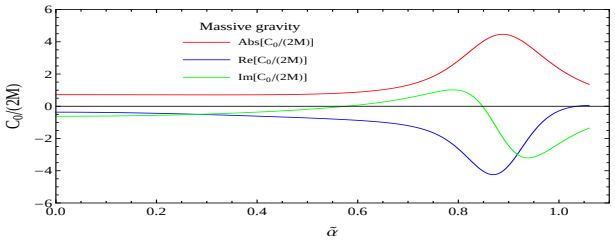

FIG. 4. Resonant behavior, in massive gravity, of the excitation coefficient $\mathcal{C}_0$ of the odd-parity ($\ell = 1, n = 0$) QNM. It is obtained from (12) by using (10) with $\phi_0 = 1$, $a = 1$ and $\beta = 10M$. The maximum of $|\mathcal{C}_0|/(2M)$ occurs for the critical value $\tilde{\alpha} \approx 0.88808$; we then have $2M\omega_0 \approx 0.85277076 - 0.04084908i$ and $\mathcal{C}_0/(2M) \approx -4.02613 - 1.93037i$.

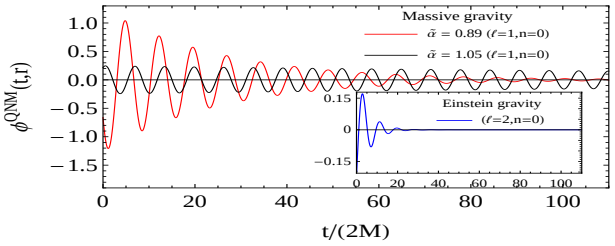

FIG. 5. Extraordinary "extrinsic" ringings induced by massive gravity and comparison with the ringing generated in Einstein gravity. The results are obtained from (11) with $r = 50M$ by using (10) with $\phi_0 = 1$, $a = 1$ and $\beta = 10M$.

of the QNM is given by $\mathcal{C}_{20}/(2M) \approx 0.50761 - 0.29210i$. Similar results as those displayed in Fig. 5 can be obtained for various values of the parameters defining the initial data (10) and for various locations of the observer. Even if the role of the perturbation is taken into account, extraordinary BH ringings exist.

Conclusion.— In this letter, by considering the massive spin-2 field in Schwarzschild spacetime, we have pointed out a new effect in BH physics : the existence around particular values of the mass parameter of a strong resonant behavior for the excitation factors of the QNMs with, as a consequence, the existence of giant and slowly-decaying ringings. Such results are, in fact, a general feature of massive field theories in the Schwarzschild BH [22]. It would be interesting to study more realistic perturbations than the distortion described here by an initial value problem (e.g., the excitation of the BH by a particle falling radially or plunging), to consider alternative massive gravity theories and to extend our study to the Kerr BH. Finally, we would like to note that :

(i) The Schwarzschild BH interacting with a massive spin-2 field is in general unstable [8, 9] (see, however, Ref. [10]). In the context of the theory considered here, the instability is due to the behavior of the propagating $\ell = 0$ mode [9]. It is a "low-mass" instability which disappears for $\tilde{\alpha}$ above the threshold value $\tilde{\alpha}_c \approx 0.86$. So, the giant ringings predicted here occurring near and above the critical value $\tilde{\alpha} \approx 0.89$ are physically relevant.

(ii) Even if the graviton is an ultralight particle, when it interacts with a supermassive BH, values of the coupling constant $\tilde{\alpha}$ leading to giant ringings can be easily reached. Indeed, supermassive BHs have their masses lying approximately between $10^6\,\mathrm{M}_\odot$ and $2 \times 10^{10}\,\mathrm{M}_\odot$; so, if we assume that $\mu \approx 1.35 \times 10^{-55}\,\mathrm{kg}$ (it seems to be the superior limit of the graviton mass in the framework of the ordinary Fierz-Pauli theory [32]), we have $\tilde{\alpha}$ lying approximately between 10^{-3} and 20. As a consequence, due to the enormous number of supermassive BHs in the Universe, the extraordinary BH ringings discussed here could be observed by the next generations of gravitational wave detectors and used to test the various massive gravity theories or their absence could allow us to impose strong constraints on the graviton mass and to support, in a new way, Einstein's general relativity.

Acknowledgments.— We wish to thank Andrei Belokogne for discussions and the "Collectivité Territoriale de Corse" for its support through the COMPA project.

* decanini@univ-corse.fr
† folacci@univ-corse.fr
‡ ould-el-hadj@univ-corse.fr

[1] H.-P. Nollert, Classical Quantum Gravity **16**, R159 (1999).
[2] K. D. Kokkotas and B. G. Schmidt, Living Rev. Rel. **2**, 2 (1999), arXiv:gr-qc/9909058.
[3] E. Berti, V. Cardoso, and A. O. Starinets, Classical Quantum Gravity **26**, 163001 (2009), arXiv:0905.2975 [gr-qc].
[4] R. Konoplya and A. Zhidenko, Rev. Mod. Phys. **83**, 793 (2011), arXiv:1102.4014 [gr-qc].
[5] K. Hinterbichler, Rev. Mod. Phys. **84**, 671 (2012), arXiv:1105.3735 [hep-th].
[6] M. Fierz and W. Pauli, Proc. Roy. Soc. Lond. A **173**, 211 (1939).
[7] A. S. Goldhaber and M. M. Nieto, Rev. Mod. Phys. **82**, 939 (2010), arXiv:0809.1003 [hep-ph].
[8] E. Babichev and A. Fabbri, Classical Quantum Gravity **30**, 152001 (2013), arXiv:1304.5992 [gr-qc].
[9] R. Brito, V. Cardoso, and P. Pani, Phys. Rev. D **88**, 023514 (2013), arXiv:1304.6725 [gr-qc].
[10] R. Brito, V. Cardoso, and P. Pani, Phys. Rev. D **87**, 124024 (2013), arXiv:1306.0908 [gr-qc].
[11] N. Deruelle and R. Ruffini, Phys. Lett. B **52**, 437 (1974).
[12] T. Damour, N. Deruelle, and R. Ruffini, Lett. Nuovo Cim. **15**, 257 (1976).
[13] T. Zouros and D. Eardley, Annals Phys. **118**, 139 (1979).
[14] S. L. Detweiler, Phys. Rev. D **22**, 2323 (1980).
[15] L. E. Simone and C. M. Will, Classical Quantum Gravity **9**, 963 (1992).
[16] R. Konoplya and A. Zhidenko, Phys. Lett. B **609**, 377 (2005), arXiv:gr-qc/0411059.
[17] S. Hod, Phys. Rev. D **84**, 044046 (2011), arXiv:1109.4080 [gr-qc].
[18] Y. Decanini, A. Folacci, and B. Raffaelli, Phys. Rev. D **84**, 084035 (2011), arXiv:1108.5076 [gr-qc].
[19] R. H. Price, Phys. Rev. D **5**, 2419 (1972).
[20] L. M. Burko and G. Khanna, Phys. Rev. D **70**, 044018 (2004), arXiv:gr-qc/0403018.
[21] S. Hod, Classical Quantum Gravity **30**, 237002 (2013).
[22] Y. Decanini, A. Folacci, and M. Ould El Hadj, *Work in preparation*.
[23] J. G. Rosa and S. R. Dolan, Phys. Rev. D **85**, 044043 (2012), arXiv:1110.4494 [hep-th].
[24] S. Hassan, A. Schmidt-May, and M. von Strauss, JHEP **1305**, 086 (2013), arXiv:1208.1515 [hep-th].
[25] C. de Rham and G. Gabadadze, Phys. Rev. D **82**, 044020 (2010), arXiv:1007.0443 [hep-th].
[26] C. de Rham, G. Gabadadze, and A. J. Tolley, Phys. Rev. Lett. **106**, 231101 (2011), arXiv:1011.1232 [hep-th].
[27] E. Berti and V. Cardoso, Phys. Rev. D **74**, 104020 (2006), arXiv:gr-qc/0605118.
[28] E. W. Leaver, Phys. Rev. D **34**, 384 (1986).
[29] N. Andersson, Phys. Rev. D **55**, 468 (1997), arXiv:gr-qc/9607064.
[30] N. Andersson and K. Glampedakis, Phys. Rev. Lett. **84**, 4537 (2000), arXiv:gr-qc/9909050.
[31] K. Glampedakis and N. Andersson, Phys. Rev. D **64**, 104021 (2001), arXiv:gr-qc/0103054.
[32] L. S. Finn and P. J. Sutton, Phys. Rev. D **65**, 044022 (2002), arXiv:gr-qc/0109049.

CHAPITRE 6

Comportement résonant des trous noirs : Champs bosoniques massifs

Comme au chapitre précédent, nous ne nous focalisons que sur les QNMs (ℓ, n) régis par l'équation de type Regge-Wheeler. Notre étude porte non seulement sur le champ de spin-2 massif (champ de Fierz-Pauli) mais nous allons aussi généraliser nos résultats au spin-0 massif (champ scalaire) et au spin-1 massif (champ de Proca).

Nous considérons les facteurs d'excitation $B_{\ell n}$ correspondants aux fréquences quasi-normales $\omega_{\ell n}$ des QNMs (ℓ, n) et nous étudions leurs évolutions en fonction du paramètre sans dimension $\tilde{\alpha}$. Nous montrons, d'abord, qu'ils présentent, en général, un comportement résonant avec un maximum aux alentours de la valeur critique $\tilde{\alpha}_{\ell n}$ qui augmente rapidement avec le moment angulaire ℓ et diminue avec l'harmonique n. Nous montrons, ensuite, quand $\tilde{\alpha}$ est proche, au-dessus et largement au-dessus de l'une des valeurs critiques $\tilde{\alpha}_{\ell n}$, qu'une sonnerie d'amplitude géante et à faible décroissance temporelle devrait être générée.

Enfin, nous étudions numériquement le rôle du moment angulaire ℓ et de l'harmonique n en comparant quelques sonneries géantes construites directement à partir des fonctions de Green retardées. Nous confirmons analytiquement certains résultats précédemment discutés en utilisant des considérations semi-classiques basées sur les propriétés des géodésiques circulaires instables suivies par les particules massives en orbite autour du trou noir de Schwarzschild.

PHYSICAL REVIEW D **89,** 084066 (2014)

Resonant excitation of black holes by massive bosonic fields and giant ringings

Yves Décanini,[*] Antoine Folacci,[†] and Mohamed Ould El Hadj[‡]

Equipe Physique Théorique, Projet COMPA, SPE, UMR 6134 du CNRS et de l'Université de Corse, Université de Corse, BP 52, F-20250 Corte, France

(Received 10 February 2014; published 22 April 2014)

We consider the massive scalar field, the Proca field, and the Fierz-Pauli field in the Schwarzschild spacetime and we focus more particularly on their long-lived quasinormal modes. We show numerically that the associated excitation factors have a strong resonant behavior and we confirm this result analytically from semiclassical considerations based on the properties of the unstable circular geodesics on which a massive particle can orbit the black hole. The conspiracy of (i) the long-lived behavior of the quasinormal modes and (ii) the resonant behavior of their excitation factors induces intrinsic giant ringings, i.e., ringings of a huge amplitude. Such ringings, which are moreover slowly decaying, are directly constructed from the retarded Green function. If we describe the source of the black hole perturbation by an initial value problem with Gaussian initial data, i.e., if we consider the excitation of the black hole from an extrinsic point of view, we can show that these extraordinary ringings are still present. This suggests that physically realistic sources of perturbations should generate giant and slowly decaying ringings and that their existence could be used to constrain ultralight bosonic field theory interacting with black holes.

DOI: 10.1103/PhysRevD.89.084066 PACS numbers: 04.70.-s, 04.25.Nx

I. INTRODUCTION

Ultralight bosonic fields are important ingredients of the fundamental theories beyond the standard model of elementary particles and the standard model of cosmology based on Einstein's general relativity. They are predicted by string theories as well as by higher-dimensional field theories and they could contribute to the dark matter content of the Universe and explain, without dark energy, its accelerated expansion. However, the particles associated with these fields are so light and are so weakly coupled with the visible sector particles that they have escaped detection so far. Thus, it is rather exciting to realize that ultralight bosonic fields interacting with black holes (BHs) could lead to "macroscopic" effects (see, e.g., Refs. [1–16] for recent works on this subject) which could be used to provide strong evidence for the existence of these new particles and to constrain the parameters defining the associated field theories.

In this context, we have highlighted in our recent work dealing with the massive spin-2 field in the Schwarzschild spacetime a new and unexpected effect in BH physics [16]: around particular values of the graviton mass, the excitation factors of the long-lived quasinormal modes (QNMs) have a strong resonant behavior. This effect has an immediate fascinating consequence: it induces giant and slowly decaying ringings when the Schwarzschild BH is excited by an external perturbation. So, if massive gravity is relevant to physics, such extraordinary BH ringings could be observed by the future gravitational wave detectors and allow us to test the various massive gravity theories. Otherwise, their absence could be used to impose constraints on the graviton mass and to further support Einstein's general relativity.

In Ref. [16], we focused only on the Fierz-Pauli theory [17,18] in the Schwarzschild spacetime, a field theory which has been developed in great details by Brito, Cardoso, and Pani in Ref. [10] and which can be obtained, e.g., by linearization of the pathology-free bimetric theory of Hassan, Schmidt-May, and von Strauss [19], an extension, in curved spacetime, of the fundamental work of de Rham, Gabadadze, and Tolley [20,21]. In our opinion, the effects we have described in this rather limited context are a general feature of all massive bosonic field theories in arbitrary BH spacetimes and, in this article, we intend to discuss more particularly, in the Schwarzschild spacetime, the cases of the real massive scalar field and of the massive vector field described by the usual Proca theory [6,22]. We shall also discuss at greater length the case of the massive gravity theory already considered in Ref. [16].

Before entering into the technical part of our work, it seems to us necessary to recall and to indicate some important points concerning the long-lived QNMs of BHs. First, we note that they should not be confused with the long-lived quasibound states (see, e.g., Refs. [23–26] for important pioneering work on this particular topic) which have been the subject of recent work dealing with ultralight scalar fields as well as with massive spin-1 and spin-2 fields [1–10,15]. The long-lived QNMs of BHs are resonant modes which can be encountered in various

[*]decanini@univ-corse.fr
[†]folacci@univ-corse.fr
[‡]ould-el-hadj@univ-corse.fr

situations and, in particular, in the two important following contexts: (i) when we consider massless fields in the Kerr spacetime and that we increase the BH angular momentum up to the extremal limit (see Ref. [27] for a pioneering work on this topic) and (ii) when we consider massive fields in the Schwarzschild spacetime and that we increase the mass field up to the QNM disappearance (see Ref. [28] for a pioneering work on this topic). These weakly damped QNMs are really interesting. Indeed, BHs are usually considered as poor oscillators but, in the two contexts previously mentioned, they have very large quality factors and one might intuitively think that the QNMs are then easier to detect. However, it is in fact important to keep in mind that a long-lived QNM can be observed only if the corresponding quasinormal excitation factor is not too small because, in that case, it can be excited easily. We recall, in particular, that the long-lived QNMs of the rapidly rotating Kerr BH have quasinormal excitation factors which vanish in the extremal limit [29]. As a consequence, contrary to initial expectations, the rapidly rotating Kerr BH is not easier to detect. As far as the long-lived QNMs of the massive fields are concerned, the situation is very different as we have already noted in Ref. [16] and as we shall explain here in more detail. In general, the quasinormal excitation factors have a huge amplitude when the QNMs are weakly damped and the conspiracy of these two behaviors induces giant ringings so that the detectability of the BH is considerably improved.

Our paper is organized as follows. We only focus on the (ℓ, n) QNMs which are governed by a Regge-Wheeler-type equation (here, ℓ denotes the angular momentum index while n is the overtone index). We are therefore concerned with all the QNMs of the scalar field (here $\ell \in \mathbb{N}$), all the odd-parity QNMs of the Proca field (here $\ell \in \mathbb{N}^*$), the even-parity $\ell = 0$ QNMs of the Proca field and the odd-parity $\ell = 1$ QNMs of the Fierz-Pauli field. In Sec. II, we consider the excitation factors $\mathcal{B}_{\ell n}$ corresponding to the complex quasinormal frequencies $\omega_{\ell n}$ of the (ℓ, n) QNMs and we study their evolution as functions of the dimensionless coupling constant $\tilde{\alpha} = 2M\mu/m_{\mathrm{P}}{}^2$ (here M, μ, and m_{P} denote, respectively, the mass of the BH, the rest mass of the field, and the Planck mass). We show numerically that, in general, they present a resonant behavior around a critical value $\tilde{\alpha}_{\ell n}$ with a maximum which increases rapidly with the angular momentum index ℓ and decreases with the overtone index n. We furthermore note that, in a large range around the critical value $\tilde{\alpha}_{\ell n}$, the imaginary part of the quasinormal frequency $\omega_{\ell n}$ is very small, i.e., that the corresponding (ℓ, n) QNM is weakly damped. So, because the quasinormal excitation factors and the quasinormal frequencies can be used to quantify intrinsically the amplitude and the decay of the BH ringing, we show that, when $\tilde{\alpha}$ is near, above and far above one of the critical values $\tilde{\alpha}_{\ell n}$, a slowly decaying giant ringing is generated. Moreover, we study numerically the role of the angular momentum index ℓ and of the overtone index n by comparing some giant ringings constructed directly from the retarded Green function. In Sec. III, we confirm analytically some of the previous results by using semiclassical considerations based on the properties of the unstable circular geodesics on which a massive particle can orbit the Schwarzschild BH. Of course, the point of view developed in Sec. II is an intrinsic one, i.e., it depends only on the BH properties. With astrophysical and physical considerations in mind, it is necessary to examine the role of the source of the field perturbation and to check that the resonant effects previously discussed are not neutralized in the presence of a realistic external perturbation. In other words, it is necessary to develop an extrinsic point of view and to study ringings constructed from the quasinormal excitation coefficients. Indeed, they permit us to include the contribution of the source of the perturbation into the BH response (see Ref. [30] for a clear analysis of the distinction between the quasinormal excitation factors and the quasinormal excitation coefficients). In Sec. IV, we describe the source of the perturbation by an initial value problem (see, e.g., Refs. [30–32] for previous works using such an approach) and we show that the use of quasinormal excitation coefficients still leads to giant ringings. In a conclusion, we discuss some limitations of our work as well as possible extensions.

Throughout this article, we adopt units such that $\hbar = c = G = 1$. We consider the exterior of the Schwarzschild BH of mass M defined by the metric

$$ds^2 = -(1 - 2M/r)dt^2 + (1 - 2M/r)^{-1}dr^2 + r^2 d\sigma_2^2, \tag{1}$$

where $d\sigma_2^2$ denotes the metric on the unit two-sphere S^2 and with the Schwarzschild coordinates (t, r) which satisfy $t \in]-\infty, +\infty[$ and $r \in]2M, +\infty[$. We also use the so-called tortoise coordinate $r_* \in]-\infty, +\infty[$ defined from the radial Schwarzschild coordinate r by $dr/dr_* = (1 - 2M/r)$ and given by $r_*(r) = r + 2M \ln[r/(2M) - 1]$ and assume a harmonic time dependence $\exp(-i\omega t)$ for all fields.

II. RESONANT BEHAVIOR OF QUASINORMAL EXCITATION FACTORS AND INTRINSIC GIANT RINGINGS

In the Schwarzschild spacetime, the time-dependent Regge-Wheeler equation

$$\left[-\frac{\partial^2}{\partial t^2} + \frac{\partial^2}{\partial r_*^2} - V_\ell(r)\right]\phi_\ell(t, r) = 0, \tag{2}$$

with the effective potential $V_\ell(r)$ given by

$$V_\ell(r) = \left(1 - \frac{2M}{r}\right)\left(\mu^2 + \frac{A(\ell)}{r^2} + \beta\frac{2M}{r^3}\right) \tag{3}$$

governs the partial amplitudes $\phi_\ell(t,r)$ of (i) the modes of the massive scalar field [we then have $\ell \in \mathbb{N}$, $A(\ell) = \ell(\ell+1)$ and $\beta = 1$], (ii) the odd-parity modes of the Proca field [we then have $\ell \in \mathbb{N}^*$, $A(\ell) = \ell(\ell+1)$ and $\beta = 0$], (iii) the even-parity $\ell = 0$ mode of the Proca field [we then have $A(\ell) = 2$ and $\beta = -3$], and (iv) the odd-parity $\ell = 1$ mode of the Fierz-Pauli field [we then have $A(\ell) = 6$ and $\beta = -8$]. This is obvious for the scalar field; for the Proca field, see Refs. [6,22] and for the Fierz-Pauli field, see Ref. [10].

The retarded Green function $G^{\rm ret}_\ell(t;r,r')$ associated with the partial amplitude $\phi_\ell(t,r)$ is a solution of

$$\left[-\frac{\partial^2}{\partial t^2}+\frac{\partial^2}{\partial r_*^2}-V_\ell(r)\right]G^{\rm ret}_\ell(t;r,r') = -\delta(t)\delta(r_*-r'_*) \tag{4}$$

satisfying the condition $G^{\rm ret}_\ell(t;r,r') = 0$ for $t \le 0$. It can be written as

$$G^{\rm ret}_\ell(t;r,r') = -\int_{-\infty+ic}^{+\infty+ic}\frac{d\omega}{2\pi}\frac{\phi^{\rm in}_{\omega\ell}(r_<)\phi^{\rm up}_{\omega\ell}(r_>)}{W_\ell(\omega)}e^{-i\omega t}, \tag{5}$$

where $c > 0$, $r_< = \min(r,r')$, $r_> = \max(r,r')$, and with $W_\ell(\omega)$ denoting the Wronskian of the functions $\phi^{\rm in}_{\omega\ell}$ and $\phi^{\rm up}_{\omega\ell}$. These two functions are linearly independent solutions of the Regge-Wheeler equation

$$\frac{d^2\phi_{\omega\ell}}{dr_*^2}+[\omega^2-V_\ell(r)]\phi_{\omega\ell} = 0. \tag{6}$$

When $\mathrm{Im}(\omega) > 0$, $\phi^{\rm in}_{\omega\ell}$ is uniquely defined by its ingoing behavior at the event horizon $r = 2M$ (i.e., for $r_* \to -\infty$)

$$\phi^{\rm in}_{\omega\ell}(r) \underset{r_*\to-\infty}{\sim} e^{-i\omega r_*} \tag{7a}$$

and, at spatial infinity $r \to +\infty$ (i.e., for $r_* \to +\infty$), it has an asymptotic behavior of the form

$$\begin{aligned}\phi^{\rm in}_{\omega\ell}(r) \underset{r_*\to+\infty}{\sim} &\left[\frac{\omega}{p(\omega)}\right]^{1/2}\\ &\times\left(A^{(-)}_\ell(\omega)e^{-i[p(\omega)r_*+[M\mu^2/p(\omega)]\ln(r/M)]}\right.\\ &\left.+A^{(+)}_\ell(\omega)e^{+i[p(\omega)r_*+[M\mu^2/p(\omega)]\ln(r/M)]}\right).\end{aligned} \tag{7b}$$

Similarly, $\phi^{\rm up}_{\omega\ell}$ is uniquely defined by its outgoing behavior at spatial infinity

$$\phi^{\rm up}_{\omega\ell}(r) \underset{r_*\to+\infty}{\sim} \left[\frac{\omega}{p(\omega)}\right]^{1/2} e^{+i[p(\omega)r_*+[M\mu^2/p(\omega)]\ln(r/M)]} \tag{8a}$$

and, at the horizon, it has an asymptotic behavior of the form

$$\phi^{\rm up}_{\omega\ell}(r) \underset{r_*\to-\infty}{\sim} B^{(-)}_\ell(\omega)e^{-i\omega r_*}+B^{(+)}_\ell(\omega)e^{+i\omega r_*}. \tag{8b}$$

In Eqs. (7) and (8), $p(\omega) = (\omega^2-\mu^2)^{1/2}$ denotes the "wave number" while $A^{(-)}_\ell(\omega)$, $A^{(+)}_\ell(\omega)$, $B^{(-)}_\ell(\omega)$, and $B^{(+)}_\ell(\omega)$ are complex amplitudes which, like the in and up modes, can be defined by analytic continuation in the full complex ω plane (or, more precisely, in a well-chosen multisheeted Riemann surface). By evaluating the Wronskian $W_\ell(\omega)$ at $r_* \to -\infty$ and $r_* \to +\infty$, we obtain

$$W_\ell(\omega) = 2i\omega A^{(-)}_\ell(\omega) = 2i\omega B^{(+)}_\ell(\omega). \tag{9}$$

If the Wronskian $W_\ell(\omega)$ vanishes, the functions $\phi^{\rm in}_{\omega\ell}$ and $\phi^{\rm up}_{\omega\ell}$ are linearly dependent and propagate inward at the horizon and outward at spatial infinity, a behavior which defines the QNMs. The zeros of the Wronskian lying in the lower part of the complex ω plane are the frequencies of the (ℓ,n) QNMs. The contour of integration in Eq. (5) may be deformed in order to capture them (see, e.g., Ref. [31]). By Cauchy's theorem and if we do not take into account the "prompt" contribution (arising from the arcs at $|\omega| = \infty$) and the "tail" contribution (associated with the various cuts), we can extract from the retarded Green function (5) a residue series over the quasinormal frequencies $\omega_{\ell n}$ lying in the fourth quadrant of the complex ω plane. We then obtain the contribution describing the BH ringing. It is given by

$$G^{\rm ret\,QNM}_\ell(t;r,r') = \sum_n G^{\rm ret\ QNM}_{\ell n}(t;r,r'), \tag{10}$$

with

$$\begin{aligned}&G^{\rm ret\ QNM}_{\ell n}(t;r,r')\\ &\quad= 2\,\mathrm{Re}[\mathcal{B}_{\ell n}\tilde\phi_{\ell n}(r)\tilde\phi_{\ell n}(r')\\ &\qquad\times e^{-i[\omega_{\ell n}t-p(\omega_{\ell n})r_*-p(\omega_{\ell n})r'_*-[M\mu^2/p(\omega_{\ell n})]\ln(rr'/M^2)]}].\end{aligned} \tag{11}$$

Here

$$\mathcal{B}_{\ell n} = \left(\frac{1}{2p(\omega)}\frac{A^{(+)}_\ell(\omega)}{\frac{dA^{(-)}_\ell(\omega)}{d\omega}}\right)_{\omega=\omega_{\ell n}} \tag{12}$$

denotes the excitation factor corresponding to the complex frequency $\omega_{\ell n}$. In Eq. (11), the real part symbol Re has been introduced to take into account the symmetry of the quasinormal frequency spectrum with respect to the imaginary ω axis and the modes $\tilde\phi_{\ell n}(r)$ are defined by

$$\begin{aligned}\tilde\phi_{\ell n}(r) \equiv{}& \phi^{\rm in}_{\omega_{\ell n}\ell}(r)/[[\omega_{\ell n}/p(\omega_{\ell n})]^{1/2}A^{(+)}_\ell(\omega_{\ell n})\\ &\times e^{i[p(\omega_{\ell n})r_*+[M\mu^2/p(\omega_{\ell n})]\ln(r/M)]}]\end{aligned} \tag{13}$$

and are therefore normalized so that $\tilde\phi_{\ell n}(r) \sim 1$ as $r \to +\infty$. In the sum (10), $n = 0$ corresponds to the

fundamental QNM (i.e., the least damped one) and $n = 1, 2, \ldots$ to the overtones.

It is important to recall that quasinormal retarded Green functions such as (11) do not provide physically relevant results at "early times" due to their exponentially divergent behavior as t decreases. In fact, it is necessary to determine, from physical considerations, the time beyond which they can be used and this time is the starting time t_{start} of the BH ringing. This is the so-called "time-shift problem" (see, e.g., Ref. [30] for a clear discussion of this problem and references therein for related works). It can be "easily" solved for massless fields. We first note that the QNMs are semiclassically associated with the peak of the effective potential located close to $r_* \approx 0$. Then, by assuming that the source at r'_* and the observer at r_* are far from the BH (i.e., that $r_*, r'_* \gg 2M$) we have $t_{\text{start}} \approx r_* + r'_*$ which is approximatively the time taken for the signal to travel from the source to the peak of the potential and then to reach the observer. For massive fields, the previous considerations must be slightly modified: it is necessary to take into account the dispersive behavior of the QNMs and therefore to define t_{start} from group velocities. From the dispersion relation $p(\omega) = (\omega^2 - \mu^2)^{1/2}$, we can show that the group velocity corresponding to the quasinormal frequency $\omega_{\ell n}$ is given by $v_{\text{g}} = \text{Re}[p(\omega_{\ell n})]/\text{Re}[\omega_{\ell n}]$. This can be confirmed by noting that the factor $\exp[-i\omega_{\ell n} t + i p(\omega_{\ell n}) r_*]$ appearing in (11) leads to the phase velocity $v_{\text{p}} = \text{Re}[\omega_{\ell n}]/\text{Re}[p(\omega_{\ell n})]$ [here it is necessary to neglect the term $i[M\mu^2/p(\omega_{\ell n})]\ln(r/M)$, an assumption formally valid for large r_*]. Because the peak of the effective

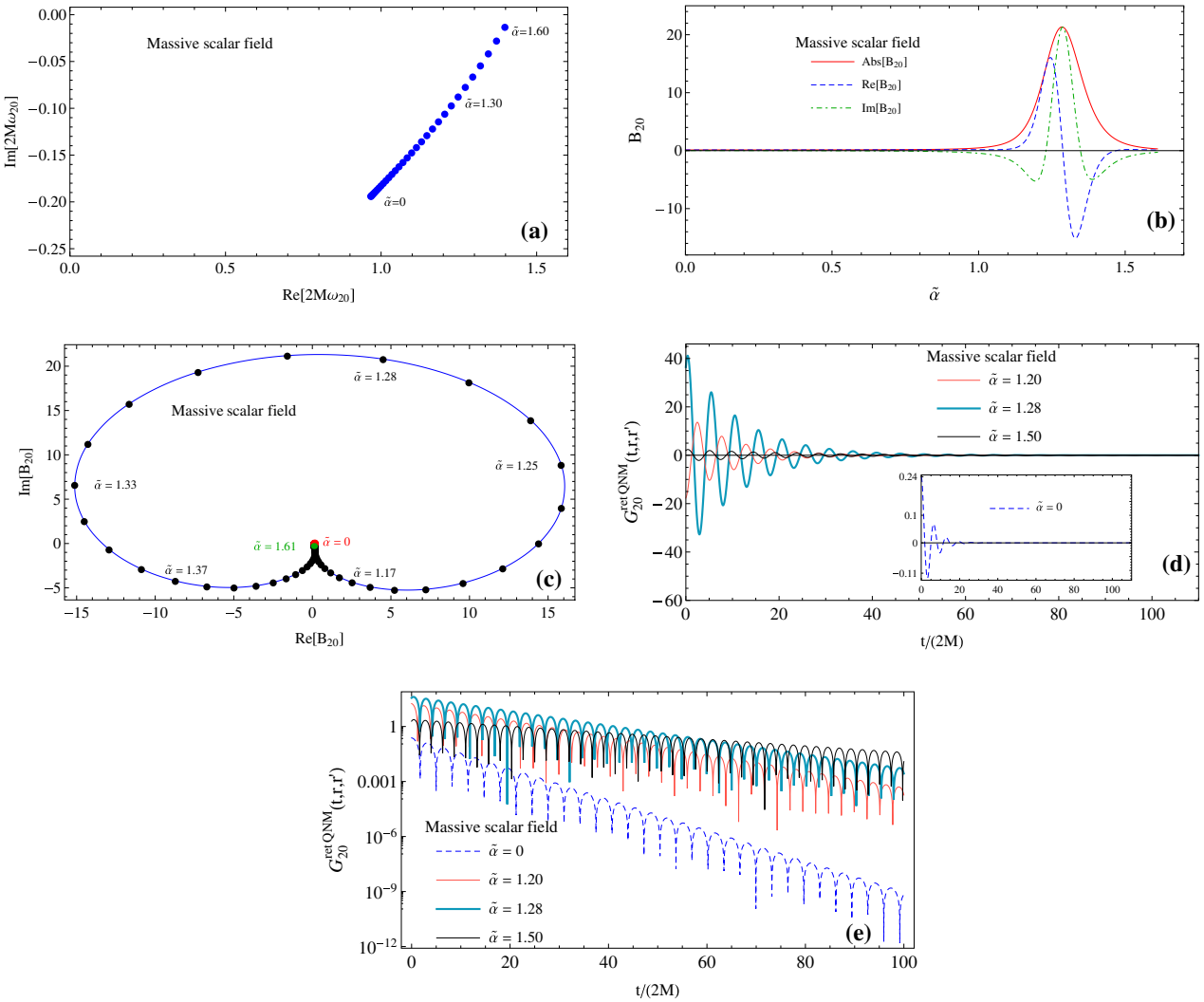

FIG. 1 (color online). The $(\ell = 2, n = 0)$ QNM of the massive scalar field. (a) The complex quasinormal frequency $2M\omega_{20}$ for $\tilde{\alpha} = 0, 0.05, \ldots, 1.55, 1.60$. (b) The resonant behavior of the excitation factor $\mathcal{B}_{20}$. (c) The excitation factor $\mathcal{B}_{20}$ for $\tilde{\alpha} = 0, 0.01, \ldots, 1.60, 1.61$. (d) and (e) Some intrinsic ringings corresponding to values of the mass near and above the critical value $\tilde{\alpha}_{20}$. We compare them with the ringing corresponding to the massless scalar field. The results are obtained from (11) with $r = 50M$ and $r' = 10M$.

potential still remains located close to $r_* \approx 0$, we then obtain $t_{\text{start}} \approx (r_* + r'_*)\text{Re}[\omega_{\ell n}]/\text{Re}[p(\omega_{\ell n})]$, a result which depends on the angular momentum index ℓ and the overtone index n.

The quasinormal frequencies $\omega_{\ell n}$ can be determined by using the method developed by Leaver [33] for massless theories and extended to massive fields by Konoplya and Zhidenko [34]. We have numerically implemented this method by modifying the Hill determinant approach of Majumdar and Panchapakesan [35]. The excitation factors $\mathcal{B}_{\ell n}$ can be obtained by integrating numerically the Regge-Wheeler equation (6) for $\omega = \omega_{\ell n}$ with the Runge-Kutta method and then by comparing its solution to asymptotic expansions with ingoing and outgoing behavior at spatial infinity. In order to obtain stable results for "large" values of the mass parameter, it has been necessary to decode, by Padé summation, the information hidden in the divergent part of the asymptotic expansions considered (see, e.g., Chap. 8 of Ref. [36] for information on Padé summation).

In Fig. 1, we consider the $(\ell = 2, n = 0)$ QNM of the massive scalar field [it should be noted that the resonant effects we shall describe for this particular QNM also exists for the $(\ell = 0, n = 0)$ and $(\ell = 1, n = 0)$ QNMs but are much more attenuated]. We display the effect of the mass on its complex quasinormal frequency ω_{20} [see Fig. 1(a)] and on the associated quasinormal excitation factor $\mathcal{B}_{20}$ [see Figs. 1(b) and 1(c)]. In Fig. 1(b), we can observe the strong resonant behavior of $\mathcal{B}_{20}$. It occurs around the critical value $\tilde{\alpha}_{20} \approx 1.28447$ and it is important to note that near, above, and "far above" $\tilde{\alpha}_{20}$ this QNM is weakly and even very

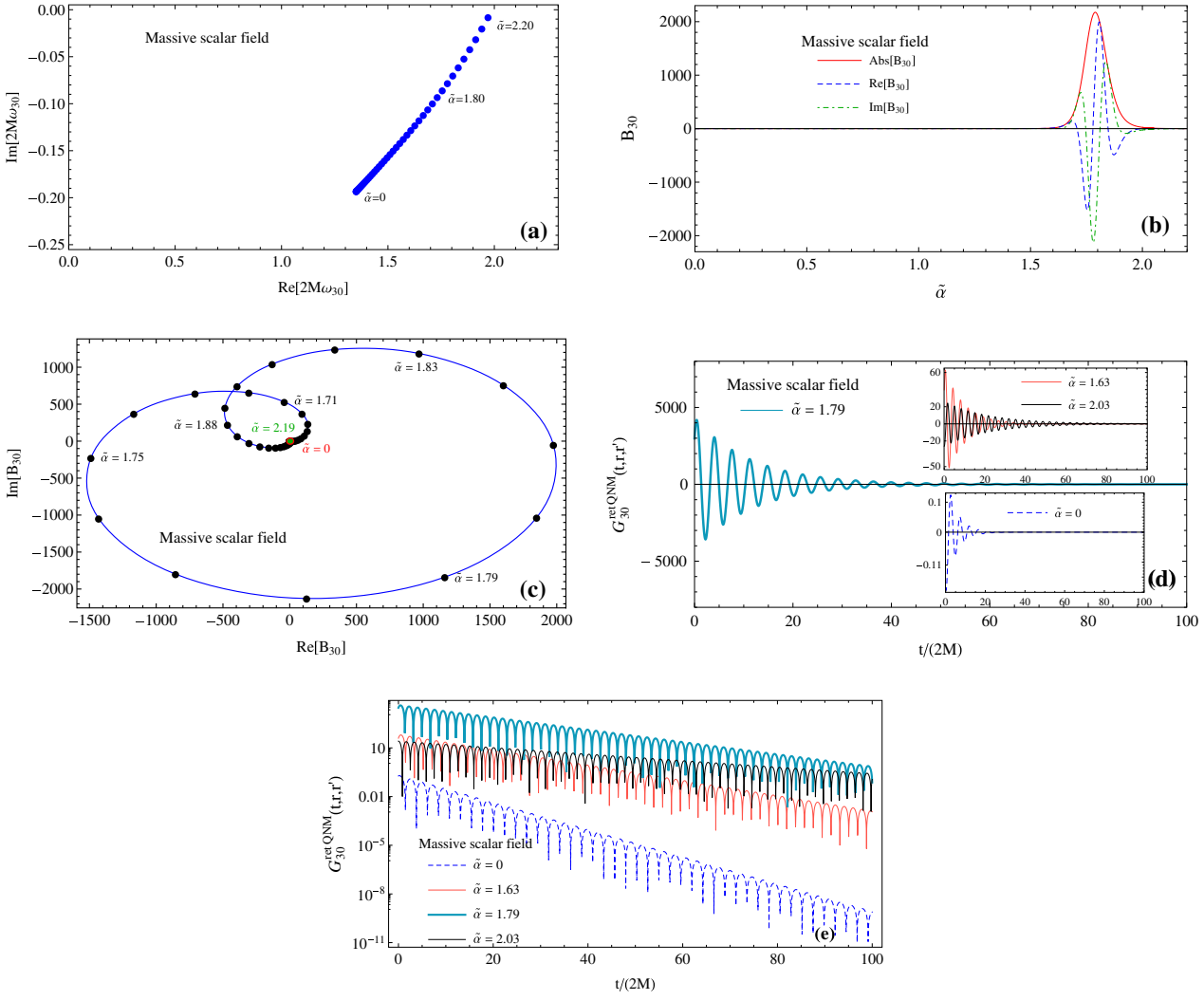

FIG. 2 (color online). The $(\ell = 3, n = 0)$ QNM of the massive scalar field. (a) The complex quasinormal frequency $2M\omega_{30}$ for $\tilde{\alpha} = 0, 0.05, \ldots, 2.15, 2.20$. (b) The resonant behavior of the excitation factor $\mathcal{B}_{30}$. (c) The excitation factor $\mathcal{B}_{30}$ for $\tilde{\alpha} = 0, 0.01, \ldots, 2.18, 2.19$. (d) and (e) Some intrinsic ringings corresponding to values of the mass near and above the critical value $\tilde{\alpha}_{30}$. We compare them with the ringing corresponding to the massless scalar field. The results are obtained from (11) with $r = 50M$ and $r' = 10M$.

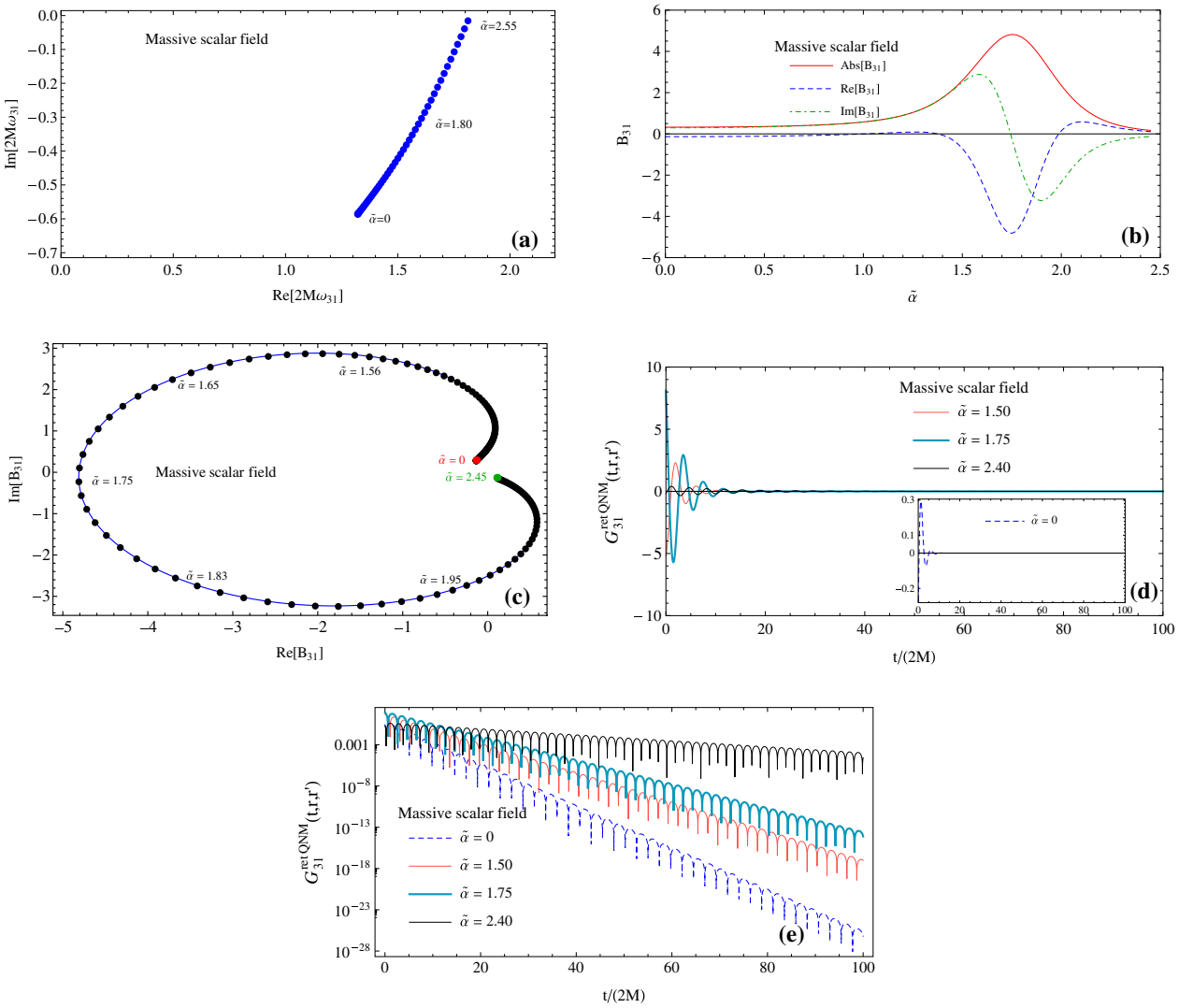

FIG. 3 (color online). The $(\ell = 3, n = 1)$ QNM of the massive scalar field. (a) The complex quasinormal frequency $2M\omega_{31}$ for $\tilde{\alpha} = 0, 0.05, \ldots, 2.50, 2.55$. (b) The resonant behavior of the excitation factor $\mathcal{B}_{31}$. (c) The excitation factor $\mathcal{B}_{31}$ for $\tilde{\alpha} = 0, 0.01, \ldots, 2.44, 2.45$. (d) and (e) Some intrinsic ringings corresponding to values of the mass near and above the critical value $\tilde{\alpha}_{31}$. We compare them with the ringing corresponding to the massless scalar field. The results are obtained from (11) with $r = 50M$ and $r' = 10M$.

weakly damped [see Fig. 1(a)]. As a consequence, for masses in a rather large range around $\tilde{\alpha}_{20}$, the BH "intrinsic" ringings constructed from the quasinormal part (11) of the retarded Green function (5) and which are generated by the scalar perturbation have a huge amplitude and are, moreover, slowly or even very slowly decaying [see Fig. 1(d) and Fig. 1(e)]. We compare them with the ringing generated by the massless scalar field which allows us to highlight the giant behavior of the ringings induced by the massive scalar field. It should be noted that we have plotted the ringings for $r = 50M$ and $r' = 10M$ but similar results can be obtained for various locations of the source and the observer. It is important to remark that, for $\tilde{\alpha} \to \tilde{\alpha}_d \approx 1.65\ldots$, $\mathrm{Im}[\omega_{20}]$ and $\mathcal{B}_{20}$ vanish and that above $\tilde{\alpha} = \tilde{\alpha}_d$ the $(\ell = 2, n = 0)$ QNM disappears. As a consequence, as $\tilde{\alpha}$ increases from $\tilde{\alpha} = 0$, the amplitude of the BH ringing increases, becomes huge in the large domain around $\tilde{\alpha}_{20}$, and then decreases when $\tilde{\alpha} \to \tilde{\alpha}_d$. However, it should be noted that when we explore the range $\tilde{\alpha} \to \tilde{\alpha}_d$, we encounter strong numerical instabilities and, in particular, it is very difficult to obtain numerically the vanishing of $\mathcal{B}_{20}$.

In Figs. 2 and 3, we respectively consider the $(\ell = 3, n = 0)$ QNM and the $(\ell = 3, n = 1)$ QNM of the massive scalar field. *Mutatis mutandis*, all the effects already noted for the $(\ell = 2, n = 0)$ QNM are still present and we shall not discuss them again. We can, however, note that the maximum of the quasinormal excitation factor seems to

TABLE I. Massive scalar field. A sample of the first quasinormal frequencies $\omega_{\ell n}$ and excitation factors $\mathcal{B}_{\ell n}$ for $\tilde{\alpha}=0$ (massless scalar field) and for $\tilde{\alpha}=\tilde{\alpha}_{\ell n}$ (massive scalar field with the mass parameter corresponding to the maximum of the excitation factor). For a given angular momentum index ℓ, only the excitation factors of the lowest overtones present a strong resonant behavior.

(ℓ,n)	$\tilde{\alpha}_{\ell n}$	$2M\omega_{\ell n}$ for $\tilde{\alpha}=0$	$\mathcal{B}_{\ell n}$ for $\tilde{\alpha}=0$	$\lvert\mathcal{B}_{\ell n}\rvert$ for $\tilde{\alpha}=0$	$2M\omega_{\ell n}$ for $\tilde{\alpha}=\tilde{\alpha}_{\ell n}$	$\mathcal{B}_{\ell n}$ for $\tilde{\alpha}=\tilde{\alpha}_{\ell n}$	$\lvert\mathcal{B}_{\ell n}\rvert$ for $\tilde{\alpha}=\tilde{\alpha}_{\ell n}$
(0,0)	0.27999	$0.220910-0.209791i$	$0.212349-0.059275i$	0.220467	$0.227442-0.179033i$	$0.263003-0.016875i$	0.263544
(1,0)	0.77371	$0.585872-0.195320i$	$-0.150670+0.022814i$	0.152388	$0.721915-0.103844i$	$-0.7542-0.5041i$	0.907094
(1,1)	0.74303	$0.528897-0.612515i$	$0.028966+0.188821i$	0.191030	$0.528356-0.524389i$	$-0.027649+0.261726i$	0.263182
(2,0)	1.28447	$0.967288-0.193517i$	$0.119355+0.013428i$	0.120108	$1.240695-0.090415i$	$1.800+21.264i$	21.340064
(2,1)	1.22223	$0.927709-0.591196i$	$0.035511-0.264290i$	0.266665	$1.033952-0.403778i$	$0.55839-0.63603i$	0.846367
(2,2)	1.23193	$0.861088-1.017117i$	$-0.286082+0.045925i$	0.289745	$0.857086-0.868873i$	$-0.462994-0.063382i$	0.467312
(3,0)	1.78928	$1.350732-0.192999i$	$-0.093638-0.040471i$	0.102010	$1.750318-0.087332i$	$1.094\times10^{3}-1.880\times10^{3}i$	2.175612×10^{3}
(3,1)	1.75358	$1.321343-0.584570i$	$-0.134112+0.294158i$	0.323288	$1.578868-0.333911i$	$-4.8046-0.3367i$	4.816410
(3,2)	1.68072	$1.267252-0.992016i$	$0.487872+0.120390i$	0.608262	$1.355312-0.741016i$	$1.08005+1.12461i$	1.559250
(3,3)	1.72590	$1.197546-1.422442i$	$-0.092651-0.517332i$	0.525563	$1.190664-1.213516i$	$0.15209-0.98334i$	0.995033
(4,0)	2.29161	$1.734831-0.192783i$	$0.068044+0.059131i$	0.090147	$2.255734-0.086470i$	$-5.54\times10^{5}+5.02\times10^{5}$	7.476094×10^{5}
(4,1)	2.28611	$1.711616-0.581782i$	$0.247593-0.275444i$	0.370367	$2.122809-0.297760i$	$22.926+49.222i$	54.299074
(4,2)	2.19818	$1.667384-0.980650i$	$-0.621067-0.421239i$	0.750444	$1.890542-0.641944i$	$0.3739-6.7715i$	6.781840
(4,3)	2.15102	$1.606576-1.394963i$	$-0.289498+0.967789i$	1.010161	$1.684235-1.084401i$	$-2.58160+2.20255i$	3.393505
(4,4)	2.22179	$1.535465-1.828039i$	$1.020115-0.205096i$	1.040528	$1.525887-1.558210i$	$2.28265+0.38472i$	2.314843

increase rapidly with the angular momentum index ℓ, a rather surprising behavior, and to decrease with the overtone index n. In Table I, where we consider a rather large sample of QMNs, we confirm these behaviors. As a consequence, for a given value of ℓ, the giant BH ringings corresponding to the fundamental tone are the most interesting ones and, moreover, as ℓ increases, their amplitudes rapidly increase. We are quite disturbed by this last result which we are not able to explain simply.

In Fig. 4 and in Table II, we consider the odd-parity QNMs of the Proca field. We can observe that their behavior (or, more precisely, the behavior of the complex quasinormal frequencies, of the quasinormal excitation factors and of the ringings) is rather similar to that of the QNMs of the massive scalar field.

In Table III, we consider the even-parity $\ell=0$ QNMs of the Proca field. We can observe that the resonant behavior of the quasinormal excitation factors is little pronounced, even for the fundamental tone.

In Fig. 5 and in Table IV, we consider the odd-parity $\ell=1$ QNMs of the Fierz-Pauli field and we observe that they presents lot of similarities with the $\ell=2$ QNMs of the massive scalar field and the odd-parity $\ell=2$ QNMs of the Proca field. We can note, in particular, the strong resonant behavior of the quasinormal excitation factor of the fundamental tone and the associated giant ringings. As already discussed in Ref. [16], such ringings could have fascinating observational consequences.

III. RESONANT BEHAVIOR OF THE QUASINORMAL EXCITATION FACTORS: A SEMICLASSICAL ANALYSIS

It is well known that the weakly damped QNMs of BHs which are associated with massless fields can be interpreted in terms of waves trapped close to the so-called photon sphere, i.e., the hypersurface on which a massless particle can orbit the BH on unstable circular null geodesics. This appealing interpretation has been suggested a long time ago by Goebel [37], has been implemented in various articles (see, e.g., Refs. [29,38,39] for an approach based on eikonal considerations and Refs. [40–43] for an approach based on Regge pole techniques) and allows us to provide analytical approximations for the complex frequencies of the QNMs. In a recent work [44], Dolan and Ottewill introduced a novel and powerful ansatz for the QNMs of spherically symmetric BHs [44]. This ansatz, which agrees with Goebel's interpretation, permitted them not only to determine the quasinormal frequencies but also to obtain an analytical expression for the quasinormal excitation factors $\mathcal{B}_{\ell n}$ of the Schwarzschild BH formally valid for large values of the angular momentum index ℓ [45]. In this section, we briefly explain how to extend the Dolan-Ottewill approach to massive fields and we then give an approximation for the quasinormal excitation factors discussed in Sec. II. It should be noted that we do not intend to enter into the technical aspects of its derivation because, *mutatis mutandis*, we extend "trivially" the calculations presented in Appendix A of Ref. [45]. We finally show that the semiclassical formula obtained describes very correctly the resonant behavior of the quasinormal excitation factors. It is important to note that, in this section, we only focus on the modes for which the large ℓ limit can be taken, i.e., on those of the scalar field and those in the odd-parity sector of the Proca field.

It is crucial to remark that two geometrical parameters are involved in the Dolan-Ottewill ansatz [see Eqs. (18) and (A13) of Ref. [45] as well as the discussion following Eq. (18) and, for more precisions and physical motivations, Sec. 5 of Ref. [44]]: the "radius" $r_c=3M$ of the photon sphere and the corresponding impact parameter $b_c=3\sqrt{3}M$. For massive fields, the situation is much more complicated (see also Ref. [43] where the Dolan-Ottewill method has been considered in the context of Regge pole techniques). Indeed, the corresponding geometrical parameters depend not only on the BH mass M but also on the rest

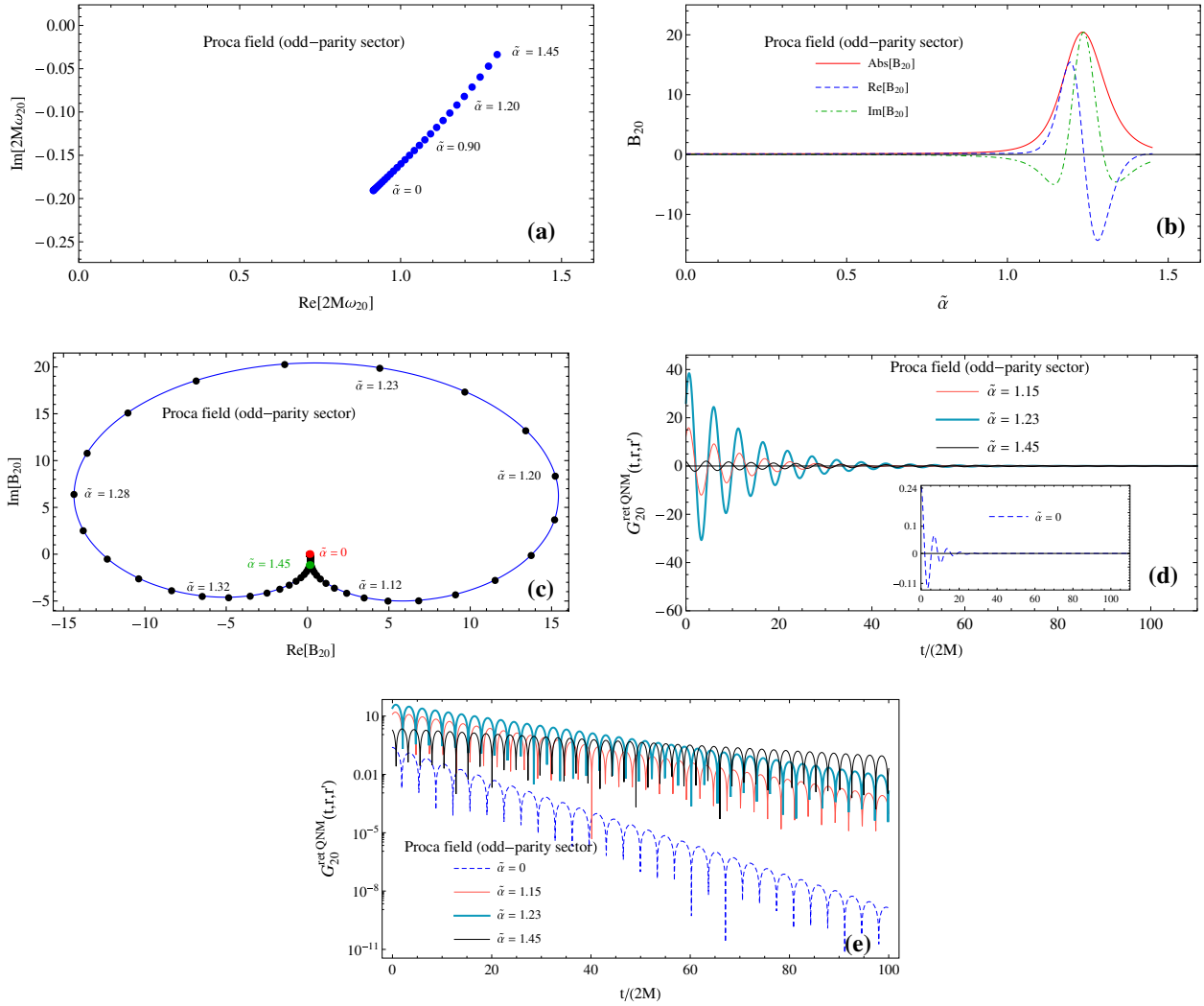

FIG. 4 (color online). The odd-parity ($\ell = 2, n = 0$) QNM of the Proca field. (a) The complex quasinormal frequency $2M\omega_{20}$ for $\tilde{\alpha} = 0, 0.05, \ldots, 1.40, 1.45$. (b) The resonant behavior of the excitation factor $\mathcal{B}_{20}$. (c) The excitation factor $\mathcal{B}_{20}$ for $\tilde{\alpha} = 0, 0.01, \ldots, 1.44, 1.45$. (d) and (e) Some intrinsic ringings corresponding to values of the mass near and above the critical value $\tilde{\alpha}_{20}$. We compare them with the ringing corresponding to the massless vector field. The results are obtained from (11) with $r = 50M$ and $r' = 10M$.

mass μ and energy ω of the particle associated with the massive field considered (see, e.g., Ref. [46]). The sphere on which the massive particle can orbit the BH on unstable circular timelike geodesics is located at $r = r_c(\omega) \in]3M, 4M[$ given by

$$r_c(\omega) = 2M\left(\frac{3 + (1 + 8v^2(\omega))^{1/2}}{1 + (1 + 8v^2(\omega))^{1/2}}\right). \tag{14}$$

Here

$$v(\omega) = \sqrt{1 - \frac{\mu^2}{\omega^2}} \tag{15}$$

denotes the particle speed at large distances from the BH which can be expressed in term of the particle momentum $p(\omega) = \sqrt{\omega^2 - \mu^2}$ by $v(\omega) = p(\omega)/\omega$. The critical radius $r_c(\omega)$ defines an associated critical impact parameter

$$b_c(\omega) = \frac{M}{\sqrt{2}v^2(\omega)}[8v^4(\omega) + 20v^2(\omega) - 1 + (1 + 8v^2(\omega))^{3/2}]^{1/2}. \tag{16}$$

We recall that any massive particle sent toward the Schwarzschild BH with an impact parameter $b < b_c(\omega)$ is captured while particles with impact parameter $b > b_c(\omega)$ are scattered. It should be also noted that, for $\mu = 0$, $v(\omega) = 1$ and from Eqs. (14) and (16) we can then recover the parameters used by Dolan and Ottewill.

These preliminary considerations permit us to understand that, in order to describe the QNMs of massive fields

TABLE II. Proca field (odd-parity sector). A sample of the first quasinormal frequencies $\omega_{\ell n}$ and excitation factors $\mathcal{B}_{\ell n}$ for $\tilde{\alpha}=0$ (massless vector field) and for $\tilde{\alpha}=\tilde{\alpha}_{\ell n}$ (massive vector field with the mass parameter corresponding to the maximum of the excitation factor). For a given angular momentum index ℓ, only the excitation factors of the lowest overtones present a strong resonant behavior.

(ℓ,n)	$\tilde{\alpha}_{\ell n}$	$2M\omega_{\ell n}$ for $\tilde{\alpha}=0$	$\mathcal{B}_{\ell n}$ for $\tilde{\alpha}=0$	$\lvert\mathcal{B}_{\ell n}\rvert$ for $\tilde{\alpha}=0$	$2M\omega_{\ell n}$ for $\tilde{\alpha}=\tilde{\alpha}_{\ell n}$	$\mathcal{B}_{\ell n}$ for $\tilde{\alpha}=\tilde{\alpha}_{\ell n}$	$\lvert\mathcal{B}_{\ell n}\rvert$ for $\tilde{\alpha}=\tilde{\alpha}_{\ell n}$
(1,0)	0.68831	$0.496527-0.184975i$	$-0.1614+0.0119i$	0.1618	$0.634396-0.086904i$	$-0.7650-0.4629i$	0.8942
(1,1)	0.70276	$0.429031-0.587335i$	$0.0118+0.1809i$	0.1813	$0.417568-0.493170i$	$-0.0428+0.2496i$	0.2533
(2,0)	1.23422	$0.915191-0.190009i$	$0.1212+0.0186i$	0.1226	$1.190479-0.084580i$	$1.9966+20.3582i$	20.4559
(2,1)	1.17146	$0.873085-0.581420i$	$0.0466-0.2590i$	0.2631	$0.974408-0.390809i$	$0.5426-0.6172i$	0.8218
(2,2)	1.21000	$0.802373-1.003175i$	$-0.2729+0.0325i$	0.2749	$0.791564-0.851199i$	$-0.4409-0.0729i$	0.4469
(3,0)	1.75351	$1.313797-0.191232i$	$-0.0934-0.0435i$	0.1031	$1.714716-0.084437i$	$1.0184\times10^{3}-1.8006\times10^{3}i$	2.0686×10^{3}
(3,1)	1.71623	$1.283475-0.579457i$	$-0.1419+0.2883i$	0.3214	$1.539459-0.326015i$	$-4.6621-0.2973i$	4.6716
(3,2)	1.64677	$1.227664-0.984133i$	$0.4725+0.1314i$	0.4905	$1.311423-0.731576i$	$1.0402+1.0982i$	1.5127

TABLE III. Proca field (even-parity $\ell=0$ QNMs). A sample of the first quasinormal frequencies $\omega_{\ell n}$ and excitation factors $\mathcal{B}_{\ell n}$ for $\tilde{\alpha}\to0$ and for $\tilde{\alpha}=\tilde{\alpha}_{\ell n}$ (Proca field with the mass parameter corresponding to the maximum of the excitation factor). For a given angular momentum index ℓ, only the excitation factors of the lowest overtones present a strong resonant behavior.

(ℓ,n)	$\tilde{\alpha}_{\ell n}$	$2M\omega_{\ell n}$ for $\tilde{\alpha}\to0$	$\mathcal{B}_{\ell n}$ for $\tilde{\alpha}\to0$	$\lvert\mathcal{B}_{\ell n}\rvert$ for $\tilde{\alpha}\to0$	$2M\omega_{\ell n}$ for $\tilde{\alpha}=\tilde{\alpha}_{\ell n}$	$\mathcal{B}_{\ell n}$ for $\tilde{\alpha}=\tilde{\alpha}_{\ell n}$	$\lvert\mathcal{B}_{\ell n}\rvert$ for $\tilde{\alpha}=\tilde{\alpha}_{\ell n}$
(0,0)	0.47912	$0.220910-0.209791i$	$-0.2123+0.0593i$	0.2205	$0.426995-0.033401i$	$-0.7147-0.1121i$	0.7234
(0,1)	0.26048	$0.172234-0.696105i$	$0.0635+0.0661i$	0.0917	$0.159227-0.682980i$	$0.0612+0.0696i$	0.0926

and to derive their excitation factors, the Dolan-Ottewill ansatz (A13) of Ref. [45] must be replaced by

$$\phi^{\pm}_{\omega\ell}(r)=\exp\left[\pm ip(\omega)\int^{r_*}\left(1+\frac{2Mb_c(\omega)^2/r_c(\omega)^2}{r'}\right)^{1/2}\times\left(1-\frac{r_c(\omega)}{r'}\right)dr'_*\right]v^{\pm}_{\omega\ell}(r), \tag{17}$$

where the functions $v^{\pm}_{\omega\ell}(r)$ are assumed to be regular for $r\to2M$, i.e., at the event horizon, and for $r\to+\infty$, i.e., at spatial infinity. It is then easy to show that the usual boundary conditions for the solutions of (6) with (3) are automatically satisfied, i.e., that $\phi^{\pm}_{\omega\ell}(r)\sim\exp[\pm i\omega r_*]$ for $r_*\to-\infty$ and $\phi^{\pm}_{\omega\ell}(r)\sim\exp[\pm i\{p(\omega)r_*+[M\mu^2/p(\omega)]\times\ln(r/M)\}]$ for $r_*\to+\infty$.

Mutatis mutandis, the derivation of the quasinormal excitation factors $\mathcal{B}_{\ell n}$ can be realized by following the different steps of Appendix A of Ref. [45] and, more precisely, by using the standard WKB techniques as well as the usual matching procedures. After a tedious calculation, we obtain

$$\mathcal{B}_{\ell n}=\frac{i(\ell+1/2)^{-1}}{\sqrt{8\pi}n!}\left(\frac{-216i(\ell+1/2)}{\xi}\right)^{n+1/2}\times\exp[2ip(\omega_{\ell n})\zeta_c(\omega_{\ell n})], \tag{18}$$

where $\xi=7+4\sqrt{3}$ and with $\zeta_c(\omega)$ given by

$$\frac{\zeta_c(\omega)}{2M}=\frac{b_c^2(\omega)}{2r_c^2(\omega)}-\frac{r_c(\omega)}{2M}\sqrt{1+\frac{2Mb_c^2(\omega)}{r_c^3(\omega)}}-\left(\frac{b_c^2(\omega)}{2r_c^2(\omega)}-\frac{r_c(\omega)}{2M}+1\right)\ln\left[\frac{b_c^2(\omega)}{2r_c^2(\omega)}+\frac{r_c(\omega)}{2M}+\frac{r_c(\omega)}{2M}\sqrt{1+\frac{2Mb_c^2(\omega)}{r_c^3(\omega)}}\right]$$
$$+\left(\frac{r_c(\omega)}{2M}-1\right)\sqrt{1+\frac{b_c^2(\omega)}{r_c^2(\omega)}}\ln\left[\left(\frac{r_c(\omega)}{2M}-1\right)\left(\frac{b_c^2(\omega)}{2r_c^2(\omega)}+1+\sqrt{1+\frac{b_c^2(\omega)}{r_c^2(\omega)}}\right)\right]-\left(\frac{r_c(\omega)}{2M}-1\right)\sqrt{1+\frac{b_c^2(\omega)}{r_c^2(\omega)}}$$
$$\times\ln\left[\frac{b_c^2(\omega)}{2r_c^2(\omega)}\left(\frac{r_c(\omega)}{2M}+1\right)+\frac{r_c(\omega)}{2M}+\frac{r_c(\omega)}{2M}\sqrt{\left(1+\frac{2Mb_c^2(\omega)}{r_c^3(\omega)}\right)\left(1+\frac{b_c^2(\omega)}{r_c^2(\omega)}\right)}\right]+\ln2. \tag{19}$$

It is straightforward to show that, for $\mu\to0$, $\zeta_c(\omega)=(3-3\sqrt{3}+4\ln2-3\ln\xi)M$ and Eq. (18) then reduces to Eq. (31) of Ref [45]. It is also important (i) to recall that the Dolan-Ottewill approach we have extended for massive fields only provides, for the quasinormal excitation factors, a leading-order expansion in $\ell+1/2$ and (ii) to note that the spin dependence, or more precisely the coefficient β in (3), does not play any role.

In Figs. 6, 7 and 8, we plot the behaviors of some quasinormal excitation factors. We consider the massive

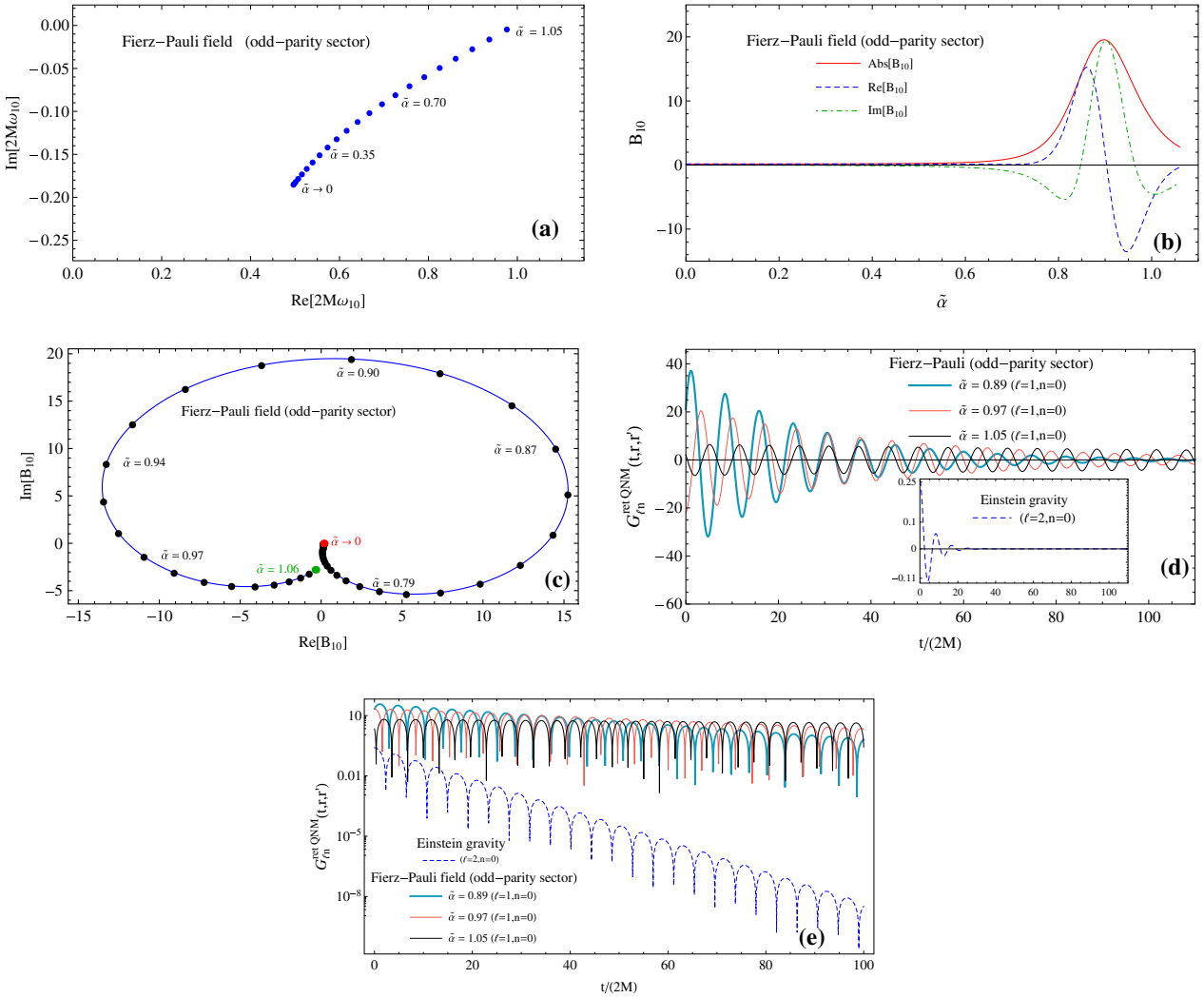

FIG. 5 (color online). The odd-parity $(\ell = 1, n = 0)$ QNM of the Fierz-Pauli field. (a) The complex quasinormal frequency $2M\omega_{10}$ for $\tilde{\alpha} = 0, 0.05, \ldots, 1.00, 1.05$. (b) The resonant behavior of the excitation factor $\mathcal{B}_{10}$. (c) The excitation factor $\mathcal{B}_{10}$ for $\tilde{\alpha} = 0, 0.01, \ldots, 1.05, 1.06$. (d) and (e) Some intrinsic ringings corresponding to values of the mass near and above the critical value $\tilde{\alpha}_{10}$. We compare them with the ringing corresponding to the odd-parity $(\ell = 2, n = 0)$ QNM of the massless spin-2 field. The results are obtained from (11) with $r = 50M$ and $r' = 10M$.

scalar field and the $(\ell = 3, n = 0)$, $(\ell = 3, n = 1)$, and $(\ell = 4, n = 0)$ QNMs. We compare the numerical results obtained in Sec. II ("exact" results) with the asymptotic results provided by formula (18). It should be noted that we have put into this formula the exact behavior of the complex quasinormal frequencies $\omega_{\ell n}$ we numerically obtained in Sec. II. For the two fundamental QNMs considered [see Figs. 6 and 8], the agreement is impressive. In particular, the strong resonant behavior of the quasinormal excitation factors is very well predicted. For the

TABLE IV. Fierz-Pauli field (odd-parity $\ell = 1$ QNMs). A sample of the first quasinormal frequencies $\omega_{\ell n}$ and excitation factors $\mathcal{B}_{\ell n}$ for $\tilde{\alpha} \to 0$ and for $\tilde{\alpha} = \tilde{\alpha}_{\ell n}$ (Fierz-Pauli field with the mass parameter corresponding to the maximum of the excitation factor). For a given angular momentum index ℓ, only the excitation factors of the lowest overtones present a strong resonant behavior.

(ℓ, n)	$\tilde{\alpha}_{\ell n}$	$2M\omega_{\ell n}$ for $\tilde{\alpha} \to 0$	$\mathcal{B}_{\ell n}$ for $\tilde{\alpha} \to 0$	$\lvert\mathcal{B}_{\ell n}\rvert$ for $\tilde{\alpha} \to 0$	$2M\omega_{\ell n}$ for $\tilde{\alpha} = \tilde{\alpha}_{\ell n}$	$\mathcal{B}_{\ell n}$ for $\tilde{\alpha} = \tilde{\alpha}_{\ell n}$	$\lvert\mathcal{B}_{\ell n}\rvert$ for $\tilde{\alpha} = \tilde{\alpha}_{\ell n}$
(1,0)	0.89757	$0.496527 - 0.184975i$	$0.1614 - 0.0119i$	0.1618	$0.859691 - 0.038782i$	$3.2524 + 19.2819i$	19.5543
(1,1)	0.82081	$0.429031 - 0.587335i$	$-0.0118 - 0.1809i$	0.1813	$0.397013 - 0.261246i$	$0.1969 - 0.4443i$	0.4860
(1,2)	1.08214	$0.349547 - 1.050375i$	$-0.0816 + 0.0721i$	0.1089	$0.223343 - 0.920334i$	$-0.1215 + 0.0669i$	0.1387

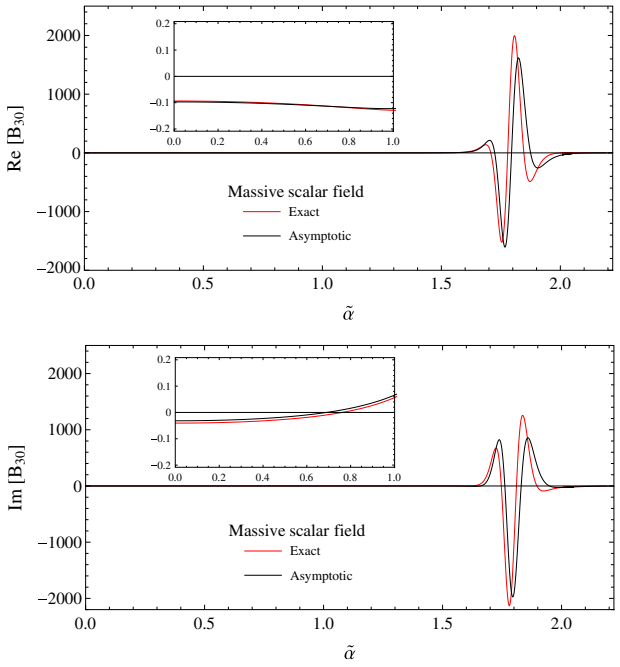

FIG. 6 (color online). The quasinormal excitation factor of the $(\ell = 3, n = 0)$ QNM of the scalar field. Exact and asymptotic behaviors.

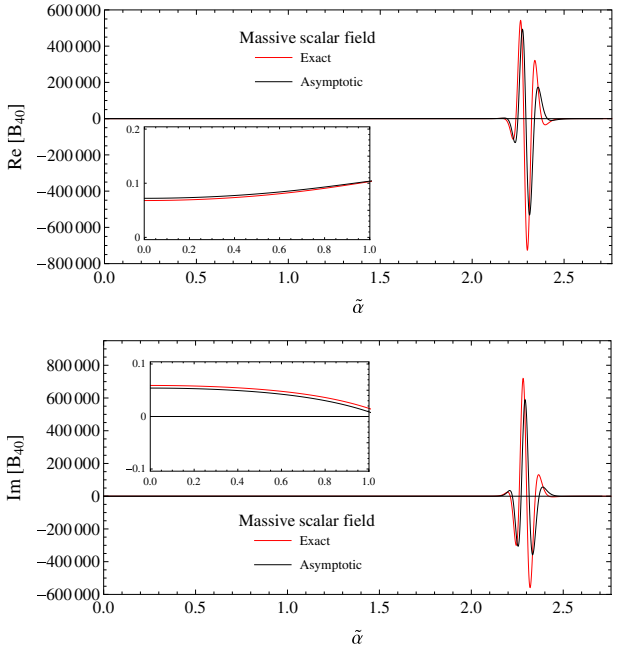

FIG. 8 (color online). The quasinormal excitation factor of the $(\ell = 4, n = 0)$ QNM of the scalar field. Exact and asymptotic behaviors.

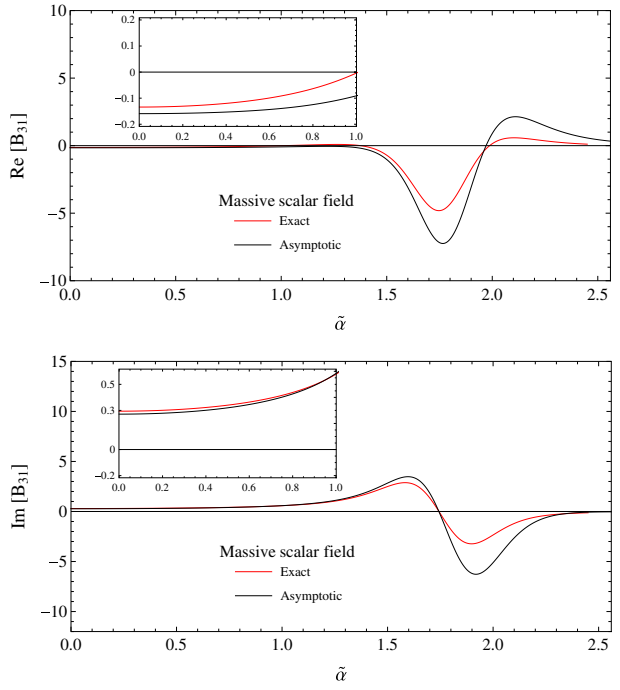

FIG. 7 (color online). The quasinormal excitation factor of the $(\ell = 3, n = 1)$ QNM of the scalar field. Exact and asymptotic behaviors.

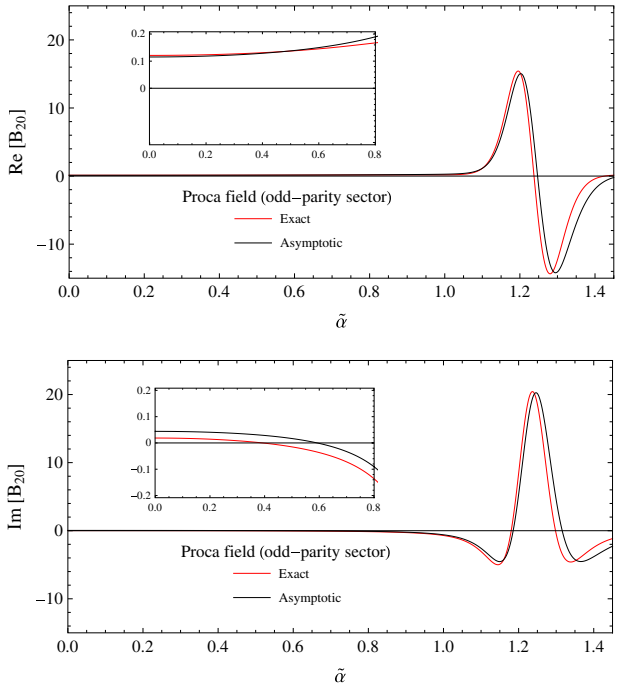

FIG. 9 (color online). The quasinormal excitation factor of the odd-parity $(\ell = 2, n = 0)$ QNM of the Proca field. Exact and asymptotic behaviors.

overtone QNM [see Fig. 7], the agreement remains satisfactory and is even very good for low values of the mass. This is also the case for the $(\ell = 2, n = 0)$ fundamental QNM while the quasinormal excitation factors of the $\ell = 0$ and 1 QNMs cannot be correctly described by formula (18). Similar considerations apply for the QNMs in the odd-parity sector of the Proca field and formula (18) can be also used efficiently in this context. It gives results that are even more accurate because the coefficient β, which has been neglected in the derivation of (18), vanishes for these QNMs. In Fig. 9, we focus on the quasinormal excitation factor of the odd-parity $(\ell = 2, n = 0)$ QNM of the Proca field. The agreement between the exact and asymptotic results is again impressive.

IV. EXTRINSIC GIANT RINGINGS

The quasinormal frequencies $\omega_{\ell n}$ and the associated excitation factors $\mathcal{B}_{\ell n}$ discussed in the two previous sections are intrinsic properties of the BH interacting with a massive bosonic field. As a consequence, the extraordinary ringings we have exhibited in Sec. II and which are constructed from the quasinormal retarded Green function (11) are not directly relevant to physics or astrophysics because they do not take into account the external mechanism which generates the BH distortion. In fact, it is necessary to check that if we consider a realistic perturbation of the BH, there still exists a giant ringing into the response obtained by convolution of the source of the perturbation with the retarded Green function. Of course, with astrophysical considerations in mind, it would be very interesting to consider as a source a "particle" falling radially or plunging into the BH but, in the framework of massive field theories, this is a very difficult problem which, to our knowledge, has never been addressed. To simplify our purpose, we shall consider a more simple problem, but despite that, it will provide us with interesting information.

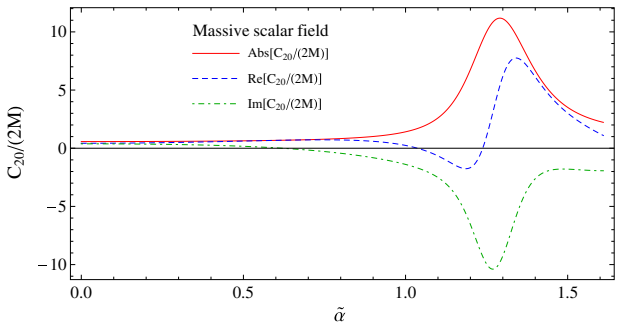

FIG. 10 (color online). Resonant behavior of the excitation coefficient $\mathcal{C}_{20}$ of the $(\ell = 2, n = 0)$ QNM of the massive scalar field. It is obtained from (24) by using (20) with $\phi_0 = 1$, $a = 1$, and $r_0 = 10M$.

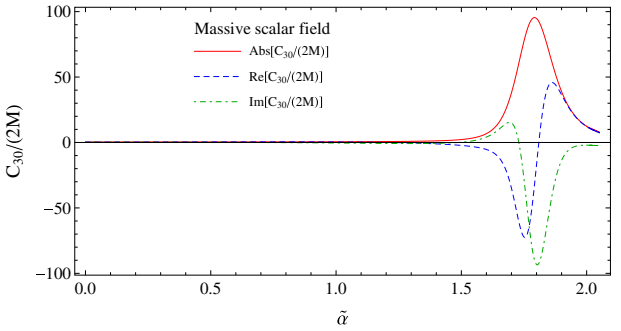

FIG. 11 (color online). Resonant behavior of the excitation coefficient $\mathcal{C}_{30}$ of the $(\ell = 3, n = 0)$ QNM of the massive scalar field. It is obtained from (24) by using (20) with $\phi_0 = 1$, $a = 1$, and $r_0 = 10M$.

We consider that the BH perturbation is generated by an initial value problem with (nonlocalized) Gaussian initial data [30–32]. More precisely, we assume that the partial amplitude $\phi_\ell(t, r)$ solution of (2) is given, at $t = 0$, by

$$\phi_\ell(t = 0, r) = \phi_0 \exp\left[-\frac{a^2}{(2M)^2}[r_*(r) - r_*(r_0)]^2\right] \quad (20)$$

and, moreover, satisfies $\partial_t \phi_\ell(t = 0, r) = 0$. By Green's theorem and using (2) and (4), we can show that

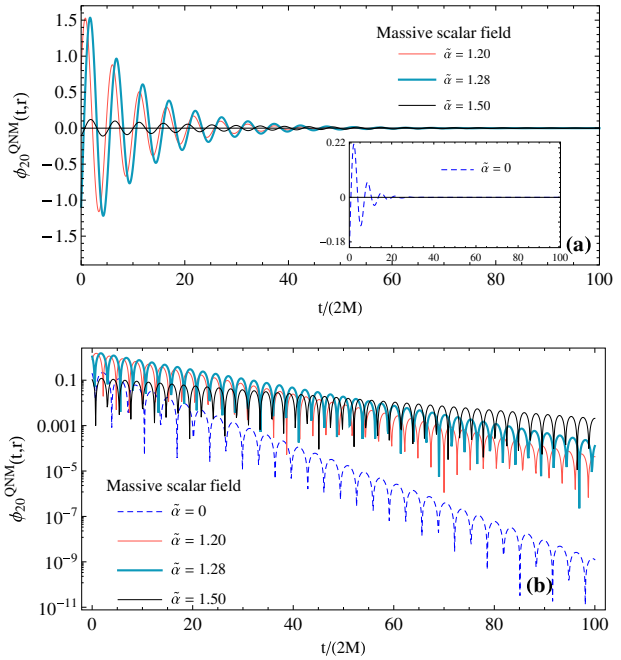

FIG. 12 (color online). The $(\ell = 2, n = 0)$ QNM of the massive scalar field. (a) and (b) Some extrinsic ringings corresponding to values of the mass near and above the critical value $\tilde{\alpha}_{20}$ and comparison with the ringing associated with the massless scalar field. Here the results are obtained from (23) with $r = 50M$ and by using (20) with $\phi_0 = 1$, $a = 1$, and $r_0 = 10M$.

$$\phi_\ell(t,r) = \int \partial_t G^{\rm ret}_\ell(t;r,r')\phi_\ell(t=0,r')dr'_* \qquad (21)$$

describes the time evolution of $\phi_\ell(t,r)$ for $t>0$. We can now insert (5) into (21) and deform again the contour of integration in the complex ω plane in order to capture the contribution of the QNMs. This allows us to isolate the BH ringing generated by the initial data. We have

$$\phi^{\rm QNM}_\ell(t,r) = \sum_n \phi^{\rm QNM}_{\ell n}(t,r) \qquad (22)$$

with

$$\phi^{\rm QNM}_{\ell n}(t,r) = 2\,{\rm Re}[i\omega_{\ell n}\mathcal{C}_{\ell n} \times e^{-i[\omega_{\ell n}t - p(\omega_{\ell n})r_* - [M\mu^2/p(\omega_{\ell n})]\ln(r/M)]}]. \qquad (23)$$

Here $\mathcal{C}_{\ell n}$ denotes the excitation coefficient of the (ℓ,n) QNM. It is defined from the corresponding excitation factor $\mathcal{B}_{\ell n}$ but, in addition, it takes explicitly into account the role of the source of the BH perturbation. We have

$$\mathcal{C}_{\ell n} = \mathcal{B}_{\ell n}\int \frac{\phi_\ell(t=0,r')\phi^{\rm in}_{\omega_{\ell n}\ell}(r')}{\sqrt{\omega_{\ell n}/p(\omega_{\ell n})}A^{(+)}_\ell(\omega_{\ell n})}dr'_*. \qquad (24)$$

The excitation coefficients $\mathcal{C}_{\ell n}$ can be easily calculated. Indeed, in order to obtain the excitation factors $\mathcal{B}_{\ell n}$ we have already constructed the functions $\phi^{\rm in}_{\omega_{\ell n}\ell}(r)$ and determined the coefficients $A^{(+)}_\ell(\omega_{\ell n})$ by solving numerically the Regge-Wheeler equation (6). The evaluation of the integral in Eq. (24) is then elementary. It should be, however, noted that the numerical instabilities we discussed in Sec. II and that occur near the values of the mass parameter for which the $\mathcal{B}_{\ell n}$ vanish are still present. They forbid us to investigate the behavior of the BH ringing (23) for the corresponding masses. It should be also noted that by describing the BH ringing by formula (23) we are again confronted with the time-shift problem. Here, we shall consider that this formula can be used beyond the starting time $t_{\rm start}\approx[r_*+r_*(r_0)]{\rm Re}[\omega_{\ell n}]/{\rm Re}[p(\omega_{\ell n})]$. This seems rather reasonable if the width of the Gaussian function (20) is not too large, i.e., if a is not too small.

In Fig. 10 where we consider the $(\ell=2,n=0)$ QNM of the massive scalar field, we exhibit the strong resonant behavior of $\mathcal{C}_{20}$ for particular values of the parameters a and r_0 defining the initial data (20). It should be noted that, in fact, it depends little on these parameters. By comparing Fig. 10 and Fig. 1(b), we can observe that the resonant behaviors of $\mathcal{C}_{20}$ and $\mathcal{B}_{20}$ are rather similar, both occurring for masses in a range where the QNM is a long-lived mode,

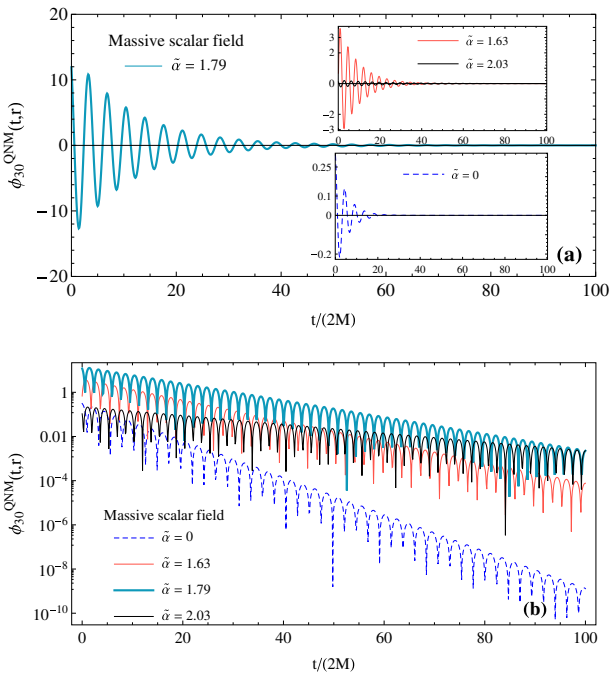

FIG. 13 (color online). The $(\ell=3,n=0)$ QNM of the massive scalar field. (a) and (b) Some extrinsic ringings corresponding to values of the mass near and above the critical value $\tilde\alpha_{30}$ and a comparison with the ringing associated with the massless scalar field. Here the results are obtained from (23) with $r=50M$ and by using (20) with $\phi_0=1$, $a=1$, and $r_0=10M$.

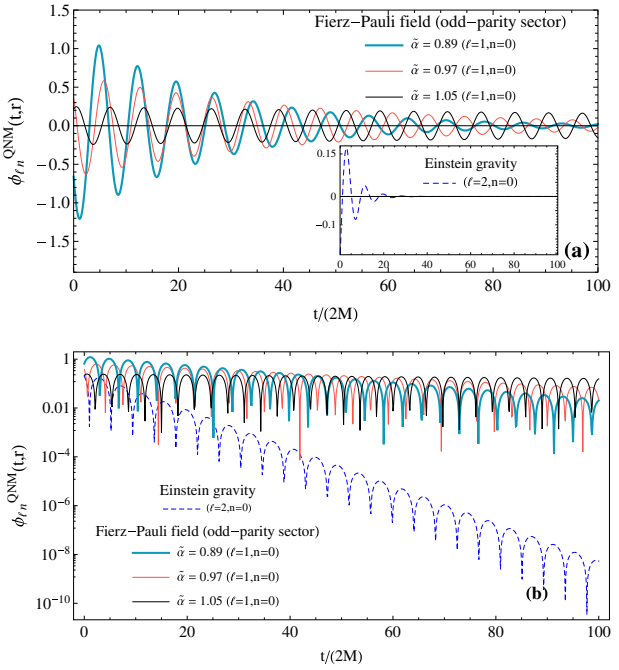

FIG. 14 (color online). The odd-parity $(\ell=1,n=0)$ QNM of the Fierz-Pauli field. (a) and (b) Some extrinsic ringings corresponding to values of the mass near and above the critical value $\tilde\alpha_{10}$ and a comparison with the ringing associated with the odd-parity $(\ell=2,n=0)$ QNM of the massless spin-2 field. Here the results are obtained from (23) with $r=50M$ and by using (20) with $\phi_0=1$, $a=1$, and $r_0=10M$.

but that the first one is more attenuated than the second one. It should be also noted that the positions of the maximums of $|\mathcal{C}_{20}|$ and $|\mathcal{B}_{20}|$ are slightly shifted. Similar considerations seem to apply for the other excitation coefficients $\mathcal{C}_{\ell n}$ of the massive scalar field [see, e.g., Fig. 11 and Fig. 2(b) where we consider, respectively, the excitation coefficient $\mathcal{C}_{30}$ and the excitation factor $\mathcal{B}_{30}$ of the $(\ell = 3, n = 0)$ QNM] and for all the other massive bosonic fields. However, it is important to note that, for overtones, the resonance phenomenon is more and more attenuated as the overtone index n increases. As a consequence, we can predict that the extrinsic ringings generated by the fundamental QNMs are certainly the most interesting and that, like the corresponding intrinsic ringings, they have huge and slowly decaying amplitudes.

In Figs. 12 and 13, we focus again on the $(\ell = 2, n = 0)$ and $(\ell = 3, n = 0)$ QNMs of the massive scalar field. We plot, for the various masses already considered in Figs. 1 and 2, the BH "extrinsic" ringings defined by (23) and we compare them with the extrinsic ringings generated by the massless scalar field. We can immediately observe that giant and slowly decaying ringings also exist when we take into account the role of the source of the BH perturbation.

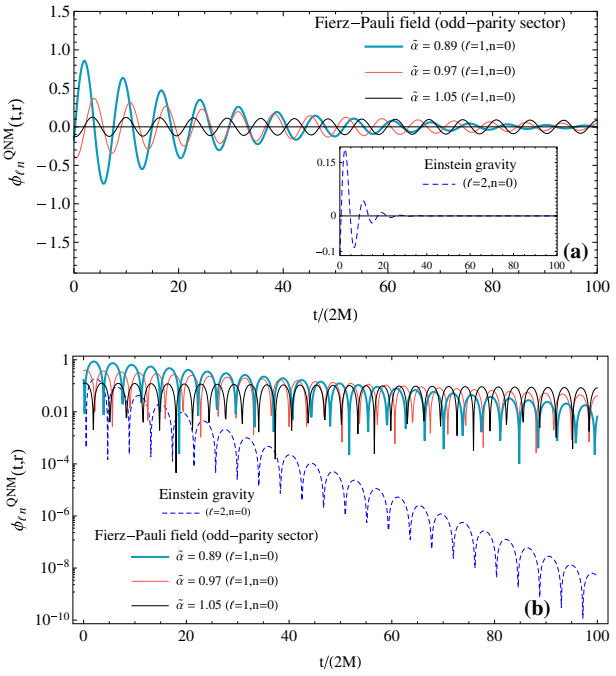

FIG. 15 (color online). The odd-parity $(\ell = 1, n = 0)$ QNM of the Fierz-Pauli field. (a) and (b) Some extrinsic ringings corresponding to values of the mass near and above the critical value $\tilde{\alpha}_{10}$ and a comparison with the ringing associated with the odd-parity $(\ell = 2, n = 0)$ QNM of the massless spin-2 field. Here the results are obtained from (23) with $r = 50M$ and by using (20) with $\phi_0 = 1$, $a = 1$, and $r_0 = 20M$.

It should be noted that, in Figs. 12 and 13, we have plotted the ringings for $r = 50M$ and $r_0 = 10M$ but similar results can be obtained for various locations of the observer and for various values of the parameters a and r_0 defining the initial data (20). In particular, in Figs. 14 and 15 where we highlight the extraordinary extrinsic ringings generated in the context of massive gravity by the odd-parity $(\ell = 1, n = 0)$ QNM of the Fierz-Pauli field, we point out the influence of r_0.

V. CONCLUSION AND PERSPECTIVES

In this article, by considering three important massive bosonic field theories in the Schwarzschild spacetime, we have shown that the excitation factors of their long-lived QNMs have a strong resonant behavior with, as a consequence, the existence of giant and slowly decaying ringings in rather large domains of the mass parameter. We have more particularly studied the role of the angular momentum index ℓ and of the overtone index n of the QNMs and we have also checked that the resonant effect and the associated giant ringing phenomenon still exist when the source of the BH perturbation is described by an initial value problem with Gaussian initial data. Of course, we should now consider more realistic BH excitations such as the excitation by a particle falling radially or plunging and, with in mind astrophysical implications, to extend our study to the Kerr BH. Furthermore, it would be necessary to examine the full response of the BH to an external perturbation and not only the part associated with QNMs. Indeed, for massless fields, the QNM contribution can be easily identified into the full response of the BH but, for massive fields, the situation might be different due to their dispersive character. But even if this is the case, i.e., if the QNM contribution is blurred, it is nevertheless clear that the resonant behavior of the excitation factors of the long-lived QNMs must induce a huge amplification of the BH response.

It should be noted that, in the present study, we have only focussed on the QNMs which are governed by a single differential equation of the Regge-Wheeler-type so our task has been greatly simplified. But what happens for the even-parity $\ell \geq 1$ QNMs of the Proca field as well as for the even-parity $\ell \geq 1$ QNMs and the odd-parity $\ell \geq 2$ QNMs of the Fierz-Pauli field? Do they generate giant ringings? Of course, this seems quite natural (we have just shown that, for the QNMs of the massive scalar field and for the odd-parity QNMs of the Proca field, giant ringings exist for all values of the angular momentum ℓ) but remains to be proved which is far from obvious: indeed, depending on the parity sector and the angular momentum index, these QNMs are governed by two or three coupled differential equations [6,10,22] and, as a consequence, the corresponding excitation factors and ringings are more challenging to compute while, at first sight, a semiclassical approach of the problem seems out of reach.

It should be also noted that we have numerically and semiclassically shown that the maximum of the amplitude

of the quasinormal excitation factors increases rapidly with the angular momentum index ℓ. We are quite disturbed by this puzzling result which we are not able to explain simply but we believe that it is harmless. Indeed,

(i) if it was limited to the spin-2 field, we might associate it with a new kind of BH instability but, because it also exists for the other two bosonic fields, such an explanation is not satisfactory,

(ii) it does not seem to lead to a divergent behavior of sums like (10) or (22) because, even if we consider a value of the mass parameter for which one of the QNM generates a huge contribution, the contributions of all the other QNMs vanish or are neglectable.

Our work is motivated by the possible implications for ultralight bosonic fields but, of course, our results could have also consequences in the context of ordinary massive bosonic fields interacting with primordial BHs. In this context, it would be interesting to consider, in addition, massive fermionic fields and to check that the resonant effects studied in this article also exist for such fields.

Let us finally note that the strong resonant behavior of the excitation factors of the long-lived QNMs is a new effect in BH physics so a lot of work remains to be done to understand all its physical consequences. This article and our previous one [16] are a first step in this direction, limited to astrophysical implications, but we think that this effect could also have interesting implications in the context of quantum field theory in curved spacetime (Hawking effect and absorption cross section, renormalized stress-energy tensors and associated correlators, etc.) and perhaps in string theory and, more particularly, in the context of the Kerr/CFT correspondence. Some of these directions will be explored shortly.

ACKNOWLEDGMENTS

We wish to thank Andrei Belokogne for various discussions and the "Collectivité Territoriale de Corse" for its support through the COMPA project. We are grateful to Vitor Cardoso for comments on our recent work [16] and for pointing us to an important reference.

[1] A. Arvanitaki, S. Dimopoulos, S. Dubovsky, N. Kaloper, and J. March-Russell, Phys. Rev. D **81**, 123530 (2010).
[2] J. Rosa, J. High Energy Phys. 06 (2010) 015.
[3] A. Arvanitaki and S. Dubovsky, Phys. Rev. D **83**, 044026 (2011).
[4] J. Barranco, A. Bernal, J. C. Degollado, A. Diez-Tejedor, M. Megevand, M. Alcubierre, D. Núñez, and O. Sarbach, Phys. Rev. D **84**, 083008 (2011).
[5] V. Cardoso, S. Chakrabarti, P. Pani, E. Berti, and L. Gualtieri, Phys. Rev. Lett. **107**, 241101 (2011).
[6] J. G. Rosa and S. R. Dolan, Phys. Rev. D **85**, 044043 (2012).
[7] J. Barranco, A. Bernal, J. C. Degollado, A. Diez-Tejedor, M. Megevand, M. Alcubierre, D. Núñez, and O. Sarbach, Phys. Rev. Lett. **109**, 081102 (2012).
[8] P. Pani, V. Cardoso, L. Gualtieri, E. Berti, and A. Ishibashi, Phys. Rev. Lett. **109**, 131102 (2012).
[9] S. R. Dolan, Phys. Rev. D **87**, 124026 (2013).
[10] R. Brito, V. Cardoso, and P. Pani, Phys. Rev. D **88**, 023514 (2013).
[11] R. Brito, V. Cardoso, and P. Pani, Phys. Rev. D **87**, 124024 (2013).
[12] E. Babichev and A. Fabbri, Classical Quantum Gravity **30**, 152001 (2013).
[13] R. Brito, V. Cardoso, and P. Pani, Phys. Rev. D **88**, 064006 (2013).
[14] S. Hod, Classical Quantum Gravity **30**, 237002 (2013).
[15] J. Barranco, A. Bernal, J. C. Degollado, A. Diez-Tejedor, M. Megevand *et al.*, arXiv:1312.5808.
[16] Y. Decanini, A. Folacci, and M. Ould El Hadj, arXiv:1401.0321.
[17] M. Fierz, Helv. Phys. Acta **12**, 3 (1939).
[18] M. Fierz and W. Pauli, Proc. R. Soc. A **173**, 211 (1939).
[19] S. Hassan, A. Schmidt-May, and M. von Strauss, J. High Energy Phys. 05 (2013) 086.
[20] C. de Rham and G. Gabadadze, Phys. Rev. D **82**, 044020 (2010).
[21] C. de Rham, G. Gabadadze, and A. J. Tolley, Phys. Rev. Lett. **106**, 231101 (2011).
[22] R. Konoplya, Phys. Rev. D **73**, 024009 (2006).
[23] N. Deruelle and R. Ruffini, Phys. Lett. **52B**, 437 (1974).
[24] T. Damour, N. Deruelle, and R. Ruffini, Lett. Nuovo Cimento Soc. Ital. Fis. **15**, 257 (1976).
[25] T. Zouros and D. Eardley, Ann. Phys. (N.Y.) **118**, 139 (1979).
[26] S. L. Detweiler, Phys. Rev. D **22**, 2323 (1980).
[27] S. L. Detweiler, Astrophys. J. **239**, 292 (1980).
[28] L. E. Simone and C. M. Will, Classical Quantum Gravity **9**, 963 (1992).
[29] V. Ferrari and B. Mashhoon, Phys. Rev. D **30**, 295 (1984).
[30] E. Berti and V. Cardoso, Phys. Rev. D **74**, 104020 (2006).
[31] E. W. Leaver, Phys. Rev. D **34**, 384 (1986).
[32] N. Andersson, Phys. Rev. D **55**, 468 (1997).
[33] E. Leaver, Proc. R. Soc. A **402**, 285 (1985).
[34] R. Konoplya and A. Zhidenko, Phys. Lett. B **609**, 377 (2005).
[35] B. Majumdar and N. Panchapakesan, Phys. Rev. D **40**, 2568 (1989).
[36] C. M. Bender and S. A. Orszag, *Advanced Mathematical Methods for Scientists and Engineers* (McGraw-Hill Book Co., Singapore, 1978).

[37] C. J. Goebel, Astrophys. J. **172**, L95 (1972).
[38] L. Vanzo and S. Zerbini, Phys. Rev. D **70**, 044030 (2004).
[39] V. Cardoso, A. S. Miranda, E. Berti, H. Witek, and V. T. Zanchin, Phys. Rev. D **79**, 064016 (2009).
[40] Y. Decanini, A. Folacci, and B. Jensen, Phys. Rev. D **67**, 124017 (2003).
[41] Y. Decanini and A. Folacci, Phys. Rev. D **81**, 024031 (2010).
[42] Y. Decanini, A. Folacci, and B. Raffaelli, Phys. Rev. D **81**, 104039 (2010).
[43] Y. Decanini, A. Folacci, and B. Raffaelli, Phys. Rev. D **84**, 084035 (2011).
[44] S. R. Dolan and A. C. Ottewill, Classical Quantum Gravity **26**, 225003 (2009).
[45] S. R. Dolan and A. C. Ottewill, Phys. Rev. D **84**, 104002 (2011).
[46] W. Unruh, Phys. Rev. D **14**, 3251 (1976).

CHAPITRE 7

Formes d'ondes en gravité massive et neutralisation des sonneries géantes

Dans les deux chapitres précédents (Chap. 5 et 6), nous avons montré l'existence d'un effet nouveau et inattendu dans la physique des trous noirs : pour les champs bosoniques massifs se propageant sur l'espace-temps de Schwarzschild, les facteurs d'excitation des QNMs ont un comportement résonant aux alentours d'une valeur critique du paramètre de masse ce qui, théoriquement, pourrait conduire à des sonneries d'amplitude géante et à faible décroissance temporelle.

Nous allons montrer, dans ce chapitre, que ces sonneries géantes sont neutralisées dans la forme d'onde en raison de la coexistence de deux phénomènes : (i) l'excitation des QBSs du trou noir de Schwarzschild qui floutent la contribution des QNMs (ii) la nature évanescente du mode partiel qui pourrait exciter le QNM concerné et générer le comportement résonant de son facteur d'excitation. Malgré cela, en gardant toujours à l'esprit la possibilité de tester la gravité massive, il est intéressant de noter que l'amplitude de la forme d'onde est néanmoins assez prononcée et à faible décroissance temporelle (ce dernier effet est dû à l'excitation des QBSs de longue durée de vie). Il est à noter également que, pour les faibles valeurs de la masse du graviton (correspondant au régime de faible instabilité du trou noir), la forme d'onde quasi-normale (sonnerie) peut être clairement identifiée et pourrait être utilisée comme une signature du graviton massif.

Pour ce faire, nous considérons toujours que la source de la perturbation est décrite par un problème de Cauchy avec des données initiales gaussiennes et nous limitons notre étude au mode impair $\ell = 1$ de la théorie du Fierz-Pauli dans l'espace-temps de Schwarzschild, tout en considérant la totalité du signal généré par la perturbation.

PHYSICAL REVIEW D **93,** 124027 (2016)

Waveforms in massive gravity and neutralization of giant black hole ringings

Yves Décanini,[*] Antoine Folacci,[†] and Mohamed Ould El Hadj[‡]

Equipe Physique Théorique—Projet COMPA, SPE, UMR 6134 du CNRS et de l'Université de Corse, Université de Corse, Faculté des Sciences, BP 52, F-20250 Corte, France

(Received 10 February 2016; published 13 June 2016)

A distorted black hole radiates gravitational waves in order to settle down in a smoother geometry. During that relaxation phase, a characteristic damped ringing is generated. It can be theoretically constructed from both the black hole quasinormal frequencies (which govern its oscillating behavior and its decay) and the associated excitation factors (which determine intrinsically its amplitude) by carefully taking into account the source of the distortion. In the framework of massive gravity, the excitation factors of the Schwarzschild black hole have an unexpected strong resonant behavior which, theoretically, could lead to giant and slowly decaying ringings. If massive gravity is relevant to physics, one can hope to observe these extraordinary ringings by using the next generations of gravitational wave detectors. Indeed, they could be generated by supermassive black holes if the graviton mass is not too small. In fact, by focusing on the odd-parity $\ell = 1$ mode of the Fierz-Pauli field, we shall show here that such ringings are neutralized in waveforms due to (i) the excitation of the quasibound states of the black hole and (ii) the evanescent nature of the particular partial modes which could excite the concerned quasinormal modes. Despite this, with observational consequences in mind, it is interesting to note that the waveform amplitude is nevertheless rather pronounced and slowly decaying (this effect is now due to the long-lived quasibound states). It is worth noting also that, for very low values of the graviton mass (corresponding to the weak instability regime for the black hole), the waveform is now very clean and dominated by an ordinary ringing which could be used as a signature of massive gravity.

DOI: 10.1103/PhysRevD.93.124027

I. INTRODUCTION

In a recent article [1] (see also the preliminary note [2]), we have discussed a new and unexpected effect in black hole (BH) physics: for massive bosonic fields in the Schwarzschild spacetime, the excitation factors of the quasinormal modes (QNMs) have a strong resonant behavior around critical values of the mass parameter leading to giant ringings which are, in addition, slowly decaying due to the long-lived character of the QNMs. We have described and analyzed this effect numerically and confirmed it analytically by semiclassical considerations based on the properties of the unstable circular geodesics on which a massive particle can orbit the BH. We have also focused on this effect for the massive spin-2 field. Here, we refer to Refs. [3,4] for recent reviews on massive gravity, to Refs. [5,6] for reviews on BH solutions in massive gravity, and to Refs. [4,6–11] for articles dealing with gravitational radiation from BHs and BH perturbations in the context of massive gravity.

In our previous works [1,2], we have considered the Fierz-Pauli theory in the Schwarzschild spacetime [8] which can be obtained by linearization of the ghost-free bimetric theory of Hassan, Schmidt-May, and von Strauss discussed in Ref. [12] and which is inspired by the fundamental work of de Rham, Gabadadze, and Tolley [13,14]. For this spin-2 field, we have considered more particularly the odd-parity ($\ell = 1, n = 0$) QNM. (Note that it is natural to think that similar results can be obtained for all the other QNMs—see also Ref. [1].) We have then shown that the resonant behavior of the associated excitation factor occurs in a large domain around a critical value $\tilde{\alpha}_0 \approx 0.90$ of the dimensionless mass parameter $\tilde{\alpha} = 2M\mu/m_{\mathrm{P}}{}^2$ (here M, μ and $m_{\mathrm{P}} = \sqrt{\hbar c/G}$ denote, respectively, the mass of the BH, the rest mass of the graviton, and the Planck mass) where the QNM is weakly damped. It is necessary to recall that the Schwarzschild BH interacting with a massive spin-2 field is, in general, unstable [7,8] (see, however, Ref. [9]). In the context of the massive spin-2 field theory we consider, this instability is due to the behavior of the (spherically symmetric) propagating $\ell = 0$ mode [8]. It is, however, important to note that

(i) It is a "low-mass" instability which disappears above a threshold value $\tilde{\alpha}_t \approx 0.86$ of the reduced mass parameter $\tilde{\alpha}$ and that the critical value around which the quasinormal resonant behavior occurs lies in the stability domain, i.e., $\tilde{\alpha}_0 > \tilde{\alpha}_t$.

(ii) Even if a part of the $\tilde{\alpha}$ domain where the quasinormal resonant behavior occurs lies outside the stability

[*]decanini@univ-corse.fr
[†]folacci@univ-corse.fr
[‡]ould-el-hadj@univ-corse.fr

domain (i.e., below $\tilde{\alpha}_t$), one can nevertheless consider the corresponding values of the reduced mass parameter; indeed, for graviton mass of the order of the Hubble scale, the instability timescale is of order of the Hubble time and the BH instability is harmless.

As a consequence, the slowly decaying giant ringings predicted in the context of massive gravity seem physically relevant (they could be generated by supermassive BHs—see also the final remark in the conclusion of Ref. [2]) and could lead to fascinating observational consequences which could be highlighted by the next generations of gravitational wave detectors.

In the present article, by assuming that the BH perturbation is generated by an initial value problem with Gaussian initial data (we shall discuss, in the conclusion, the limitation of this first hypothesis), an approach which has regularly provided interesting results (see, e.g., Refs. [15–17]), and by restricting our study to the odd-parity $\ell = 1$ mode of the Fierz-Pauli theory in the Schwarzschild spacetime (we shall come back, in the conclusion, on this second hypothesis) but by considering the full signal generated by the perturbation and not just the purely quasinormal contribution, we shall show that, in fact, the extraordinary BH ringings are neutralized in waveforms due to the coexistence of two phenomena:

(i) The excitation of the quasibound states (QBSs) of the Schwarzschild BH. Indeed, it is well known that, for massive fields, the resonance spectrum of a BH includes, in addition to the complex frequencies associated with QNMs, those corresponding to QBSs. Here, we refer to Refs. [18–21] for important pioneering works on this topic and to Refs. [6,8] for recent articles dealing with the QBS of BHs in massive gravity. In a previous article [22], we have considered the role of QBSs in connection with gravitational radiation from BHs. By using a toy model in which the graviton field is replaced with a massive scalar field linearly coupled to a plunging particle, we have highlighted in particular that, in waveforms, the excitation of QBSs blurs the QNM contribution. Unfortunately, due to numerical instabilities, we have limited our study to the low-mass regime. Now, we are able to overcome these numerical difficulties and we shall observe that, near the critical mass $\tilde{\alpha}_0$, the QBSs of the BH not only blur the QNM contribution but provide the main contribution to waveforms.

(ii) The evanescent nature of the particular partial mode which could excite the concerned QNM and generate the resonant behavior of its associated excitation factor. Indeed, if the mass parameter lies near the critical value $\tilde{\alpha}_0$, we shall show that the real part of the quasinormal frequency is smaller than the mass parameter and lies into the cut of the retarded Green function. In other words, the QNM is excited by an evanescent partial mode and, as a consequence, this leads to a significant attenuation of its amplitude.

It is interesting to note that, despite the neutralization process, the waveform amplitude remains rather pronounced (if we compare it with those generated in the framework of Einstein's general relativity) and slowly decaying, this last effect being now due to the excited long-lived QBSs.

In the article, even if it was not our main initial concern, we have also briefly consider the behavior of the waveform for very small values of the reduced mass parameter $\tilde{\alpha}$ corresponding to the weak instability regime. Indeed, our results concerning the QNMs as well as the QBSs of the Schwarzschild BH have permitted us to realize that the waveform associated with the odd-parity $\ell = 1$ mode of the Fierz-Pauli theory could be helpful to test massive gravity even if the graviton mass is very small: the fundamental QNM generates a ringing which is neither giant nor slowly decaying but which is not blurred by the QBS contribution.

Throughout this article, we adopt units such that $\hbar = c = G = 1$. We consider the exterior of the Schwarzschild BH of mass M defined by the metric $ds^2 = -(1-2M/r)dt^2 + (1-2M/r)^{-1}dr^2 + r^2 d\sigma_2^2$ (here $d\sigma_2^2$ denotes the metric on the unit 2-sphere S^2) with the Schwarzschild coordinates (t, r) which satisfy $t \in]-\infty, +\infty[$ and $r \in]2M, +\infty[$. We also use the so-called tortoise coordinate $r_* \in]-\infty, +\infty[$ defined from the radial Schwarzschild coordinate r by $dr/dr_* = (1-2M/r)$ and given by $r_*(r) = r + 2M\ln[r/(2M) - 1]$ and assume a harmonic time dependence $\exp(-i\omega t)$ for the spin-2 field.

II. WAVEFORMS GENERATED BY AN INITIAL VALUE PROBLEM AND NEUTRALIZATION OF GIANT RINGINGS

A. Theoretical considerations

1. Construction of the waveform

We consider the massive spin-2 field in the Schwarzschild spacetime and we focus on the odd-parity $\ell = 1$ mode of this field theory (see Ref. [8]). The corresponding partial amplitude $\phi(t, r)$ satisfies (to simplify the notation, the angular momentum index $\ell = 1$ will be, from now on, suppressed in all formulas)

$$\left[-\frac{\partial^2}{\partial t^2} + \frac{\partial^2}{\partial r_*^2} - V(r)\right]\phi(t, r) = 0, \tag{1}$$

with the effective potential $V(r)$ given by

$$V(r) = \left(1 - \frac{2M}{r}\right)\left(\mu^2 + \frac{6}{r^2} - \frac{16M}{r^3}\right). \tag{2}$$

We describe the source of the BH perturbation by an initial value problem with Gaussian initial data. More precisely, we consider that the partial amplitude $\phi(t,r)$ is given, at $t=0$, by $\phi(t=0,r)=\phi_0(r)$ with

$$\phi_0(r)=\phi_0\exp\left[-\frac{a^2}{(2M)^2}(r_*(r)-r_*(r_0))^2\right] \tag{3}$$

and satisfies $\partial_t\phi(t=0,r)=0$. By Green's theorem, we can show that the time evolution of $\phi(t,r)$ is described, for $t>0$, by

$$\phi(t,r)=\int_{-\infty}^{+\infty}\partial_t G_{\rm ret}(t;r,r')\phi_0(r')dr'_*. \tag{4}$$

Here we have introduced the retarded Green function $G_{\rm ret}(t;r,r')$ solution of

$$\left[-\frac{\partial^2}{\partial t^2}+\frac{\partial^2}{\partial r_*^2}-V(r)\right]G_{\rm ret}(t;r,r')=-\delta(t)\delta(r_*-r'_*) \tag{5}$$

and satisfying the condition $G_{\rm ret}(t;r,r')=0$ for $t\leq 0$. We recall that it can be written as

$$G_{\rm ret}(t;r,r')=-\int_{-\infty+ic}^{+\infty+ic}\frac{d\omega}{2\pi}\frac{\phi^{\rm in}_\omega(r_<)\phi^{\rm up}_\omega(r_>)}{W(\omega)}e^{-i\omega t}, \tag{6}$$

where $c>0$, $r_<=\min(r,r')$, $r_>=\max(r,r')$ and with $W(\omega)$ denoting the Wronskian of the functions $\phi^{\rm in}_\omega$ and $\phi^{\rm up}_\omega$. These two functions are linearly independent solutions of the Regge-Wheeler equation

$$\frac{d^2\phi_\omega}{dr_*^2}+[\omega^2-V(r)]\phi_\omega=0. \tag{7}$$

When $\mathrm{Im}(\omega)>0$, $\phi^{\rm in}_\omega$ is uniquely defined by its ingoing behavior at the event horizon $r=2M$ (i.e., for $r_*\to-\infty$),

$$\phi^{\rm in}_\omega(r)\underset{r_*\to-\infty}{\sim}e^{-i\omega r_*}, \tag{8a}$$

and, at spatial infinity $r\to+\infty$ (i.e., for $r_*\to+\infty$), it has an asymptotic behavior of the form

$$\begin{aligned}\phi^{\rm in}_\omega(r)\underset{r_*\to+\infty}{\sim}&\left[\frac{\omega}{p(\omega)}\right]^{1/2}\\&\times(A^{(-)}(\omega)e^{-i[p(\omega)r_*+[M\mu^2/p(\omega)]\ln(r/M)]}\\&+A^{(+)}(\omega)e^{+i[p(\omega)r_*+[M\mu^2/p(\omega)]\ln(r/M)]}).\end{aligned} \tag{8b}$$

Similarly, $\phi^{\rm up}_\omega$ is uniquely defined by its outgoing behavior at spatial infinity,

$$\phi^{\rm up}_\omega(r)\underset{r_*\to+\infty}{\sim}\left[\frac{\omega}{p(\omega)}\right]^{1/2}e^{+i[p(\omega)r_*+[M\mu^2/p(\omega)]\ln(r/M)]}, \tag{9a}$$

and, at the horizon, it has an asymptotic behavior of the form

$$\phi^{\rm up}_\omega(r)\underset{r_*\to-\infty}{\sim}B^{(-)}(\omega)e^{-i\omega r_*}+B^{(+)}(\omega)e^{+i\omega r_*}. \tag{9b}$$

In Eqs. (8) and (9),

$$p(\omega)=(\omega^2-\mu^2)^{1/2} \tag{10}$$

denotes the "wave number," while $A^{(-)}(\omega)$, $A^{(+)}(\omega)$, $B^{(-)}(\omega)$, and $B^{(+)}(\omega)$ are complex amplitudes which, like the in- and up- modes, can be defined by analytic continuation in the full complex ω plane or, more precisely, in an appropriate Riemann surface taking into account the cuts associated with the functions $p(\omega)$ and $[\omega/p(\omega)]^{1/2}$. By evaluating the Wronskian $W(\omega)$ at $r_*\to-\infty$ and $r_*\to+\infty$, we obtain

$$W(\omega)=2i\omega A^{(-)}(\omega)=2i\omega B^{(+)}(\omega). \tag{11}$$

Using (6) into (4) and assuming that the source $\phi_0(r)$ given by (3) is strongly localized near $r=r_0$ (this can be easily achieved if we assume that the width of the Gaussian function is not too large, i.e., if a is not too small) while the observer is located at a rather large distance from the source, we obtain

$$\begin{aligned}\phi(t,r)=-\frac{1}{2\pi}\mathrm{Re}\Bigg[&\int_{0+ic}^{+\infty+ic}d\omega\left(\frac{e^{-i\omega t}}{A^{(-)}(\omega)}\right)\\&\times\phi^{\rm up}_\omega(r)\int_{-\infty}^{+\infty}dr'_*\phi_0(r')\phi^{\rm in}_\omega(r')\Bigg].\end{aligned} \tag{12}$$

This formula will permit us to construct numerically the waveform for an observer at (t,r).

2. Extraction of the QNM contribution

The zeros of the Wronskian $W(\omega)$ are the resonances of the BH. Here, it is worth recalling that if $W(\omega)$ vanishes, the functions $\phi^{\rm in}_\omega$ and $\phi^{\rm up}_\omega$ are linearly dependent. The zeros of the Wronskian lying in the lower part of the first Riemann sheet associated with the function $p(\omega)$ (see Fig. 16 in Ref. [22]) are the complex frequencies of the $\ell=1$ QNMs. Their spectrum is symmetric with respect to the imaginary ω axis. Similarly, the zeros of the Wronskian lying in the lower part of the second Riemann sheet associated with the function $p(\omega)$ are the complex frequencies of the $\ell=1$ QBSs and their spectrum is symmetric with respect to the imaginary ω axis.

The contour of integration in Eq. (12) may be deformed in order to capture the QNM contribution [15], i.e., the extrinsic ringing of the BH. By Cauchy's theorem and if we do not take into account all the other contributions (those arising from the arcs at $|\omega|=\infty$, from the various cuts and from the complex frequencies of the QBSs), we can extract

a residue series over the quasinormal frequencies ω_n lying in the fourth quadrant of the first Riemann sheet associated with the function $p(\omega)$. We then isolate the BH ringing generated by the initial data. It is given by

$$\phi^{\mathrm{QNM}}(t,r) = 2\mathrm{Re}\left[\sum_n i\omega_n \mathcal{C}_n e^{-i\omega_n t}\left[\frac{p(\omega_n)}{\omega_n}\right]^{1/2}\phi^{\mathrm{up}}_{\omega_n}(r)\right]. \tag{13}$$

In this sum, $n=0$ corresponds to the fundamental QNM (i.e., the least damped one) and $n=1,2,\ldots$ to the overtones. Moreover, $\mathcal{C}_n$ denotes the excitation coefficient of the QNM with overtone index n. It is defined from the corresponding excitation factor

$$\mathcal{B}_n = \left(\frac{1}{2p(\omega)}\frac{A^{(+)}(\omega)}{\frac{dA^{(-)}(\omega)}{d\omega}}\right)_{\omega=\omega_n} \tag{14}$$

but, in addition, it takes explicitly into account the role of the BH perturbation. We have

$$\mathcal{C}_n = \mathcal{B}_n \int_{-\infty}^{+\infty} \frac{\phi_0(r')\phi^{\mathrm{in}}_{\omega_n}(r')}{\sqrt{\omega_n/p(\omega_n)}A^{(+)}(\omega_n)}dr'_*. \tag{15}$$

For more precisions concerning the excitation factors (intrinsic quantities) and the excitation coefficients (extrinsic quantities), we refer to Refs. [1,2,17].

B. Numerical results and discussions

1. Numerical methods

To construct the waveform (12), we have to obtain numerically the functions $\phi^{\mathrm{in}}_\omega(r)$ and $\phi^{\mathrm{up}}_\omega(r)$ as well as the coefficient $A^{(-)}(\omega)$ for $\omega\in\mathbb{R}^+$. This can be achieved by integrating numerically the Regge-Wheeler equation (7) with the Runge-Kutta method by using a sufficiently large working precision. It is necessary to initialize the process with Taylor series expansions converging near the horizon and to compare the solutions to asymptotic expansions with ingoing and outgoing behavior at spatial infinity. In order to obtain reliable results for "large" values of the mass parameter, it necessary to decode systematically, by Padé summation, the information hidden in the divergent part of the asymptotic expansions considered but also to work very carefully for frequencies near the branch point $+\mu$. Moreover, in Eq. (12), we have to discretize the integral over ω. In order to obtain numerically stable waveforms, we can limit the range of frequencies to $-8\leq 2M\omega\leq +8$ and take for the frequency resolution $2M\delta\omega = 1/10000$.

The quasinormal frequencies ω_n (as well as the complex frequencies of the QBSs) can be determined by using the method developed for massive fields by Konoplya and Zhidenko [23] and which can be numerically implemented by modifying the Hill determinant approach of Majumdar and Panchapakesan [24] (for more precision, see Sec. II of Ref. [1] as well as Appendixes B and C of Ref. [22]).

The coefficients $A^{(+)}(\omega_n)$, the excitation factors $\mathcal{B}_n$ and the excitation coefficients $\mathcal{C}_n$ can be obtained from $\phi^{\mathrm{in}}_\omega(r)$ by integrating numerically the Regge-Wheeler equation (7) for $\omega=\omega_n$ and $\omega=\omega_n+\epsilon$ (we have taken $\epsilon\sim 10^{-10}$) with the Runge-Kutta method and then by comparing the solution to asymptotic expansions (decoded by Padé summation) with ingoing and outgoing behavior at spatial infinity.

To construct the ringing (13), we need, in addition to the quasinormal frequencies ω_n and the excitation coefficients $\mathcal{C}_n$, the functions $\phi^{\mathrm{up}}_{\omega_n}(r)$. They can be obtained by noting that $\phi^{\mathrm{up}}_{\omega_n}(r) = \phi^{\mathrm{in}}_{\omega_n}(r)/A^{(+)}(\omega_n)$. It is also important to recall that the quasinormal contribution (13) does not provide physically relevant results at "early times" due to its exponentially divergent behavior as t decreases. In our previous works [1,2], we have proposed to construct the starting time t_{start} of the BH ringing from the group velocity corresponding to the quasinormal frequency ω_n which is given by $v_g = \mathrm{Re}[p(\omega_n)]/\mathrm{Re}[\omega_n]$. By assuming again that the source is strongly localized while the observer is located at a rather large distance r from the source, we can use for the starting time

$$t_{\mathrm{start}} \approx \frac{r_*(r)+r_*(r_0)}{\mathrm{Re}[p(\omega_n)]/\mathrm{Re}[\omega_n]}. \tag{16}$$

2. Numerical results and comments

In Fig. 1, we display the effect of the graviton mass on the complex frequency ω_0 of the fundamental QNM and in Fig. 2, we exhibit the strong resonant behavior of the associated excitation factor $\mathcal{B}_0$ occurring around the critical value $\tilde{\alpha}_0\approx 0.90$. Here, we focus on the least damped QNM but it is worth noting that the same kind of quasinormal resonant behavior also exists for the overtones but with excitation factors $\mathcal{B}_n$ of much lower amplitude. In Fig. 3, we exhibit the strong resonant behavior of the excitation coefficient $\mathcal{C}_0$ for particular values of the parameters defining the initial data (3). It occurs around the critical

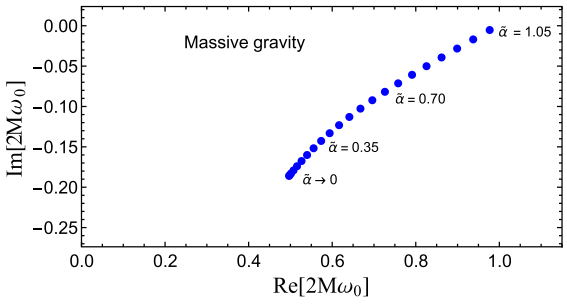

FIG. 1. Complex frequency ω_0 of the odd-parity ($\ell=1, n=0$) QNM (massive spin-2 field). $2M\omega_0$ is followed from $\tilde{\alpha}\to 0$ to $\tilde{\alpha}=1.05$. Above $\tilde{\alpha}\approx 1.06$, the QNM disappears.

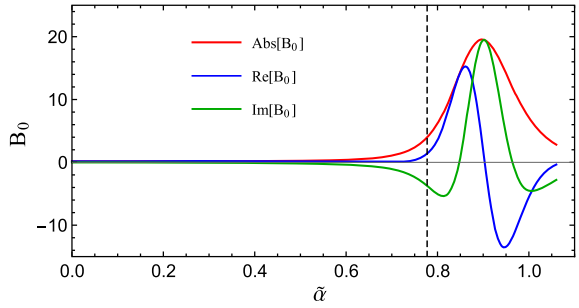

FIG. 2. Resonant behavior, in massive gravity, of the excitation factor $\mathcal{B}_0$ of the odd-parity ($\ell = 1$, $n = 0$) QNM. The maximum of $|2M\mathcal{B}_0|$ occurs for the critical value $\tilde{\alpha}_0 \approx 0.89757$; we then have $2M\omega_0 \approx 0.85969073–0.03878222i$, $2M\mathcal{B}_0 \approx 3.25237 + 19.28190i$ and $|2M\mathcal{B}_0| \approx 19.5543$.

value $\tilde{\alpha}_0 \approx 0.89$ and is rather similar to the behavior of the corresponding excitation factor $\mathcal{B}_0$. It depends very little on the parameters defining the Cauchy problem. Of course, for overtones, the quasinormal resonant behavior is more and more attenuated as the overtone index n increases. It is also important to note that the quasinormal resonant behavior occurs for masses in a range where the fundamental QNM is a long-lived mode (see Fig. 1). From a theoretical point of view, if we focus our attention exclusively on Eq. (13) (see also Refs. [1,2]), it is logical to think that this leads to giant and slowly decaying ringings. In fact, this way of thinking is rather naive and it seems that, in waveforms, it is not possible to exhibit such extraordinary ringings for two main reasons (here we restrict our discussion to the fundamental QNM because it provides the most interesting contribution):

(i) The quasinormal ringing (13) is excited when a real frequency ω in the integral (12) defining the waveform coincides with (or is very close to) the excitation frequency $\mathrm{Re}[\omega_0]$ of the $n = 0$ QNM. In the low-mass regime, the wave number $p(\omega = \mathrm{Re}[\omega_0])$ is a real positive number and the partial

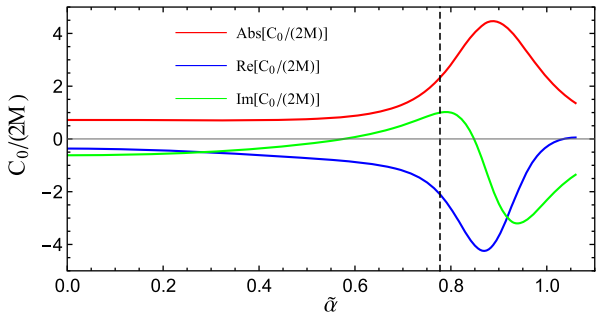

FIG. 3. Resonant behavior, in massive gravity, of the excitation coefficient $\mathcal{C}_0$ of the odd-parity ($\ell = 1$, $n = 0$) QNM. It is obtained from (15) by using (3) with $\phi_0 = 1$, $a = 1$ and $r_0 = 10M$. The maximum of $|2M\mathcal{C}_0|$ occurs for the critical value $\tilde{\alpha}_0 \approx 0.88808$; we then have $2M\omega_0 \approx 0.85277076–0.04084908i$, $2M\mathcal{C}_0 \approx -4.02613–1.93037i$ and $|2M\mathcal{C}_0| \approx 4.46498$.

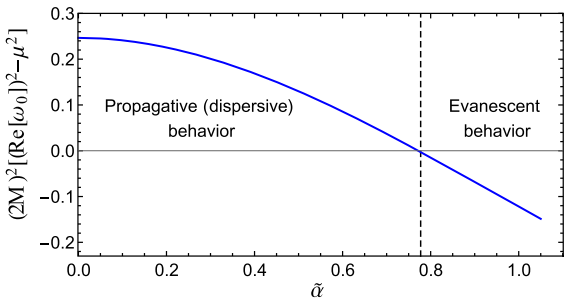

FIG. 4. The square of the wave number $p(\omega = \mathrm{Re}[\omega_0])$ as a function of the mass. In the low-mass regime, the partial wave exciting the quasinormal ringing has a propagative behavior while, for masses in the range where the excitation factor $\mathcal{B}_0$ and the excitation coefficient $\mathcal{C}_0$ have a strong resonant behavior, its has an evanescent behavior.

wave which excites the ringing has a propagative behavior (see Fig. 4). The ringing can be clearly identify in the waveform (see Fig. 5) even if, as the mass parameter increases, the quality of the superposition of the signals decreases. For masses in the range where the excitation factor $\mathcal{B}_0$ and the excitation coefficient $\mathcal{C}_0$ have a strong resonant behavior, the wave number $p(\omega = \mathrm{Re}[\omega_0])$ is an imaginary number (the real part of the quasinormal frequency is smaller than the mass parameter and lies into the cut of the retarded Green function) and,

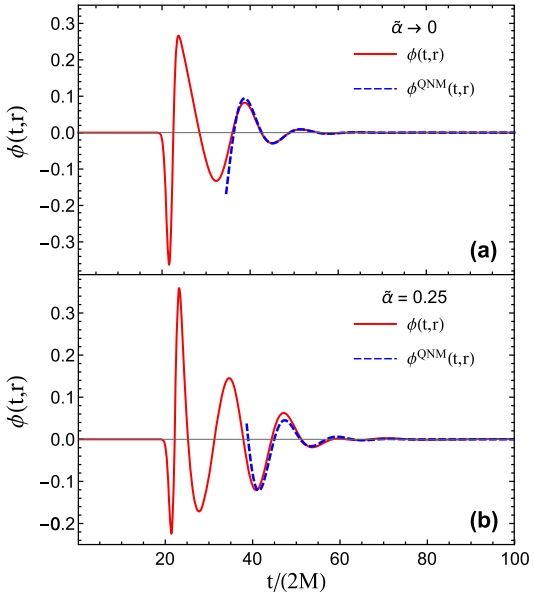

FIG. 5. Comparison of the waveform (12) with the quasinormal waveform (13). The results are obtained for (a) $\tilde{\alpha} \to 0$ and (b) $\tilde{\alpha} = 0.25$. The parameters of the Gaussian source (3) are $\phi_0 = 1$, $a = 1$ and $r_0 = 10M$. The observer is located at $r = 50M$. The quality of the superposition of the two signals decreases as the mass increases due to the dispersive nature of the massive field (the excitation of QBSs playing a negligible role).

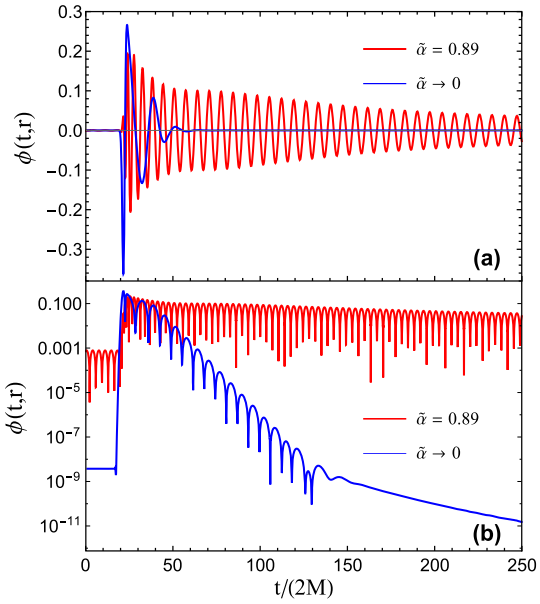

FIG. 6. Comparison of the waveforms obtained for $\tilde{\alpha} \to 0$ and for $\tilde{\alpha} = 0.89$. The parameters of the Gaussian source (3) are $\phi_0 = 1$, $a = 1$ and $r_0 = 10M$. The observer is located at $r = 50M$. (a) Normal plot and (b) semi-log plot.

TABLE I. Odd-parity $\ell = 1$ mode of massive gravity. A sample of the first quasibound frequencies $\omega_{\ell n}$.

(ℓ, n)	$\tilde{\alpha}$	$2M\omega_{\ell n}$
$(1, n)$	0	/
(1,0)	0.25	$0.24978–9.37148 \times 10^{-13} i$
(1,1)		$0.24988–5.63842 \times 10^{-13} i$
(1,2)		$0.24992–3.30927 \times 10^{-13} i$
(1,3)		$0.24995–2.05049 \times 10^{-13} i$
(1,4)		$0.24996–1.34298 \times 10^{-13} i$
(1,0)	0.82	$0.81077–0.00007i$
(1,1)		$0.81494–0.00004i$
(1,2)		$0.81684–0.00003i$
(1,3)		$0.81784–0.00002i$
(1,4)		$0.81844–0.00001i$
(1,0)	0.89	$0.87756–0.00030i$
(1,1)		$0.88324–0.00019i$
(1,2)		$0.88580–0.00011i$
(1,3)		$0.88715–0.00006i$
(1,4)		$0.88795–0.00004i$
(1,0)	1.30	$1.25689–0.01719i$
(1,1)		$1.27712–0.00724i$
(1,2)		$1.28590–0.00362i$
(1,3)		$1.29049–0.00204i$
(1,4)		$1.29317–0.00125i$

as a consequence, the partial wave which could excite the ringing has an evanescent behavior (see Fig. 4 as well as Figs. 2 and 3). Theoretically, this leads to a significant attenuation of the ringing amplitude in the waveform. In Fig. 6, we display the waveform for a value of the reduced mass $\tilde{\alpha}$ very close to the critical value $\tilde{\alpha}_0$. We cannot identify the ringing but we can, however, observe that the amplitude of the waveform is more larger than in the massless limit and that it decays very slowly. Such a behavior is a consequence of the excitation of QBSs (see below).

(ii) For any nonvanishing value of the reduced mass $\tilde{\alpha}$, the QBSs of the Schwarzschild BH are excited. Of course, their influence is negligible for $\tilde{\alpha} \to 0$ (see Table I and Fig. 5) but increases with $\tilde{\alpha}$ (see Fig. 7 where we displays the spectral content of the late-time tail of the waveform for $\tilde{\alpha} = 0.25$) and, for higher values of $\tilde{\alpha}$, they can even blur the QNM contribution (as we have already noted in another context in Ref. [22]). But near and above the critical value $\tilde{\alpha}_0$ of the reduced mass, the QBSs of the BH not only blur the QNM contribution but provide the main contribution to waveforms (see Figs. 6 and 8).

It is interesting to also consider waveforms for reduced mass parameters:

(i) Near the critical value $\tilde{\alpha}_0$ but outside the stability domain (see Figs. 9 and 10 where we display the waveform corresponding to $\tilde{\alpha} = 0.82$ and its spectral content).

(ii) Far above the critical value $\tilde{\alpha}_0$ (see Figs. 11 and 12 where we display the waveform corresponding to $\tilde{\alpha} = 1.30$ and its spectral content) and, in particular, for values for which the fundamental QNM does not exist (see Fig. 1).

In both cases, we can observe the neutralization of the giant ringing. It is worth noting that the amplitude of the waveforms is smaller than that corresponding to the critical value $\tilde{\alpha}_0$. In fact, we can observe that this amplitude increases from $\tilde{\alpha} \to 0$ to $\tilde{\alpha} \approx \tilde{\alpha}_0$ and then decreases from $\tilde{\alpha} = \tilde{\alpha}_0$ to $\tilde{\alpha} \to \infty$. It reaches a maximum for the critical mass parameter $\tilde{\alpha}_0$. In our opinion, this fact is reminiscent

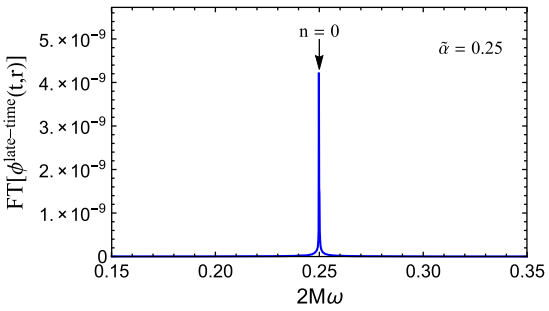

FIG. 7. The spectral content of the "late-time" phase of the waveform for $\tilde{\alpha} = 0.25$. The parameters of the Gaussian source (3) are $\phi_0 = 1$, $a = 1$ and $r_0 = 10M$. The observer is located at $r = 50M$. We only observe the signature of the first long-lived QBS (see Table I); it is weakly excited (note its very low amplitude) and has little influence on the waveform (see Fig. 5).

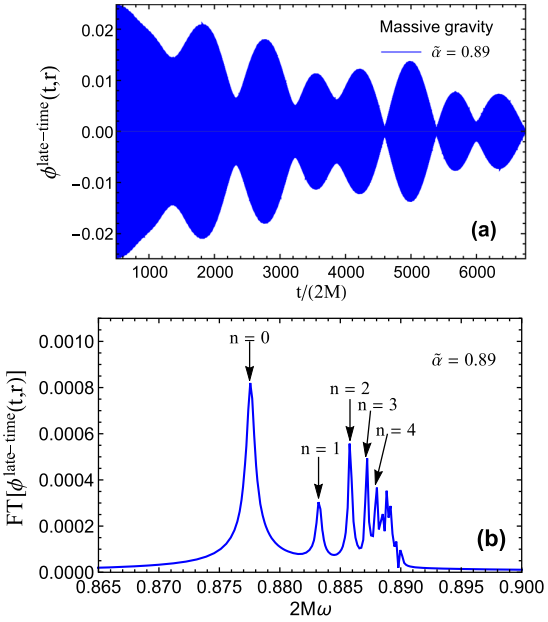

FIG. 8. (a) The late-time phase of the waveform for $\tilde{\alpha} = 0.89$ and (b) the spectral content of the full waveform. The parameters of the Gaussian source (3) are $\phi_0 = 1$, $a = 1$ and $r_0 = 10M$. The observer is located at $r = 50M$. We observe the signature of the first long-lived QBSs (see also Table I) and beats due to interference between QBSs of neighboring frequencies.

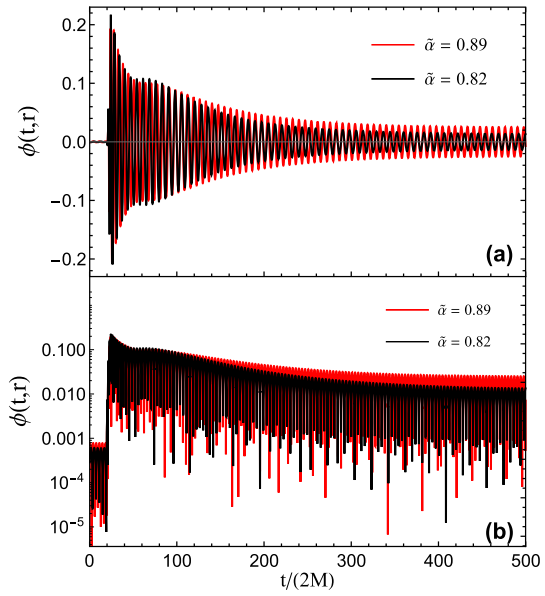

FIG. 9. Comparison of the waveforms obtained for $\tilde{\alpha} = 0.89$ and for $\tilde{\alpha} = 0.82$. The parameters of the Gaussian source (3) are $\phi_0 = 1$, $a = 1$ and $r_0 = 10M$. The observer is located at $r = 50M$. (a) Normal plot and (b) semi-log plot.

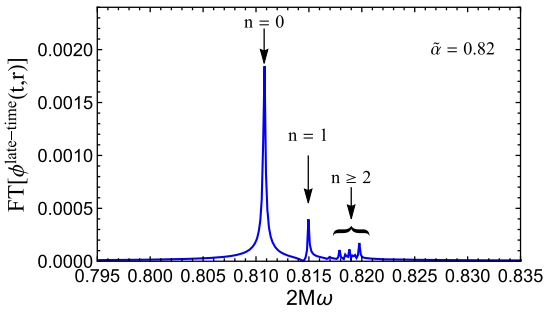

FIG. 10. The spectral content of the full waveform for $\tilde{\alpha} = 0.82$ (see also Table I). The parameters of the Gaussian source (3) are $\phi_0 = 1$, $a = 1$ and $r_0 = 10M$. The observer is located at $r = 50M$. We observe, in particular, that the first long-lived QBSs are not excited.

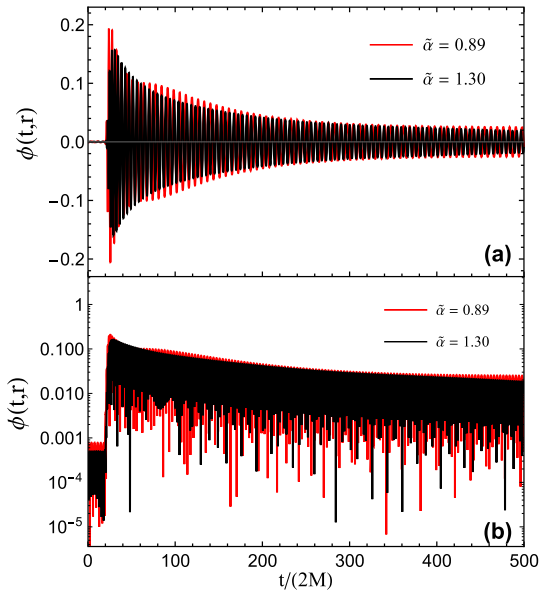

FIG. 11. Comparison of the waveforms obtained for $\tilde{\alpha} = 0.89$ and for $\tilde{\alpha} = 1.30$. The parameters of the Gaussian source (3) are $\phi_0 = 1$, $a = 1$ and $r_0 = 10M$. The observer is located at $r = 50M$. (a) Normal plot and (b) semi-log plot.

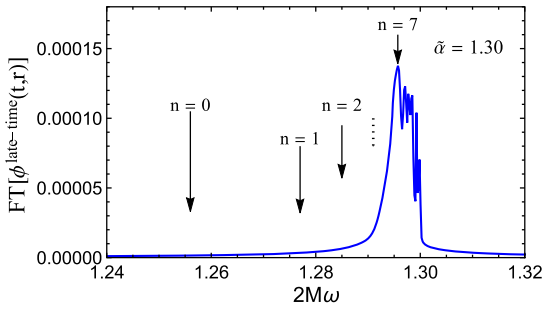

FIG. 12. The spectral content of the full waveform for $\tilde{\alpha} = 1.30$ (see also Table I). The parameters of the Gaussian source (3) are $\phi_0 = 1$, $a = 1$ and $r_0 = 10M$. The observer is located at $r = 50M$. We observe, in particular, that the first long-lived QBSs are not excited.

of the theoretical existence of giant ringings. We can also observe in Fig. 12 that the first long-lived QBSs are not excited. Indeed, they disappear because (i) their complex frequencies lie deeper in the complex plane and (ii) the real part of their complex frequencies is more smaller than the mass parameter and lies into the cut of the retarded Green function (see Table I). As a consequence, the partial waves which could excite them have an evanescent behavior. It is the mechanism which operates for the fundamental QNM around the critical value $\tilde{\alpha}_0$ and which leads to the non-observability of giant ringings.

III. CONCLUSION

In this article, we have shown that the giant and slowly decaying ringings which could be generated in massive gravity due to the resonant behavior of the quasinormal excitation factors of the Schwarzschild BH are neutralized in waveforms. This is mainly a consequence of the coexistence of two effects which occur in the frequency range of interest: (i) the excitation of the QBSs of the BH and (ii) the evanescent nature of the particular partial modes which could excite the concerned QNMs. It should be noted that this neutralization process occurs for values of the reduced mass parameter $\tilde{\alpha}$ into the BH stability range (we have considered $\tilde{\alpha} = 0.89$ and $\tilde{\alpha} = 1.30$) but also outside this range (we have considered $\tilde{\alpha} = 0.82$). Despite the neutralization, the waveform characteristics remain interesting from the observational point of view.

It is also interesting to note that, for values of $\tilde{\alpha}$ below and much below the threshold value $\tilde{\alpha}_t$ (we have considered $\tilde{\alpha} = 0.25$ and $\tilde{\alpha} \to 0$ corresponding to the weak instability regime for the BH), the situation is very different. Of course, the ringing is neither giant nor slowly decaying but it is not blurred by the QBS contribution. As a consequence, it could be clearly observed in waveforms and used to test massive gravity theories with gravitational waves even if the graviton mass is very small.

In order to simplify our task, we have restricted our study to the odd-parity $\ell = 1$ partial mode of the Fierz-Pauli theory in the Schwarzschild spacetime (here it is important to recall that its behavior is governed by a single differential equation of the Regge-Wheeler type [see Eq. (1)] while all the other partial modes are governed by two or three coupled differential equations depending on the parity sector and the angular momentum) and we have, moreover, described the distortion of the Schwarzschild BH by an initial value problem. Of course, it would be very interesting to consider partial modes with higher angular momentum as well as more realistic perturbation sources but these configurations are much more challenging to treat in massive gravity. However, even if we are not able currently to deal with such problems, we believe that they do not lead to very different results. Our opinion is supported by some calculations we have achieved by replacing the massive spin-2 field with the massive scalar field. Indeed, in this context and when we consider partial modes with higher angular momentum, we can observe results rather similar to those of Sec. II:

(i) If we still describe the distortion of the Schwarzschild BH by an initial value problem [25].
(ii) If we consider the excitation of the BH by a particle plunging from slightly below the innermost stable circular orbit into the Schwarzschild BH, i.e., if we use the toy model we developed in Ref. [22] (see Figs. 13 and 14 and comments in figure captions).

It would be important to extend our study to a rotating BH in massive gravity. Indeed, in that case, because the BH is described by two parameters and not just by its mass, the existence of the resonant behavior of the quasinormal excitation factors might not be accompanied by the neutralization of the associated giant ringings.

We would like to conclude with some remarks inspired by our recent articles [1,2,22] as well as by the present work. The topic of classical radiation from BHs when massive fields are involved has been the subject of a large number of studies since the 1970s but, in general, they focus on very particular aspects such as the numerical determination of the quasinormal frequencies, the excitation of the corresponding resonant modes, the numerical determination of QBS complex frequencies, their role in the context of BH instability, the behavior of the late-time tail of the signal due to a BH perturbation … and, moreover,

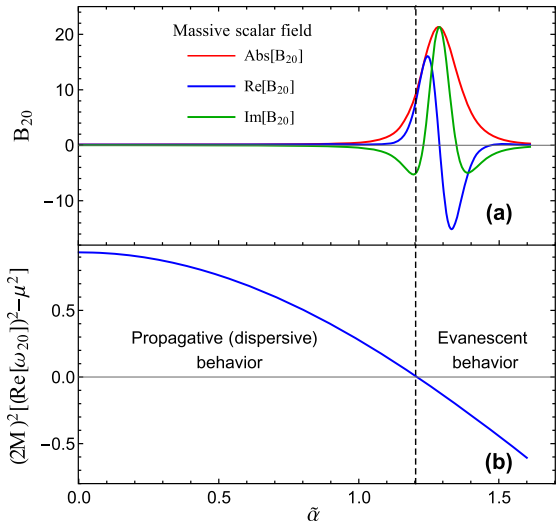

FIG. 13. The ($\ell = 2$, $n = 0$) QNM of the massive scalar field. We denote by ω_{20} its complex frequency and by $\mathcal{B}_{20}$ the associated excitation factor. (a) Resonant behavior of $\mathcal{B}_{20}$. (b) The square of the wave number $p(\omega = \mathrm{Re}[\omega_{20}])$ as a function of the mass parameter. For masses in the range where the excitation factor $\mathcal{B}_{20}$ has a strong resonant behavior, the partial wave exciting the quasinormal ringing has an evanescent behavior. This leads to a significant attenuation of the ringing amplitude in the waveform (see Fig. 14).

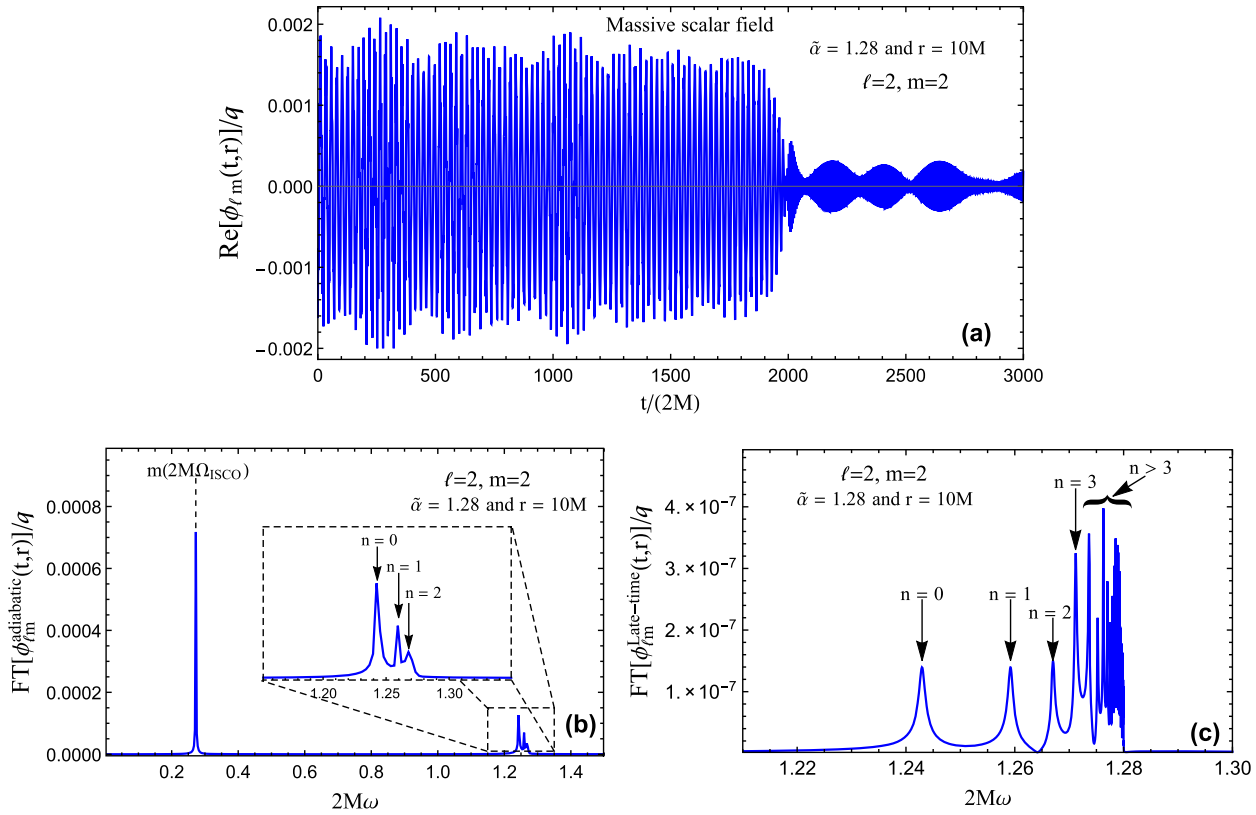

FIG. 14. Quadrupolar waveform $\phi_{22}(t,r)$ associated with the ($\ell = 2$, $m = 2$) mode of the massive scalar field and generated by a scalar point particle on a plunge trajectory (see Ref. [22] for the theory). The mass parameter corresponds to the maximum of $|\mathcal{B}_{20}|$ (see Fig. 13) and the observer is located at $r = 10M$. (a) The quasinormal ringing does not appear in the waveform. The beats are caused by interferences between QBSs. (b) Spectral content of the adiabatic phase. We observe, in addition to the signature of the quasicircular motion of the plunging particle, that of the first long-lived QBSs. (c) Spectral content of the late-time phase. We observe a profusion of long-lived QBSs with an accumulation which converges to the limiting frequency $2M\omega = \tilde{\alpha}$.

they consider these aspects rather independently of each other. When addressing the problem of the construction of the waveform generated by an arbitrary BH perturbation and its physical interpretation, these various aspects must be considered together and this greatly complicates the task. If we work in the low-mass regime, its seems that, *mutatis mutandis*, the lessons we have learned from massless fields provide a good guideline but, if this is not the case, we face numerous difficulties. It is possible to overcome the numerical difficulties encountered (see Sec. II B 1) but, from the theoretical point of view, the situation is much more tricky and, in particular, the unambiguous identification of the different contributions (the "prompt" contribution, the QNM and QBS contributions, the tail contribution …) in waveforms or in the retarded Green function is not so easy and natural as for massless fields. In fact, it would be interesting to extend rigorously, for massive fields, the nice work of Leaver in Ref. [15] but, in our opinion, due to the structure of the Riemann surfaces involved as well as to the presence of the cuts associated with the wave number $p(\omega)$ [see Eq. (10)] and with the function $[\omega/p(\omega)]^{1/2}$ [see, e.g., in Eqs. (8b) and (9a)], this is far from obvious and certainly requires uniform asymptotic techniques.

ACKNOWLEDGMENTS

We wish to thank Andrei Belokogne for various discussions and the Collectivité Territoriale de Corse for its support through the COMPA project.

[1] Y. Decanini, A. Folacci, and M. Ould El Hadj, Phys. Rev. D **89**, 084066 (2014).
[2] Y. Decanini, A. Folacci, and M. Ould El Hadj, arXiv: 1401.0321.
[3] K. Hinterbichler, Rev. Mod. Phys. **84**, 671 (2012).
[4] C. de Rham, Living Rev. Relativ. **17**, 7 (2014).
[5] M. S. Volkov, Classical Quantum Gravity **30**, 184009 (2013).
[6] E. Babichev and R. Brito, Classical Quantum Gravity **32**, 154001 (2015).
[7] E. Babichev and A. Fabbri, Classical Quantum Gravity **30**, 152001 (2013).
[8] R. Brito, V. Cardoso, and P. Pani, Phys. Rev. D **88**, 023514 (2013).
[9] R. Brito, V. Cardoso, and P. Pani, Phys. Rev. D **87**, 124024 (2013).
[10] S. Hod, Classical Quantum Gravity **30**, 237002 (2013).
[11] E. Babichev, R. Brito, and P. Pani, Phys. Rev. D **93**, 044041 (2016).
[12] S. Hassan, A. Schmidt-May, and M. von Strauss, J. High Energy Phys. 05 (2013) 086.
[13] C. de Rham and G. Gabadadze, Phys. Rev. D **82**, 044020 (2010).
[14] C. de Rham, G. Gabadadze, and A. J. Tolley, Phys. Rev. Lett. **106**, 231101 (2011).
[15] E. W. Leaver, Phys. Rev. D **34**, 384 (1986).
[16] N. Andersson, Phys. Rev. D **55**, 468 (1997).
[17] E. Berti and V. Cardoso, Phys. Rev. D **74**, 104020 (2006).
[18] N. Deruelle and R. Ruffini, Phys. Lett. B **52**, 437 (1974).
[19] T. Damour, N. Deruelle, and R. Ruffini, Lett. Nuovo Cimento Soc. Ital. Fis. **15**, 257 (1976).
[20] T. Zouros and D. Eardley, Ann. Phys. (N.Y.) **118**, 139 (1979).
[21] S. L. Detweiler, Phys. Rev. D **22**, 2323 (1980).
[22] Y. Decanini, A. Folacci, and M. Ould El Hadj, Phys. Rev. D **92**, 024057 (2015).
[23] R. Konoplya and A. Zhidenko, Phys. Lett. B **609**, 377 (2005).
[24] B. Majumdar and N. Panchapakesan, Phys. Rev. D **40**, 2568 (1989).
[25] Y. Decanini, A. Folacci, and M. Ould El Hadj (unpublished).

Conclusion et perspectives

L'observation récente des ondes gravitationnelles par la nouvelle génération d'interféromètres de Michelson kilométriques [3] marque le début de l'astronomie gravitationnelle et ouvre une nouvelle fenêtre sur l'Univers. En effet, c'est la première fois qu'un messager (onde gravitationnelle) autre que le rayonnement électromagnétique (ondes lumineuses, ondes radio et micro-ondes, rayons gamma et rayons X) et les astroparticules (neutrinos, rayons cosmiques) a permis de mettre en évidence et d'une manière directe l'existence d'un nouvel objet (le trou noir binaire), d'étudier son évolution et de déterminer ses caractéristiques physiques (masse, moment angulaire...).

La nouvelle génération de détecteurs terrestres [212] ainsi que les futurs détecteurs spatiaux [213] permettront au cours des décennies à venir de développer une nouvelle vision du Cosmos (observation des fluctuations quantiques de l'Univers primordial, étude des trous noirs, étude de l'effondrement gravitationnel des étoiles massives...) mais aussi de tester en champ fort les différentes théories de la gravitation et de l'espace-temps alternatives à celle d'Einstein. Il est donc en particulier très intéressant de reconsidérer dans le cadre de la gravité massive le rayonnement gravitationnel des trous noirs et d'étudier notamment leurs perturbations. C'est dans cette optique que s'est développé notre travail de thèse et nous avons réussi à mettre en évidence quelques effets nouveaux en physique des trous noirs.

Afin d'éviter de nombreuses complications théoriques liées à la gravité massive, nous avons choisi de travailler d'abord avec un "modèle-jouet" où un champ de graviton massif est remplacé par un champ scalaire massif couplé linéairement à une particule en chute libre dans le trou noir. Ainsi, l'étude du rayonnement généré par une particule plongeant dans un trou noir de Schwarzschild nous a permis d'exhiber quelques effets physiques qui doivent être présents pour le problème analogue en gravité massive. Ils sont effectivement directement liés aux propriétés partagées par le champ scalaire massif et le champ de graviton massif, à savoir (i) la nature évanescente et dispersive des modes partiels et (ii) l'existence des QBSs. Nous avons en particulier montré que :

(i) La forme d'onde produite par une particule plongeant dans le trou noir de Schwarzschild à partir de l'ISCO peut être grossièrement décomposée en trois phases (pour les faibles valeurs du paramètre de couplage sans dimension $\tilde{\alpha}$ donné par Eq. (1)) qui sont une phase adiabatique correspondant au mouvement quasi-circulaire de la particule au voisinage de l'ISCO, la phase de sonnerie due à l'excitation des résonances du trou noir et la phase de fin du signal.

(ii) Dans la phase adiabatique, pour un observateur à grande distance du trou noir, le comportement de la forme d'onde dépend d'une valeur seuil $\tilde{\alpha}_t$ du paramètre sans dimension $\tilde{\alpha}$, valeur seuil proportionnelle à la fréquence orbitale $\Omega_{\rm ISCO}$ d'une particule se

mouvant sur l'ISCO. Cette valeur seuil sépare le régime dispersif du régime évanescent. Au-dessus de la valeur seuil, pour un observateur à l'infini spatial, l'amplitude de la forme d'onde s'annule. A une distance r du trou noir, l'amplitude de la forme d'onde décroit en fonction du paramètre sans dimension $\tilde{\alpha}$ et s'annule pour les grandes valeurs.

(iii) La phase de sonnerie (les oscillations et l'atténuation) est bien décrite par l'excitation du premier mode quasi-normal du trou noir dans le cas de faibles valeurs du paramètre $\tilde{\alpha}$.

(iv) Dans la phase de fin du signal, on a mis en évidence la présence des QBSs. On peut faire remarquer qu'ils sont présents aussi dans la phase adiabatique. Par contre, dans cette phase, ils ne peuvent être perçus que pour des valeurs du paramètre sans dimension $\tilde{\alpha}$ au-dessus de la valeur seuil (dans le régime évanescent) et, à grande, distance ils devraient dominer le signal.

(v) Pour les "grandes" valeurs du paramètre sans dimension $\tilde{\alpha}$, les sonneries seront floutées par l'excitation des QBSs.

Nous avons, ensuite, considéré les perturbations du trou noir de Schwarzschild dans le cadre de la théorie de la gravité massive. Nous avons limité notre étude aux QNMs du fait de leur importance dans la compréhension théorique du comportement des trous noirs et parce que d'un point de vue observationnel ils fournissent une preuve directe de leur existence. Cette étude nous a permis de montrer plus particulièrement l'existence d'un comportement résonant de leurs facteurs d'excitation. Ce comportement se produit dans un large domaine autour d'une valeur critique $\tilde{\alpha}_c$ où, de plus, les QNMs sont faiblement amortis. En conséquence, il devrait induire des sonneries d'amplitude géante et à faible décroissance temporelle. Dans le chapitre 6, nous avons vu que ce comportement n'est pas propre au champ de graviton massif et nous l'avons généralisé à d'autres champs bosoniques (spin-0 et spin-1). Nous avons aussi confirmé analytiquement certains de ces résultats en nous appuyant sur des considérations semi-classiques basées sur les propriétés des géodésiques circulaires instables suivies par des particules massives en orbite autour du trou noir.

Enfin, nous avons montré que ces sonneries d'amplitude géante et à faible décroissance temporelle qui devraient être générées en gravité massive sont neutralisées dans les formes d'ondes du fait de la coexistence de deux phénomènes :

(i) L'excitation des QBSs du trou noir de Schwarzschild qui floutent la contribution des QNMs.

(ii) La nature évanescente du mode partiel qui pourrait exciter le QNM concerné et générer le comportement résonant de son facteur d'excitation.

Nous allons conclure par quelques remarques inspirées par nos travaux en vue de leurs éventuelles extensions :

(i) Il serait intéressant, par exemple, d'étendre notre travail aux trous noirs en rotation en gravité massive. Dans ce cas précis, étant donné que les trous noirs sont décrits par deux paramètres et non plus uniquement par leur masse, l'existence du comportement résonant des facteurs d'excitation des QNMs pourrait induire des sonneries d'amplitude

géante et à faible décroissance temporelle non neutralisées dans les formes d'onde. Notons que ce comportement résonant des facteurs d'excitation des QNMs à longue durée de vie est un effet nouveau en physique des trous noirs. Aussi, beaucoup de travail reste à faire pour une compréhension profonde et complète de ce phénomène et ses conséquences physiques. Notre étude, bien que limitée à des considérations astrophysiques est une première entreprise dans cette voie. Nous pensons aussi que cet effet pourrait avoir d'intéressantes implications dans le contexte de la théorie des champs quantiques en espace-temps courbe (effet Hawking, sections d'absorption, tenseur d'énergie-impulsion renormalisé et fonctions de corrélations associées...). Quelques-unes de ces pistes pourraient être explorées prochainement.

(ii) Il serait aussi intéressant et encore plus important de considérer l'influence des QBSs dans le rayonnement gravitationnel émis par les trous noirs en rotation en gravité massive car leur mise en évidence observationnelle trancherait en défaveur de la théorie d'Einstein. Il faut cependant noter qu'en gravité massive l'étude des perturbations du trou noir de Schwarzschild est fort délicate et que celle des trous noirs en rotation pourrait être inextricable. Rappelons en effet que dans le cas du trou noir de Schwarzschild en gravité massive le comportement du mode partiel impair $\ell = 1$ est gouverné par une seule équation différentielle de type Regge-Wheeler tandis que les autres modes partiels sont gouvernés par deux ou trois équations différentielles couplées qui dépendent de la parité et du moment angulaire ℓ.

ANNEXE A

Méthodes numériques : Généralisation aux champs bosoniques massifs

Nous considérons, ici, le champ scalaire massif, le champ de Proca, le champ d'Einstein et le champ de Fierz-Pauli. Nous commençons par déterminer numériquement les modes solutions ϕ^{in} et ϕ^{up} de l'équation de type-Regge-Wheeler homogène qui permettent de construire les réponses partielles $\phi_{\omega\ell}(r)$, ainsi que leurs formes d'ondes associées $\phi_\ell(t,r)$ (Annexe. A.2). Nous généralisons ensuite la méthode du *balayage dans le plan complexe* pour la recherche des fréquences quasi-normales et des fréquences quasi-liées associées, respectivement, aux QNMs et QBSs de ces différents champs bosoniques (Annexe. A.2 et Annexe. A.3).

A.1. Résolution numérique de l'équation de Regge-Wheeler

Dans l'espace-temps de Schwarzschild, l'équation de Regge-Wheeler homogène

$$\left[\frac{d^2}{dr_*^2} + \omega^2 - V_\ell(r)\right]\phi_{\omega\ell} = 0, \tag{A.1.1}$$

avec le potentiel effectif donné par

$$V_\ell(r) = \left(1 - \frac{2M}{r}\right)\left(\mu^2 + \frac{A(\ell)}{r^2} + \beta\frac{2M}{r^3}\right). \tag{A.1.2}$$

gouverne les modes partiels $\phi_{\omega\ell}(r)$ du :

(i) Champ scalaire massif

$$\ell \in \mathbb{N}, \qquad A(\ell) = \ell(\ell+1) \qquad \text{et} \qquad \beta = 1$$

(ii) Champ de Proca

- Parité impaire

$$\ell \in \mathbb{N}^*, \qquad A(\ell) = \ell(\ell+1) \qquad \text{et} \qquad \beta = 0$$

- Parité paire

$$\ell = 0, \qquad A(\ell) = 2 \qquad \text{et} \qquad \beta = -3$$

(iii) Champ d'Einstein

- parité impaire

$$\mu = 0, \qquad \ell \geqslant 2, \qquad \mathrm{A}(\ell) = \ell(\ell+1) \qquad \text{et} \qquad \beta = -3$$

(iv) Champ de Fierz-Pauli

- parité impaire

$$\ell = 1, \qquad \mathrm{A}(\ell) = 6 \qquad \text{et} \qquad \beta = -8$$

Nous déterminons, pour commencer et comme nous l'avons déjà fait au Chap. 3, numériquement les fonctions ϕ^{in} et ϕ^{up} pour construire les réponses partielles. Pour cela, nous décrivons d'abord la solution de l'équation de Regge-Wheeler (A.1.1) à l'aide d'un développement en série de Taylor convergent rapidement à l'horizon pour $r_* \to -\infty$ ou $r \to 2\mathrm{M}$, et qui est donné par l'expression (3.1.3), avec les $a_n^{\pm}$ vérifiant, maintenant, la relation de récurrence à 5 termes (cf. (3.1.4)) généralisée aux différents champs bosoniques

$$\begin{aligned}
&n\Big[n \pm 2i\,(2\mathrm{M}\omega)\Big]a_n^{\pm} \\
&+\Big[\mp 4i\,(2\mathrm{M}\omega)(n-1) - 2\,(n-1)(2n-1) - \mathrm{A}(\ell) - \beta - (2\mathrm{M}\mu)^2\Big]a_{n-1}^{\pm} \\
&+\Big[\pm 2i\,(2\mathrm{M}\omega)(n-2) + 6\,(n-2)(n-1) + 2\,\mathrm{A}(\ell) + 3\beta\Big]a_{n-2}^{\pm} \\
&+\Big[-2\,(n-3)(2n-3) - \mathrm{A}(\ell) - 3\beta\Big]a_{n-3}^{\pm} \\
&+\Big[(n-2)(n-4) + \beta\Big]a_{n-4}^{\pm} = 0
\end{aligned} \tag{A.1.3}$$

et les conditions initiales

$$a_{-3}^{\pm} = a_{-2}^{\pm} = a_{-1}^{\pm} = 0 \quad \text{et} \quad a_0 = 1. \tag{A.1.4}$$

Nous décrivons aussi, à l'aide d'un développement asymptotique la solution de l'équation de Regge-Wheeler (A.1.1) à l'infini spatial pour $r_* \to +\infty$ ou $r \to +\infty$ donné par l'expression (3.1.6), où les $\tau_n^{\pm}$ vérifient la relation de récurrence à 4 termes (cf. (3.1.7)) généralisée aux différents champs bosoniques

$$\begin{aligned}
&\mp\Big[2i\,(2\mathrm{M}p(\omega))\,n\Big]\tau_n^{\pm} \\
&+\Big[(2\mathrm{M}\mu)^2 \pm 2i\,(2\mathrm{M}p(\omega))(n-1) \mp 2i\left(\frac{\mathrm{M}\mu^2}{p(\omega)}\right)(n-1) \\
&\mp i\left(\frac{\mathrm{M}\mu^2}{p(\omega)}\right) - \left(\frac{\mathrm{M}\mu^2}{p(\omega)}\right)^2 + n(n-1) - \mathrm{A}(\ell)\Big]\tau_{n-1}^{\pm} \\
&+\left[\pm 4i\left(\frac{\mathrm{M}\mu^2}{p(\omega)}\right)(n-2) \pm 3i\left(\frac{\mathrm{M}\mu^2}{p(\omega)}\right) + 2\left(\frac{\mathrm{M}\mu^2}{p(\omega)}\right)^2 - (n-2)(2n-1) - \beta + \mathrm{A}(\ell)\right]\tau_{n-2}^{\pm} \\
&+\left[\mp 2i\left(\frac{\mathrm{M}\mu^2}{p(\omega)}\right)(n-3) \mp 2i\left(\frac{\mathrm{M}\mu^2}{p(\omega)}\right) - \left(\frac{\mathrm{M}\mu^2}{p(\omega)}\right)^2 + (n-3)(n-1) + \beta\right]\tau_{n-3}^{\pm} = 0
\end{aligned} \tag{A.1.5}$$

et les conditions initiales suivantes

$$\tau_{-2}^{\pm} = \tau_{-1}^{\pm} = 0 \quad \text{et} \quad \tau_{0}^{\pm} = 1. \tag{A.1.6}$$

Nous utilisons, *mutatis mutandis*, la même démarche décrite dans le Chap. 3, dans le but d'obtenir à la fois les $\phi^{\text{in}}_{\omega\ell}$, les coefficients $A_\ell^{(-)}$ et les $\phi^{\text{up}}_{\omega\ell}$ pour construire les réponses partielles ainsi que les formes d'ondes associées.

A.2. Construction du spectre des fréquences quasi-normales

Nous généralisons, maintenant, la méthode du déterminant de Hill, décrite dans le Chap. 3.1 et que nous avons modifiée, au cas du champ scalaire massif pour la recherche des fréquences quasi-normales. Pour que cela soit possible, les QNMs, comme nous l'avons déjà fait remarquer (cf. Chap. 3), doivent vérifier les conditions aux limites données par les expressions (3.2.1a) et (3.2.1b). Les solutions de l'équation de Regge-Wheeler homogène (A.1.1) peuvent donc s'écrire sous la forme donnée par l'expression (3.2.2), tout en généralisant la relation de récurrence à 3 termes

$$\alpha_n a_{n+1} + \beta_n a_n + \gamma_n a_{n-1} = 0, \tag{A.2.1}$$

avec comme conditions initiales

$$\alpha_0 a_1 + \beta_0 a_0 = 0, \tag{A.2.2}$$

où

$$\alpha_n = (n+1)(n+1-4i\mathrm{M}\omega), \tag{A.2.3a}$$

$$\beta_n = \frac{\mathrm{M}(\omega+p(\omega))\Big[4\mathrm{M}(\omega+p(\omega))^2 + i(2n+1)(\omega+3p(\omega))\Big]}{p(\omega)} - 2n(n+1) - \beta - A(\ell), \tag{A.2.3b}$$

$$\gamma_n = \left[n - \frac{\mathrm{M}i(\omega+p(\omega))^2}{p(\omega)}\right]^2 - 1 + \beta. \tag{A.2.3c}$$

Nous utilisons, dans la pratique, la méthode du *balayage du plan complexe* décrite dans le Chap. 3, tout en spécifiant le $A(\ell)$ et le β pour chaque champ considéré.

A.3. Construction du spectre des fréquences quasi-liées

En ce qui concerne le spectre des fréquences quasi-liées, la recherche se fait exactement de la même manière. On doit simplement tenir compte du fait que l'on travaille dans le second feuillet de Riemann associé à la fonction $p(\omega)$, d'où la nécessité de changer $p(\omega)$ en $-p(\omega)$ (voir Fig. 3.4).

Bibliographie

[1] A. Einstein, "Die Feldgleichungen der Gravitation", Sitzungsberichte der Königlich Preußischen Akademie der Wissenschaften (Berlin), 844 (1915).

[2] A. Einstein, "Näherungsweise Integration der Feldgleichungen der Gravitation", Sitzungsberichte der Königlich Preußischen Akademie der Wissenschaften (Berlin), 688 (1916).

[3] B. P. Abbott et al., "Observation of Gravitational Waves from a Binary Black Hole Merger", Phys. Rev. Lett. **116**, 061102 (2016), arXiv :1602.03837 [gr-qc].

[4] R. A. Hulse et J. H. Taylor, "Discovery of a pulsar in a binary system", Astrophys. J. **195**, L51 (1975).

[5] J. H. Taylor et J. M. Weisberg, "A new test of general relativity: Gravitational radiation and the binary pulsar PS R 1913+16", Astrophys. J. **253**, 908 (1982).

[6] K. D. Kokkotas et B. G. Schmidt, "Quasinormal modes of stars and black holes", Living Rev. Rel. **2**, 2 (1999), arXiv :gr-qc/9909058.

[7] H.-P. Nollert, "Topical review: Quasinormal modes: the characteristic 'sound' of black holes and neutron stars", Classical Quantum Gravity **16**, R159 (1999).

[8] E. Berti, V. Cardoso et A. O. Starinets, "Quasinormal modes of black holes and black branes", Classical Quantum Gravity **26**, 163001 (2009), arXiv :0905.2975 [gr-qc].

[9] R. Konoplya et A. Zhidenko, "Quasinormal modes of black holes: From astrophysics to string theory", Rev. Mod. Phys. **83**, 793 (2011), arXiv :1102.4014 [gr-qc].

[10] B. P. Abbott et al., "Properties of the binary black hole merger GW150914", (2016), arXiv :1602.03840 [gr-qc].

[11] B. P. Abbott et al., "GW150914: First results from the search for binary black hole coalescence with Advanced LIGO", (2016), arXiv :1602.03839 [gr-qc].

[12] S. W. Hawking et G. F. R. Ellis, *The Large Scale Structure of Space-Time*, Cambridge Monographs on Mathematical Physics (Cambridge University Press, 2011).

[13] E. Berti et al., "Testing General Relativity with Present and Future Astrophysical Observations", Class. Quant. Grav. **32**, 243001 (2015), arXiv :1501.07274 [gr-qc].

[14] L. S. Finn et P. J. Sutton, "Bounding the mass of the graviton using binary pulsar observations", Phys. Rev. D **65**, 044022 (2002).

[15] C. Talmadge, J. P. Berthias, R. W. Hellings et al., "Model Independent Constraints on Possible Modifications of Newtonian Gravity", Phys. Rev. Lett. **61**, 1159 (1988).

[16] C. M. Will, "Bounding the mass of the graviton using gravitational wave observations of inspiralling compact binaries", Phys. Rev. D **57**, 2061 (1998), arXiv :gr-qc/9709011 [gr-qc].

[17] B. P. Abbott et al., "Tests of general relativity with GW150914", (2016), arXiv :1602.03841 [gr-qc].

[18] A. S. Goldhaber et M. M. Nieto, "Photon and Graviton Mass Limits", Rev. Mod. Phys. **82**, 939 (2010), arXiv :0809.1003 [hep-ph].

[19] S. Gillessen, F. Eisenhauer, S. Trippe et al., "Monitoring stellar orbits around the Massive Black Hole in the Galactic Center", Astrophys. J. **692**, 1075 (2009), arXiv :0810.4674 [astro-ph].

[20] R. C. van den Bosch, K. Gebhardt, K. Gultekin et al., "An Over-Massive Black Hole in the Compact Lenticular Galaxy NGC1277", Nature **491**, 729 (2012), arXiv :1211.6429 [astro-ph.CO].

[21] L. Ferrarese et D. Merritt, "A Fundamental relation between supermassive black holes and their host galaxies", Astrophys. J. **539**, L9 (2000), arXiv :astro-ph/0006053 [astro-ph].

[22] P. A. Seoane et al., "The Gravitational Universe", (2013), arXiv :1305.5720 [astro-ph.CO].

[23] R. P. Kerr, "Gravitational field of a spinning mass as an example of algebraically special metrics", Phys. Rev. Lett. **11**, 237 (1963).

[24] T. Regge et J. A. Wheeler, "Stability of a Schwarzschild singularity", Phys. Rev. **108**, 1063 (1957).

[25] C. V. Vishveshwara, "Stability of the schwarzschild metric", Phys. Rev. D **1**, 2870 (1970).

[26] F. J. Zerilli, "Effective potential for even-parity regge-wheeler gravitational perturbation equations", Phys. Rev. Lett. **24**, 737 (1970).

[27] V. Moncrief, "Gravitational perturbations of spherically symmetric systems. I. The exterior problem.", Annals Phys. **88**, 323 (1974).

[28] F. J. Zerilli, "Gravitational field of a particle falling in a schwarzschild geometry analyzed in tensor harmonics", Phys. Rev. D **2**, 2141 (1970).

[29] M. Davis, R. Ruffini, W. H. Press et al., "Gravitational radiation from a particle falling radially into a schwarzschild black hole", Phys. Rev. Lett. **27**, 1466 (1971).

[30] M. Davis, R. Ruffini et J. Tiomno, "Pulses of gravitational radiation of a particle falling radially into a schwarzschild black hole", Phys. Rev. D **5**, 2932 (1972).

[31] S. A. Teukolsky, "Gravitational perturbations of a rotating black hole", (1971).

[32] S. A. Teukolsky, "Rotating black holes - separable wave equations for gravitational and electromagnetic perturbations", Phys. Rev. Lett. **29**, 1114 (1972).

[33] S. A. Teukolsky, "Perturbations of a rotating black hole. 1. Fundamental equations for gravitational electromagnetic and neutrino field perturbations", Astrophys. J. **185**, 635 (1973).

[34] W. H. Press et S. A. Teukolsky, "Perturbations of a Rotating Black Hole. II. Dynamical Stability of the Kerr Metric", Astrophys. J. **185**, 649 (1973).

[35] S. A. Teukolsky et W. H. Press, "Perturbations of a rotating black hole. III - Interaction of the hole with gravitational and electromagnet ic radiation", Astrophys. J. **193**, 443 (1974).

[36] S. L. Detweiler et E. Szedenits, " Black holes and gravitational waves. II. Trajectories plunging into a nonrotating hole", Astrophys. J. **231**, 211 (1979).

[37] V. Moncrief, C. T. Cunningham et R. H. Price, "Radiation from slightly nonspherical models of gravitational collapse", in Proceedings, Sources of Gravitational Radiation (1979), p. 231–243.

[38] C. T. Cunningham, R. H. Price et V. Moncrief, "Radiation from collapsing relativistic stars. I - Linearized odd-parity radiation", Astrophys. J. **224**, 643 (1978).

[39] C. T. Cunningham, R. H. Price et V. Moncrief, "Radiation from collapsing relativistic starts. II. Linearized even parity radiation", Astrophys. J. **230**, 870 (1979).

[40] K. Oohara et T. Nakamura, "Energy, momentum and angular momentum of gravitational waves induced by a particle plunging into a Schwarzschild black hole", Prog. Theor. Phys. **70**, 757 (1983).

[41] Y. Mino, M. Sasaki et T. Tanaka, "Gravitational radiation reaction to a particle motion", Phys. Rev. D **55**, 3457 (1997), arXiv :gr-qc/9606018 [gr-qc].

[42] T. C. Quinn et R. M. Wald, "An Axiomatic approach to electromagnetic and gravitational radiation reaction of particles in curved space-time", Phys. Rev. D **56**, 3381 (1997), arXiv :gr-qc/9610053 [gr-qc].

[43] A. Ori et K. S. Thorne, "The Transition from inspiral to plunge for a compact body in a circular equatorial orbit around a massive, spinning black hole", Phys. Rev. D **62**, 124022 (2000), arXiv :gr-qc/0003032 [gr-qc].

[44] R. J. Gleiser, C. O. Nicasio, R. H. Price et al., "Gravitational radiation from Schwarzschild black holes: The Second order perturbation formalism", Phys. Rept. **325**, 41 (2000), arXiv :gr-qc/9807077 [gr-qc].

[45] J. G. Baker, B. Bruegmann, M. Campanelli et al., "Plunge wave forms from inspiralling binary black holes", Phys. Rev. Lett. **87**, 121103 (2001), arXiv :gr-qc/0102037 [gr-qc].

[46] M. Sasaki et H. Tagoshi, "Analytic black hole perturbation approach to gravitational radiation", Living Rev. Rel. **6**, 6 (2003), arXiv :gr-qc/0306120 [gr-qc].

[47] M. Campanelli, C. Lousto et Y. Zlochower, "The Last orbit of binary black holes", Phys. Rev. D **73**, 061501 (2006), arXiv :gr-qc/0601091 [gr-qc].

[48] U. Sperhake, E. Berti, V. Cardoso et al., "Eccentric binary black-hole mergers: The Transition from inspiral to plunge in general relativity", Phys. Rev. D **78**, 064069 (2008), arXiv :0710.3823 [gr-qc].

[49] S. E. Gralla et R. M. Wald, "A Rigorous Derivation of Gravitational Self-force", Class. Quant. Grav. **25**, [Erratum: Class. Quant. Grav.28,159501(2011)], 205009 (2008), arXiv :0806.3293 [gr-qc].

[50] Y. Mino et J. Brink, "Gravitational Radiation from Plunging Orbits: Perturbative Study", Phys. Rev. D **78**, 124015 (2008), arXiv :0809.2814 [gr-qc].

[51] L. Barack, "Gravitational self force in extreme mass-ratio inspirals", Class. Quant. Grav. **26**, 213001 (2009), arXiv :0908.1664 [gr-qc].

[52] S. Hadar et B. Kol, "Post-ISCO Ringdown Amplitudes in Extreme Mass Ratio Inspiral", Phys. Rev. D **84**, 044019 (2011), arXiv :0911.3899 [gr-qc].

[53] S. L. Detweiler, "Elementary development of the gravitational self-force", Fundam. Theor. Phys. **162**, [,271(2009)], 271 (2011), arXiv :0908.4363 [gr-qc].

[54] R. M. Wald, "Introduction to Gravitational Self-Force", Fundam. Theor. Phys. **162**, [,253(2009)], 253 (2011), arXiv :0907.0412 [gr-qc].

[55] J. Thornburg, "The Capra Research Program for Modelling Extreme Mass Ratio Inspirals", GW Notes **5**, 3 (2011), arXiv :1102.2857 [gr-qc].

[56] S. Hadar, B. Kol, E. Berti et al., "Comparing numerical and analytical calculations of post-ISCO ringdown amplitudes", Phys. Rev. D **84**, 047501 (2011), arXiv :1105.3861 [gr-qc].

[57] E. Poisson, A. Pound et I. Vega, "The Motion of point particles in curved spacetime", Living Rev. Rel. **14**, 7 (2011), arXiv :1102.0529 [gr-qc].

[58] R. H. Price, G. Khanna et S. A. Hughes, "Black hole binary inspiral and trajectory dominance", Phys. Rev. D **88**, 104004 (2013), arXiv :1306.1159 [gr-qc].

[59] S. Hadar, A. P. Porfyriadis et A. Strominger, "Gravity Waves from Extreme-Mass-Ratio Plunges into Kerr Black Holes", Phys. Rev. D **90**, 064045 (2014), arXiv :1403.2797 [hep-th].

[60] S. Hadar, A. P. Porfyriadis et A. Strominger, "Fast plunges into Kerr black holes", (2015), arXiv :1504.07650 [hep-th].

[61] P. Amaro-Seoane, J. R. Gair, A. Pound et al., "Research Update on Extreme-Mass-Ratio Inspirals", J. Phys. Conf. Ser. **610**, 012002 (2015), arXiv :1410.0958 [astro-ph.CO].

[62] R. H. Price, S. Nampalliwar et G. Khanna, "Black hole binary inspiral: Analysis of the plunge", Phys. Rev. D **93**, 044060 (2016), arXiv :1508.04797 [gr-qc].

[63] K. Postnov et L. Yungelson, "The Evolution of Compact Binary Star Systems", Living Rev. Rel. **9**, 6 (2006), arXiv :astro-ph/0701059 [astro-ph].

[64] H. A. Lorentz et J. Droste, "Collected papers: volume v", in (Springer Netherlands, Dordrecht, 1937) chap. The Motion of a System of Bodies under the Influence of their Mutual Attraction, According to Einstein's Theory, p. 330–355.

[65] A. Einstein, L. Infeld et B. Hoffmann, "The Gravitational equations and the problem of motion", Annals Math. **39**, 65 (1938).

[66] S. Chandrasekhar, "The Post-Newtonian Equations of Hydrodynamics in General Relativity.", Astrophys. J. **142**, 1488 (1965).

[67] S. Chandrasekhar, "Conservation Laws in General Relativity and in the Post-Newtonian Approximations", Astrophys. J. **158**, 45 (1969).

[68] S. Chandrasekhar et F. P. Esposito, "The 2(1/2)-Post-Newtonian Equations of Hydrodynamics and Radiation Reaction in General Relativity", Astrophys. J. **160**, 153 (1970).

[69] R. Blandford et S. A. Teukolsky, "Arrival-time analysis for a pulsar in a binary system.", Astrophys. J. **205**, 580 (1976).

[70] R. Epstein, "The binary pulsar - Post-Newtonian timing effects", Astrophys. J. **216**, 92 (1977).

[71] T. Damour et J. H. Taylor, "On the orbital period change of the binary pulsar PSR 1913 + 16", Astrophys. J. **366**, 501 (1991).

[72] C. M. Will, "Gravitational waves from inspiraling compact binaries: A PostNewtonian approach", in Relativistic cosmology. Proceedings, 8th Nishinomiya-Yukawa Memorial Symposium, NYMSS-8, Nishinomiya, Japan, October 28-29, 1993 (1994), p. 83–98, arXiv :gr-qc/9403033 [gr-qc].

[73] L. Blanchet, B. R. Iyer, C. M. Will et al., "Gravitational wave forms from inspiralling compact binaries to second postNewtonian order", Class. Quant. Grav. **13**, 575 (1996), arXiv :gr-qc/9602024 [gr-qc].

[74] C. M. Will et A. G. Wiseman, "Gravitational radiation from compact binary systems: Gravitational wave forms and energy loss to second postNewtonian order", Phys. Rev. D **54**, 4813 (1996), arXiv :gr-qc/9608012 [gr-qc].

[75] P. Jaranowski et G. Schaefer, "Third postNewtonian higher order ADM Hamilton dynamics for two-body point mass systems", Phys. Rev. D **57**, [Erratum: Phys. Rev.D63,029902(2001)], 7274 (1998), arXiv :gr-qc/9712075 [gr-qc].

[76] L. Blanchet, "On the multipole expansion of the gravitational field", Class. Quant. Grav. **15**, 1971 (1998), arXiv :gr-qc/9801101 [gr-qc].

[77] L. Blanchet, G. Faye et B. Ponsot, "Gravitational field and equations of motion of compact binaries to 5/2 postNewtonian order", Phys. Rev. D **58**, 124002 (1998), arXiv :gr-qc/9804079 [gr-qc].

[78] C. M. Will, "Generation of postNewtonian gravitational radiation via direct integration of the relaxed Einstein equations", Prog. Theor. Phys. Suppl. **136**, 158 (1999), arXiv :gr-qc/9910057 [gr-qc].

[79] M. E. Pati et C. M. Will, "PostNewtonian gravitational radiation and equations of motion via direct integration of the relaxed Einstein equations. 1. Foundations", Phys. Rev. D **62**, 124015 (2000), arXiv :gr-qc/0007087 [gr-qc].

[80] T. Damour, P. Jaranowski et G. Schaefer, "Poincare invariance in the ADM Hamiltonian approach to the general relativistic two-body problem", Phys. Rev. D **62**, [Erratum: Phys. Rev.D63,029903(2001)], 021501 (2000), arXiv :gr-qc/0003051 [gr-qc].

[81] V. C. de Andrade, L. Blanchet et G. Faye, "Third postNewtonian dynamics of compact binaries: Noetherian conserved quantities and equivalence between the harmonic coordinate and ADM Hamiltonian formalisms", Class. Quant. Grav. **18**, 753 (2001), arXiv :gr-qc/0011063 [gr-qc].

[82] L. Blanchet et G. Faye, "General relativistic dynamics of compact binaries at the third postNewtonian order", Phys. Rev. D **63**, 062005 (2001), arXiv :gr-qc/0007051 [gr-qc].

[83] L. Blanchet, B. R. Iyer et B. Joguet, "Gravitational waves from inspiralling compact binaries: Energy flux to third postNewtonian order", Phys. Rev. D **65**, [Erratum: Phys. Rev.D71,129903(2005)], 064005 (2002), arXiv :gr-qc/0105098 [gr-qc].

[84] L. Blanchet, G. Faye, B. R. Iyer et al., "Gravitational wave inspiral of compact binary systems to 7/2 postNewtonian order", Phys. Rev. D **65**, [Erratum: Phys. Rev.D71,129902(2005)], 061501 (2002), arXiv :gr-qc/0105099 [gr-qc].

[85] T. Damour, P. Jaranowski et G. Schaefer, "Dimensional regularization of the gravitational interaction of point masses", Phys. Lett. **B513**, 147 (2001), arXiv :gr-qc/0105038 [gr-qc].

[86] Y. Itoh, T. Futamase et H. Asada, "Equation of motion for relativistic compact binaries with the strong field point particle limit: The Second and half postNewtonian order", Phys. Rev. D **63**, 064038 (2001), arXiv :gr-qc/0101114 [gr-qc].

[87] M. E. Pati et C. M. Will, "PostNewtonian gravitational radiation and equations of motion via direct integration of the relaxed Einstein equations. 2. Two-body equations of motion to second postNewtonian order, and radiation reaction to 3.5 postNewtonia order", Phys. Rev. D **65**, 104008 (2002), arXiv :gr-qc/0201001 [gr-qc].

[88] Y. Itoh, "Equation of motion for relativistic compact binaries with the strong field point particle limit: Third postNewtonian order", Phys. Rev. D **69**, 064018 (2004), arXiv :gr-qc/0310029 [gr-qc].

[89] L. Blanchet, T. Damour, G. Esposito-Farese et al., "Gravitational radiation from inspiralling compact binaries completed at the third post-Newtonian order", Phys. Rev. Lett. **93**, 091101 (2004), arXiv :gr-qc/0406012 [gr-qc].

[90] W. D. Goldberger et I. Z. Rothstein, "An Effective field theory of gravity for extended objects", Phys. Rev. D **73**, 104029 (2006), arXiv :hep-th/0409156 [hep-th].

[91] L. Blanchet, T. Damour, G. Esposito-Farese et al., "Dimensional regularization of the third post-Newtonian gravitational wave generation from two point masses", Phys. Rev. D **71**, 124004 (2005), arXiv :gr-qc/0503044 [gr-qc].

[92] T. Mitchell et C. M. Will, "Post-Newtonian gravitational radiation and equations of motion via direct integration of the relaxed Einstein equations. V. The Strong equivalence principle to second post-Newtonian order", Phys. Rev. D **75**, 124025 (2007), arXiv :0704.2243 [gr-qc].

[93] L. Blanchet, G. Faye, B. R. Iyer et al., "The Third post-Newtonian gravitational wave polarisations and associated spherical harmonic modes for inspiralling compact binaries in quasi-circular orbits", Class. Quant. Grav. **25**, [Erratum: Class. Quant. Grav.29,239501(2012)], 165003 (2008), arXiv :0802.1249 [gr-qc].

[94] G. Schaefer, "Post-Newtonian methods: Analytic results on the binary problem", Fundam. Theor. Phys. **162**, [,167(2009)], 167 (2011), arXiv :0910.2857 [gr-qc].

[95] L. Blanchet, "Post-Newtonian theory and the two-body problem", Fundam. Theor. Phys. **162**, [,125(2009)], 125 (2011), arXiv :0907.3596 [gr-qc].

[96] S. Foffa et R. Sturani, "Dynamics of the gravitational two-body problem at fourth post-Newtonian order and at quadratic order in the Newton constant", Phys. Rev. D **87**, 064011 (2013), arXiv :1206.7087 [gr-qc].

[97] L. Blanchet, "Gravitational Radiation from Post-Newtonian Sources and Inspiralling Compact Binaries", Living Rev. Rel. **17**, 2 (2014), arXiv :1310.1528 [gr-qc].

[98] P. Jaranowski et G. Schäfer, "Dimensional regularization of local singularities in the 4th post-Newtonian two-point-mass Hamiltonian", Phys. Rev. D **87**, 081503 (2013), arXiv :1303.3225 [gr-qc].

[99] T. Damour, P. Jaranowski et G. Schäfer, "Nonlocal-in-time action for the fourth post-Newtonian conservative dynamics of two-body systems", Phys. Rev. D **89**, 064058 (2014), arXiv :1401.4548 [gr-qc].

[100] A. Buonanno et T. Damour, "Effective one-body approach to general relativistic two-body dynamics", Phys. Rev. D **59**, 084006 (1999), arXiv :gr-qc/9811091 [gr-qc].

[101] A. Buonanno et T. Damour, "Transition from inspiral to plunge in binary black hole coalescences", Phys. Rev. D **62**, 064015 (2000), arXiv :gr-qc/0001013 [gr-qc].

[102] T. Damour, "The General Relativistic Two Body Problem and the Effective One Body Formalism", Fundam. Theor. Phys. **177**, 111 (2014), arXiv :1212.3169 [gr-qc].

[103] T. Damour, "The general relativistic two body problem", (2013), arXiv :1312.3505 [gr-qc].

[104] T. Damour, "Coalescence of two spinning black holes: an effective one-body approach", Phys. Rev. D **64**, 124013 (2001), arXiv :gr-qc/0103018 [gr-qc].

[105] T. Damour, P. Jaranowski et G. Schaefer, "Effective one body approach to the dynamics of two spinning black holes with next-to-leading order spin-orbit coupling", Phys. Rev. D **78**, 024009 (2008), arXiv :0803.0915 [gr-qc].

[106] E. Barausse et A. Buonanno, "An Improved effective-one-body Hamiltonian for spinning black-hole binaries", Phys. Rev. D **81**, 084024 (2010), arXiv :0912.3517 [gr-qc].

[107] A. Nagar, "Effective one body Hamiltonian of two spinning black-holes with next-to-next-to-leading order spin-orbit coupling", Phys. Rev. D **84**, [Erratum: Phys. Rev.D88,no.8,089901(2013)], 084028 (2011), arXiv :1106.4349 [gr-qc].

[108] E. Barausse et A. Buonanno, "Extending the effective-one-body Hamiltonian of black-hole binaries to include next-to-next-to-leading spin-orbit couplings", Phys. Rev. D **84**, 104027 (2011), arXiv :1107.2904 [gr-qc].

[109] S. Balmelli et P. Jetzer, "Effective-one-body Hamiltonian with next-to-leading order spin-spin coupling for two nonprecessing black holes with aligned spins", Phys. Rev. D **87**, [Erratum: Phys. Rev.D90,no.8,089905(2014)], 124036 (2013), arXiv :1305.5674 [gr-qc].

[110] L. Barack, T. Damour et N. Sago, "Precession effect of the gravitational self-force in a Schwarzschild spacetime and the effective one-body formalism", Phys. Rev. D **82**, 084036 (2010), arXiv :1008.0935 [gr-qc].

[111] T. Damour, "Gravitational Self Force in a Schwarzschild Background and the Effective One Body Formalism", Phys. Rev. D **81**, 024017 (2010), arXiv :0910.5533 [gr-qc].

[112] E. Barausse, A. Buonanno et A. Le Tiec, "The complete non-spinning effective-one-body metric at linear order in the mass ratio", Phys. Rev. D **85**, 064010 (2012), arXiv :1111.5610 [gr-qc].

[113] S. Akcay, L. Barack, T. Damour et al., "Gravitational self-force and the effective-one-body formalism between the innermost stable circular orbit and the light ring", Phys. Rev. D **86**, 104041 (2012), arXiv :1209.0964 [gr-qc].

[114] T. Damour et A. Nagar, "Comparing Effective-One-Body gravitational waveforms to accurate numerical data", Phys. Rev. D **77**, 024043 (2008), arXiv :0711.2628 [gr-qc].

[115] T. Damour, B. R. Iyer et A. Nagar, "Improved resummation of post-Newtonian multipolar waveforms from circularized compact binaries", Phys. Rev. D **79**, 064004 (2009), arXiv :0811.2069 [gr-qc].

[116] Y. Pan, A. Buonanno, M. Boyle et al., "Inspiral-merger-ringdown multipolar waveforms of nonspinning black-hole binaries using the effective-one-body formalism", Phys. Rev. D **84**, 124052 (2011), arXiv :1106.1021 [gr-qc].

[117] T. Damour, A. Nagar et S. Bernuzzi, "Improved effective-one-body description of coalescing nonspinning black-hole binaries and its numerical-relativity completion", Phys. Rev. D **87**, 084035 (2013), arXiv :1212.4357 [gr-qc].

[118] Y. Pan, A. Buonanno, A. Taracchini et al., "Inspiral-merger-ringdown waveforms of spinning, precessing black-hole binaries in the effective-one-body formalism", Phys. Rev. D **89**, 084006 (2014), arXiv :1307.6232 [gr-qc].

[119] Y. Pan, A. Buonanno, A. Taracchini et al., "Stability of nonspinning effective-one-body model in approximating two-body dynamics and gravitational-wave emission", Phys. Rev. D **89**, 061501 (2014), arXiv :1311.2565 [gr-qc].

[120] A. Taracchini et al., "Effective-one-body model for black-hole binaries with generic mass ratios and spins", Phys. Rev. D **89**, 061502 (2014), arXiv :1311.2544 [gr-qc].

[121] T. Damour et A. Nagar, "New effective-one-body description of coalescing nonprecessing spinning black-hole binaries", Phys. Rev. D **90**, 044018 (2014), arXiv :1406.6913 [gr-qc].

[122] F. Pretorius, "Binary Black Hole Coalescence", (2007), arXiv :0710.1338 [gr-qc].

[123] J. Centrella, J. G. Baker, B. J. Kelly et al., "Black-hole binaries, gravitational waves, and numerical relativity", Rev. Mod. Phys. **82**, 3069 (2010), arXiv :1010.5260 [gr-qc].

[124] I. Hinder, "The Current Status of Binary Black Hole Simulations in Numerical Relativity", Class. Quant. Grav. **27**, 114004 (2010), arXiv :1001.5161 [gr-qc].

[125] S. T. McWilliams, "The Status of Black-Hole Binary Merger Simulations with Numerical Relativity", Class. Quant. Grav. **28**, 134001 (2011), arXiv :1012.2872 [gr-qc].

[126] U. Sperhake, E. Berti et V. Cardoso, "Numerical simulations of black-hole binaries and gravitational wave emission", Comptes Rendus Physique **14**, 306 (2013), arXiv :1107.2819 [gr-qc].

[127] H. P. Pfeiffer, "Numerical simulations of compact object binaries", Class. Quant. Grav. **29**, 124004 (2012), arXiv :1203.5166 [gr-qc].

[128] R. Konoplya et A. Zhidenko, "Detection of gravitational waves from black holes: Is there a window for alternative theories?", (2016), arXiv :1602.04738 [gr-qc].

[129] M. Fierz, "Force-free particles with any spin", Helv. Phys. Acta **12**, 3 (1939).

[130] M. Fierz et W. Pauli, "On relativistic wave equations for particles of arbitrary spin in an electromagnetic field", Proc. Roy. Soc. Lond. A **173**, 211 (1939).

[131] G. Dvali, G. Gabadadze et M. Porrati, "4-D gravity on a brane in 5-D Minkowski space", Phys. Lett. B **485**, 208 (2000), arXiv :hep-th/0005016.

[132] K. Hinterbichler, "Theoretical Aspects of Massive Gravity", Rev. Mod. Phys. **84**, 671 (2012), arXiv :1105.3735 [hep-th].

[133] C. de Rham, "Massive Gravity", Living Rev. Relativity. **17**, 7 (2014), arXiv :1401.4173 [hep-th].

[134] M. S. Volkov, "Hairy black holes in the ghost-free bigravity theory", Phys. Rev. **D85**, 124043 (2012), arXiv :1202.6682 [hep-th].

[135] M. S. Volkov, "Self-accelerating cosmologies and hairy black holes in ghost-free bigravity and massive gravity", Classical Quantum Gravity **30**, 184009 (2013), arXiv :1304.0238 [hep-th].

[136] R. Brito, V. Cardoso et P. Pani, "Massive spin-2 fields on black hole spacetimes: Instability of the Schwarzschild and Kerr solutions and bounds on the graviton mass", Phys. Rev. D **88**, 023514 (2013), arXiv :1304.6725 [gr-qc].

[137] R. Brito, V. Cardoso et P. Pani, "Partially massless gravitons do not destroy general relativity black holes", Phys. Rev. D **87**, 124024 (2013), arXiv :1306.0908 [gr-qc].

[138] E. Babichev et A. Fabbri, "Instability of black holes in massive gravity", Classical Quantum Gravity **30**, 152001 (2013), arXiv :1304.5992 [gr-qc].

[139] E. Babichev et R. Brito, "Black holes in massive gravity", Classical Quantum Gravity. **32**, 154001 (2015), arXiv :1503.07529 [gr-qc].

[140] E. Babichev, R. Brito et P. Pani, "Linear stability of nonbidiagonal black holes in massive gravity", (2015), arXiv :1512.04058 [gr-qc].

[141] N. Deruelle et R. Ruffini, "Quantum and classical relativistic energy states in stationary geometries", Phys. Lett. B **52**, 437 (1974).

[142] T. Damour, N. Deruelle et R. Ruffini, "On Quantum Resonances in Stationary Geometries", Lett. Nuovo Cim. **15**, 257 (1976).

[143] T. Zouros et D. Eardley, "Instabilities of massive scalar perturbations of a rotating black hole", Annals Phys. **118**, 139 (1979).

[144] S. L. Detweiler, "Klein-Gordon equation and rotating black holes", Phys. Rev. D **22**, 2323 (1980).

[145] J. G. Rosa et S. R. Dolan, "Massive vector fields on the Schwarzschild spacetime: quasi-normal modes and bound states", Phys. Rev. D **85**, 044043 (2012), arXiv :1110.4494 [hep-th].

[146] A. Arvanitaki, S. Dimopoulos, S. Dubovsky et al., "String Axiverse", Phys. Rev. D **81**, 123530 (2010), arXiv :0905.4720 [hep-th].

[147] J. Rosa, "The Extremal black hole bomb", JHEP **1006**, 015 (2010), arXiv :0912.1780 [hep-th].

[148] A. Arvanitaki et S. Dubovsky, "Exploring the String Axiverse with Precision Black Hole Physics", Phys. Rev. D **83**, 044026 (2011), arXiv :1004.3558 [hep-th].

[149] J. Barranco, A. Bernal, J. C. Degollado et al., "Are black holes a serious threat to scalar field dark matter models?", Phys. Rev. D **84**, 083008 (2011), arXiv :1108.0931 [gr-qc].

[150] V. Cardoso, S. Chakrabarti, P. Pani et al., "Floating and sinking: The Imprint of massive scalars around rotating black holes", Phys. Rev. Lett. **107**, 241101 (2011), arXiv :1109.6021 [gr-qc].

[151] J. Barranco, A. Bernal, J. C. Degollado et al., "Schwarzschild black holes can wear scalar wigs", Phys. Rev. Lett. **109**, 081102 (2012), arXiv :1207.2153 [gr-qc].

[152] P. Pani, V. Cardoso, L. Gualtieri et al., "Black hole bombs and photon mass bounds", Phys. Rev. Lett. **109**, 131102 (2012), arXiv :1209.0465 [gr-qc].

[153] S. R. Dolan, "Superradiant instabilities of rotating black holes in the time domain", Phys. Rev. D **87**, 124026 (2013), arXiv :1212.1477 [gr-qc].

[154] R. Brito, V. Cardoso et P. Pani, "Black holes with massive graviton hair", Phys. Rev. D **88**, 064006 (2013), arXiv :1309.0818 [gr-qc].

[155] S. Hod, "Asymptotic late-time tails of massive spin-2 fields", Classical Quantum Gravity **30**, 237002 (2013).

[156] J. Barranco, A. Bernal, J. C. Degollado et al., "Schwarzschild scalar wigs: spectral analysis and late time behavior", (2013), arXiv :1312.5808 [gr-qc].

[157] Y. Decanini, A. Folacci et M. Ould El Hadj, "Giant black hole ringings induced by massive gravity", (2014), arXiv :1401.0321 [gr-qc].

[158] Y. Décanini, A. Folacci et M. Ould El Hadj, "Resonant excitation of black holes by massive bosonic fields and giant ringings", Phys. Rev. D **89**, 084066 (2014), arXiv :1402.2481 [gr-qc].

[159] Y. Decanini, A. Folacci et M. Ould El Hadj, "Waveforms produced by a scalar point particle plunging into a Schwarzschild black hole: Excitation of quasinormal modes and quasibound states", Phys. Rev. D **92**, 024057 (2015), arXiv :1506.09133 [gr-qc].

[160] Y. Décanini, A. Folacci et M. Ould El Hadj, "Waveforms in massive gravity and neutralization of giant black hole ringings", (2016), arXiv :1602.03460 [gr-qc].

[161] C. W. Misner, K. S. Thorne et J. A. Wheeler, *Gravitation* (W. H. Freeman et Company, 1973).

[162] K. Schwarzschild, "Über das gravitationsfeld eines massenpunktes nach der einsteinschen theorie", Sitzungsber. K. Preuss. Akad. Wiss. Phys.-Math. Kl, 189 (1916).

[163] R. M. Wald, *General relativity* (University of Chicago Press, 1984).

[164] S. Chandrasekhar, *The mathematical theory of black holes* (Oxford University Press, 1983).

[165] C. Darwin, "The gravity field of a particule", Proc. R. Soc. London **249**, 180 (1959).

[166] C. Darwin, "The gravity field of a particule II", Proc. R. Soc. London **263**, 39 (1961).

[167] V. P. Frolov et I. D. Novikov, *Black hole physics* (Kluwer AcademicPublishers, 1998).

[168] P. M. Morse et H. Feshbach, *Methods of theoretical physics* (McGraw-Hill Book Co, New York, 1953).

[169] R. Breuer, P. Chrzanowksi, H. Hughes et al., "Geodesic synchrotron radiation", Phys. Rev. D **8**, 4309 (1973).

[170] A. Sommerfeld, *Partial differential equations in physics* (Academic Press, New York, New York, 1949).

[171] W. H. Press, "Long Wave Trains of Gravitational Waves from a Vibrating Black Hole", Astrophys. J. **170**, L105 (1971).

[172] C. J. Goebel, "Comments on the "vibrations" of a Black Hole.", Astrophys. J. **172**, L95 (1972).

[173] V. Ferrari et B. Mashhoon, "New approach to the quasinormal modes of a black hole", Phys. Rev. D **30**, 295 (1984).

[174] L. Vanzo et S. Zerbini, "Asymptotics of quasinormal modes for multihorizon black holes", Phys. Rev. D **70**, 044030 (2004), arXiv :hep-th/0402103 [hep-th].

[175] V. Cardoso, A. S. Miranda, E. Berti et al., "Geodesic stability, Lyapunov exponents and quasinormal modes", Phys. Rev. D **79**, 064016 (2009), arXiv :0812.1806 [hep-th].

[176] Y. Decanini, A. Folacci et B. Jensen, "Complex angular momentum in black hole physics and the quasinormal modes", Phys. Rev. D **67**, 124017 (2003), arXiv :gr-qc/0212093 [gr-qc].

[177] Y. Decanini et A. Folacci, "Regge poles of the Schwarzschild black hole: A WKB approach", Phys. Rev. D **81**, 024031 (2010), arXiv :0906.2601 [gr-qc].

[178] Y. Decanini, A. Folacci et B. Raffaelli, "Unstable circular null geodesics of static spherically symmetric black holes, Regge poles and quasinormal frequencies", Phys. Rev. D **81**, 104039 (2010), arXiv :1002.0121 [gr-qc].

[179] Y. Decanini, A. Folacci et B. Raffaelli, "Resonance and absorption spectra of the Schwarzschild black hole for massive scalar perturbations: a complex angular momentum analysis", Phys. Rev. D **84**, 084035 (2011), arXiv :1108.5076 [gr-qc].

[180] S. Chandrasekhar et S. Detweiler, "The quasi-normal modes of the schwarzschild black hole", Proceedings of the Royal Society of London A **344**, 441 (1975).

[181] I. M. Ternov, V. R. Khalilov, G. A. Chizhov et al., "Finite Movement of Massive Particles in Kerr and Schwarzschild Fields", Sov. Phys. J. **21**, [Izv. Vuz. Fiz.21N9,109(1978)], 1200 (1978).

[182] I. M. Ternov, A. B. Gaina et G. A. Chizhov, "Finite motion of electrons in the field of microscopically small black holes", Sov. Phys. J. **23**, [Izv. Vuz. Fiz.23N8,56(1980)], 695 (1980).

[183] I. M. Ternov, A. B. Gaina et G. A. Chizhov, "Spectral properties of a charged black hole", Sov. J. Nucl. Phys. **44**, [Yad. Fiz.44,533(1986)], 343 (1986).

[184] A. B. Gaina et I. M. Ternov, "Boson Instability of charged black holes", Sov. Astron. Lett. **12**, 394 (1986).

[185] A. B. Gaina et I. M. Ternov, "energy spectrum of the Klein-Gordon equation in Schwarzschild and Kerr fields", Sov. Phys. J. **31**, 830 (1988).

[186] I. M. Ternov et A. B. Gaina, "energy spectrum of the Dirac equation for the Schwarzschild and Kerr fields", Sov. Phys. J. **31**, 157 (1988).

[187] A. B. Gaina et I. M. Ternov, "Quantum mechanics near the black hole", Vestn. Mosk. Univ. Fiz. Astron. **30N2**, [Moscow Univ. Phys. Bull.44N2,22(1989)], 22 (1989).

[188] C. L. Pekeris et K. Frankowski, "Hyperfine Splitting in Muonium, Positronium, and Hydrogen, Deduced From a Solution of Dirac's Equation in Kerr-Newman Geometry", Phys. Rev. A **39**, 518 (1989).

[189] A. Lasenby, C. Doran, J. Pritchard et al., "Bound states and decay times of fermions in a Schwarzschild black hole background", Phys. Rev. D **72**, 105014 (2005), arXiv :gr-qc/0209090 [gr-qc].

[190] H. Furuhashi et Y. Nambu, "Instability of massive scalar fields in Kerr-Newman spacetime", Prog. Theor. Phys. **112**, 983 (2004), arXiv :gr-qc/0402037 [gr-qc].

[191] V. Cardoso, O. J. C. Dias, J. P. S. Lemos et al., "The Black hole bomb and superradiant instabilities", Phys. Rev. D **70**, [Erratum: Phys. Rev.D70,049903(2004)], 044039 (2004), arXiv :hep-th/0404096 [hep-th].

[192] Yu. P. Laptev et M. L. Fil'chenkov, "Electromagnetic and gravitational radiation of graviatoms", Astron. Astrophys. Trans. **25**, 33 (2006), arXiv :gr-qc/0606019 [gr-qc].

[193] I. Sturm et F. M. C. Witte, "Groundstate splitting around rotating mini blackholes", (2007), arXiv :0707.2676 [gr-qc].

[194] S. R. Dolan, "Instability of the massive Klein-Gordon field on the Kerr spacetime", Phys. Rev. D **76**, 084001 (2007), arXiv :0705.2880 [gr-qc].

[195] J. Grain et A. Barrau, "Quantum bound states around black holes", Eur. Phys. J. **C53**, 641 (2008), arXiv :hep-th/0701265 [HEP-TH].

[196] T. Hartman, W. Song et A. Strominger, "The Kerr-Fermi Sea", (2009), arXiv :0912.4265 [hep-th].

[197] S. R. Dolan et D. Dempsey, "Bound states of the Dirac equation on Kerr spacetime", Class. Quant. Grav. **32**, 184001 (2015), arXiv :1504.03190 [gr-qc].

[198] P. Anninos, C. DeWitt-Morette, R. A. Matzner et al., "Orbiting cross sections: application to black hole scattering", Phys. Rev. D **46**, 4477 (1992).

[199] C. M. Bender et S. A. Orszag, *Advanced mathematical methods for scientists and engineers* (McGraw-Hill Book Co, Singapore, 1978).

[200] C. V. Vishveshwara, "Scattering of Gravitational Radiation by a Schwarzschild Black-hole", Nature **227**, 936 (1970).

[201] B. F. Schutz et C. M. Will, "Black hole normal modes : A semianalytic approach", Astrophys. J. **291**, L33 (1985).

[202] E. Leaver, "An Analytic representation for the quasi normal modes of Kerr black holes", Proc. Roy. Soc. Lond. A **402**, 285 (1985).

[203] E. W. Leaver, "Quasinormal modes of Reissner-Nordstrom black holes", Phys. Rev. D **41**, 2986 (1990).

[204] R. Konoplya et A. Zhidenko, "Decay of massive scalar field in a Schwarzschild background", Phys. Lett. B **609**, 377 (2005), arXiv :gr-qc/0411059.

[205] B. Majumdar et N. Panchapakesan, "Schwarzschild black-hole normal modes using the Hill determinant", Phys. Rev. D **40**, 2568 (1989).

[206] L. Blanchet, M. S. Qusailah et C. M. Will, "Gravitational recoil of inspiralling black-hole binaries to second post-Newtonian order", Astrophys. J. **635**, 508 (2005), arXiv :astro-ph/0507692 [astro-ph].

[207] T. Damour et A. Nagar, "Faithful effective-one-body waveforms of small-mass-ratio coalescing black-hole binaries", Phys. Rev. D **76**, 064028 (2007), arXiv :0705.2519 [gr-qc].

[208] C. de Rham et G. Gabadadze, "Generalization of the Fierz-Pauli Action", Phys. Rev. D **82**, 044020 (2010).

[209] C. de Rham, G. Gabadadze et A. J. Tolley, "Resummation of Massive Gravity", Phys. Rev. Lett. **106**, 231101 (2011).

[210] S. Hassan, A. Schmidt-May et M. von Strauss, "On Consistent Theories of Massive Spin-2 Fields Coupled to Gravity", JHEP **1305**, 086 (2013).

[211] E. Berti et V. Cardoso, "Quasinormal ringing of Kerr black holes. I. The Excitation factors", Phys. Rev. D **74**, 104020 (2006).

[212] J. Aasi et al., "Prospects for Observing and Localizing Gravitational-Wave Transients with Advanced LIGO and Advanced Virgo", [Living Rev. Rel.19,1(2016)] (2013) 10.1007/lrr-2016-1, arXiv :1304.0670 [gr-qc].

[213] A. Klein et al., "Science with the space-based interferometer eLISA: Supermassive black hole binaries", Phys. Rev. **D93**, 024003 (2016), arXiv :1511.05581 [gr-qc].

Rayonnement des trous noirs en interaction avec des champs bosoniques massifs

Cette thèse porte sur le rayonnement des trous noirs en interaction avec des champs bosoniques massifs (champ scalaire, champ électromagnétique de Proca et champ des gravitons de Fierz-Pauli). Nous avons étudié plus particulièrement l'influence du spectre des résonances (quasi-normales ou quasi-liées) sur la réponse du trou noir à une perturbation extérieure. Ce travail est un premier pas pour mettre en évidence des effets nouveaux dans le rayonnement des trous noirs supermassifs qui permettraient de tester les théories de gravité massive ou de trancher en faveur de la relativité générale d'Einstein.

Plus précisément :

– Afin de contourner les nombreuses difficultés liées aux théories de gravité massive et à leurs perturbations en présence de trous noirs, nous avons d'abord travaillé sur un modèle où le champ des gravitons est remplacé par un champ scalaire massif couplé linéairement à une "particule" plongeant dans le trou noir de Schwarzschild. Nous avons étudié l'influence de la masse du champ sur la structure des réponses du trou noir et comparé nos résultats à ceux du champ non massif. Nous avons mis en évidence des effets nouveaux dus au paramètre de masse comme l'excitation des modes quasi-liés du trou noir en plus de celle de ses modes quasi-normaux ainsi que l'effondrement de la forme d'onde lorsque la particule se déplace sur une trajectoire quasi-circulaire.

– Nous nous sommes ensuite intéressés à l'excitation des modes quasi-normaux du trou noir de Schwarzschild parce que, d'un point de vue observationnel, ils sont censés fournir une preuve directe de l'existence des trous noirs. Nous avons montré numériquement et analytiquement la présence d'un comportement résonant de leurs facteurs d'excitation qui, théoriquement, devrait induire des sonneries d'amplitude géante et à faible décroissance temporelle. Ce comportement a été mis en évidence sur le champ de Fierz-Pauli et nous l'avons généralisé aux autres champs bosoniques (scalaire et de Proca). Cependant, en travaillant sur un problème de Cauchy, nous avons aussi montré que, contrairement à ce qui se passe pour les champs non-massifs, la sonnerie quasi-normale ne peut être clairement individualisée sur une forme d'onde et que son caractère géant est même neutralisé du fait de la coexistence de deux phénomènes : (i) l'excitation des modes quasi-liés qui floutent la contribution des modes quasi-normaux et (ii) la nature évanescente des modes partiels particuliers supposés exciter les modes quasi-normaux dont le facteur d'excitation a un comportement résonant.

Mots clés : Rayonnement des trous noirs, champs bosoniques massifs, modes quasi-normaux, modes quasi-liés, formes d'ondes.

Università di Corsica Pasquale Paoli

Equipe Physique Théorique - Projet COMPA
SPE, UMR 6134 du CNRS et de l'Université de Corse

cnrs dépasser les frontières